COLLEGE OF ENGINEERING
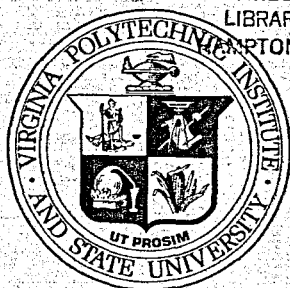
ANALYSIS, TESTING, AND EVALUATION

OF FAULTED AND UNFAULTED WYE,

DELTA, AND OPEN DELTA CONNECTED

ELECTROMECHANICAL ACTUATORS

NAS 9-16211

VIRGINIA POLYTECHNIC INSTITUTE AND STATE UNIVERSITY

NF01841

**BLACKSBURG,
VIRGINIA**

ANALYSIS, TESTING, AND EVALUATION
OF FAULTED AND UNFAULTED WYE,
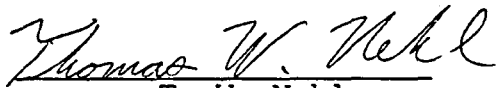DELTA, AND OPEN DELTA CONNECTED
ELECTROMECHANICAL ACTUATORS

NAS 9-16281

ANALYSIS, TESTING, AND EVALUATION OF FAULTED AND UNFAULTED WYE, DELTA, AND OPEN DELTA CONNECTED ELECTROMECHANICAL ACTUATORS

by

T. W. Nehl
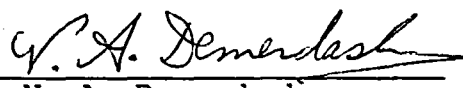Principal Investigator

N. A. Demerdash
Co-Principal Investigator

Personnel: T. A. Nyamusa
T. L. McHale

Virginia Polytechnic Institute and State University
Blacksburg, VA 24061

submitted to

TABLE OF CONTENTS

1.0 INTRODUCTION

This report presents the final results of contract number NAS 9-16281 of the NASA Johnson Space Center. The main goal of this research contract was the development of mathematical models capable of simulating the transient, steady state, and faulted performance characteristics of various brushless dc machine-PSA (power switching assembly) configurations. These systems are intended for possible future use as primemovers in EMAs (electromechanical actuators) for flight control applications. These machine-PSA configurations include wye, delta, and open-delta connected systems, see Figures (1.0-1), (1.0-2), and (1.0-3), respectively. The research performed under this contract was initially broken down into the following six tasks:

1. Development of mathematical models for various machine-PSA configurations,

2. Experimental validation of the mathematical model,

3. Shorted turn model for failure modes,

4. Experimental validation of the mathematical model for shorted turn-failure modes,

5. Tradeoff study, and

6. Documentation of results and methodology.

The fourth task was ultimately eliminated due to problems in procuring the required equipment.

The developed actuator model is very general and can handle a large variety of machine-PSA configurations. The model includes mutual coupling between the armature phase windings as well as the ability to handle nonlinearities in both the inductances and capacitances of the system. This program automatically generates the state model from the network topology without any tedious hand derivations. This model has the capability of handling PSAs with or without separate choppers. Furthermore the chopping can be either hysteresis or PWM controlled as desired.

This program has already been applied successfully to wye, delta, and open delta connected machines as well as machines with shorted turns in the armature windings.

The model was verified against test data obtained from a 15 HP samarium cobalt permanent magnet brushless dc machine system designed and built for use in electric vehicles. The correlation between measured and simulated data was excellent in all cases; thereby satisfying the second task listed above.

The third task is concerned with the development and verification of a shorted turn model. The shorted turn model was successfully implemented and applied to the wye connected machine mentioned earlier. Due to the problems in securing the required test equipment, the parameters in this case were assumed to be linear.

Because of the lack of adequate test facilities, the fourth task was cancelled.

The tradeoff study was not completed because of the large computer resource outlays required for the finite element field analysis and associated calculations. The derivation of this model and results obtained are given in the following chapters.

DC SUPPLY   SEPARATE CHOPPER   INVERTER/CONVERTER   PM MACHINE
(OPTIONAL)

Figure (1.0-1)   Wye Configuration

DR

Q7   D7

CHOKE

Q8   D8

Q1   D1

Q2   D2

Q3   D3

Q4   D4

Q5   D5

Q6   D6

C

A

B

DC SUPPLY   SEPARATE CHOPPER   INVERTER/CONVERTER   PM MACHINE
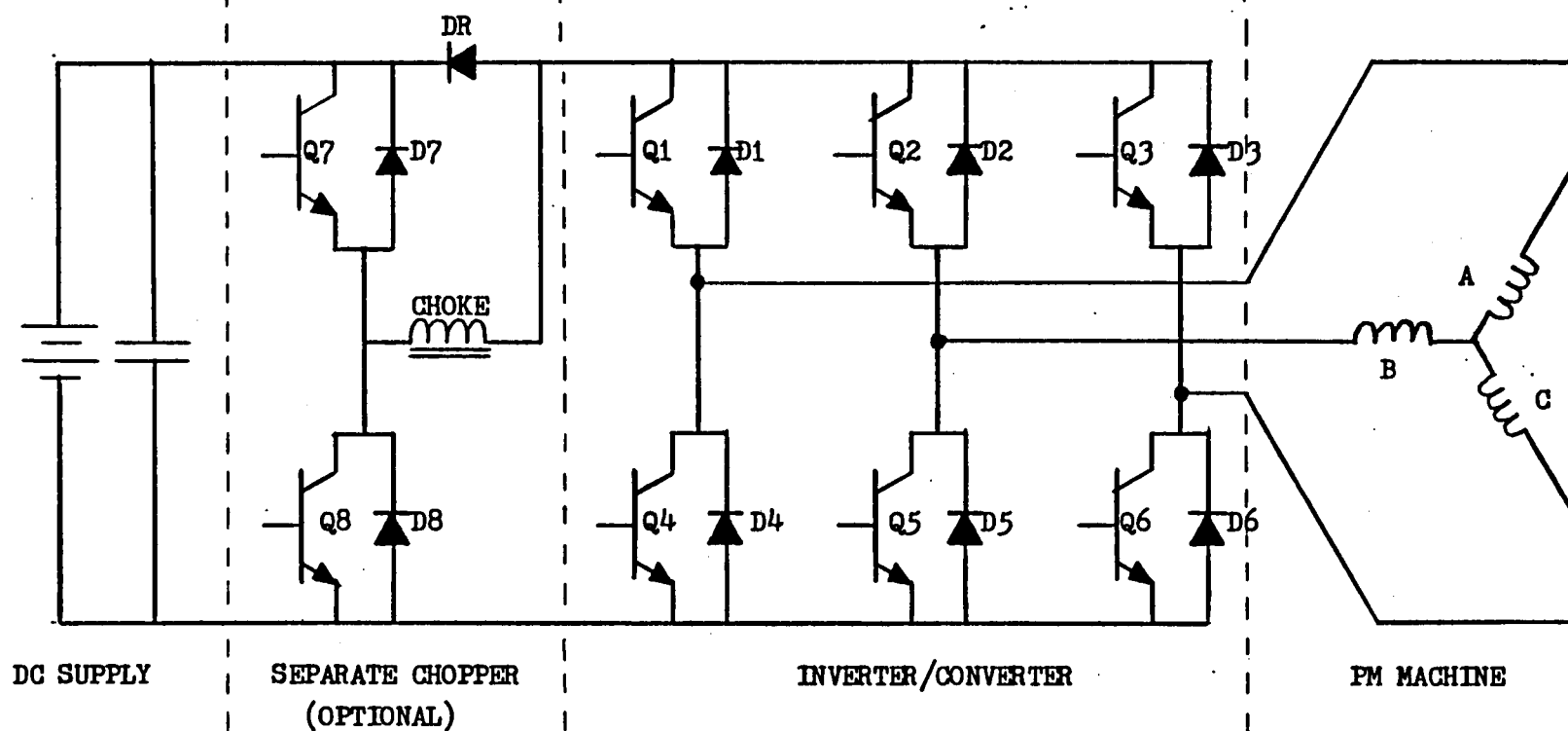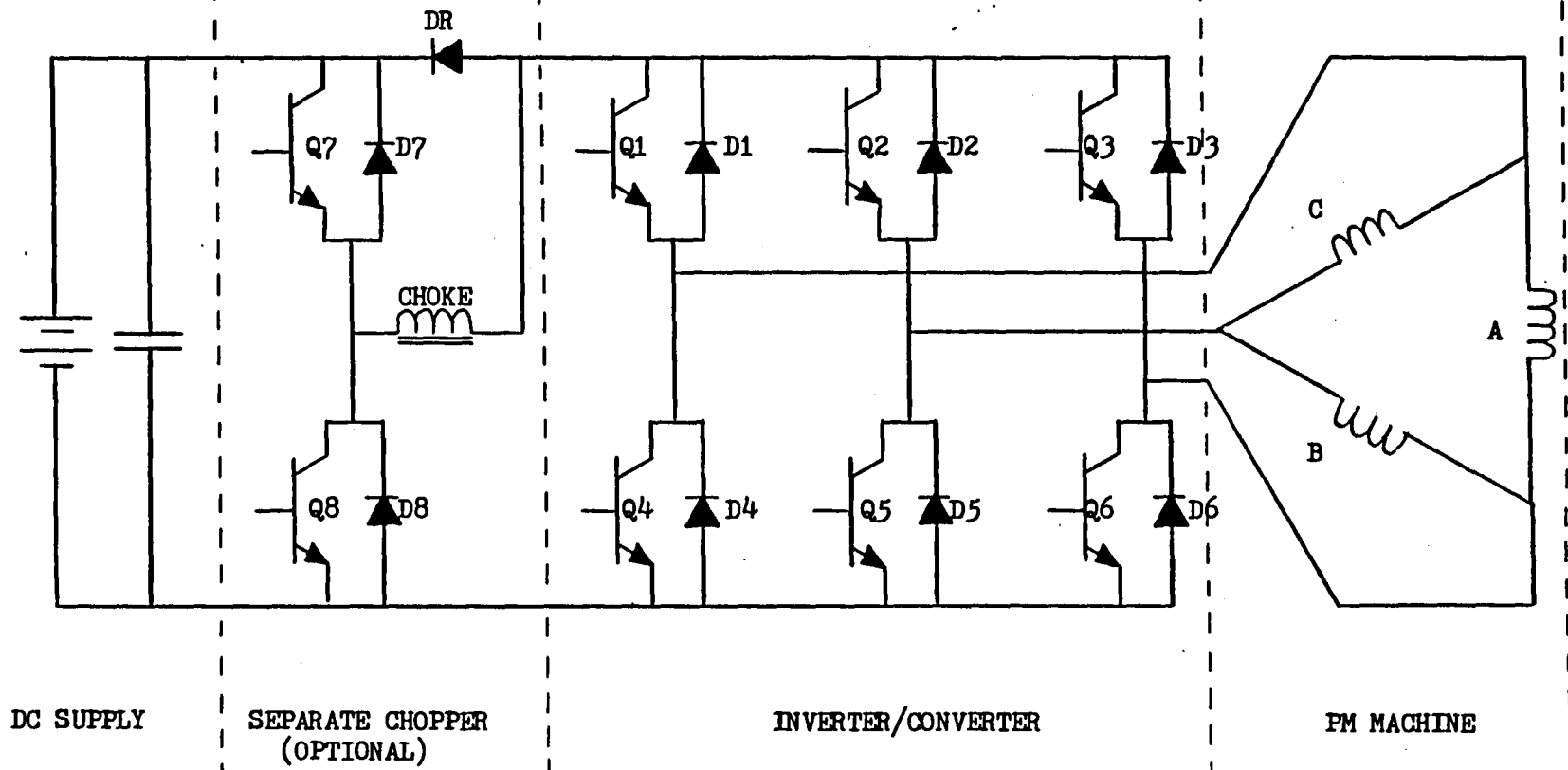   (OPTIONAL)

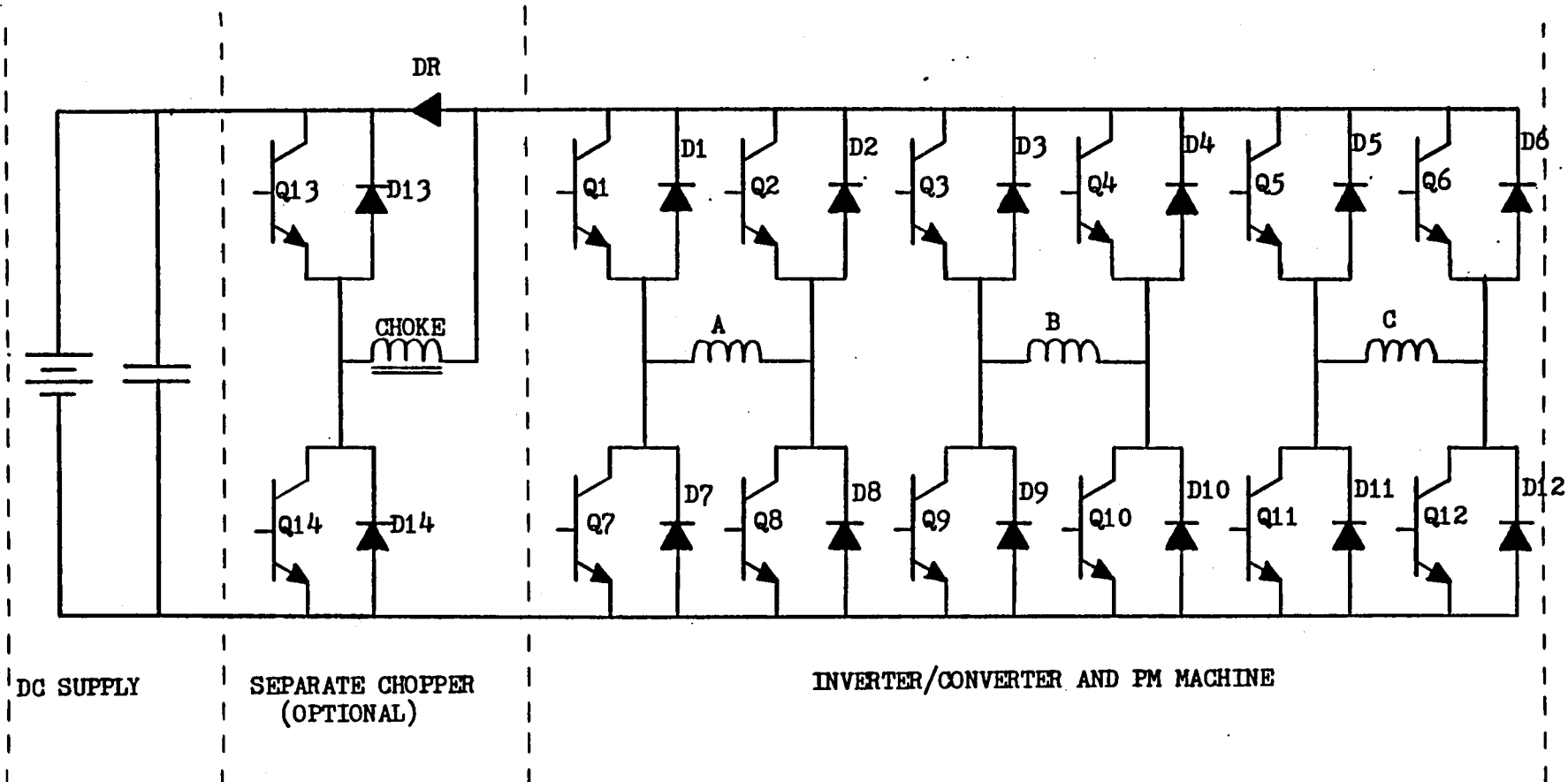Figure (1.0-2)   Delta Configuration

Figure (1.0-3) Open Delta Configuration

2.0 THE ACTUATOR MODEL

A generalized hybrid matrix modeling approach, suitable for the simulation of electromechanical systems consisting of solid state switching devices, capacitors (linear or nonlinear), inductors (linear or nonlinear) as well as rotating machines with mutual coupling between all of the machine windings, is presented in this chapter. This approach was chosen because it facilitates the automatic generation of the system state model directly from the network topology.

The systems that were analyzed using this modeling approach were divided into two subsystems: the power electronics and the rotating machine. A brief description of these two subsystems, as well as their impact on the overall modeling approach, is given below:

1. The power electronics was the first subsystem considered here. The state-of-the-art functions of power electronics subsystems are to control and process the flow of power from the dc source to the machine and vice versa. The power diodes and transistors are assumed to be the basic switching components of the power electronics. These diodes and/or transistors take on either very small or very large equivalent resistances depending upon their "on"/"off" status. This

nonlinearity requires that the state equations be updated whenever a diode or transistor changes state (status). The large spread of these resistance values causes a correspondingly large spread in the time constants of the overall system. Therefore, for this class of systems, the governing state equations are very stiff.

2. The second subsystem, which requires special attention, is the machine. In general, both the machine winding inductances and induced emfs are functions of the winding currents (state variables) and rotor angle. The nonlinearities associated with these parameters are typically much less severe than those produced by the switching action of the power diodes within the rectifier bridge.

Both of these subsystems are susceptible to failures or faults. Therefore additional consideration was given to the allowed possibility of faults in the various components, such as the diodes, transistors, fuses, and capacitors of the power electronics as well as faults within the machine itself. Some of these faults may lead to further stiffness of the system state equations.

The intrinsic characteristics of such electromechanical systems, during both normal and faulted operation, requires

that the modeling approach be designed to handle very stiff, nonlinear differential equations. Hence, the modeling approach presented in this report utilizes a commercially available implicit integration routine designed specifically for stiff differential equations. This is necessary in order to accurately simulate the dynamics of the system with a minimum expenditure of computer resources. Also the wide variety of topologies encountered in these type of machine systems, together with the large number of capacitances and inductances associated with these systems, makes it mandatory that the state model be generated automatically from the system topology and component parameters. Therefore the modeling approach, presented in this report has the following features:

1. The model is generated automatically from the system topology and component parameters;

2. the model is capable of handling nonlinear component parameters; and

3. the solution routines can handle extremely stiff (ill-conditioned) differential equations.

The theoretical background of a modeling approach with these three attributes is the subject of this chapter. The

modeling approach makes heavy use of network graph theory [1,2], and is based upon a hybrid matrix formulation, [2]. This approach is presented in the seven sections of this chapter. A brief description of each section follows.

In the first section, the nonlinear components typically found in such electromechanical systems are identified and described. A suitable network model for each of these components is presented.

In the second section, the basic concepts of network graph theory relevant to the chosen modeling approach are discussed. The use of network graph theory allows for compact notation and facilitates the actual implementation of the model on the digital computer.

In the third section, the hybrid matrix approach for automatically generating the state equations is discussed in detail. This approach was chosen since it easily handles the various nonlinear components as well as mutual coupling present in these types of systems.

In the fourth section, the output equations (branch voltages and currents) are obtained in terms of the hybrid matrix representation used to obtain the state model. The output equations express all of the branch voltages and currents in terms of the state variables and forcing functions.

The fifth section outlines the procedure used to determine the operating point "on"/"off" of the diodes at each point in time. The accuracy of the overall solution is closely related to the degree of stiffness and the accuracy in determining the precise switching points of these diodes.

The procedure for integrating the state variables forward in time is given in the sixth section. The effects of stiffness on the solution accuracy and model performance are discussed.

In the last section, the modeling approach is verified by comparison of simulated results with test data obtained from a 15 hp samarium cobalt based brushless dc machine designed and built for vehicle propulsion.

2.1 Models for the Nonlinear Components

Typical EMA systems contain a number of nonlinearities which must be dealt with separately. The nonlinearities of greatest concern can be catagorized into four groups:

1. The first group of nonlinearities is associated with the switching action of the power diodes, see Figure (2.1-1). This switching action causes extreme changes in the electrical time constants of the system. This is due to the extremely large change in the conduction properties of the diodes between their "on" and "off" states. The slope of the switch I-V characteristic, shown in Figure (2.1-1), is equal to the reciprocal of the equivalent diode resistance at a given operating point. The "on" state of the diode is represented by the first quadrant in Figure (2.1-1), where the slope is large (low equivalent diode resistance). Conversely, the "off" state is represented by the third quadrant of this figure. The slope of the diode characteristic, in this quadrant, is very small and hence can be represented by a very large equivalent resistance.

2. The second group of nonlinearities is associated with the switching action of the power transistors. This switching action also causes extreme changes in the time
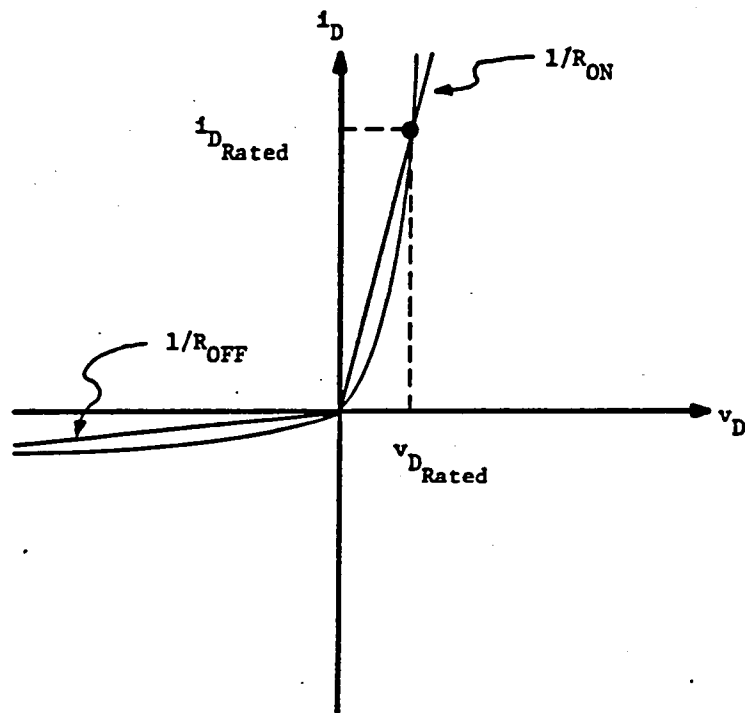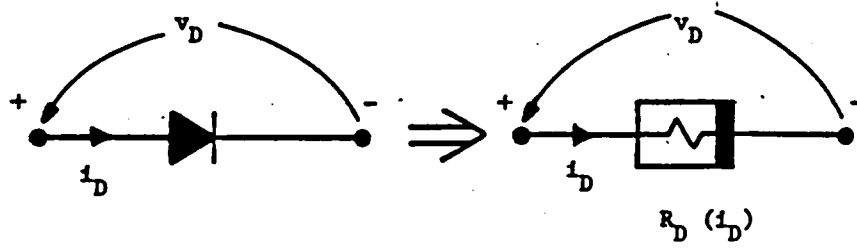
Fig. (2.1-1) Piecewise Linear Diode Model
Approximating the I-V Characteristics

constants of the electromechanical system. Like the diodes, this is due to the extremely large change in the conduction properties of the transistors between their "on" and "off" states. The "on" state of the transistor is represented by a low equivalent resistance. Conversely, the "off" state is represented by a very large equivalent resistance. The only difference between the diode and transistor models is the way in which the equivalent resistance value is determined throughout a given simulation run.

3. The machine parameters (inductances and emfs) of the ac machine form the second group of nonlinearities within the system. These nonlinearities are due to saturation effects within the iron portions of the machine. The winding inductances and emfs are influenced also by the angular displacement between the rotor and stator. Details on the numerical calculation of these parameters are given in reference [3, 4, 5]

4. The last group of nonlinearities considered here is due to failures which may occur in the various components of the system. The faults or failures considered in this work consist of the following:

    a) Open fuses due to electrical or mechanical reasons;

    b) open capacitors due to mechanical reasons;

c) shorted capacitors due to dielectric breakdown;

d) open circuited diodes due to electrical or mechanical reasons; and

e) short circuited diodes due to electrical or mechanical reasons.

Nonlinear Network Model of the Diodes and Transistors

The nonlinearity due to the switching action of a diode is modeled by a piecewise-linear representation of the specific diode's I-V characteristic, as shown in Figure (2.1-1). In terms of an equivalent network component model, the diode is modeled as a nonlinear or bi-valued resistance, see reference [6, 7]. The "on" (or first quadrant) value of this resistance is defined as the forward voltage drop of the actual diode divided by the forward diode current at rated conditions for the given system under study. This data is obtained from the actual manufacturer's data sheets of the power diodes. A similar model is used for the transistor; however, the resistance value (between collector and emitter) is assumed not to be polarity sensitive. These simplified switch models were chosen because it was found from past experience that the excessive computation required to include the dynamics during the actual switching

process would add little in the way of improved accuracy in the predicted system response. This is primarily due to to the fact that the percent of the total simulation duration which these switching devices spend within the highly nonlinear region of their IV-characteristics is small. This is true for these types of machine systems primarily because of their relatively low frequency application. The modeling approach presented in this report can incorporate equivalent network models for these switching devices if additional accuracy is required.

The algorithm used to switch from one diode state to the other is described in detail in Section 2.5. On the otherhand, the control logic used for determining the "on"/"off" state of each transistor is a function of the state variables, forcing functions, the rotor angle, the machine speed, the mode of operation, and the commanded machine torque.

Machine Model Including Shorted Turns

The second nonlinear system component modeled was the multiwinding machine. The electromagnetic interactions

between the various windings was modeled by means of n-coupled coils, one for each of the n windings. The model of each winding consists of three series connected components; the coil resistance, the incremental self and mutual inductances, and the open circuit back emf. The inductances and emf's are functions of the level of saturation and hence this model is nonlinear. Also, these parameters are functions of the rotor angle, hence the model is time dependent as well. This machine model is general enough to be applied to machines similar to the permanent-magnet dc-machine systems described in Chapter 1. For simplicity, the multiple armature machine will be treated as having two separate armatures. One of these armatures is assumed to be normal or healthy (h) while the other is faulted or defective (d). The n-coupled coil approach is quite general and can easily be extended to any number of armatures and fault configurations.

The spatial relationships among the axes of the seven windings of this machine is displayed in Figure (2.1-2). Notice that there are two windings for each of three phases (a,b,c) as well as a seperate field winding (f). The coil axis or positive MMF direction of each coil is indicated by the arrows labeled (a,b,c,f). The angle between the

MMF (FIELD)

MMF (C)

MMF (A)

"phasor diagram"

MMF (B)

phase B

R_2

L_2

e_2

R_5

L_5

e_5

e_f

R_f

L_f

e_4 L_4 R_4

phase A

e_1 L_1 R_1

e_3

L_3

R_3

e_6

L_6

R_6

phase C

$$v_{L_1} = L_1 \frac{d}{dt}(\underline{i})$$

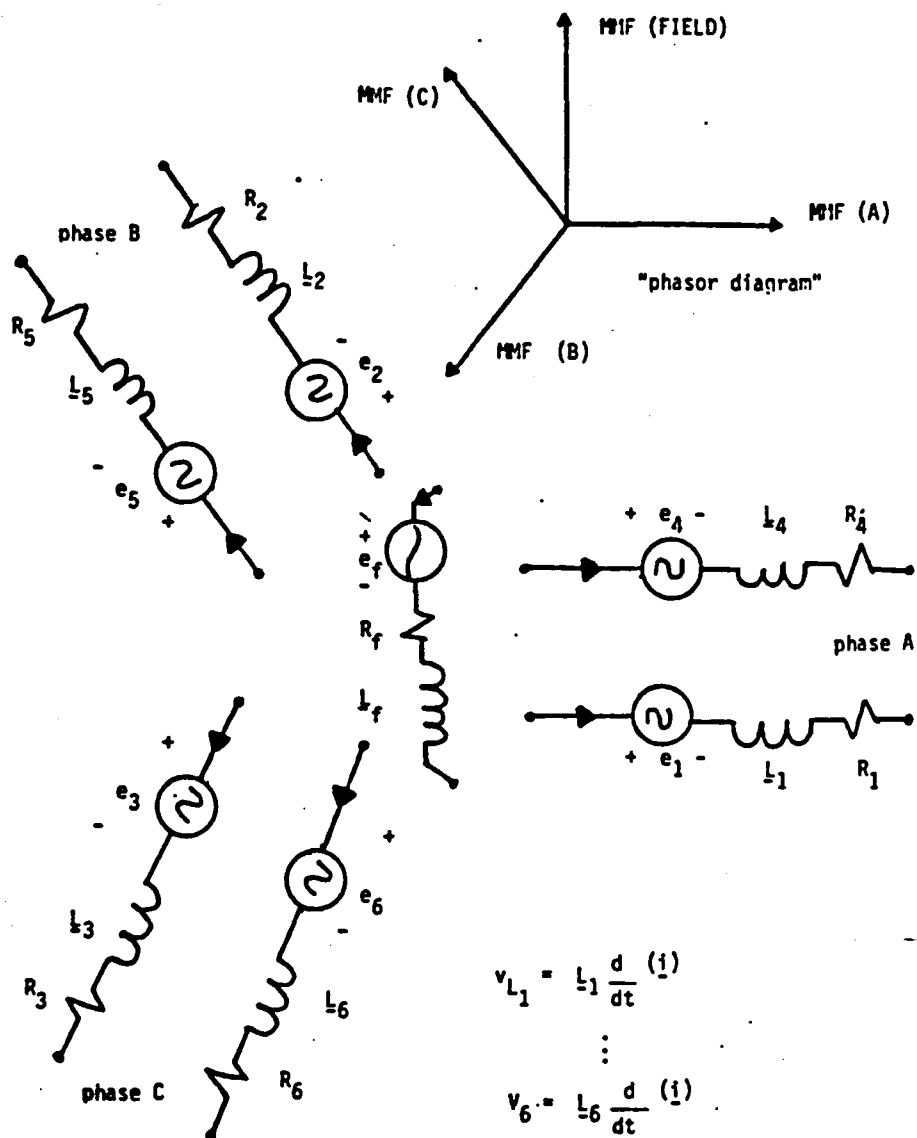$$\vdots$$

$$v_6 = L_6 \frac{d}{dt}(\underline{i})$$

Figure (2.1-2)   Lumped Parameter Machine Model

positive MMF of phase A and positive field MMF is denoted by
an angle theta. The behavior of the field winding is
assumed to be controlled by the value of the field current,
which is treated as an external known forcing function and
hence not a state variable. In the case of a permanent
magnet machine, this field current would be held constant.
Based upon these assumptions, the voltage equations for the
seven winding machine model can be expressed in matrix form
as follows:

$$
\begin{vmatrix} v_1 \\ v_2 \\ v_3 \\ -- \\ v_4 \\ v_5 \\ v_6 \end{vmatrix} = \begin{vmatrix} R_1 & 0 & 0 & 0 & 0 & 0 \\ 0 & R_2 & 0 & 0 & 0 & 0 \\ 0 & 0 & R_3 & 0 & 0 & 0 \\ ---&---&---&---&---&--- \\ 0 & 0 & 0 & R_4 & 0 & 0 \\ 0 & 0 & 0 & 0 & R_5 & 0 \\ 0 & 0 & 0 & 0 & 0 & R_6 \end{vmatrix} * \begin{vmatrix} i_1 \\ i_2 \\ i_3 \\ -- \\ i_4 \\ i_5 \\ i_6 \end{vmatrix} + d/dt \begin{vmatrix} \lambda_1 \\ \lambda_2 \\ \lambda_3 \\ -- \\ \lambda_4 \\ \lambda_5 \\ \lambda_6 \end{vmatrix}
$$

(2.1-1)

Notice that the effect of the field winding was incorporated
into the vector of winding flux linkages since the field
current was assumed to be a known function of time because
of the permanent magnets. Equation (2.1-1) can be expressed
in shorthand matrix notation, specifically advantageous for
partial fault analysis, as follows:

$$
\begin{vmatrix} \underline{v}_h \\ -- \\ \underline{v}_d \end{vmatrix} = \begin{vmatrix} \underline{R}_h & | & \underline{0} \\ ---- & | & ---- \\ \underline{0} & | & \underline{R}_d \end{vmatrix} * \begin{vmatrix} \underline{i}_h \\ -- \\ \underline{i}_d \end{vmatrix} + d/dt \begin{vmatrix} \underline{\lambda}_h \\ -- \\ \underline{\lambda}_d \end{vmatrix} \qquad (2.1-2)
$$

where, $\underline{v}_h$ and $\underline{v}_d$ represent the voltage vectors of the healthy (h) and faulted or defective (d) armature phase windings (terminal voltages), respectively;

$\underline{R}_h$ and $\underline{R}_d$ represent the resistance matrices of the healthy and faulted phase windings, respectively;

$\underline{i}_h$ and $\underline{i}_d$ represent the current vectors of the healthy (h) and faulted (d) phase windings, respectively; and,

$\underline{\lambda}_h$ and $\underline{\lambda}_d$ represent the flux linkage vectors of the healthy and faulted phase windings, respectively.

The flux linkage vectors, $\underline{\lambda}_h$ and $\underline{\lambda}_d$, are functions of the six armature currents, $\{i_1, \ldots, i_6\}$, the field current, i_f, and the rotor position, θ. Hence, by the chain rule:

$$
[d\underline{\lambda}_h/dt] = [\partial\underline{\lambda}_h/\partial i_1]*[di_1/dt] + \ldots + [\partial\underline{\lambda}_h/\partial i_6]*[di_6/dt]
$$
$$
+ [\partial\underline{\lambda}_h/\partial i_f]*[di_f/dt] + [\partial\underline{\lambda}_h/\partial\theta]*[d\theta/dt] \qquad (2.1-3)
$$

$$
[d\underline{\lambda}_d/dt] = [\partial\underline{\lambda}_d/\partial i_1]*[di_1/dt] + \ldots + [\partial\underline{\lambda}_d/\partial i_6]*[di_6/dt]
$$
$$
+ [\partial\underline{\lambda}_d/\partial i_f]*[di_f/dt] + [\partial\underline{\lambda}_d/\partial\theta]*[d\theta/dt] \qquad (2.1-4)
$$

The first derivative of the rotor angle, θ, with respect to time, t, is defined as the radian velocity, ω, of the machine as follows:

$$\omega = d\theta/dt \qquad (2.1-5)$$

The "induced armature emf" can be obtained from equations (2.1-3) and (2.1-4) as follows:

$$
\begin{vmatrix} e_h \\ \hline e_d \end{vmatrix}
=
\begin{vmatrix} [\partial\lambda_h/\partial i_f] \\ \hline [\partial\lambda_d/\partial i_f] \end{vmatrix}
*[di_f/dt]
+
\begin{vmatrix} [\partial\lambda_h/\partial\theta] \\ \hline [\partial\lambda_d/\partial\theta] \end{vmatrix}
*\omega
$$

$$(2.1-6)$$

The partials of λ_h and λ_d with respect to the currents are, by definition, the machine incremental inductances. These inductances are given in matrix form as: L_{hh}, L_{hd}, L_{hf}, L_{dh}, L_{dd}, and L_{df}, and are defined as follows:

$$
L_{hh} = \begin{vmatrix} \partial\lambda_h/\partial i_1 & \partial\lambda_h/\partial i_2 & \partial\lambda_h/\partial i_3 \end{vmatrix} \qquad (2.1-7)
$$

$$
L_{hd} = \begin{vmatrix} \partial\lambda_h/\partial i_4 & \partial\lambda_h/\partial i_5 & \partial\lambda_h/\partial i_6 \end{vmatrix} \qquad (2.1-8)
$$

$$
L_{hf} = \begin{vmatrix} \partial\lambda_h/\partial i_f \end{vmatrix} \qquad (2.1-9)
$$

- 18 -

$$\underline{L}_{dh} = \begin{array}{|c|c|c|} \hline \partial\underline{\lambda}_d/\partial i_1 & \partial\underline{\lambda}_d/\partial i_2 & \partial\underline{\lambda}_f/\partial i_3 \\ \hline \end{array}$$

(2.1-10)

$$\underline{L}_{dd} = \begin{array}{|c|c|c|} \hline \partial\underline{\lambda}_d/\partial i_4 & \partial\underline{\lambda}_d/\partial i_5 & \partial\underline{\lambda}_d/\partial i_6 \\ \hline \end{array}$$

(2.1-11)

$$\underline{L}_{df} = \begin{array}{|c|} \hline \partial\underline{\lambda}_d/\partial i_f \\ \hline \end{array}$$

(2.1-12)

Using equations (2.1-3) through (2.1-12) one can rewrite the armature terminal voltage vector, equation (2.1-2), as follows:

$$\begin{array}{|c|} \hline \underline{v}_h \\ \hline \underline{v}_d \\ \hline \end{array} = \begin{array}{|c|c|} \hline \underline{R}_h & \underline{0} \\ \hline \underline{0} & \underline{R}_d \\ \hline \end{array} * \begin{array}{|c|} \hline \underline{i}_h \\ \hline \underline{i}_d \\ \hline \end{array} + \begin{array}{|c|} \hline \underline{e}_h \\ \hline \underline{e}_d \\ \hline \end{array} +$$

$$\begin{array}{|c|c|}
\hline
\underline{L}_{hh} & \underline{L}_{hd} \\
\hline
\underline{L}_{dh} & \underline{L}_{dd} \\
\hline
\end{array} * d/dt
\begin{array}{|c|}
\hline
\underline{i}_h \\
\hline
\underline{i}_d \\
\hline
\end{array}
\qquad (2.1\text{-}13)$$

In expanded form, the terminal voltages of the armature can now be written as follows:

$$
\begin{vmatrix} v_1 \\ v_2 \\ v_3 \\ v_4 \\ v_5 \\ v_6 \end{vmatrix}
=
\begin{vmatrix}
R_1 & 0 & 0 & 0 & 0 & 0 \\
0 & R_2 & 0 & 0 & 0 & 0 \\
0 & 0 & R_3 & 0 & 0 & 0 \\
0 & 0 & 0 & R_4 & 0 & 0 \\
0 & 0 & 0 & 0 & R_5 & 0 \\
0 & 0 & 0 & 0 & 0 & R_6
\end{vmatrix}
*
\begin{vmatrix} i_1 \\ i_2 \\ i_3 \\ i_4 \\ i_5 \\ i_6 \end{vmatrix}
+
\begin{vmatrix} e_1 \\ e_2 \\ e_3 \\ e_4 \\ e_5 \\ e_6 \end{vmatrix}
$$

$$
+
\begin{vmatrix}
L_{11} & L_{12} & L_{13} & L_{14} & L_{15} & L_{16} \\
L_{21} & L_{22} & L_{23} & L_{24} & L_{25} & L_{26} \\
L_{31} & L_{32} & L_{33} & L_{34} & L_{35} & L_{36} \\
L_{41} & L_{42} & L_{43} & L_{44} & L_{45} & L_{46} \\
L_{51} & L_{52} & L_{53} & L_{54} & L_{55} & L_{56} \\
L_{61} & L_{62} & L_{63} & L_{64} & L_{65} & L_{66}
\end{vmatrix}
* d/dt
\begin{vmatrix} i_1 \\ i_2 \\ i_3 \\ i_4 \\ i_5 \\ i_6 \end{vmatrix}
\qquad (2.1\text{-}14)
$$

Equation (2.1-14) is the governing matrix equation of the seven winding machine. This equation corresponds to the lumped parameter network model shown in Figure (2.1-2).

The vectors and matricies employed in Figure (2.1-2) are related to this discusion by the following identities:

$$\underline{i} = \left[\begin{array}{c|c} \underline{i}_h & \underline{i}_d \end{array} \right]^t \tag{2.1-15}$$

$$\left[\begin{array}{c} \underline{L}_1 \\ \hline \underline{L}_2 \\ \hline \underline{L}_3 \end{array} \right] = \left[\begin{array}{c|c} \underline{L}_{hh} & \underline{L}_{hd} \end{array} \right] \tag{2.1-16}$$

and

$$\left[\begin{array}{c} \underline{L}_4 \\ \hline \underline{L}_5 \\ \hline \underline{L}_6 \end{array} \right] = \left[\begin{array}{c|c} \underline{L}_{hd} & \underline{L}_{dd} \end{array} \right] \tag{2.1-17}$$

A procedure used to obtain these emf and inductance parameters using the finite element method is described in detail in references [8, 9, 10].

Nonlinear Network Models of the Faulted Components

One important application of the simulation model presented in this work is to analyze the effects of component faults in the PSA. These faults may occur in the fuses, the snubber capacitors, and in the diode and transistor switches. The failures or faults within these components may be due to both electrical and/or mechanical reasons.

Nonlinear Component Model of the Fuses

The nonlinearity of the fuse model results from the incorporation of its failure modes mentioned previously. The first fuse failure mode considered here results from the fuse thermal rating ($i^2 T$) being exceeded. This is due to sustained excessive fuse current. Once a fuse opens and clears, the open fuse is modeled as a very large resistance. Thus, the fuse model is somewhat similar to the diode model in that it also is modeled as a nonlinear resistor.

The second failure mode, considered here, results from mechanical fatigue. It is assumed that this type of failure

mode results in an open (large resistance). The only difference in these two failure modes is in their initiations. The first failure mode is initiated when the accumulated energy exceeds the i^2T rating of the fuse. The second type of failure mode is initiated by the USER at a specified time within a given simulation run.

The use of the low or high values of resistance to simulate the state of each fuse makes it possible to use just one network topology during both the faulted and unfaulted modes of operation. This greatly simplifies the analysis.

The unfaulted state of the fuse is modeled as a very low resistance. This resistance value as well as the i^2T rating are obtained directly from the fuse data sheets supplied by the manufacturer. An example, [10], of such a data sheet, in graphical form, can be seen in Figure (2.1-3).

The data, given in this figure, which is pertinent to the fuse model is summarized below:

1. THE RATED CURRENT (I_{RATED}) specifies the rated current that can pass through the fuse indefinitely without causing the fuse to open and clear.
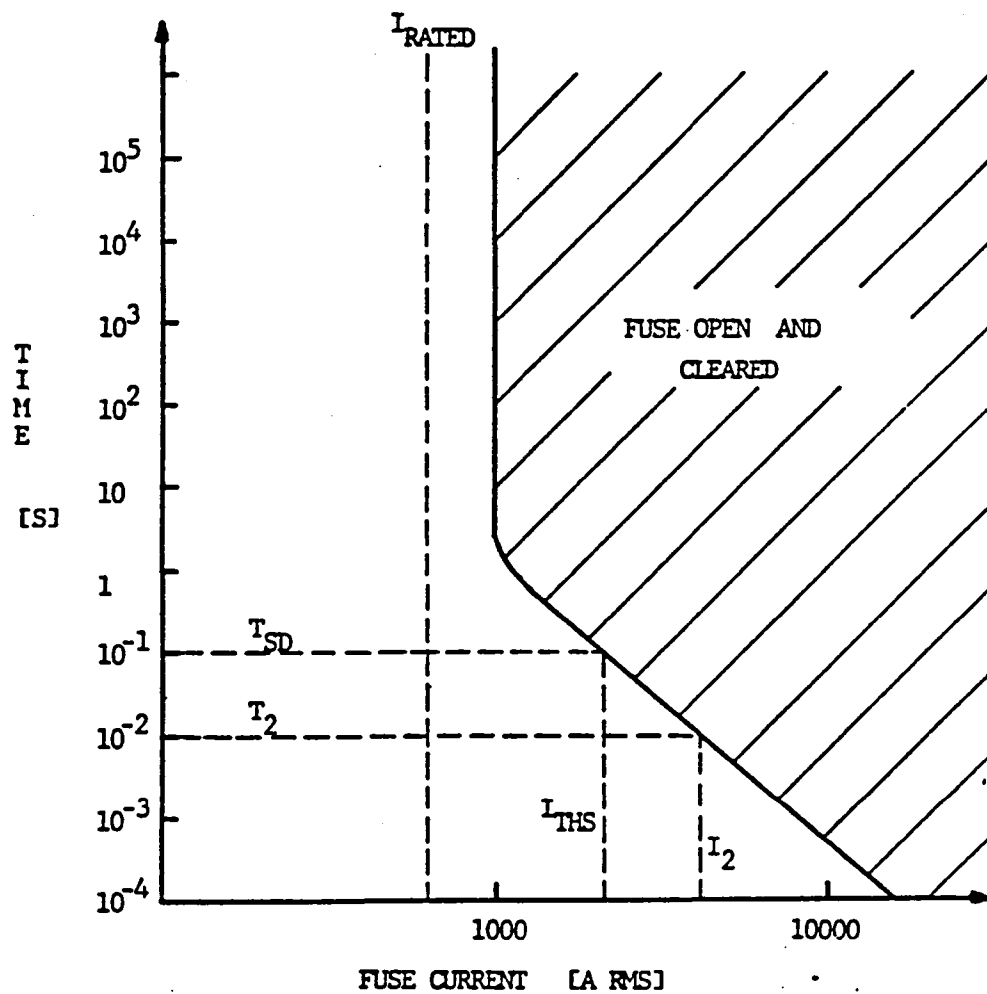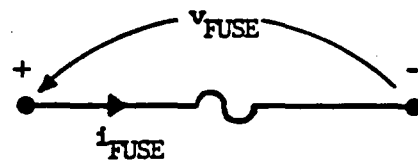
Figure (2.1-3)   Example Fuse Characteristic

2. The I^2T rating of the fuse can be obtained from this figure by squaring the RMS value of any current, I_2, within the specified "section for calculating I^2T" as shown in Figure (2.1-3) and multiplying this result by its corresponding time, T_2, as follows:
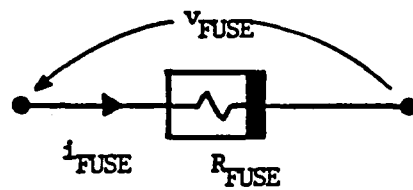
$$I^2T = (I_2)^2 * T_2 \qquad\qquad (2.1-18)$$

3. The Total Simulation Duration (T_{SD}) is USER specified and is defined as the total duration of the computer simulation run. The intersection of T_{SD} with the boundary between safe and open operation regions gives the value of the threshold current I_{THS}. This current represents the minimum value of the fuse current for which the fuse energy is accumulated. If this accumulated energy exceeds the i^2T rating then the fuse is opened and cleared. Notice for the specified time period, T_{SD}, any value of sustained fuse current below I_{THS} will not result in a fuse open.

These parameters are incorporated in the fuse network component model for a given simulation. The schematic and corresponding network component symbols of this model are given in Figure (2.1-4).

Schematic
Symbol

v_{FUSE}

+   —

i_{FUSE}

v_{FUSE}

Fuse Model

i_{FUSE} R_{FUSE}

R_{FUSE}

(LATCHED)

R_{open}

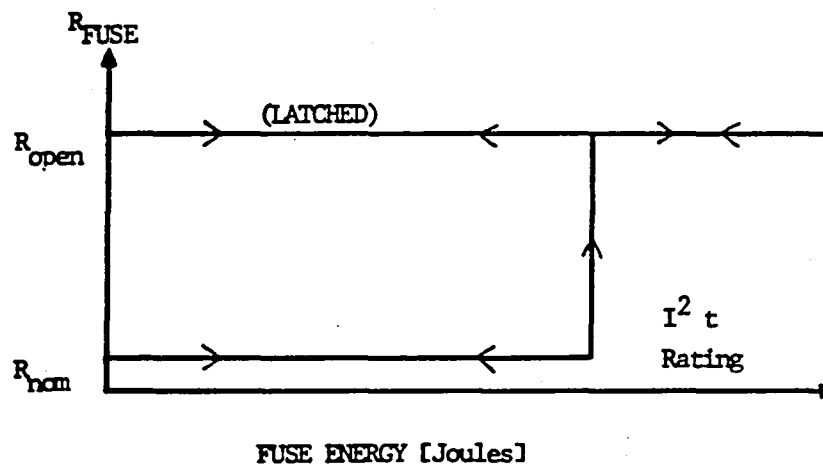$I^2 t$
Rating

R_{nom}

FUSE ENERGY [Joules]

Figure (2.1-4)   Latching Hysteresis Type of Network
Component Fuse Model

The latching-hysterisis behavior of the fuse model is shown also within this figure. The fuse is modeled as a piecewise (latching) linear resistor which can take on two distinct and very widely spread values. The nominal (unfaulted) value of the fuse resistance (R_{NOM}) can be obtained from the manufacturer's data sheet. The fuse will always have this low resistance value if the energy dissipated within the fuse never exceeds its I^2T rating. This safe region of operation is shown in Figure (2.1-4) and corresponds to the region bounded by the shaded (FUSE OPEN AND CLEARED) region and the two axes (time versus current) as illustrated in Figure (2.1-3). Once the fuse exceeds its I^2T rating, the resistance value of its corresponding network component model (R_{FUSE}) is made very high (R_{OPEN}), to simulate the open circuit condition.

The second fuse failure mode, that is the mechanical opening of a fuse, is USER initiated. This is accomplished by setting the fuse resistance, R_{FUSE}, to be equal to R_{OPEN} at some predetermined time during the computer simulation run. These two modes for initiating a fuse failure can be considered as natural (I^2T) and forced (mechanical). The latching behavior of the fuse model, as shown in Figure (2.1-4), is necessary since once the fuse is opened, it will remain open for the remainder of the simulation.

Nonlinear Component Model of Faulted Capacitors

The nonlinearity of the capacitor model is strictly due to the incorporation of its failure modes.
These failure modes are:

1. An open circuit due to mechanical fatigue; and

2. a short circuit due to dielectric failure.

The equivalent network model of the fault capacitor during the normal, open, and shorted modes of operation, is illustrated in Figure (2.1-5). The two resistors (R_{CS} and R_{CO}) within this equivalent component model are bi-valued piecewise linear resistors. The very large (open) value and the very small (shorted) value of these resistances are determined by the specific capacitor mode of operation.

These three modes of operation of the fault capacitors (normal, open, or shorted) can be implemented by the various combinations of the resistance values for R_{CO} and R_{CS} as illustrated in Figure (2.1-5).

The failure modes of the fault capacitor are initiated in the following manner:
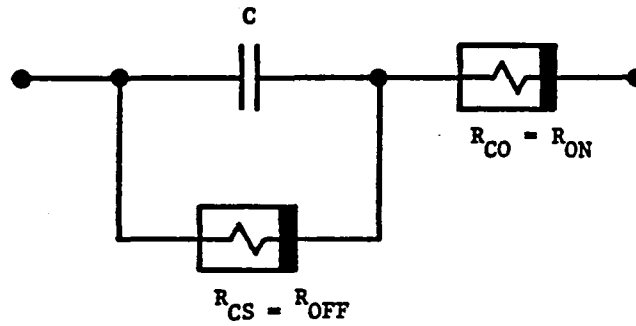
1. A shorted capacitor (R_{OC} and R_{SC} are set to small values) is initiated if the fault capacitor's voltage (which is typically a state variable) exceeds its breakdown value. This breakdown voltage value, called

V_{CBD}, is obtainable from the manufacturer's data sheet. Even though a breakdown can occur for different voltages (ac or dc), it is the responsibility of the engineer when incorporating these voltages to use his/her judgement in determining a suitable peak breakdown voltage, V_{CBD}, to be used in a given simulation. Once the breakdown (shorted fault) has occurred, the values of R_{OC} and R_{SC}, in Figure (2.1-5) are latched at very small resistive values.
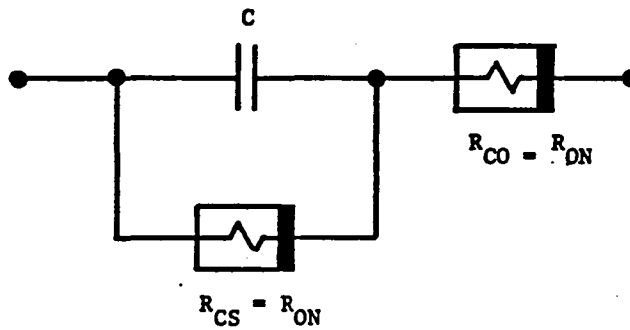
2. The open capacitor (R_{OC} and R_{SC} are set to very large values) is assumed to occur due to mechanical fatigue. This type of fault is initiated by the USER at a specified time during the simulation run. Once the open failure mode has occurred, the values of R_{OC} and R_{SC} are latched at very large values of resistance for the remaining duration of the simulation.

The initiation of these two failure modes of the capacitors can be considered as 1) natural, in the case of the short, and 2) forced, in the case of the open. The latching behavior of this model is necessary since it is assumed that these failures (faults) are permanent during a particular simulation run.

a) **Unfaulted Capacitor**

$R_{CO} = R_{ON}$

$R_{CS} = R_{OFF}$

b) **Shorted Capacitor**

$R_{CO} = R_{ON}$

$R_{CS} = R_{ON}$

c) **Open Capacitor**

$R_{CO} = R_{OFF}$

$R_{CS} = R_{OFF}$

R_{ON} = Very small resistance,
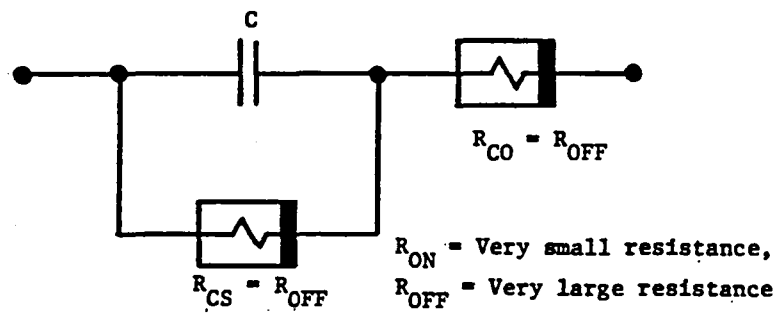R_{OFF} = Very large resistance

Figure (2.1-5) Faulted Capacitor Equivalent Network Model

2.2 Network Graph Theory Concepts

The computer-aided analysis of relatively complex systems, such as the EMA systems introduced in Chapter 1, requires a systematic procedure for formulating the governing state equations on the digital computer. This can be accomplished by applying generalized graph theory concepts, [1,2], and matrix algebra to the lumped-parameter network model of the system under study. The economical advantage of this approach becomes apparent when it is required to model a number of different topologies (or systems) using the same simulation program, as is the case here with the various types of power conditioners and brushless dc-machine systems considered in this report.

In this section, a brief background on the fundamental concepts and definitions of network graph theory are presented. For further detail, see references [1,2].

A lumped-parameter network model of a system can be represented by means of a directed graph. A directed graph consists of a set of branches which are interconnected at nodes. A branch is a one-port representation of a network component. The relationship between the branch voltage and branch current is defined by the component model. Typical components encountered in EMA systems include resistors, capacitors, inductors, diodes, sources, rotating machines,

etc. Models of multi-port components are represented by a
set of branches (one-ports).

In this work, the positive direction of the current
through a branch and the positive direction of the voltage
rise across a branch are defined using the consumer
notation, as shown in Figure (2.2-1). In the consumer
notation, positive branch power is defined as power consumed
within the branch, thus the branch is said to be acting as a
sink. On the other hand, negative branch power is defined as
power generated from within the branch, thus the branch is
said to be acting as a source.

Branch power is defined as the product of the branch
voltage and the branch current. For the k-th branch, as
shown in Figure (2.2-1), the branch power is defined as:

$$p_{b_k} = v_{b_k} * i_{b_k} \qquad (2.2-1)$$

The branch voltage, v_{b_k}, is defined as the difference
between the node voltages v_{N_m} and v_{N_n}, taking the assumed
positive direction (from node m to node n in this case) of
the current, i_{b_k}, as follows:

$$v_{b_k} = v_{N_m} - v_{N_n} \qquad (2.2-2)$$

The node voltages v_{N_m} and v_{N_n} are defined in terms of a
reference (ground) node voltage, v_{ref}.
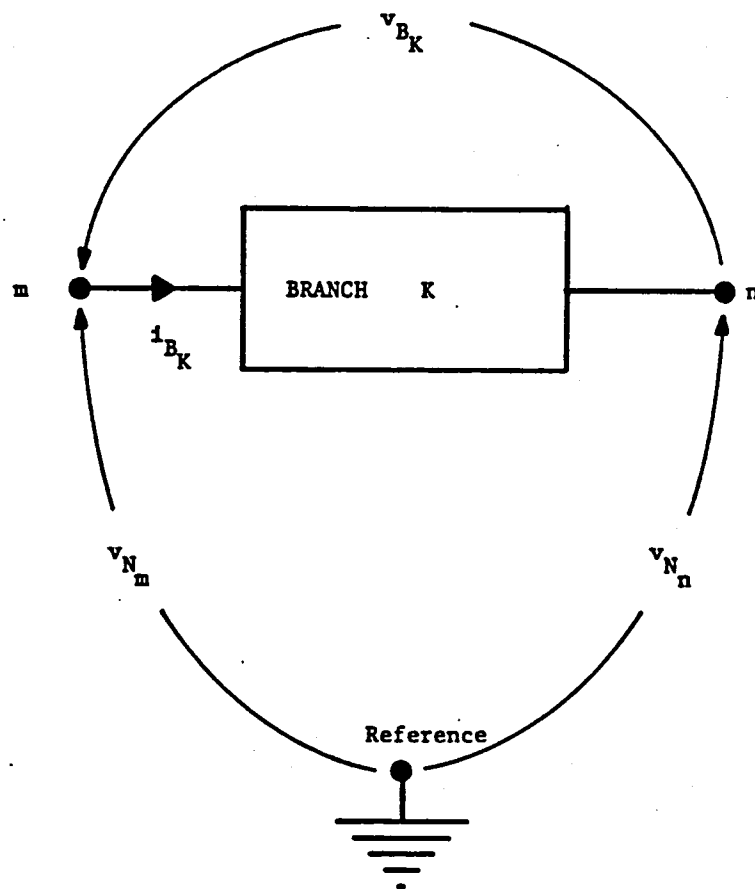
Figure(2.2-1) Branch Voltage and Current References

Consider for example, an arbitrary network with a total of NB branches and NN nodes. In this network, it is assumed that at least two branches are connected to each node. At this point, it would be advantageous to define some of the basic network graph terms used thoughout the remainder of this report.

Loop   A loop is a set of two or more branches which form a closed path

Tree   A tree is a subgraph of a network graph which must satisfy three conditions.
        1. All NN nodes must be contained in the tree.

        2. All NN nodes must be connected by branches. These branches are called twigs.

        3. The twigs may not form any loops

Cotree The cotree consists of all branches of the original network not contained within the chosen tree.   The cotree branches are called links. The insertion of any link into the tree results in a closed loop.

Cut-Set A cut-set is a "set" of branches which when "cut" away from the original network graph will totally isolate it into two separate subgraphs.

It must be noted that for any network graph there exists more than one choice for a tree and its corresponding cotree. The particular type of tree which is employed here is called a "normal-tree". A normal-tree is defined as a tree whose branches are selected in a specified sequence according to their component types.

In particular, the selection of a normal tree requires that all the independent voltage sources, E, and capacitors, C, within the original network model be chosen with the highest priority as twigs. All voltage sources are selected first. It is assumed that there are no all voltage source loops. Next, all of the capacitors, except for those belonging to a C-E loop, are selected as twigs. A C-E loop is defined as a loop consisting entirely of capacitors and/or independent voltage sources. Only one of the capacitors within every C-E loop must be chosen as a link (branch of the cotree) and the remaining C-E loop branches are chosen as twigs (branches of the normal tree). It should be noted that only the normal tree capacitor voltages are members of the set state variables. A dual situation for determining which inductor currents are chosen as state variables, is discussed next.

The selection of a normal tree requires that no independent current sources, J, and as few as possible inductors, L, be chosen as twigs. This is to say, the selection of the cotree requires that all the independent current sources and inductors within the original network be chosen with the highest priority as links. All current sources are chosen first. It is assumed that there are no all-current-source cutsets. Next, all of the inductors, except for those belonging to a L-J cutset, are selected as links. A L-J cutset is defined as a cutset consisting entirely of inductors and/or independent current sources. Only one of the inductors within every L-J cutset must be chosen as a twig (branch of the normal tree) and the remaining L-J cutset branches are chosen as links (branches of the cotree). It should be noted that only the cotree inductor currents are members of the set of state variables.

2.3 Hybrid-Matrix Approach for Automatic Generation of the State Model

Conventional modeling methods based upon frequency-domain techniques, when applied to the analysis of electronically commutated dc machine systems, often leave much to be desired. This is because of the nonlinear components associated within these systems, such as the rectifier

diodes and the magnetic core of the machine. The incorporation of such components into an overall system model requires a nonlinear time-domain approach that can easily accommodate these component nonlinearities. Also, in order to use the many available integration routines, the governing differential equations of the actuator network model must be explicitly obtained as the normal form state equations, [2], as follows:

$$p(\ \underline{x}\ ) = \underline{f}(\ \underline{x}, t\ ) \qquad\qquad (2.3\text{-}1)$$

where $\underline{x}$ is the state vector of the system and $\underline{f}$ explicitly defines the relationship between the first derivative of the state vector with respect to time, $p(\ \underline{x}\ )$, in terms of the state vector and the independent variable time, t. It is assumed that all the forcing functions are known functions of time and/or the state variables, and therefore, are incorporated in $\underline{f}$ of equation (2.3-1).

In this section, an algorithm which is used to automatically generate the normal form state equations from the network graph of the system under study, is presented. This algorithm is based upon a hybrid matrix approach, [2,5], which is well suited for the analysis of nonlinear electrical networks. There are basically six steps involved

in the formulation of the normal form state model. These
are:

Step 1   Translate the electromechanical system into a
         lumped-parameter network model using the component
         models given in Section 2.1.

Step 2   Choose a "normal tree" for this lumped-parameter
         network model.

Step 3   From the chosen tree and cotree, obtain a linear
         resistive n-port of this network. Express the
         behavior of this n-port using a hybrid matrix
         formulation.

Step 4   Determine the operating point of the nonlinear
         resistors.

Step 5   Solve for the currents of the cotree capacitors and
         the voltages of the tree inductors.

Step 6   Obtain the normal-form state equations using the
         results of steps three, four, and five.

These six steps will now be discussed in detail.

Translate System into Lumped Parameter Network (Step 1)

The first step in the derivation of the normal form state
equations for a system is to choose a suitable lumped

- 38 -

parameter network model. In the case of the brushless exciter, described in Section 1.2, this consists of:

1. Replacing the permanent magnet machine with a machine model, similar to one given in Figure (2.1-2);

2. Replacing the components of the power conditioner by the components models described in Section (2.1).

Choose a Normal Tree (Step 2)

Once a lumped-parameter network model of the system has been obtained, the choice of a normal tree must then be considered. A normal tree is a member of a subset of the set of all possible trees. The normal tree is chosen using a component selection hierarchy. The order or selection hierarchy for the twig and link branches must conform to the order given in Table (2.3-1). Furthermore, the numbering of the branches (twigs and links) must also follow this hierarcy. It is extremely important that this hierarchy procedure be followed; otherwise, the matrix partitioning employed later in this section would be meaningless.

If the network topology does not change then the branch hierarchy and normal tree selection needs to be implemented only once per simulation. However, the remaining steps relating to component value changes must be implemented each

time any change occurs.

Notice, the branch hierarchy (allowable branch types) given in Table (2.3-1) does not include dependent sources. In this report, mutual inductances and capacitances are included within the formulation of the state equations. By eliminating the dependent sources as allowable components within Table (2.3-1), there are no topological restrictions placed upon the these mutuals. This is most desirable for the types of power-conditioner fed machine systems considered in this research.

Table (2.3-1) Tree and Cotree Branch Numbering

ORDER	BRANCH TYPE	VARIABLE SUBSCRIPT
---------- (Tree Branches) ---------------- (t) ------		
1-st	Independent Voltage Sources	E_t
2-nd	Capacitors (linear or nonlinear)	C_t
3-rd	Resistors (nonlinear)	R_t
4-th	1 Inductor (linear or nonlinear) per (L-J) Cutset .	L_t
5-th	Resistors (linear)	R
---------- (Cotree Branches) -------------- (c) -------		
6-th	Resistors (linear)	G
7-th	Independent Current Sources	J_c
8-th	Inductors (linear or nonlinear)	L_c
9-th	Resistors (nonlinear)	G_c
10-th	1 Capacitor (linear or nonlinear) per (C-E) Loop .	C_c

Obtain a Linear Resistive n-port from the Chosen Normal Tree and Represent the n-port using Hybrid Matrix Formulation (Step 3)

Once a normal tree has been chosen, the next step is to segregate all the linear resistors from the other components of the overall network and place them into an n-port sub-network as shown in Figure (2.3-1). The motivation for forming this n-port is to isolate the linear, time-invariant components of the network and incorporate their influence upon the other components by using hybrid parameters. Using this approach, the states of the nonlinear components become boundary conditions for the n-port. Furthermore, the relationship between the port voltages and currents are defined by means of a linear time invariant hybrid matrix, $\underline{H}$. This relationship is given by the following matrix equation:

$$\begin{bmatrix} \underline{i}_t \\ \underline{v}_c \end{bmatrix} = \underline{H} \begin{bmatrix} \underline{v}_t \\ \underline{i}_c \end{bmatrix} \qquad (2.3-2)$$

where $\underline{H}$ is defined in terms of the linear resistors of the n-port and is partitioned as follows:

$$\underline{H} = \begin{bmatrix} \underline{H}_{tt} & \underline{H}_{tc} \\ \underline{H}_{ct} & \underline{H}_{cc} \end{bmatrix} \qquad (2.3-3)$$
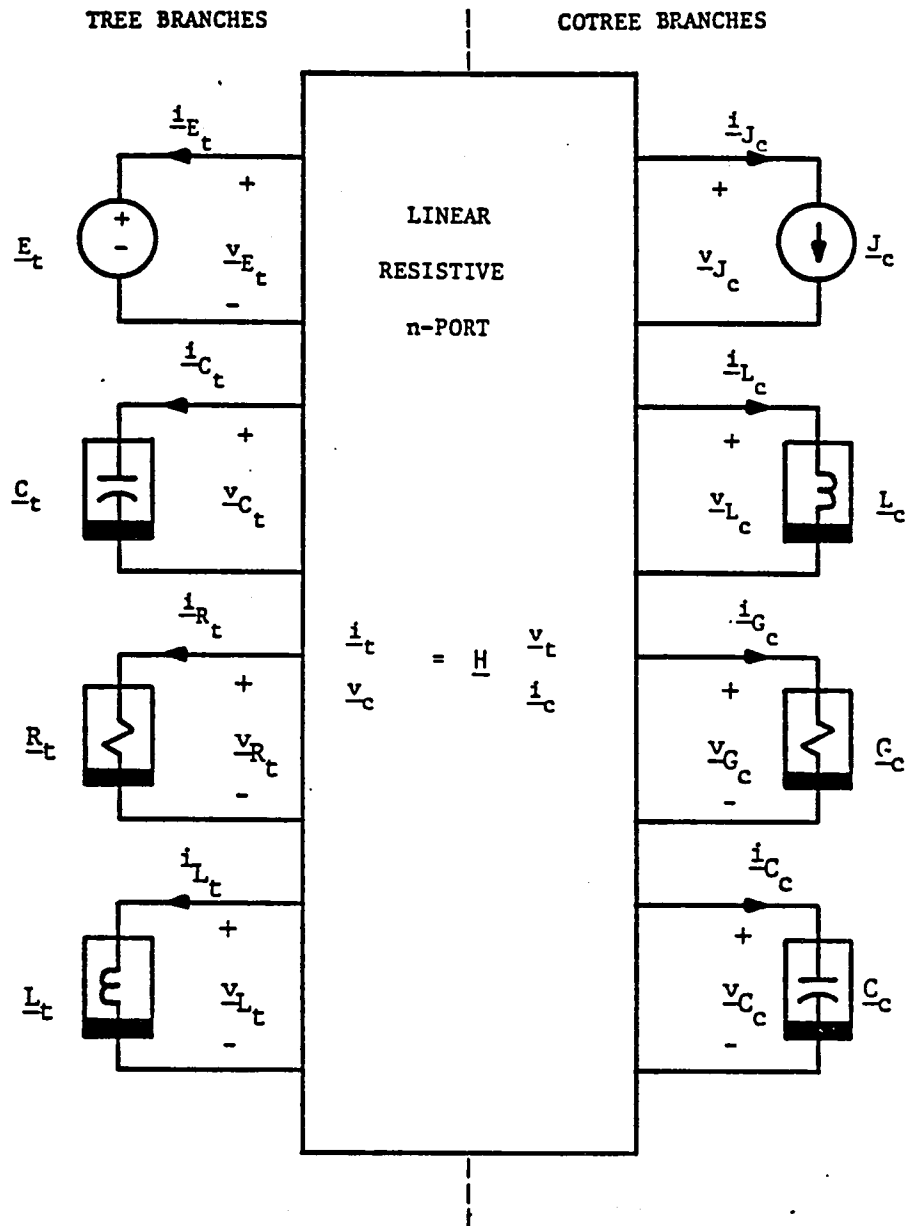
Figure(2.3-1) Isolation of the Linear Resistors into the
Resistive n-Port Network

The tree, t, and cotree, c, port voltage and current vectors of equation (2.3-2) are defined in terms of the port vectors shown in Figure (2.3-1) as follows:

$$
\underline{v}_t = \begin{bmatrix} \underline{v}_{E_t} \\ \underline{v}_{C_t} \\ \hline \underline{v}_{R_t} \\ \underline{v}_{L_t} \end{bmatrix}
\tag{2.3-4}
$$

$$
\underline{v}_c = \begin{bmatrix} \underline{v}_{J_c} \\ \underline{v}_{L_c} \\ \hline \underline{v}_{G_c} \\ \underline{v}_{C_c} \end{bmatrix}
\tag{2.3-5}
$$

$$
\underline{i}_t = \begin{bmatrix} \underline{i}_{E_t} \\ \underline{i}_{C_t} \\ \hline \underline{i}_{R_t} \\ \underline{i}_{L_t} \end{bmatrix}
\tag{2.3-6}
$$

$$\underline{i}_c = \begin{array}{|c|} \hline \underline{i}_{J_c} \\ \underline{i}_{L_c} \\ \hline \underline{i}_{G_c} \\ \underline{i}_{C_c} \\ \hline \end{array} \qquad (2.3\text{-}7)$$

The $\underline{H}$ matrix is obtained by applying KCL to the entire network in such a way that each twig current is written as a linear combination of the link currents as follows:

$$\underline{D}\,\underline{i} = \begin{array}{c} \text{<--twigs-->|<--links-->} \\ \left[\begin{array}{cc|cc} \underline{I}_{tt} & \underline{0}_{tR} & \underline{D}_{tG} & \underline{D}_{tc} \\ \hline \underline{0}_{Rt} & \underline{I}_{RR} & \underline{D}_{RG} & \underline{D}_{Rc} \end{array}\right] \end{array} \begin{array}{|c|} \hline \underline{i}_t \\ \underline{i}_R \\ \hline \underline{i}_G \\ \underline{i}_c \\ \hline \end{array} = \underline{0}$$

$$(2.3\text{-}8)$$

Notice that the current vectors $\underline{i}_R$ and $\underline{i}_G$ are internal to the linear resistive n-port and belong to the tree and cotree, respectively. Equation (2.3-8) can be written in a more compact form as follows:

$$\underline{D}\,\underline{i} = \begin{array}{c} \text{<--twigs-->|<--links-->} \\ \left[\begin{array}{c|c} \underline{I}_{tree} & \underline{D}_{cotree} \end{array}\right] \end{array} \begin{array}{|c|} \hline \underline{i}_{tree} \\ \hline \underline{i}_{cotree} \\ \hline \end{array} = \underline{0}$$

$$(2.3\text{-}9)$$

Similarly using KVL, one can write the fundamental loop equations as follows:

$$
\underline{B}\,\underline{v} =
\begin{array}{c}
\overset{\text{<--twigs-->}|\text{<--links-->}}{}\\
\left[
\begin{array}{cc|cc}
\underline{B}_{Gt} & \underline{B}_{GR} & \underline{I}_{GG} & \underline{0}_{Gc} \\
\underline{B}_{ct} & \underline{B}_{cR} & \underline{0}_{cG} & \underline{I}_{cc}
\end{array}
\right]
\end{array}
\begin{bmatrix}
\underline{v}_t \\
\underline{v}_R \\
\hline
\underline{v}_G \\
\underline{v}_c
\end{bmatrix}
= \underline{0}
$$

$$(2.3\text{-}10)$$

or in compact form as:

$$
\underline{B}\,\underline{v} =
\begin{array}{c}
\overset{\text{<--twigs-->}|\text{<--links-->}}{}\\
\left[
\begin{array}{c|c}
\underline{B}_{tree} & \underline{I}_{cotree}
\end{array}
\right]
\end{array}
\begin{bmatrix}
\underline{v}_{tree} \\
\hline
\underline{v}_{cotree}
\end{bmatrix}
= \underline{0}
$$

$$(2.3\text{-}11)$$

From network graph theory,[3], one can relate $\underline{D}_{cotree}$ and $\underline{B}_{tree}$ as follows:

$$
\underline{B}_{tree} = -\underline{D}^t_{cotree} \qquad (2.3\text{-}12)
$$

Substituting equation (2.3-12) into equation (2.3-10) yields:

$$
\underline{B}\ \underline{v} =
\begin{array}{c}
\text{<--twigs-->} \quad \text{<--links-->} \\
\left[
\begin{array}{cc|cc}
-\underline{D}_{tG}^{t} & -\underline{D}_{RG}^{t} & \underline{I}_{GG} & \underline{0}_{Gc} \\
-\underline{D}_{tc}^{t} & -\underline{D}_{Rc}^{t} & \underline{0}_{cG} & \underline{I}_{cc}
\end{array}
\right]
\left[
\begin{array}{c}
\underline{v}_t \\
\underline{v}_R \\
---- \\
\underline{v}_G \\
\underline{v}_c
\end{array}
\right]
= \underline{0}
\end{array}
$$

$$(2.3-13)$$

The relationship between the voltage and current vectors of the resistors in the linear resistive n-port network are related by Ohms law as follows:

$$\underline{v}_R = \underline{Z}_R\ \underline{i}_R \tag{2.3-14}$$

for the linear tree resistors and

$$\underline{v}_G = \underline{Z}_G\ \underline{i}_G \tag{2.3-15}$$

for the linear cotree resistors.

Inspection of the hybrid matrix equation of the n-port, equation (2.3-2), reveals that the internal variables $\{\underline{v}_G, \underline{i}_G, \underline{v}_R, \underline{i}_R\}$ have been eliminated by incorporating their influence, on the port variables, in $\underline{H}$. This is accomplished by using equations (2.3-8) and (2.3-13) to relate the port variables $\underline{v}_t$ and $\underline{i}_c$ as shown in equation (2.3-2).

Using the lower partition of equation (2.3-8) and the component equations given in equations (2.3-14) and (2.3-15), one can write the following:

$$\underline{Z}_R^{-1} \underline{v}_R + \underline{D}_{RG} \underline{Z}_G^{-1} \underline{v}_G + \underline{D}_{Rc} \underline{i}_c = \underline{0}$$

(2.3-16)

Solving for $\underline{v}_G$ using the upper partition of equation (2.3-13) yields:

$$\underline{v}_G = \underline{D}_{tG}^t \underline{v}_t + \underline{D}_{RG}^t \underline{v}_R$$

(2.3-17)

Substituting this equation into (2.3-16) gives:

$$\underline{Z}_R^{-1} \underline{v}_R + \underline{D}_{RG} \underline{Z}_G^{-1} [\underline{D}_{tG}^t \underline{v}_t + \underline{D}_{RG}^t \underline{v}_R] + \underline{D}_{Rc} \underline{i}_c = \underline{0}$$

(2.3-18)

Solving for $\underline{v}_R$ in terms of the port variables yields:

$$\underline{v}_R = [\underline{Z}_R^{-1} + \underline{D}_{RG} \underline{Z}_G^{-1} \underline{D}_{RG}^t]^{-1} [-\underline{D}_{RG} \underline{Z}_G^{-1} \underline{D}_{tG}^t \underline{v}_t - \underline{D}_{Rc} \underline{i}_c]$$

(2.3-19)

Now define a matrix $\underline{Y}$ as follows:

$$\underline{Y} = [\underline{Z}_R^{-1} + \underline{D}_{RG} \underline{Z}_G^{-1} \underline{D}_{RG}^t]$$

(2.3-20)

Using this definition of $\underline{Y}$, equation (2.3-19) can be simplified to the expression:

$$\underline{v}_R = \underline{Y}^{-1} \; [-\underline{D}_{RG} \; \underline{Z}_G^{-1} \; \underline{D}_{tG}^t \; \underline{v}_t - \underline{D}_{Rc} \; \underline{i}_c]$$

(2.3-21)

A similar procedure will now be followed to obtain $\underline{i}_G$ in terms of the port variables. Using the upper partition of equation (2.3-13) and the component equations given in equations (2.3-14) and (2.3-15), one can write the following:

$$-\underline{D}_{tG}^t \; \underline{v}_t - \underline{D}_{RG}^t \; \underline{Z}_R \; \underline{i}_R + \underline{Z}_G \; \underline{i}_G = \underline{0}$$

(2.3-22)

Solving for $\underline{i}_R$ using the lower partition of equation (2.3-8) yields:

$$\underline{i}_R = -\underline{D}_{RG} \; \underline{i}_G - \underline{D}_{Rc} \; \underline{i}_c$$

(2.3-23)

Substituting this equation into (2.3-22) gives:

$$-\underline{D}_{tG}^t \; \underline{v}_t + \underline{D}_{RG}^t \; \underline{Z}_R \; [\underline{D}_{RG} \; \underline{i}_G + \underline{D}_{Rc} \; \underline{i}_c] + \underline{Z}_G \; \underline{i}_G = \underline{0}$$

(2.3-24)

Solving for $\underline{i}_G$ in terms of the port variables yields:

$$\underline{i}_G = [\underline{Z}_G + \underline{D}_{RG}^t \; \underline{Z}_R \; \underline{D}_{RG}]^{-1} \; [\underline{D}_{tG}^t \; \underline{v}_t - \underline{D}_{RG}^t \; \underline{Z}_R \; \underline{D}_{Rc} \; \underline{i}_c]$$

(2.3-25)

Now define a matrix $\underline{Z}$ as follows:

$$\underline{Z} = [\underline{Z}_G + \underline{D}_{RG}^t \, \underline{Z}_R \, \underline{D}_{RG}]$$

(2.3-26)

Therefore, equation (2.3-25) can be simplified to

$$\underline{i}_G = \underline{Z}^{-1}[-\underline{D}_{tG}^t \, \underline{v}_t - \underline{D}_{RG}^t \, \underline{Z}_R \, \underline{D}_{Rc} \, \underline{i}_c \,]$$

(2.3-27)

The final step in obtaining $\underline{H}$ is accomplished by solving $\underline{i}_t$ and $\underline{v}_c$ in terms of $\underline{v}_t$ and $\underline{i}_c$. To obtain $\underline{i}_t$ in this form, substitute equation (2.3-27) into the top partition of equation (2.3-8). This yields the following matrix relationship:

$$\underline{i}_t = -\underline{D}_{tG} \, \underline{Z}^{-1} \, [\underline{D}_{tG}^t \, \underline{v}_t - \underline{D}_{RG}^t \, \underline{Z}_R \, \underline{D}_{Rc} \, \underline{i}_c] - \underline{D}_{tc} \, \underline{i}_c$$

$$\underline{i}_t = \quad [-\underline{D}_{tG} \, \underline{Z}^{-1} \, \underline{D}_{tG}^t] \, \underline{v}_t$$
$$+ \, [\underline{D}_{tG} \, \underline{Z}^{-1} \, \underline{D}_{RG}^t \, \underline{Z}_R \, \underline{D}_{Rc} - \underline{D}_{tc}] \, \underline{i}_c$$

(2.3-28)

Similarly, to obtain $\underline{v}_c$, substitute equation (2.3-25) into the bottom partition of equation (2.3-13). This yields the following matrix relationship:

$$\underline{v}_c = \underline{D}_{tc}^t \, \underline{v}_t + \underline{D}_{Rc}^t \, \underline{Y}^{-1} \, [-\underline{D}_{RG} \, \underline{Z}_G^{-1} \, \underline{D}_{tG}^t \, \underline{v}_t - \underline{D}_{Rc} \, \underline{i}_c]$$

$$\underline{v}_c = [\underline{D}_{tc}^t - \underline{D}_{Rc}^t \, \underline{Y}^{-1} \, \underline{D}_{RG} \, \underline{Z}_G^{-1} \, \underline{D}_{tG}^t] \, \underline{v}_t$$
$$+ \, [-\underline{D}_{Rc}^t \, \underline{Y}^{-1} \, \underline{D}_{Rc}] \, \underline{i}_c$$

$$(2.3\text{-}29)$$

Combining equations (2.3-28) and (2.3-29) into one matrix equation gives the following relationship:

$$
\begin{array}{|c|}
\hline
\underline{i}_t \\
\hline
\underline{v}_c \\
\hline
\end{array}
=
\begin{array}{|c|}
\hline
\text{tree response port vector} \\
\hline
\text{cotree response port vector} \\
\hline
\end{array}
=
$$

$$
\begin{array}{|c|c|}
\hline
[-\underline{D}_{tG} \, \underline{Z}^{-1} \, \underline{D}_{tG}^t] & [\underline{D}_{tG} \, \underline{Z}^{-1} \, \underline{D}_{RG}^t \, \underline{Z}_R \, \underline{D}_{Rc} - \underline{D}_{tc}] \\
\hline
[\underline{D}_{tc}^t - \underline{D}_{Rc}^t \, \underline{Y}^{-1} [-\underline{D}_{RG} \, \underline{Z}_G^{-1} \underline{D}_{tG}^t]] & [-\underline{D}_{Rc}^t \, \underline{Y}^{-1} \, \underline{D}_{Rc}] \\
\hline
\end{array}
$$

$$
*\;
\begin{array}{|c|}
\hline
\underline{v}_t \\
\hline
\underline{i}_c \\
\hline
\end{array}
$$

$\longleftarrow$ tree stimulus port vector

$\longleftarrow$ cotree stimulus port vector

$$(2.3\text{-}30)$$

Comparison of this equation with (2.3-2) and (2.3-3) reveals that this is the desired hybrid matrix equation originally defined in compact form in equation (2.3-2). It is now obvious that the influences of the internal linear n-port resistors manifest themselves as entries within the hybrid matrix, $\underline{H}$. The entries of the matrix, $\underline{H}$, are functions of the network topology and linear resistors only. Therefore, for a fixed topology, the matrix, $\underline{H}$, needs to be calculated only once per simulation run.

At this point, it is necessary to expand the $\underline{H}$ matrix, defined in equation (2.3-30), into a partitioned form which relates all of the voltage and current port vectors of the linear resistive n-port, as shown in Figure (2.3-1). This is given on the next page as equation (2.3-31).

A number of the sub-matricies of $\underline{H}$ given in equation (2.3-31) are null. Substitution of these null submatricies into equation (2.3-31), on the next page, yields equation (2.3-32).

$$\begin{bmatrix} \underline{i}_t \\ \underline{v}_c \end{bmatrix} \;=\; \underline{H} \begin{bmatrix} \underline{v}_t \\ \underline{i}_c \end{bmatrix} \qquad \text{which expands to}$$

$$\begin{bmatrix} \underline{i}_{E_t} & \underline{i}_{C_t} & \underline{i}_{R_t} & \underline{i}_{L_t} & \underline{v}_{J_c} & \underline{v}_{L_c} & \underline{v}_{G_c} & \underline{v}_{C_c} \end{bmatrix}^t \;=$$

$$\begin{bmatrix}
\underline{H}_{E_t E_t} & \underline{H}_{E_t C_t} & \underline{H}_{E_t R_t} & \underline{H}_{E_t L_t} & \underline{H}_{E_t J_c} & \underline{H}_{E_t L_c} & \underline{H}_{E_t G_c} & \underline{H}_{E_t C_c} \\
\underline{H}_{C_t E_t} & \underline{H}_{C_t C_t} & \underline{H}_{C_t R_t} & \underline{H}_{C_t L_t} & \underline{H}_{C_t J_c} & \underline{H}_{C_t L_c} & \underline{H}_{C_t G_c} & \underline{H}_{C_t C_c} \\
\underline{H}_{R_t E_t} & \underline{H}_{R_t C_t} & \underline{H}_{R_t R_t} & \underline{H}_{R_t L_t} & \underline{H}_{R_t J_c} & \underline{H}_{R_t L_c} & \underline{H}_{R_t G_c} & \underline{H}_{R_t C_c} \\
\underline{H}_{L_t E_t} & \underline{H}_{L_t C_t} & \underline{H}_{L_t R_t} & \underline{H}_{L_t L_t} & \underline{H}_{L_t J_c} & \underline{H}_{L_t L_c} & \underline{H}_{L_t G_c} & \underline{H}_{L_t C_c} \\
\underline{H}_{J_c E_t} & \underline{H}_{J_c C_t} & \underline{H}_{J_c R_t} & \underline{H}_{J_c L_t} & \underline{H}_{J_c J_c} & \underline{H}_{J_c L_c} & \underline{H}_{J_c G_c} & \underline{H}_{J_c C_c} \\
\underline{H}_{L_c E_t} & \underline{H}_{L_c C_t} & \underline{H}_{L_c R_t} & \underline{H}_{L_c L_t} & \underline{H}_{L_c J_c} & \underline{H}_{L_c L_c} & \underline{H}_{L_c G_c} & \underline{H}_{L_c C_c} \\
\underline{H}_{G_c E_t} & \underline{H}_{G_c C_t} & \underline{H}_{G_c R_t} & \underline{H}_{G_c L_t} & \underline{H}_{G_c J_c} & \underline{H}_{G_c L_c} & \underline{H}_{G_c G_c} & \underline{H}_{G_c C_c} \\
\underline{H}_{C_c E_t} & \underline{H}_{C_c C_t} & \underline{H}_{C_c R_t} & \underline{H}_{C_c L_t} & \underline{H}_{C_c J_c} & \underline{H}_{C_c L_c} & \underline{H}_{C_c G_c} & \underline{H}_{C_c C_c}
\end{bmatrix} \;*$$

$$\begin{bmatrix} \underline{v}_{E_t} & \underline{v}_{C_t} & \underline{v}_{R_t} & \underline{v}_{L_t} & \underline{i}_{J_c} & \underline{i}_{L_c} & \underline{i}_{G_c} & \underline{i}_{C_c} \end{bmatrix}^t$$

$$(2.3\text{-}31)$$

$$\begin{vmatrix} \underline{i}_t \\ \hline \underline{v}_c \end{vmatrix} = \underline{H} \begin{vmatrix} \underline{v}_t \\ \hline \underline{i}_c \end{vmatrix}$$ which expands to

$$\left| \underline{i}_{E_t} \mid \underline{i}_{C_t} \mid \underline{i}_{R_t} \mid \underline{i}_{L_t} \mid \underline{v}_{J_c} \mid \underline{v}_{L_c} \mid \underline{v}_{G_c} \mid \underline{v}_{C_c} \right|^t =$$

$\underline{H}_{E_t E_t}$	$\underline{H}_{E_t C_t}$	$\underline{H}_{E_t R_t}$	$\underline{O}_{E_t L_t}$	$\underline{H}_{E_t J_c}$	$\underline{H}_{E_t L_c}$	$\underline{H}_{E_t G_c}$	$\underline{H}_{E_t C_c}$
$\underline{H}_{C_t E_t}$	$\underline{H}_{C_t C_t}$	$\underline{H}_{C_t R_t}$	$\underline{O}_{C_t L_t}$	$\underline{H}_{C_t J_c}$	$\underline{H}_{C_t L_c}$	$\underline{H}_{C_t G_c}$	$\underline{H}_{C_t C_c}$
$\underline{H}_{R_t E_t}$	$\underline{H}_{R_t C_t}$	$\underline{H}_{R_t R_t}$	$\underline{O}_{R_t L_t}$	$\underline{H}_{R_t J_c}$	$\underline{H}_{R_t L_c}$	$\underline{H}_{R_t G_c}$	$\underline{O}_{R_t C_c}$
$\underline{O}_{L_t E_t}$	$\underline{O}_{L_t C_t}$	$\underline{O}_{L_t R_t}$	$\underline{O}_{L_t L_t}$	$\underline{H}_{L_t J_c}$	$\underline{H}_{L_t L_c}$	$\underline{O}_{L_t G_c}$	$\underline{O}_{L_t C_c}$
$\underline{H}_{J_c E_t}$	$\underline{H}_{J_c C_t}$	$\underline{H}_{J_c R_t}$	$\underline{H}_{J_c L_t}$	$\underline{H}_{J_c J_c}$	$\underline{H}_{J_c L_c}$	$\underline{H}_{J_c G_c}$	$\underline{O}_{J_c C_c}$
$\underline{H}_{L_c E_t}$	$\underline{H}_{L_c C_t}$	$\underline{H}_{L_c R_t}$	$\underline{H}_{L_c L_t}$	$\underline{H}_{L_c J_c}$	$\underline{H}_{L_c L_c}$	$\underline{H}_{L_c G_c}$	$\underline{O}_{L_c C_c}$
$\underline{H}_{G_c E_t}$	$\underline{H}_{G_c C_t}$	$\underline{H}_{G_c R_t}$	$\underline{O}_{G_c L_t}$	$\underline{H}_{G_c J_c}$	$\underline{H}_{G_c L_c}$	$\underline{H}_{G_c G_c}$	$\underline{O}_{G_c C_c}$
$\underline{H}_{C_c E_t}$	$\underline{H}_{C_c C_t}$	$\underline{O}_{C_c R_t}$	$\underline{O}_{C_c L_t}$	$\underline{O}_{C_c J_c}$	$\underline{O}_{C_c L_c}$	$\underline{O}_{C_c G_c}$	$\underline{O}_{C_c C_c}$

$*$

$$\left| \underline{v}_{E_t} \mid \underline{v}_{C_t} \mid \underline{v}_{R_t} \mid \underline{v}_{L_t} \mid \underline{i}_{J_c} \mid \underline{i}_{L_c} \mid \underline{i}_{G_c} \mid \underline{i}_{C_c} \right|^t$$

(2.3-32)

Additional properties of the $\underline{H}$ matrix are given below:

$$\underline{H}_{tt} = \underline{H}_{tt}^t \tag{2.3-33}$$

$$\underline{H}_{cc} = \underline{H}_{cc}^t \tag{2.3-34}$$

$$\underline{H}_{tc} = -\underline{H}_{ct}^t \tag{2.3-35}$$

Determine Operating Point of Nonlinear Resistors (Step 4)

The hybrid matrix equation (2.3-31) relates the constraints on the port voltages $(\underline{v}_c, \underline{v}_t)$ and currents $(\underline{i}_c, \underline{i}_t)$ imposed by the linear resistive portion of the overall network, as illustrated in Figure (2.3-1). The topological constraints imposed by choosing a normal tree, as defined in section 2.2, gives the hybrid matrix as partitioned in equation (2.3-32). This equation does not include the effects of the nonlinear components, or of the energy storage elements and independent sources. The effect of these variables is included by imposing the I-V characteristics (constraints) of these elements as boundary conditions to the n (two terminal) ports of the linear time-invariant resistive n-port sub-network.

At any given instant of time, it is assumed that the state of the network is fixed; that is, the stored energy of each energy storage element remains constant. In this work, the state varables are the tree capacitor voltages, $\underline{v}_{C_t}$, and the cotree inductor currents, $\underline{i}_{C_c}$. The state (energy) of the network is fixed at any given instant of time by holding these state variables constant (along with the independent sources). In the case of the nonlinear capacitors and inductors, it is assumed that their incremental component values are functions of the state variables. The derivatives of the state variables as well as branch variables of the nonlinear resistors are not considered "frozen" for any given instant of time, in the sense that these variables must be determined iteratively for that instant. The term "frozen" is used to represent variables that are "known" for a given instant of time. Specifically, "frozen" variables are the voltages and/or currents which:

1. are simply a known function of time (forcing functions or independent sources),

2. are known as a result of integration (state variables), or

3. are linear combinations of the state variables and
    forcing functions.

The I-V characteristics of the nonlinear resistors are
assumed to be independent of the state variables and forcing
functions. Thus, the values or operating points of these
nonlinear resistors must simultaneously satisfy their own
I-V characteristics as well as the constraints imposed by
the rest of the network. The procedure for obtaining the
operating points of the nonlinear resistors will now be
described.

As previously mentioned, the nonlinear components as well
as the independent sources are all connected externally to
the n (two terminal) ports of the linear resistive n-port,
as shown in Figure (2.3-1). The influence of the rest of the
network upon the port varables, $\underline{i}_{R_t}$ and $\underline{v}_{G_c}$, of the
nonlinear resistors can be isolated out of equation (2.3-32)
as follows:

$$
\begin{bmatrix} \underline{i}_{R_t} \\ \hline \underline{v}_{G_c} \end{bmatrix} =
\left[
\begin{array}{c|c|c|c|c|c|c|c}
\underline{H}_{R_t E_t} & \underline{H}_{R_t C_t} & \underline{H}_{R_t R_t} & \underline{0}_{R_t L_t} & \underline{H}_{R_t J_c} & \underline{H}_{R_t L_c} & \underline{H}_{R_t G_c} & \underline{0}_{R_t C_c} \\
\hline
\underline{H}_{G_c E_t} & \underline{H}_{G_c C_t} & \underline{H}_{G_c R_t} & \underline{0}_{G_c L_t} & \underline{H}_{G_c J_c} & \underline{H}_{G_c L_c} & \underline{H}_{G_c G_c} & \underline{0}_{G_c C_c}
\end{array}
\right] *
$$

$$
\left[
\begin{array}{c|c|c|c|c|c|c|c}
\underline{v}_{E_t} & \underline{v}_{C_t} & \underline{v}_{R_t} & \underline{v}_{L_t} & \underline{i}_{J_c} & \underline{i}_{L_c} & \underline{i}_{G_c} & \underline{i}_{C_c}
\end{array}
\right]^t
$$

<div align="right">(2.3-36)</div>

The presence of the four null submatricies within this equation indicates that $\underline{i}_{R_t}$ and $\underline{v}_{G_c}$ are independent of $\underline{v}_{L_t}$ and $\underline{i}_{C_c}$. Therefore, equation (2.3-26) can be reduced as follows:

$$
\begin{bmatrix} \underline{i}_{R_t} \\ \hline \underline{v}_{G_c} \end{bmatrix} =
\left[
\begin{array}{c|c|c|c|c|c}
\underline{H}_{R_t E_t} & \underline{H}_{R_t C_t} & \underline{H}_{R_t R_t} & \underline{H}_{R_t J_c} & \underline{H}_{R_t L_c} & \underline{H}_{R_t G_c} \\
\hline
\underline{H}_{G_c E_t} & \underline{H}_{G_c C_t} & \underline{H}_{G_c R_t} & \underline{H}_{G_c J_c} & \underline{H}_{G_c L_c} & \underline{H}_{G_c G_c}
\end{array}
\right] *
$$

$$
\left[
\begin{array}{c|c|c|c|c|c}
\underline{v}_{E_t} & \underline{v}_{C_t} & \underline{v}_{R_t} & \underline{i}_{J_c} & \underline{i}_{L_c} & \underline{i}_{G_c}
\end{array}
\right]^t
$$

<div align="right">(2.3-37)</div>

At any given instant of time, the state variables, $\underline{v}_{C_t}$ and $\underline{i}_{L_c}$, as well as the forcing functions, $\underline{v}_{E_t}$ and $\underline{i}_{J_c}$, are fixed (frozen). Hence, the operating points of the nonlinear resistive port variables can be determined by means of an iterative procedure such that both the I-V characteristics of these resistors and equation (2.3-37) are satisfied.

The state variables and forcing functions can be considered as fixed boundary conditions to the linear resistive n-port. This is accomplished by representing these frozen variables as independent sources for that fixed instant of time. Therefore, the behavior of the network shown in Figure (2.3-1), can be represented for that instant of time, as shown in Figure (2.3-2). In this figure, the frozen independent port variables are contained within the outer box while those which can vary are placed outside. The independent port variables, $\underline{v}_{L_t}$ and $\underline{i}_{C_c}$, outside this box are free to vary. The nonlinear resistors are also placed outside this box since their values must be determined iteratively, for that given instant in time.

The operating points of the nonlinear resistors are independent of $\underline{v}_{L_t}$ and $\underline{i}_{L_c}$ as can be seen in equations (2.3-36) and (2.3-37). This is due to the fact that the state (stored energy) of the tree inductors and the cotree
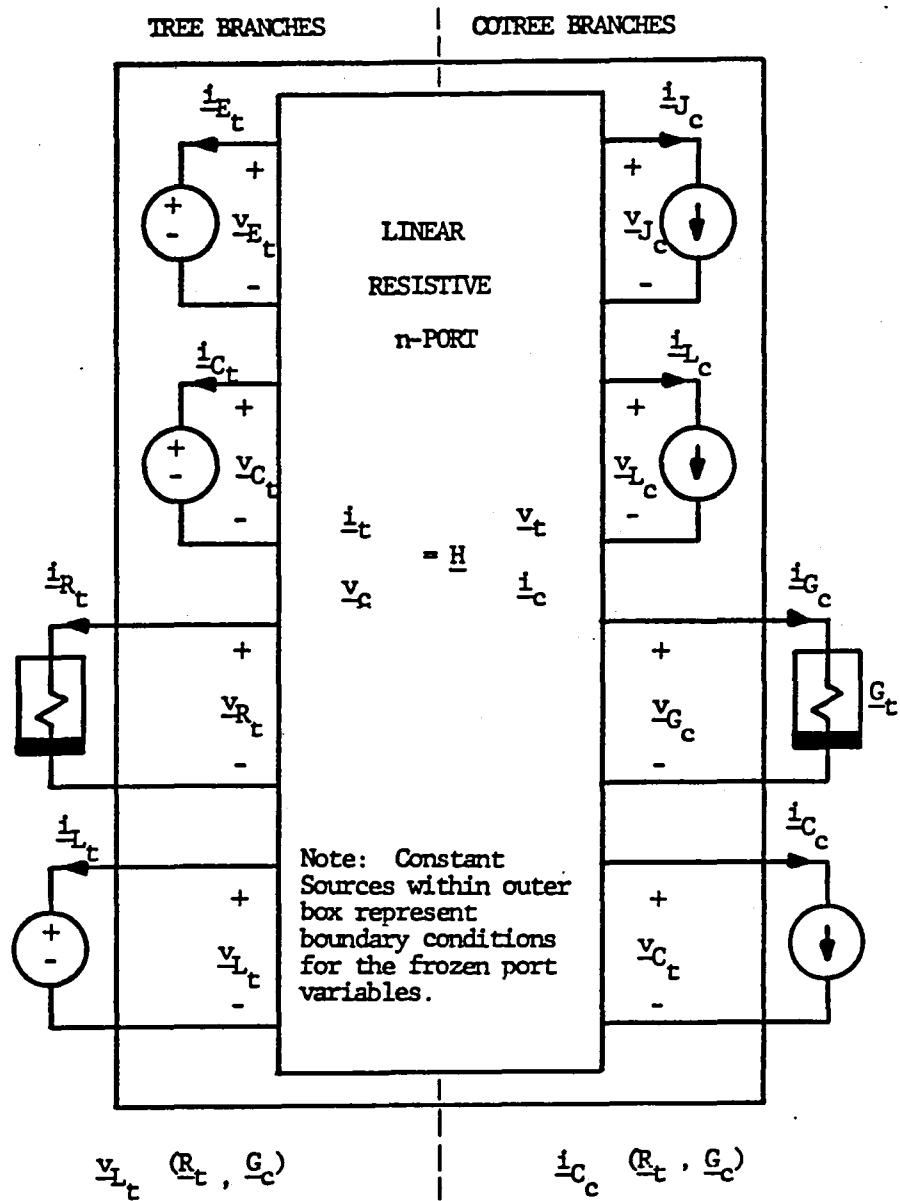
Figure(2.3-2) Port Variables held Constant (Frozen) while Determining the Operating Points of the Nonlinear Resistors, $\underline{R}_t$ and $\underline{G}_c$

capacitors are linear functions of the fixed (frozen) state variables and independent sources, as given by rows four and eight of the matrix equation (2.3-32), respectively. These equations in reduced form are:

$$\underline{i}_{L_t} = \underline{H}_{L_t J_c} \; \underline{i}_{J_c} + \underline{H}_{L_t L_c} \; \underline{i}_{L_c}$$

(2.3-38)

$$\underline{v}_{C_c} = \underline{H}_{C_c E_t} \; \underline{v}_{E_t} + \underline{H}_{C_c C_t} \; \underline{v}_{C_t}$$

(2.3-39)

Therefore, the response of the tree inductors and cotree capacitors is known and fixed for the instant in time under consideration as depicted in Figure (2.3-3)

Based upon this discussion, equation (2.3-37) can be conceptualized as the sum of a constant source vector, due to the fixed state variables and forcing functions (represented as "frozen" inputs in Figure (2.3-3)), and a vector which is a nonlinear function representing the I-V characteristics of the nonlinear resistors. This can be represented in matrix form as follows:

$$
\begin{bmatrix} \underline{i}_{R_t} \\ \hline \underline{v}_{G_c} \end{bmatrix}
=
\begin{bmatrix} \underline{f}_{R_t} \\ \hline \underline{f}_{G_c} \end{bmatrix}
+
\begin{bmatrix} \underline{s}_{R_t} \\ \hline \underline{s}_{G_c} \end{bmatrix}
$$

(2.3-40)
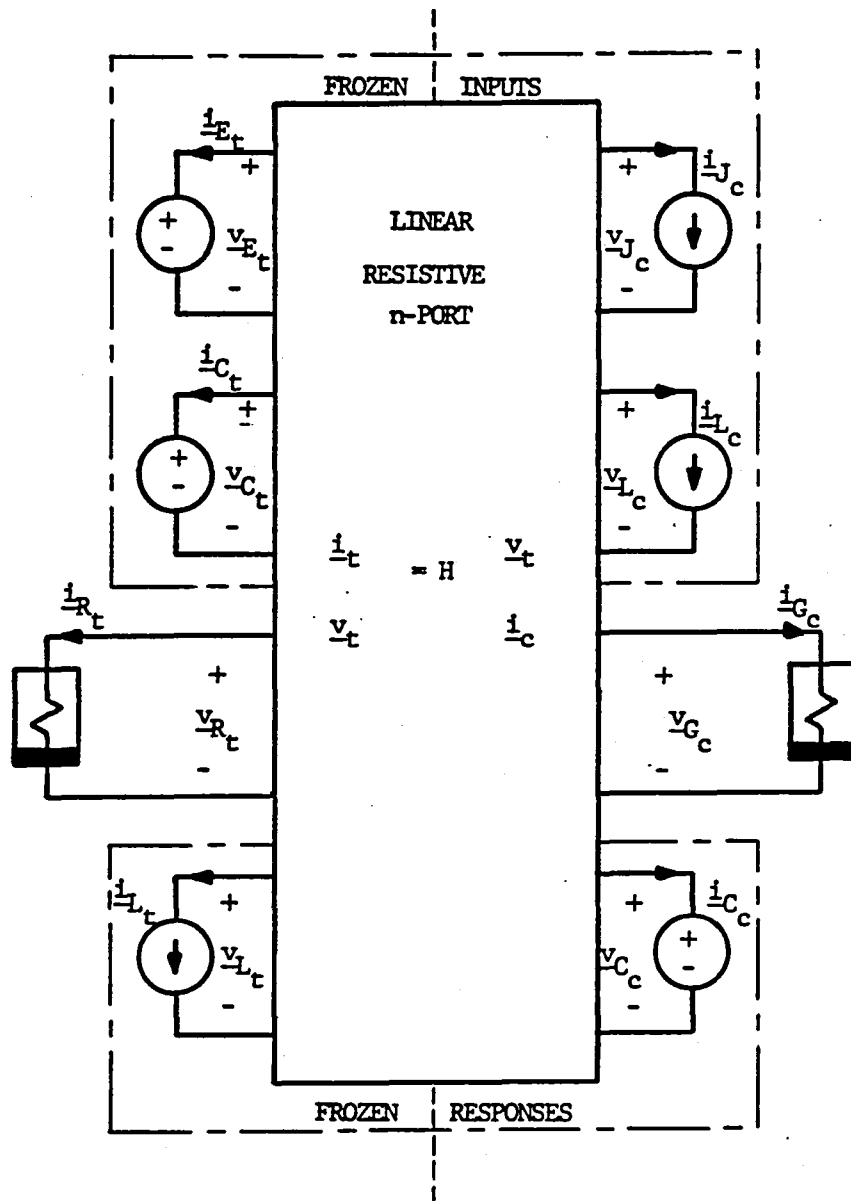
Figure (2.3-3) Frozen or Fixed Port Variables
While Determining the Operating Points
of the Nonlinear Resistors, R_t and G_c.

where the source vector is defined as

$$
\begin{vmatrix} \underline{s}_{R_t} \\ \underline{s}_{G_c} \end{vmatrix} = \begin{vmatrix} \underline{H}_{R_t C_t} & \underline{H}_{R_t L_c} & \underline{H}_{R_t E_t} & \underline{H}_{R_t J_c} \\ \underline{H}_{G_c C_t} & \underline{H}_{G_c L_c} & \underline{H}_{G_c E_t} & \underline{H}_{G_c J_c} \end{vmatrix} *
$$

$$
\begin{vmatrix} \underline{v}_{C_t} & \underline{i}_{L_c} & \underline{v}_{E_t} & \underline{i}_{J_c} \end{vmatrix}^t \qquad (2.3\text{-}41)
$$

and the vector representing the nonlinear behavior of these resistors, obtained from equation (2.3-31) and their nonlinear I-V characteristics, is defined as follows:

$$
\begin{vmatrix} \underline{f}_{R_t} \\ \underline{f}_{G_c} \end{vmatrix} = \begin{vmatrix} \underline{H}_{R_t R_t} & \underline{H}_{R_t G_c} \\ \underline{H}_{G_c R_t} & \underline{H}_{G_c G_c} \end{vmatrix} * \begin{vmatrix} \underline{v}_{R_t} \\ \underline{i}_{G_c} \end{vmatrix} \qquad (2.3\text{-}42)
$$

In this work, it is assumed that the I-V characteristics of the nonlinear resistors can be explicitly written as follows:

$$
\begin{vmatrix} \underline{v}_{R_t} \end{vmatrix} = \begin{vmatrix} r_1(\, i_{Rt}(1)) \\ r_2(\, i_{Rt}(2)) \\ \vdots \\ r_{n_{Rt}}(\, i_{Rt}(n_{Rt})) \end{vmatrix} = \begin{vmatrix} \underline{r}(\underline{i}_{R_t}) \end{vmatrix} \qquad (2.3\text{-}43)
$$

$$
\begin{vmatrix} \underline{i}_{G_c} \end{vmatrix}
=
\begin{vmatrix}
g_1(\ v_{Gc}\ (1)) \\
\hline
g_2(\ v_{Gc}\ (2)) \\
\vdots \\
\vdots \\
\hline
g_{n_{Gc}}(\ v_{Gc}\ (n_{Gc}))
\end{vmatrix}
=
\begin{vmatrix} \underline{g}(\underline{v}_{G_c}) \end{vmatrix}
\qquad (2.3\text{-}44)
$$

where $i_{Rt}(k)$ is current through the kth nonlinear resistor with a corresponding branch voltage of $v_{Rt}(k)$.

Therefore, in more compact form, the nonlinear equations employed in the iterative process to obtain the operating points of the nonlinear resistors, $(\underline{v}_{R_t}, \underline{i}_{R_t})$ and $(\underline{v}_{G_c}, \underline{i}_{G_c})$, is given as follows:

$$
\begin{vmatrix} \underline{i}_{R_t} \\ \hline \underline{v}_{G_c} \end{vmatrix}
-
\begin{vmatrix} \underline{H}_{R_tR_t} & \underline{H}_{R_tG_c} \\ \hline \underline{H}_{G_cR_t} & \underline{H}_{G_cG_c} \end{vmatrix}
*
\begin{vmatrix} \underline{r}(\underline{i}_{R_t}) \\ \hline \underline{g}(\underline{v}_{G_c}) \end{vmatrix}
-
\begin{vmatrix} \underline{s}_{R_t} \\ \hline \underline{s}_{G_c} \end{vmatrix}
= \underline{0}
$$

$$(2.3\text{-}45)$$

Note that equations (2.3-43) and (2.3-44) represent either the voltage or current of each nonlinear resistor explicitly in terms of the other variable. In order to obtain a matrix equation, similar to (2.3-45) strictly in

terms of one variable (i or v) for each nonlinear resistor, all of the nonlinear resistors must have I-V characteristics that are single valued. The incorporation of diodes within the overall system model does not present any problem since their I-V characteristics are monotonic and therefore possess an inverse. In other words, either variable (i or v) can be written explicitly in terms of the other for the diode model presented in this work.

It is assumed that at each fixed instant of time or (equivalently for frozen port sources as shown in Figure (2.3-3)), that a unique operating point for all of the nonlinear resistors can be determined, [2, 11]. Such a unique operating point, the solution to equation (2.3-45), is symbolized as follows:

$$
\begin{bmatrix} \underline{v}'_{R_t} \\ \underline{i}'_{G_c} \end{bmatrix} = \begin{bmatrix} \underline{r}\,(\underline{i}'_{R_t}) \\ \underline{g}\,(\underline{v}'_{R_t}) \end{bmatrix} = \underline{h}'_{RG} \qquad (2.3\text{-}47)
$$

The primes above these variables indicate that they are the unique solution of the nonlinear equation (2.3-45). Notice that this solution is uniquely determined by the state variables and forcing functions at each instant of time.

Solve for the Currents of the Cotree Capacitors and the Voltages of the Tree Inductors (Step 5)

Once the operating points of the nonlinear resistors, $(\underline{i}_{R_t}, \underline{v}_{R_t})$ and $(\underline{i}_{G_c}, \underline{v}_{G_c})$, within the original network have been determined as $\underline{h}'_{RG}$; the unknown tree inductor voltages, $\underline{v}_{L_t}$, and the unknown cotree capacitor currents, $\underline{i}_{C_c}$, can be determined, independent of the nonlinear resistors, for the given instant in time as illustrated in Figure (2.3-2).

It is assumed, in this work, that component equations for all inductors and capacitors (including mutuals) can be expressed (on an instant by instant basis) in matrix form as follows:

$$
\begin{vmatrix} \underline{v}_{L_t} \\ \hline \underline{v}_{L_c} \end{vmatrix} = \begin{vmatrix} \underline{L}_{tt} & \underline{L}_{tc} \\ \hline \underline{L}_{ct} & \underline{L}_{cc} \end{vmatrix} * d/dt \begin{vmatrix} \underline{i}_{L_t} \\ \hline \underline{i}_{L_c} \end{vmatrix} \qquad (2.3\text{-}48)
$$

$$
\begin{vmatrix} \underline{i}_{C_t} \\ \hline \underline{i}_{C_c} \end{vmatrix} = \begin{vmatrix} \underline{C}_{tt} & \underline{C}_{tc} \\ \hline \underline{C}_{ct} & \underline{C}_{cc} \end{vmatrix} * d/dt \begin{vmatrix} \underline{v}_{C_t} \\ \hline \underline{v}_{C_c} \end{vmatrix} \qquad (2.3\text{-}49)
$$

The entries of these coefficients matrices contain incremental values of inductances and capacitances, respectively. The arbitrary (m,n) entries for these two coefficient matrices are defined as follows:

$$L_{mn} = \frac{\partial(\,\lambda_m(i_{L_t}, i_{L_c})\,)}{\partial(\,i_n\,)} = \frac{\partial(\,\lambda_m(i_{L_c})\,)}{\partial(\,i_n\,)} \qquad (2.3\text{-}50)$$

$$C_{mn} = \frac{\partial(\,q_m(v_{C_t}, v_{C_c})\,)}{\partial(\,v_n\,)} = \frac{\partial(\,q_m(v_{C_t})\,)}{\partial(\,v_n\,)} \qquad (2.3\text{-}51)$$

where $\lambda_m(\underline{i}_{L_t}, \underline{i}_{L_c})$ is the total flux linkage of the m-th inductor and $q_m(\underline{v}_{C_t}, \underline{v}_{C_c})$ is the total charge of the m-th capacitor. The current, i_n, represents the n-th current within the set of currents , $\{\underline{i}_{L_t}, \underline{i}_{L_c}\}$. Similarly the voltage v_n represents the n-th voltage within the set of capacitor voltages , $\{\underline{v}_{C_t}, \underline{v}_{C_c}\}$. Finally, the partial derivative, $\partial(\,\lambda_m\,)/\partial(\,i_n\,)$, in equation (2.3-50), represents the instantaneous change of the total flux linkage, λ_m, with respect to that n-th winding current, i_n. Similarily, the partial derivative in equation (2.3-51) represents the instantaneous rate of change of the charge on the m-th capacitor with respect to the voltage across the n-th capacitor.

In the types of electromechanical systems considered here, it was assumed that mutual capacitances could be

neglected. In that case, the capacitance matrix, in equation (2.3-49), is diagonal.

Using these component equations and the contraints imposed on them by the linear resistive n port; the unknown link capacitor currents and twig inductor voltages can now be determined. The constraints on these port variables are obtained from the fourth and eighth rows of equation (2.3-32) as follows:

$$
\begin{bmatrix} \underline{v}_{C_c} \\ \underline{i}_{L_t} \end{bmatrix} =
\begin{bmatrix} \underline{H}_{C_c C_t} & \underline{0}_{C_c L_c} & \underline{H}_{C_c E_t} & \underline{0}_{C_c J_c} \\ \underline{0}_{L_t C_t} & \underline{H}_{L_t L_c} & \underline{0}_{L_t E_t} & \underline{H}_{L_t J_c} \end{bmatrix} *
$$

$$
\begin{bmatrix} \underline{v}_{C_t} & \underline{i}_{L_c} & \underline{v}_{E_t} & \underline{i}_{J_c} \end{bmatrix}^t
$$

$$(2.3\text{-}52)$$

Differentiating both sides of this equation yields the following:

$$
\frac{d}{dt}\begin{bmatrix} \underline{v}_{C_c} \\ \underline{i}_{L_t} \end{bmatrix} =
\begin{bmatrix} \underline{H}_{C_c C_t} & \underline{0}_{C_c L_c} & \underline{H}_{C_c E_t} & \underline{0}_{C_c J_c} \\ \underline{0}_{L_t C_t} & \underline{H}_{L_t L_c} & \underline{0}_{L_t E_t} & \underline{H}_{L_t J_c} \end{bmatrix} *
$$

$$
\frac{d}{dt}\begin{bmatrix} \underline{v}_{C_t} & \underline{i}_{L_c} & \underline{v}_{E_t} & \underline{i}_{J_c} \end{bmatrix}^t
$$

$$(2.3\text{-}53)$$

Using equations (2.3-48) and (2.3-49) one can write

$$
\begin{vmatrix} \underline{i}_{C_c} \\ \hline \underline{v}_{L_t} \end{vmatrix} =
\begin{vmatrix} \underline{C}_{ct} & \underline{0}_{cc} \\ \hline \underline{0}_{tt} & \underline{L}_{tc} \end{vmatrix} * d/dt
\begin{vmatrix} \underline{v}_{C_t} \\ \hline \underline{i}_{L_c} \end{vmatrix} +
\begin{vmatrix} \underline{C}_{cc} & \underline{0}_{ct} \\ \hline \underline{0}_{tc} & \underline{L}_{tt} \end{vmatrix} * d/dt
\begin{vmatrix} \underline{v}_{C_c} \\ \hline \underline{i}_{L_t} \end{vmatrix}
$$

$$(2.3\text{-}54)$$

Substitution of equation (2.3-53) into equation (2.3-54) yields:

$$
\begin{vmatrix} \underline{i}_{C_c} \\ \hline \underline{v}_{L_t} \end{vmatrix} =
\begin{vmatrix} \underline{C}_{ct} & \underline{0}_{cc} \\ \hline \underline{0}_{tt} & \underline{L}_{tc} \end{vmatrix} * d/dt
\begin{vmatrix} \underline{v}_{C_t} \\ \hline \underline{i}_{L_c} \end{vmatrix} +
\begin{vmatrix} \underline{C}_{cc} & \underline{0}_{ct} \\ \hline \underline{0}_{tc} & \underline{L}_{tt} \end{vmatrix} *
$$

$$
\left[
\begin{vmatrix} \underline{H}_{C_c C_t} & \underline{0}_{C_c L_c} \\ \hline \underline{0}_{L_t C_t} & \underline{H}_{L_t L_c} \end{vmatrix} * d/dt
\begin{vmatrix} \underline{v}_{C_t} \\ \hline \underline{i}_{L_c} \end{vmatrix} +
\begin{vmatrix} \underline{H}_{C_c E_t} & \underline{0}_{C_c J_c} \\ \hline \underline{0}_{L_t E_t} & \underline{H}_{L_t J_c} \end{vmatrix} * d/dt
\begin{vmatrix} \underline{v}_{E_t} \\ \hline \underline{i}_{J_c} \end{vmatrix}
\right]
$$

$$(2.3\text{-}55)$$

Collecting terms yields:

$$
\begin{bmatrix} \underline{i}_{C_c} \\ \underline{v}_{L_t} \end{bmatrix} =
$$

$$
\left[\begin{array}{cc|cc} \underline{C}_{ct} & \underline{0}_{cc} \\ \hline \underline{0}_{tt} & \underline{L}_{tc} \end{array} + \begin{array}{cc} \underline{C}_{cc} & \underline{0}_{ct} \\ \hline \underline{0}_{tc} & \underline{L}_{tt} \end{array} * \begin{array}{cc} \underline{H}_{C_cC_t} & \underline{0}_{C_cL_c} \\ \hline \underline{0}_{L_tC_t} & \underline{H}_{L_tL_c} \end{array} \right] * \frac{d}{dt} \begin{bmatrix} \underline{v}_{C_t} \\ \underline{i}_{L_c} \end{bmatrix}
$$

$$
+ \begin{bmatrix} \underline{C}_{cc} & \underline{0}_{ct} \\ \hline \underline{0}_{tc} & \underline{L}_{tt} \end{bmatrix} * \begin{bmatrix} \underline{H}_{C_cE_t} & \underline{H}_{C_cJ_c} \\ \hline \underline{H}_{L_tE_t} & \underline{H}_{L_tJ_c} \end{bmatrix} * \frac{d}{dt} \begin{bmatrix} \underline{v}_{E_t} \\ \underline{i}_{J_c} \end{bmatrix}
$$

$$(2.3\text{-}56)$$

Thus we have expressed $\underline{i}_{C_c}$ and $\underline{v}_{L_t}$ in terms of the derivatives of both the state variables and forcing functions. This completes step 5.

Derivation of the Normal Form State Equations (Step 6)

The final step in obtaining the normal form state equations uses the results from steps three, four, and five. The response port variables, $\underline{i}_{C_t}$ and $\underline{v}_{L_c}$, of the state variables $\underline{v}_{C_t}$ and $\underline{i}_{L_c}$, respectively are defined by rows two and six of equation (2.3-32).

These two equations can be expressed as follows:

$$
\begin{bmatrix} \underline{i}_{C_t} \\ \hline \underline{v}_{L_c} \end{bmatrix} =
$$

$$
\begin{bmatrix} \underline{H}_{C_tC_t} & \underline{H}_{C_tL_c} \\ \hline \underline{H}_{L_cC_t} & \underline{H}_{L_cL_c} \end{bmatrix} * \begin{bmatrix} \underline{i}_{C_t} \\ \hline \underline{v}_{L_c} \end{bmatrix} + \begin{bmatrix} \underline{H}_{C_tE_t} & \underline{H}_{C_tJ_c} \\ \hline \underline{H}_{L_cE_t} & \underline{H}_{L_cJ_c} \end{bmatrix} * \begin{bmatrix} \underline{v}_{E_t} \\ \hline \underline{i}_{J_c} \end{bmatrix}
$$

$$
+ \begin{bmatrix} \underline{H}_{C_tR_t} & \underline{H}_{C_tG_c} \\ \hline \underline{H}_{L_cR_t} & \underline{H}_{L_cG_c} \end{bmatrix} * \begin{bmatrix} \underline{v}'_{R_t} \\ \hline \underline{i}'_{G_c} \end{bmatrix} + \begin{bmatrix} \underline{H}_{C_tC_c} & \underline{0}_{C_tL_t} \\ \hline \underline{0}_{L_cC_c} & \underline{H}_{L_cL_t} \end{bmatrix} * \begin{bmatrix} \underline{i}_{C_c} \\ \hline \underline{v}_{L_t} \end{bmatrix}
$$

$$
(2.3-57)
$$

The primes above the nonlinear resistor port variables, $\underline{v}'_{R_t}$ and $\underline{i}'_{G_c}$, indicate the that these satisfy equation (2.3-45).

Next, the substitution of equation (2.3-56) into (2.3-57) yields the matrix equation on the next page.

$$
\begin{vmatrix} \underline{i}_{C_t} \\ \hline \underline{v}_{L_c} \end{vmatrix} =
$$

$$
\begin{vmatrix} \underline{H}_{C_tC_t} & \underline{H}_{C_tL_c} \\ \hline \underline{H}_{L_cC_t} & \underline{H}_{L_cL_c} \end{vmatrix} * \begin{vmatrix} \underline{v}_{C_t} \\ \hline \underline{i}_{L_c} \end{vmatrix} + \begin{vmatrix} \underline{H}_{C_tE_t} & \underline{H}_{C_tJ_c} \\ \hline \underline{H}_{L_cE_t} & \underline{H}_{L_cJ_c} \end{vmatrix} * \begin{vmatrix} \underline{v}_{E_t} \\ \hline \underline{i}_{J_c} \end{vmatrix}
$$

$$
+ \begin{vmatrix} \underline{H}_{C_tR_t} & \underline{H}_{C_tG_c} \\ \hline \underline{H}_{L_cR_t} & \underline{H}_{L_cG_c} \end{vmatrix} * \begin{vmatrix} \underline{v}'_{R_t} \\ \hline \underline{i}'_{G_c} \end{vmatrix} + \begin{vmatrix} \underline{H}_{C_tC_c} & \underline{0}_{C_tL_t} \\ \hline \underline{0}_{L_cC_c} & \underline{H}_{L_cL_t} \end{vmatrix} *
$$

$$
\left[\begin{vmatrix} \underline{C}_{ct} & \underline{0}_{cc} \\ \hline \underline{0}_{tt} & \underline{L}_{tc} \end{vmatrix} + \begin{vmatrix} \underline{C}_{cc} & \underline{0}_{ct} \\ \hline \underline{0}_{tc} & \underline{L}_{tt} \end{vmatrix} * \begin{vmatrix} \underline{H}_{C_cC_t} & \underline{0}_{C_cL_c} \\ \hline \underline{0}_{L_tC_t} & \underline{H}_{L_tL_c} \end{vmatrix}\right] * d/dt \begin{vmatrix} \underline{v}_{C_t} \\ \hline \underline{i}_{L_c} \end{vmatrix}
$$

$$
+ \begin{vmatrix} \underline{C}_{cc} & \underline{0}_{ct} \\ \hline \underline{0}_{tc} & \underline{L}_{tc} \end{vmatrix} * \begin{vmatrix} \underline{H}_{C_cE_t} & \underline{0}_{C_cJ_c} \\ \hline \underline{0}_{L_tE_t} & \underline{H}_{L_tJ_c} \end{vmatrix} * d/dt \begin{vmatrix} \underline{v}_{E_t} \\ \hline \underline{i}_{J_c} \end{vmatrix} \right]
$$

(2.3-58)

Furthermore, using equation (2.3-56) one can express the vectors $\underline{i}_{C_t}$ and $\underline{v}_{L_c}$ as follows:

$$\begin{bmatrix} \underline{i}_{C_t} \\ \hline \underline{v}_{L_c} \end{bmatrix} = \begin{bmatrix} \underline{C}_{tt} & \underline{0}_{tc} \\ \underline{0}_{ct} & \underline{L}_{cc} \end{bmatrix} * \frac{d}{dt}\begin{bmatrix} \underline{v}_{C_t} \\ \underline{i}_{L_c} \end{bmatrix} + \begin{bmatrix} \underline{C}_{tc} & \underline{0}_{tt} \\ \underline{0}_{cc} & \underline{L}_{ct} \end{bmatrix} * \frac{d}{dt}\begin{bmatrix} \underline{v}_{C_c} \\ \underline{i}_{L_t} \end{bmatrix}$$

<div align="right">(2.3-59)</div>

Substituting for the derivatives of $\underline{v}_{C_c}$ and $\underline{i}_{L_t}$ from equation (2.3-53) yields:

$$\begin{bmatrix} \underline{i}_{C_t} \\ \hline \underline{v}_{L_c} \end{bmatrix} = \begin{bmatrix} \underline{C}_{tt} & \underline{0}_{tc} \\ \underline{0}_{ct} & \underline{L}_{cc} \end{bmatrix} * \frac{d}{dt}\begin{bmatrix} \underline{v}_{C_t} \\ \underline{i}_{L_c} \end{bmatrix} + \begin{bmatrix} \underline{C}_{tc} & \underline{0}_{tt} \\ \underline{0}_{cc} & \underline{L}_{ct} \end{bmatrix} *$$

$$\left[\begin{bmatrix} \underline{H}_{C_c C_t} & \underline{0}_{C_c L_c} \\ \underline{0}_{L_t C_t} & \underline{H}_{L_t L_c} \end{bmatrix} * \frac{d}{dt}\begin{bmatrix} \underline{v}_{C_t} \\ \underline{i}_{L_c} \end{bmatrix} + \begin{bmatrix} \underline{H}_{C_c E_t} & \underline{0}_{C_c J_c} \\ \underline{0}_{L_t E_t} & \underline{H}_{L_t J_c} \end{bmatrix} * \frac{d}{dt}\begin{bmatrix} \underline{v}_{E_t} \\ \underline{i}_{J_c} \end{bmatrix}\right]$$

<div align="right">(2.3-60)</div>

Regrouping equation (2.3-60) and substituting the result for the left side of equation (2.3-58) yields:

$$\left[\begin{bmatrix} \underline{C}_{tt} & \underline{0}_{tc} \\ \underline{0}_{ct} & \underline{L}_{cc} \end{bmatrix} + \begin{bmatrix} \underline{C}_{tc} & \underline{0}_{tt} \\ \underline{0}_{cc} & \underline{L}_{ct} \end{bmatrix} * \begin{bmatrix} \underline{H}_{C_cC_t} & \underline{0}_{C_cL_c} \\ \underline{0}_{L_tC_t} & \underline{H}_{L_tL_c} \end{bmatrix}\right] * d/dt \begin{bmatrix} \underline{v}_{C_t} \\ \underline{i}_{L_c} \end{bmatrix}$$

$$+ \begin{bmatrix} \underline{C}_{tc} & \underline{0}_{tt} \\ \underline{0}_{cc} & \underline{L}_{ct} \end{bmatrix} * \begin{bmatrix} \underline{H}_{C_cE_t} & \underline{0}_{C_cJ_c} \\ \underline{0}_{L_tE_t} & \underline{H}_{L_tJ_c} \end{bmatrix} * d/dt \begin{bmatrix} \underline{v}_{E_t} \\ \underline{i}_{J_c} \end{bmatrix}$$

$$= (\text{Right side of equation (2.3-58)}$$

$$(2.3-61)$$

Finally, by performing the necessary matrix algebra on equation (2.3-61), the derivative of the state variables can be explicitly expressed in terms of the state variables, the forcing functions and their derivatives, as well as the (iterated upon) nonlinear resistor port variables as shown in equation (2.3-62).

Thus the general form for equation (2.3-62), where $\underline{x}$ is the state variable vector, $\underline{u}$, is the forcing function vector, and $\underline{h}'_{RG}$ is the previously solved for nonlinear

$$
\frac{d}{dt}\begin{bmatrix} \underline{v}_{C_t} \\ \hline \underline{i}_{L_c} \end{bmatrix} = \left[\begin{bmatrix} \underline{C}_{tt} & \underline{O}_{tc} \\ \hline \underline{O}_{ct} & \underline{L}_{cc} \end{bmatrix} + \begin{bmatrix} \underline{C}_{tc} & \underline{O}_{tt} \\ \hline \underline{O}_{cc} & \underline{L}_{ct} \end{bmatrix} * \begin{bmatrix} \underline{H}_{C_cC_t} & \underline{O}_{C_tL_c} \\ \hline \underline{O}_{L_tC_t} & \underline{H}_{L_tL_c} \end{bmatrix} \right.
$$

$$
- \begin{bmatrix} \underline{H}_{C_tC_c} & \underline{O}_{C_tL_t} \\ \hline \underline{O}_{L_cC_c} & \underline{H}_{L_cL_t} \end{bmatrix} * \left(\begin{bmatrix} \underline{C}_{ct} & \underline{O}_{cc} \\ \hline \underline{O}_{tt} & \underline{L}_{tc} \end{bmatrix} + \begin{bmatrix} \underline{C}_{cc} & \underline{O}_{ct} \\ \hline \underline{O}_{tc} & \underline{L}_{tt} \end{bmatrix} * \begin{bmatrix} \underline{H}_{C_cC_t} & \underline{O}_{C_cL_c} \\ \hline \underline{O}_{L_tL_t} & \underline{H}_{L_tL_c} \end{bmatrix} \right)^{-1}
$$

$$
* \left[\begin{bmatrix} \underline{H}_{C_tC_t} & \underline{H}_{C_tL_c} \\ \hline \underline{H}_{L_cC_t} & \underline{H}_{L_cL_c} \end{bmatrix} * \begin{bmatrix} \underline{v}_{C_t} \\ \hline \underline{i}_{L_c} \end{bmatrix} + \begin{bmatrix} \underline{H}_{C_tE_t} & \underline{H}_{C_tJ_c} \\ \hline \underline{H}_{L_cE_t} & \underline{H}_{L_cJ_c} \end{bmatrix} * \begin{bmatrix} \underline{v}_{E_t} \\ \hline \underline{i}_{J_c} \end{bmatrix} \right.
$$

$$
+ \left(\begin{bmatrix} \underline{H}_{C_tC_c} & \underline{O}_{C_tL_t} \\ \hline \underline{O}_{L_cC_c} & \underline{H}_{L_cL_t} \end{bmatrix} * \begin{bmatrix} \underline{C}_{cc} & \underline{O}_{ct} \\ \hline \underline{O}_{tc} & \underline{L}_{tt} \end{bmatrix} * \begin{bmatrix} \underline{H}_{C_cE_t} & \underline{O}_{C_cJ_c} \\ \hline \underline{O}_{L_tE_t} & \underline{H}_{L_tJ_c} \end{bmatrix} - \begin{bmatrix} \underline{C}_{tc} & \underline{O}_{tt} \\ \hline \underline{O}_{cc} & \underline{L}_{ct} \end{bmatrix} \right.
$$

$$
\left. \left. * \begin{bmatrix} \underline{H}_{C_cE_t} & \underline{O}_{C_cJ_c} \\ \hline \underline{O}_{L_tE_t} & \underline{H}_{L_tJ_c} \end{bmatrix} \right) * \frac{d}{dt}\begin{bmatrix} \underline{v}_{E_t} \\ \hline \underline{i}_{J_c} \end{bmatrix} + \begin{bmatrix} \underline{H}_{C_tR_t} & \underline{H}_{C_tG_c} \\ \hline \underline{H}_{L_cR_t} & \underline{H}_{L_cG_c} \end{bmatrix} * \frac{d}{dt}\begin{bmatrix} \underline{v}'_{R_t} \\ \hline \underline{i}'_{G_c} \end{bmatrix} \right]
$$

<div align="right">(2.3-62)</div>

resistors' port vector as given in equation (2.3-47), can be expressed as follows:

$$d(\underline{x})/dt = \underline{A}\,\underline{x} + \underline{B}\,\underline{u} + \underline{C}\,d(\underline{u})/dt + \underline{D}\,\underline{h}'_{RG}$$

$$(2.3-63)$$

.Details on how equation (2.3-62) is numerically integrated are discussed in Section 2.5.

Inspection of the expanded form of the state model, equation (2.3-62), reveals that the inverse of the matrix, $\underline{M}_{CL}$ is required. In order to numerically evaluate the above matricies $\{\underline{A},\underline{B},\underline{C},$ and,$\underline{D}\}$ given in equation (2.3-63), the matrix $\underline{M}_{CL}$ must be inverted only once for networks not containing any nonlinear capacitances and/or inductances. Fortunately, this matrix has some properties that simplify the numerical calculations for its inverse for networks containing nonlinear inductors and/or capacitors. These properties are discussed next.

$\underline{M}_{CL}$ can be obtained from equation (2.3-62) as follows:

$$\underline{M}_{CL} = \left| \begin{array}{c|c} \underline{C}_{tt} & \underline{0}_{tc} \\ \hline \underline{0}_{ct} & \underline{L}_{cc} \end{array} \right| - \left| \begin{array}{c|c} \underline{H}_{C_tC_c}\, \underline{C}_{cc}\, \underline{H}_{C_cC_t} & \underline{0}_{C_tL_c} \\ \hline \underline{0}_{L_cC_c} & \underline{H}_{L_cL_t}\, \underline{L}_{tt}\, \underline{H}_{L_tL_c} \end{array} \right|$$

$$+ \left[\left| \begin{array}{c|c} \underline{C}_{tc}\, \underline{H}_{C_cC_t} & \underline{0}_{C_tL_c} \\ \hline \underline{0}_{L_cC_t} & \underline{L}_{ct}\, \underline{H}_{L_tL_c} \end{array} \right| + \left| \begin{array}{c|c} \underline{H}_{C_tC_c}\, \underline{C}_{ct} & \underline{0}_{C_tL_c} \\ \hline \underline{0}_{L_cC_t} & \underline{H}_{L_cL_t}\, \underline{L}_{tt} \end{array} \right| \right]$$

<div align="right">(2.3-64)</div>

All of the hybrid sub-matrices within $\underline{M}_{CL}$ are skew symmetric and hence one can use this information to reduce computer memory requirements. Incorporating this fact, $\underline{M}_{CL}$ can be expressed as follows:

$$
\underline{M}_{CL} \; = \;
\begin{array}{|c|c|}
\hline
\underline{M}_C & \underline{0} \\
\hline
\underline{0} & \underline{M}_L \\
\hline
\end{array}
$$

$$
=
\begin{array}{|c|c|}
\hline
\begin{array}{l}
\underline{C}_{tt} \;+\; \underline{C}_{tc} \, \underline{H}_{C_c C_t} \\[4pt]
+\; (\, \underline{C}_{ct}^{t} \, \underline{H}_{C_c C_t} \;)^{t} \\[4pt]
+\; \underline{H}_{C_c C_t}^{t} \, \underline{C}_{cc} \, \underline{H}_{C_c C_t}
\end{array}
&
\underline{0}_{tc} \\
\hline
\underline{0}_{ct}
&
\begin{array}{l}
\underline{L}_{cc} \;+\; \underline{L}_{ct} \, \underline{H}_{L_t L_c} \\[4pt]
+\; (\, \underline{L}_{tc}^{t} \, \underline{H}_{L_t L_c} \;)^{t} \\[4pt]
+\; \underline{H}_{L_t L_c}^{t} \, \underline{L}_{tt} \, \underline{H}_{L_t L_c}
\end{array} \\
\hline
\end{array}
$$

$$(2.3\text{-}65)$$

From matrix algebra, the inverse of $\underline{M}_{CL}$ should be calculated by taking the inverse of $\underline{M}_C$ and $\underline{M}_L$ individually as follows:

$$
\underline{M}_{CL}^{-1} \; = \;
\begin{array}{|c|c|}
\hline
\underline{M}_C^{-1} & \underline{0} \\
\hline
\underline{0} & \underline{M}_L^{-1} \\
\hline
\end{array}
\qquad (2.3\text{-}66)
$$

This approach greatly reduces both computer memory and computation time to form the required inverse of $\underline{\underline{M}}_{CL}$.

Further simplifications of $\underline{\underline{M}}_{CL}$ are possible if the capacitors and inductors are bilateral, or

$$\underline{\underline{C}}_{tc} = \underline{\underline{C}}_{ct}^t \quad , \quad \underline{\underline{C}}_{tt} = \underline{\underline{C}}_{tt}^t \quad , \quad \underline{\underline{C}}_{cc} = \underline{\underline{C}}_{cc}^t$$
$$\underline{\underline{L}}_{tc} = \underline{\underline{L}}_{ct}^t \quad , \quad \underline{\underline{L}}_{tt} = \underline{\underline{L}}_{tt}^t \quad , \quad \underline{\underline{L}}_{cc} = \underline{\underline{L}}_{cc}^t$$

$$(2.3-67)$$

Substitution of these identities into equation (2.3-65) yields the following:

$$\underline{\underline{M}}_{CL} = \left[\begin{array}{c|c} \underline{\underline{C}}_{TT} + \underline{\underline{C}}_{TC} + \underline{\underline{C}}_{CC} & \underline{0} \\ \hline \underline{0} & \underline{\underline{L}}_{TT} + \underline{\underline{L}}_{TC} + \underline{\underline{L}}_{CC} \end{array} \right]$$

where
$$\underline{\underline{C}}_{TT} = \underline{\underline{C}}_{tt}$$
$$\underline{\underline{C}}_{TC} = \underline{\underline{C}}_{tc} \, \underline{\underline{H}}_{C_c C_t} + (\underline{\underline{C}}_{tc} \, \underline{\underline{H}}_{C_c C_t})^t$$
$$\underline{\underline{C}}_{CC} = \underline{\underline{H}}_{C_t C_c} \, \underline{\underline{C}}_{cc} \, \underline{\underline{H}}_{C_t C_c}^t$$
and
$$\underline{\underline{L}}_{CC} = \underline{\underline{L}}_{cc}$$
$$\underline{\underline{L}}_{CT} = \underline{\underline{L}}_{ct} \, \underline{\underline{H}}_{L_t L_c} + (\underline{\underline{L}}_{ct} \, \underline{\underline{H}}_{L_t L_c})^t$$
$$\underline{\underline{L}}_{TT} = \underline{\underline{H}}_{L_t L_c}^t \, \underline{\underline{L}}_{tt} \, \underline{\underline{H}}_{L_t L_c}$$

$$(2.3-68)$$

2.4 Automatic Generation of the Output Equations

At any given instant in time, the values of all branch voltages and currents are completely determined by the state variables and forcing functions of the system. In matrix form, this statement can be expressed as follows:

$$\underline{y} = \underline{E}\,\underline{x} + \underline{F}\,\underline{\dot{x}} + \underline{P}\,\underline{u} + \underline{Q}\,\underline{\dot{u}} + \underline{K}\,\underline{h}'_{RG}$$

$$(2.4-1)$$

where $\underline{y}$ is the (output) vector of all the branch voltages and currents within the overall network. The vectors, $\underline{x}$, $\underline{u}$, and $\underline{h}'_{RG}$, were previously defined in equation (2.3-63). The dot notation represents the first derivative with respect to time (i.e. $d(\underline{x})/dt = \underline{\dot{x}}$). The output vector, $\underline{y}$, can be expanded in terms of the previously defined branch variables, equations (2.3-4) through (2.3-7), as shown in Table (2.4-1).

The tree port voltages, $\underline{v}_t$, are defined in equation (2.3-4). The first two vectors of $\underline{v}_t$ are the independent voltage sources, $\underline{v}_{E_t}$, and the twig capacitor voltages, $\underline{v}_{C_t}$. Remember $\underline{v}_{C_t}$ is one of two components of the state vector, $\underline{x}$, and $\underline{v}_{E_t}$ is one of two components of the forcing function vector $\underline{u}$. The other two components of $\underline{u}$ and $\underline{x}$ are the first two elements of $\underline{i}_c$, equation (2.3-7), respectively. Again, these four components, $\underline{v}_{C_t}$, $\underline{i}_{L_c}$, $\underline{v}_{E_t}$, and $\underline{i}_{J_c}$, are known for any instant in time.

Table (2.4-1) Partitioning of Network Branch Variables

$\underline{v}_t$	Tree Port	(stimulus)	
$\underline{i}_t$	Variables	(response)	
$\underline{v}_R$	Tree Non-port	Internal	
$\underline{i}_R$	Variables	to the	
$\underline{v}_G$	Cotree Non-port	Linear Resistive	
$\underline{i}_G$	Variables	n-port	
$\underline{v}_C$	Cotree Port	(response)	
$\underline{i}_C$	Variables	(stimulus)	

The next two components of the output equations are $\underline{v}_{R_t}$ and $\underline{i}_{G_c}$, which occur as the third entries of $\underline{v}_t$ and $\underline{i}_c$, see equations (2.3-4) and (2.3-7), respectively. These two vectors can be obtained by using equations (2.3-43) through (2.3-45). Since the nonlinear resistors are modeled by piecewise linear, continuous, passive and strictly monotonically increasing I-V characteristics, the inverse of their component equations exist. Therefore $\underline{v}_{R_t}$ and $\underline{i}_{G_c}$ can be written as follows:

$$\underline{v}'_{R_t} = r^{-1} (\underline{i}'_{R_t}) \qquad\qquad (2.4\text{-}2)$$

$$\underline{i}'_{G_c} = g^{-1} (\underline{v}'_{G_c}) \qquad\qquad (2.4\text{-}3)$$

Since the operating points of the nonlinear resistors are fixed at any given instant in time, the nonlinear operators r^{-1} and g^{-1} can be replaced by the constant coefficient matrices $\underline{R}^{-1}_{R_t R_t}$ and $\underline{G}^{-1}_{G_c G_c}$, respectively, for that instant in time. Thus for that instant, equations (2.4-2) and (2.4-3) can be combined into one matrix equation which define these nonlinear resistors by the linear relationship given in the matrix equation (2.4-4) on the next page.

$$
\left[\begin{array}{c} \underline{i}_{R_t} \\ \hline \underline{v}_{G_c} \end{array} \right] = \left[\begin{array}{c|c} \underline{R}^{-1}_{R_t R_t} & \underline{0}_{R_t G_c} \\ \hline \underline{0}_{G_c R_t} & \underline{G}^{-1}_{G_c G_c} \end{array} \right] * \left[\begin{array}{c} \underline{v}_{R_t} \\ \hline \underline{i}_{G_c} \end{array} \right]
\qquad (2.4-4)
$$

Within this matrix equation, $\underline{R}^{-1}_{R_t R_t}$ and $\underline{G}^{-1}_{G_c G_c}$ are both, in general, constant diagonal matrices only for that instant in time.

Substituting equation (2.4-4) into equation (2.3-45) and regrouping, one can write the output equations for $\underline{v}_{R_t}$ and $\underline{i}_{G_c}$ as shown in equation (2.4-5). The corresponding output equations for the variables, $\underline{i}_{R_t}$ and $\underline{v}_{G_c}$, are obtained by direct substitution of equation (2.4-5) in equation (2.4-4).

The last components of the port stimulus vectors, $\underline{v}_t$ and $\underline{i}_c$, are the twig inductor voltages, $\underline{v}_{L_t}$, and the link capacitor currents, $\underline{i}_{C_c}$ These variables are defined in equation (2.3-56) in terms of the time derivatives of the state variables and the forcing functions.

Since all of the port stimulus variables, $\underline{v}_t$ and $\underline{i}_c$, are known, the remaining response port variables, $\underline{i}_t$ and $\underline{v}_c$, can be obtained directly from equation (2.3-32).

$$
\begin{bmatrix}
\underline{v}_{R_t} \\
\hline
\underline{i}_{G_c}
\end{bmatrix}
=
$$

$$
\left(
\begin{bmatrix}
\underline{R}^{-1}_{R_t R_t} & \underline{0}_{R_t G_c} \\
\hline
\underline{0}_{G_c R_t} & \underline{G}^{-1}_{G_c G_c}
\end{bmatrix}
-
\begin{bmatrix}
\underline{H}_{C_c C_t} & \underline{0}_{C_c L_c} \\
\hline
\underline{0}_{L_t C_t} & \underline{H}_{L_t L_c}
\end{bmatrix}
\right)^{-1}
*
$$

$$
\left[
\begin{bmatrix}
\underline{H}_{R_t C_t} & \underline{H}_{R_t L_c} \\
\hline
\underline{H}_{G_c E_t} & \underline{H}_{G_c L_c}
\end{bmatrix}
*
\begin{bmatrix}
\underline{v}_{C_t} \\
\hline
\underline{i}_{L_c}
\end{bmatrix}
+
\begin{bmatrix}
\underline{H}_{R_t E_t} & \underline{H}_{R_t J_c} \\
\hline
\underline{H}_{G_c E_t} & \underline{H}_{G_c J_c}
\end{bmatrix}
*
\begin{bmatrix}
\underline{v}_{E_t} \\
\hline
\underline{i}_{J_c}
\end{bmatrix}
\right]
$$

<div align="right">(2.4-5)</div>

The only remaining components of $\underline{y}$ which still need to be defined are the branch voltages and currents, $\underline{v}_R$, $\underline{v}_G$, $\underline{i}_R$, and $\underline{i}_G$, of the linear resistive n-port. These branches are all resistive and internal to the n-port subnetwork.

The vectors $\underline{v}_R$ and $\underline{i}_G$ can be obtained directly in terms of the stimulus port vectors, $\underline{v}_t$ and $\underline{i}_c$, using equations (2.3-21) and (2.3-25), respectively. The associated current and voltage vectors, $\underline{i}_R$ and $\underline{v}_G$, are defined in terms of $\underline{v}_R$ and $\underline{i}_G$ by the component equations (2.3-14) and (2.3-15), respectively. The component coefficient matrices of these linear resistors are diagonal and hence their inverses are trivial. This completes the process for obtaining the output equations of all the branch voltages and currents, $\underline{y}$, as defined in equations (2.4-1) and (2.4-2).

2.5 Determination of Network Operating Point

The state model for many electromechanical systems derived in Section (2.3) is nonlinear due to the presence of the nonlinear machine parameters (inductances) and solid state switching devices (represented by nonlinear resistances). This model also has the capability of handling nonlinear capacitors; however, this nonlinearity is often neglected in the simulation of typical electromechanical machine systems.

The nonlinear inductances are assumed to be functions of the state variables, $\underline{i}_{L_c}$, as defined in equation (2.3-50). Since the state variables are fixed or frozen at any instant of time, the inductances, therefore, are known and fixed at

- 85 -

that particular instant of time. The same holds true for the nonlinear capacitances.

The nonlinear resistances, however, must be determined iteratively, at each given point in time such that both the network constraints and the I-V characteristics of these resistors are simultaneously satisfied.

The nonlinear resistances considered in this work are piecewise linear as described earlier in Section (2.1). In order to realistically model the switching action of the solid state components, a large variation in the slope of the I-V characteristics between the "on" and "off" states of these switches is required. This slope ratio is of the order of six or more magnitudes. Consequently, the associated system time constants of the natural response also vary by approximately the same orders of magnitude. This results in a state model in which the eigenvalues of the matrix, $\underline{A}$, equation (2.3-63), are very widely separated. Such systems are inherently very difficult to solve numerically on the digital computer. This problem is referred to as the "time constant or stiffness" problem.

The larger the "off" to "on" ratio of the resistance values, the stiffer the governing set of differential equations (state model) becomes. Therefore, it is very important that the chosen integration routine be able to handle this class of differential equations.

Furthermore, it will be shown that stiffness affects not only the integration process but also the calculation of the diode operating points. This is due to the fact that errors in the calculation of the diode switching times results in entremely large voltage and current transients due to the inductive and capacitive nature of the systems under study. It will be shown that the "stiffer" the system, the larger the magnitude of these fictitious transients.

An algorithm for determining the operating points of these nonlinear resistances will now be discussed. The effects of stiffness on the performance of the algorithm will also be examined. This algorithm can be broken down into the following steps:

Step 1   Given an updated set of state variables and forcing functions at time, t=T1, determine the present values of the nonlinear inductances and capacitances.

Step 2   Solve for the operating points of the nonlinear resistances, at t=T1, by iterating upon equation (2.3-45).

Step 3   Update the matrices given in equation (2.3-62) and proceed to integrate the updated state model forward in time to t=T2, using an appropriate integration routine.

Since the solid state switching devices are modeled as piecewise linear resistances, Step 2 requires special attention at the zero crossing point of the I-V characteristic, as illustrated in Figure (2.1-1).

The most critical step in this algorithm involves the precise determination of the all diode switching points (times). In previous work, [12-14], these switching points were not precisely determined but were merely constrained to occur at the chosen solution points. This earlier approach was adequate at the time because of the relatively small integration steps sizes (5 μs) and because of the relatively mild degree of stiffness ($R_{OFF}/R_{ON} > 10000$) used by these investigators. It was found here, however, that this approach for changing the diode states presents serious problems for increasing values of "off" resistance and increasing integration step sizes. Also, it was found that the previous approach, [6-8], required excessive computer execution time due to the constraint of smaller integration step sizes, required by the explicit integration routine employed, for increasing degrees of stiffness. In fact, ratios of R_{OFF}/R_{ON} greater than 10000 resulted in numerical problems when using this previous approach.

The impact of constraining the switching times of the diodes to occur precisely at the preceeding integration point, which may be different than the true switching times, results in the appearance of very large voltage transients or spikes within the given numerical simulation run. This phenomena can best be understood by examination of the example given in Figure (2.5-1). The example consists of a series connected voltage source, diode, and inductor in which the diode is undergoing a change in state from "on" to "off". It is assumed that this change in state occurs between the integration points t_k and t_{k+1} at a time $t=t_s$. Assuming an initial inductor current of 1 ampere at $t=t_k$ and a sinusoidal source voltage, v_s, the diode current is assumed to reach a value of -1 ampere at $t=t_{k+1}$. If the diode is constrained to switch at $t=t_{k+1}$ rather than at the correct time, $t=t_s$, then a false voltage transient of almost 10KV is generated across the inductor assuming that v_s is negligible in comparison. In fact, inspection of the equation for the inductor voltage,

$$v_L = L(di/dt) = v_S - iR_D \qquad (2.5-1)$$

reveals that the magnitude of this voltage transient is approximately a linear function of the "off" resistance. Since the magnitude of the series inductor's current is constant at any given instant, the change of the equivalent

diode resistance at time $t=t_{k+1}$ results in a large increase of the diode voltage. This large voltage reflects the drastic drop in inductor current as illustrated in Figure (2.5-1). The relationship of the integration time step, $t_{k+1}-t_k$, to the voltage spike is not as defined at the "off" resistance value of the diode. But, the larger the time step, the more negative the inductive current can become, in this example, befor the switch in status occurs. This larger (more negative) inductor current is directly proportional to the voltage spike, as given in equation (2.5-1). A dual argument can be made for currents spikes if capacitors are present in the system, particlarity if they are in parallel with the diode.

To eliminate these artificial voltage and current transients, an improved diode switching algorithm was developed. This routine determines all of the diode switching times to within a USER specified tolerance. The diode status "on"/"off" is only changed at these points in time, thereby eliminating the artifical voltage and current transients which would have occured using the previous approaches. Details of this diode switching algorithm will be discussed next.

DIODE OFF STATE

$v_D \leqslant 0$

$R_D = 10K\Omega$

$v_L = v_S + i_D R_D$

$= v_S + 10KV$

$\approx 10KV$

for $t = t_{K+1}^+$

DIODE ON STATE

$v_D > 0$

$R_D = 0.01$

$v_L = v_S - i_D R_D$

$= v_S + 0.01$

$\approx v_S$

for $t = t_{K+1}^-$
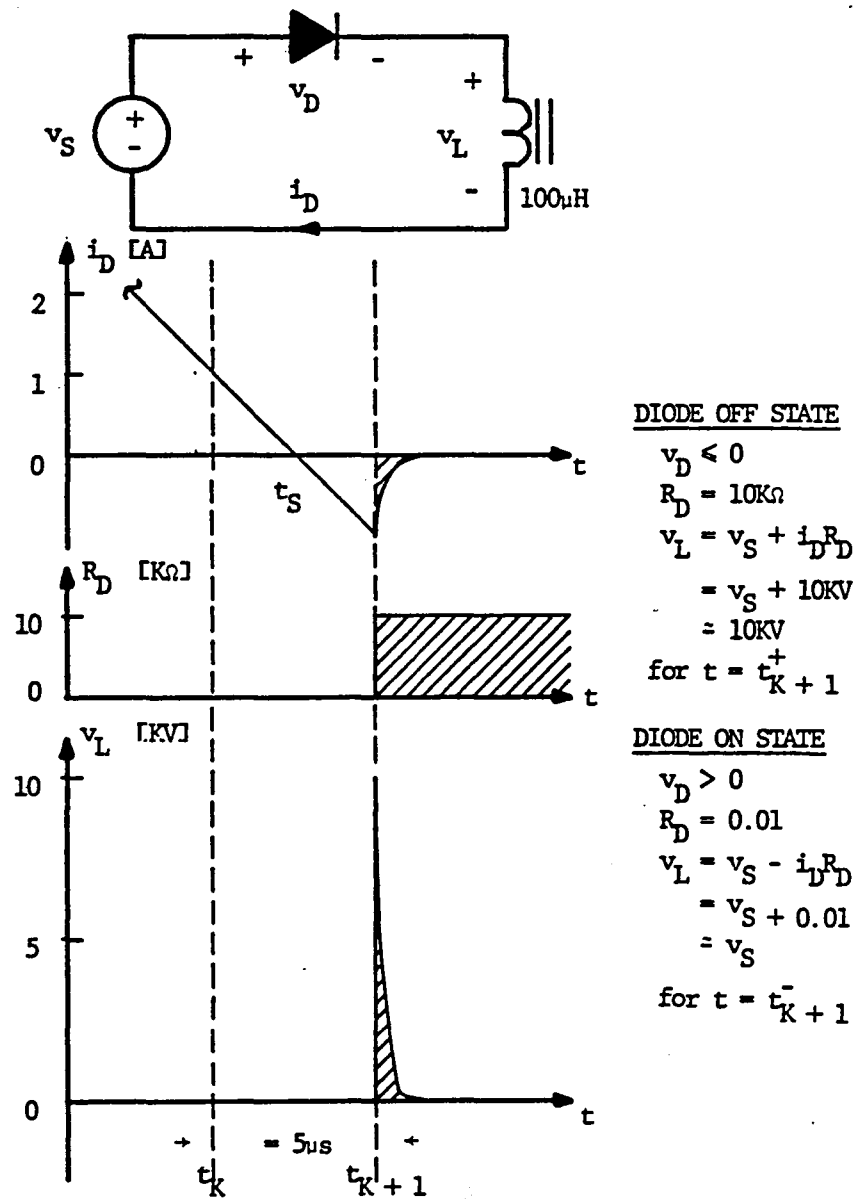
Figure (2.5-1)   Voltage Transient Due to Time Error in Diode Switching

Diode Switching Algorithm

The diode switching algorithm was designed to calculate the zero crossing time for each diode. In general these switching times may occur in between the discrete integration points. Furthermore, this algorithm also updates the state model everytime such a change in status is detected. The model updating is only done at the calculated time of the zero crossing. The basic assumptions upon which this algorithm is based are listed below:

1. The diode components are modeled as piecewise linear resistors;

2. the time interval, Δt, between integration points is small enough so that fast transients are not overstepped;

3. the change of status occurs only at the zero crossings of the diodes (within a user specified tolerance); and

4. a given diode will remain in the "on" state as long as its branch voltage is positive and will remain in the "off" state as long as its branch voltage is negative.

The second assumption is stated to make the reader aware of the possibility that this algorithm could miss a rapid change of sign within a diode's voltage or current since a polarity comparison is done only at the beginning of the time interval, Δt, and at the end; t_k and t_{k+1}, respectively. This blindness is illustrated in Figure (2.5-2). Note the polarity check shows that the product of the diode current values, at times t_k and t_{k+1}, is positive, thus falsely indicating there was no zero crossing. Since a change in polarity would indicate a zero crossing for the diode, this particular example illustrates the possibility of not detecting such a zero crossing if Δt is too large. Thus, assumption 2 reveals the need to reduce the time interval, Δt, if one desires to track rapid switching transients accurately.

This type of algorithm can be extended to other switching devices, such as a silicon controlled rectifiers (SCRs) and triacs (back to back SCRs) with some minor modifications. These two devices also require the accurate determination of their zero crossing times in the same manner as the conventional diode, in order to prevent erroneous voltage spikes. Details of the necessary logic required for modeling such devices will not be discussed here. Also,
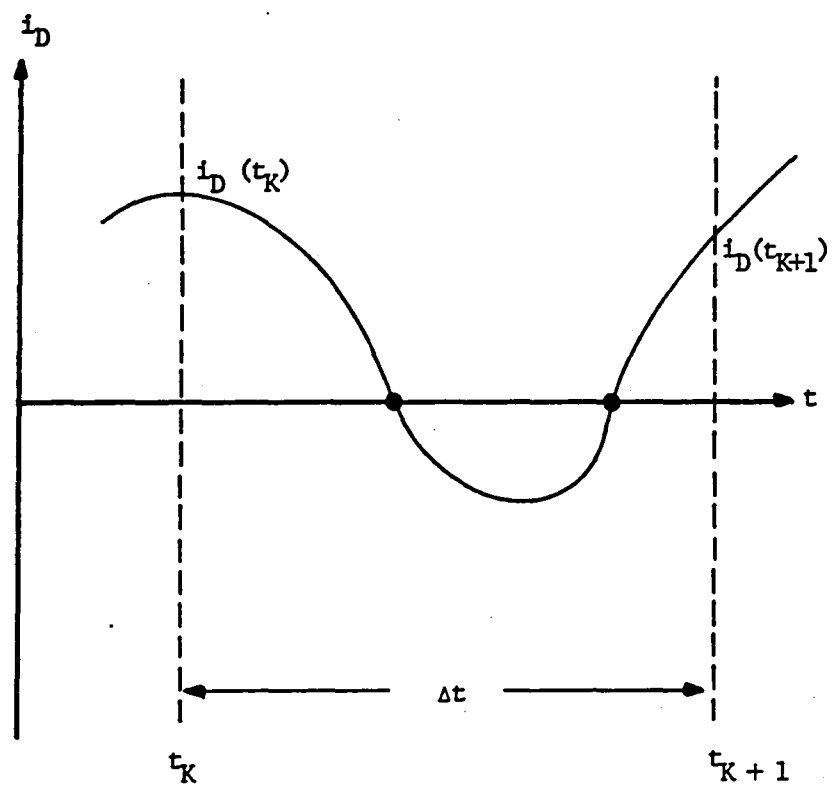
Figure (2.5-2) Blindness of the Switching Algorithm

this algorithm is not limited to one switch point simply at the origin.

The essential features of this algorithm will now be discussed. If a change in diode current polarity is detected between times t_k and t_{k+1}, for any diode, then there exists at least one diode zero crossing within Δt. Once this zero crossing has been detected, the zero crossing algorithm (diode switching algorithm) is called. This routine is not exited until all of the diodes which cross zero within this time interval are identified and dealt with properly. This routine entails the following:

1. Estimate each detected diode zero crossing time.

2. Rank each crossing time from first to last.

3. Integrate forward in time, using the unswitched (previous) diode status at time t_k, to the first estimated crossing time, t_s.

4. Check the accuracy of the estimated zero crossing time by using the calculated diode currents to determine the diode voltage at that point in time.

5. Change status of the diodes experiencing the zero crossing at this time, t_s, if the diode voltage (and current) spikes are within a USER specified tolerance, then update the state model.

6. If t_s occurs prior to the actual zero crossing time consider this estimate to be t_k, Figure (2.5-2), and go to 1.

7. In general, either integrate forward or move backward in order to determine a more accurate crossing time, if needed.

8. Continue this process until the entire integration interval, Δt, is covered. This could entail subdividing Δt into a number of subintervals to obtain all of the zero crossings.

Notice that the implementation of item 5 requires updating the overall state model due to any change in the diode resistances associated with any change in diode status.

The algorithm employed to model the switching action of all the diodes is nested inside the main integration loop of the overall simulation program. This algorithm continually

checks for any change in polarity between successive diode voltage or current values. The major integration loop supplies all the branch voltages and currents at every Δt time increment througout the entire simulation duration. This algorithm does not interrupt the calculation and storage of the solution points at their fixed time interval, Δt.

Using this improved diode switching algorithm, in conjunction with an appropriate implicit integration routine, it was possible to more accurately solve stiff systems where the ratio between the "off" and "on" values of the diode resistance ranged between 10^5 and 10^8. In addition, there were savings in computer execution time since the implicit routine allows much larger time steps. Both of these improvements are discussed in the next section.

2.6 Integration and Stiffness Considerations

The network operating point and the branch voltages and currents, for any given instant in time, are dependent only upon the state of the energy storage elements and forcing functions ($\underline{v}_{C_t}, \underline{i}_{L_c}, \underline{v}_{E_t}$, and $\underline{i}_{J_c}$). Hence in order to obtain a time solution for all of the branch variables, the state equations, given in equation (2.3-62), need to be integrated forward in time from one instant to the next using an

appropriate integration routine. The selection of an appropriate integration routine is based upon solution accuracy and the corresponding computational costs for extremely stiff systems.

State equations, associated with power switching type networks, are extremely stiff as was mentioned earlier. The integration of such stiff differential equations poses a number of numerical problems. For example, it is well known that the general class of explicit integration routines does not compare favorably in terms of accuracy and cost, to the implicit predictor-corrector routines when applied to these types of systems [5,26]. This and other points will be illustrated in the first part of this section by means of a numerical example.

The chosen numerical example is the simple stiff network presented in Figure (2.6-1). The numerical solutions from these routines are compared with the exact (analytical) solution of this network. This comparison is conducted for various degrees of stiffness in order to determine which type of integration routine is appropriate.

First, the concept of stiffness will be examined in detail using the simple network example. Next, the exact solution of this network will be compared with those obtained from two commercially available integration routines. These two routines are available from the

$R_s = 1\Omega$

$v_s = 1\,u(t)$

$i_1(t)$

$R_1 = 1\Omega$

$L_1 = 1H$

$i_2(t)$

$R_2 = \sigma\Omega$

$L_2 = 1H$
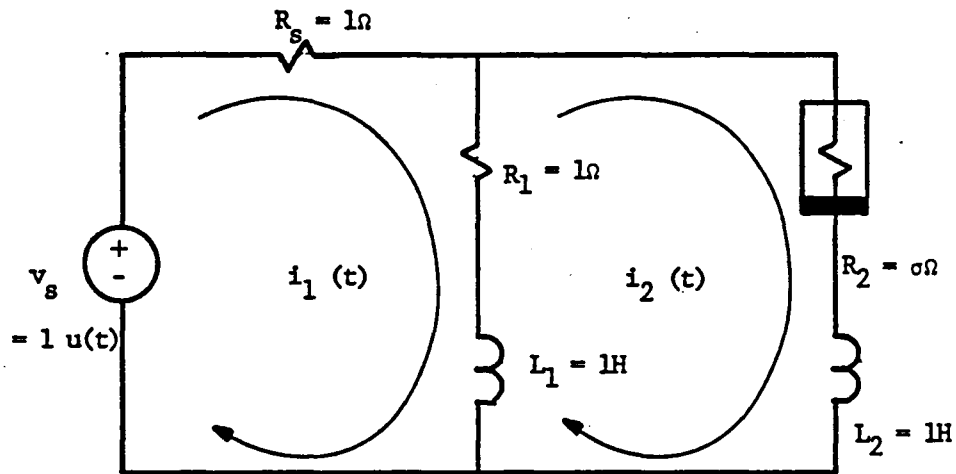
State Equations:

$$\frac{d}{dt}\begin{bmatrix} i_1 \\ i_2 \end{bmatrix} = \begin{bmatrix} -3 & 1-\sigma \\ -1 & -\sigma \end{bmatrix} \cdot \begin{bmatrix} i_1 \\ i_2 \end{bmatrix} + \begin{bmatrix} 2 & 1 \\ 1 & 1 \end{bmatrix} \cdot \begin{bmatrix} u(t) \\ 0 \end{bmatrix}$$

or

$$\dot{\underline{x}} = \underline{A}\,\underline{x} + \underline{B}\,\underline{u}$$

Figure (2.6-1)   Example Network Illustrating Stiffness
of State Equations

International Mathematical and Statistical Library, IMSL, [15]. The chosen explicit routine is a fifth and sixth order Runge-Kutta-Verner integration algorithm named DVERK, [15, 16]. The chosen implicit routine is a variable order Adams predictor-corrector method (or Gears Method) named DGEAR, [15, 16].

The algorithms employed by these two routines are given in Table (2.6-1). These algorithms were obtained from reference [17]. DVERK is an explicit routine, by definition, since the projected state vector for the next time instant, $y(t_{k+1})$, is solely determined by information calculated from past history. Considering explicit integration algorithms as recursive difference equations reveals the relationship between the (maximum allowable) step size, $h=\Delta t$, and the algorithm's numerical stability [3, 5, 20]. DGEAR, on the other hand, is not restricted to small integration time steps because of its implicit nature. Specifically, the homogeneous solution to the difference equation for an implicit routine (algorithm) is bounded for all positive h. Details of these types of routines can be obtained in references [2, 17, 18, 19]. The application and blackbox performance of the two integration routines under study, for the class of initial valued differential equations which are considered stiff, is the concern of this section. The concept of stiffness and its probable manifestation within a network shall be discussed next.

Table (2.6-1) Typical Integration Algorithms

let, $dy/dx = f(x,y)$ normal-form first-order differential equations

and, $f_i = f(x_i, y_i) = f(x_i, y(x_i))$

$x_i = x_{i-1} + h$

Runge-Kutta algorithms have the form : $y_{i+1} = y_i + h\ O$
(similar to DVERK)

    where, for a fourth order algorithm;

    $O = 1/6[k_1 + 2(1-.707)k_2 + 2(1+.707)k_3 + k_4]$

    and;

     $k_1 = f_i$,
     $k_2 = f(x_i + h/2\ ,\ y_i + hk_1/2)$,
     $k_3 = f[x_i + .707h\ ,\ y_i + (-1/2 + .707)hk_1 + (1-.707)hk_2]$
     $k_4 = f[x_i + h\ ,\ y_i - .707hk_2 + (1+.707)hk_3]$

Predictor-Corrector algorithm;   (similar to DGEAR)

    Predictor:

$y_{i+1} = y_i + h/24(55f_i - 59f_{i-1} + 37f_{i-2} - 9f_{i-3})$

    Corrector:

$y_{i+1} = y_i + h/24(9f_{i+1} - 19f_i - 5f_{i-1} + f_{i-2})$

The example network, along with its defining state equations, is shown in Figure (2.6-1). This particular example was chosen because it illustrates how the natural response of a network can possess two extremely spread time constants. The numerical difficulties encountered with the integration of such systems is referred to as the "time constant" problem. By increasing the resistance value R_2, which is in series with the inductor, L_2, the step response of the example network becomes more and more difficult to calculate accurately using numerical integration routines. This is due to the fact that the magnitude of the resistance value for R_2 is equal to the stiffness value, σ of the network under study.

The stiffness value, σ, is defined here as the ratio of the two resistor values, $\sigma = R_2/R_1$. Thus, by increasing only one of these resistance values, R_2 for example, while holding the other constant ($R_1 = 1$ ohm), one can directly vary the degree of stiffness of the network example under study. The exact relationship between the stiffness value, σ, defined here, and the ratio of the actual time constants of the network's natural response shall be discussed next.

The analytical unit step response for the two loop currents, $i_1(t)$ and $i_2(t)$, shown in Figure (2.6-1) is given below:

$$i_1(t) = C_1 e^{s_1 t} + C_2 e^{s_2 t} + \sigma + 1/s_1 s_2 \qquad (2.6-2)$$

$$i_2(t) = C_3 e^{s_1 t} + C_4 e^{s_2 t} + 1/s_1 s_2 \qquad (2.6\text{-}3)$$

where

$$C_1 = (2s_1 + \sigma + 1)/(s_1 - s_2) \qquad (2.6\text{-}4)$$

$$C_2 = (2s_1 + \sigma + 1)/(s_1 - s_2) \qquad (2.6\text{-}5)$$

$$C_3 = (s_1 + 1)/s_1(s_1 - s_2) \qquad (2.6\text{-}6)$$

$$C_4 = (s_2 + 1)/s_2(s_1 - s_2) \qquad (2.6\text{-}7)$$

$$s_1, s_2 = -(\sigma+3)/2 \pm .5[\sigma^2 - 2\sigma + 5]^{.5} \qquad (2.6\text{-}8)$$

Furthermore, the steady state response due to the unit step input is

$$i_1(\infty) = (\sigma+1)/s_1 s_2 \qquad (2.6\text{-}9)$$

$$i_2(\infty) = (1)/s_1 s_2 \qquad (2.6\text{-}10)$$

Examination of equation (2.6-8) reveals that for an increasing stiffness value, σ, the poles or time constants, which are symbolized as s_1 and s_2, approach $-\sigma$ and $-3/2$, respectively. Also, the root loci for these two poles always remain on the negative real axis of the s-plane (Laplace transformation). Notice also that these two poles spread apart (system becomes stiffer), as shown in Figure (2.6-2), when σ is increased from zero to infinity.

To characterize the concept of stiffness further; one can express the stiffness of the network's state equation in terms of the maximum ratio of its "time constants" (or eigenvalues of the matrix $\underline{A}$ in Figure (2.6-1)).
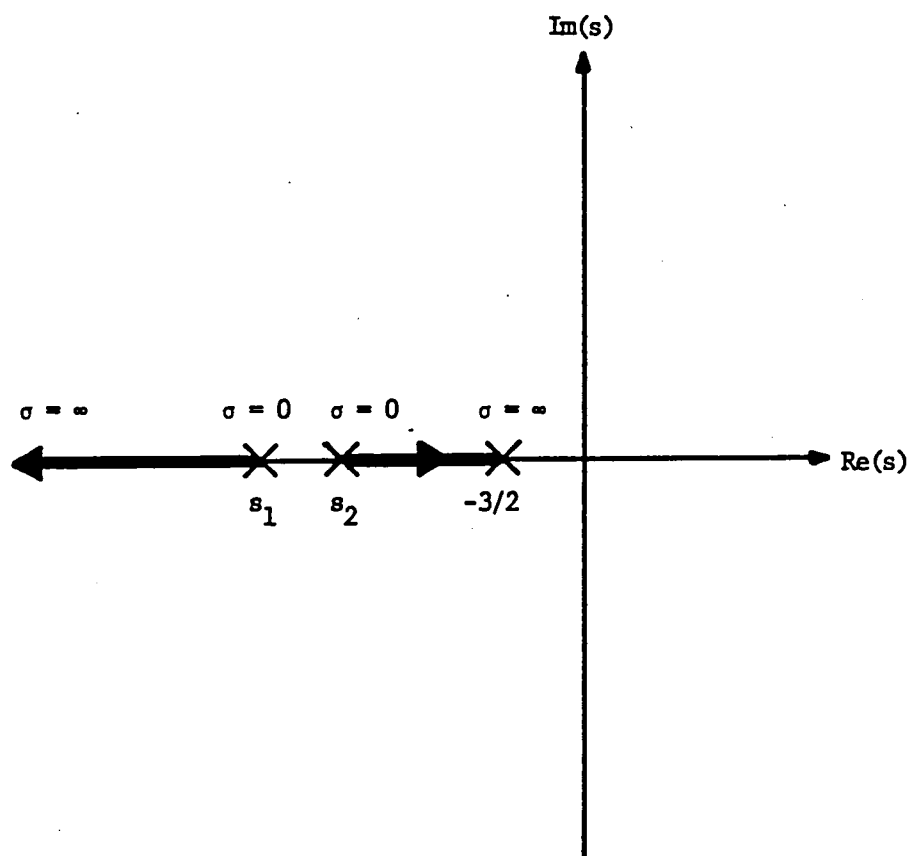
Figure (2.6-2)   Root locus of s_1 and s_2

The "stiffness" of a set of first order differential equations can also be associated with the degree of ill-conditioning of the $\underline{A}$ matrix. More precisely, ill-conditioning of a matrix is defined in terms of the ratio of its largest to smallest eigenvalue magnitudes. The larger this ratio, the more ill-conditioned the $\underline{A}$ matrix. There is a condition number which can be assigned to any matrix in terms of its largest and smallest eigenvalues that indicates the degree of ill-conditioning of the matrix, [7]. This number is sometimes defined as follows:

$$CN = \frac{||\lambda large||}{||\lambda small||} \qquad (2.6-11)$$

where

> $||\lambda large||$ is the modulus of the largest eigenvalue
> of the $\underline{A}$ matrix

and

> $||\lambda small||$ is the modulus of the smallest eigenvalue
> of the $\underline{A}$ matrix

In the network example presented in this section, there are only two eigenvalues and they are real negative numbers. Hence, the condition number, as defined in equation (2.6-11), for the $\underline{A}$ matrix given in Figure (2.6-1) can be written as follows:

$$CN = [s_1/s_2] = [(\sigma+3)+(\sigma^2-2\sigma + 5)^{.5}/((\sigma+3)-(\sigma^2-2\sigma +5)^{.5})$$
$$(2.6-12)$$

Notice that as σ is increased, the condition number, CN, of the A matrix also increases. A large condition number indicates difficulties in numerical calculations associated the A matrix, such as its inverse for example. A good estimate for the number of significant digits of accuracy when numerically calculating the inverse of the A matrix can be related to the condition number approximately, [17], as follows:

$$NSD = WLENGTH - [\ INT(LOG_{10}(CN)) + 1\ ]$$

where:

NSD = number of significant digits

WLENGTH = number of digits (decimal places) stored in a computer word used in computation.

    a) Single Precision = 7 digits

    b) Double Precision = 14 digits

INT (*) = Truncates the fractional part of the real number, hence making it an integer.

CN = the condition number of the matrix, A.

For example, if the stiffness value, σ, is set equal to 1000, then the CN is equal to 500.75 and the number of digits of round-off that can be expected is 3. On the other hand, if σ is set equal to 10^6 then CN is equal to 0.50000075×10^6 and the number of digits of round-off that can be expected when taking the inverse of the A matrix is 6. These two computations illustrate the direct significance of the stiffness value, σ, with the round-off error expected

using the digital computer. Further, in this particular example network, $INT(\log_{10}CN) + 1$ represents the number of digits round-off to be expected when taking the inverse of the $\underline{A}$ matrix.

Similarly, the ill conditioning of some matrix $\underline{M}$ can also have pronounced effects when operating numerically on systems of the form $\underline{M}\ \underline{x}=\underline{b}$; where $\underline{b}$ is the vector of known forcing functions or measured data and $\underline{x}$ is the response of the system (characterized by $\underline{M}$) to the data $\underline{b}$. These pronounced effects, manifested as large changes in the response $\underline{x}$ due to very small variations or errors in the data $\underline{b}$, may be caused by numerical round-off of the measured data for example. This sensitivity to the data is a direct result of the wide spread in the magnitudes of the eigenvalues of the matrix $\underline{M}$. If a perturbation, $\Delta\underline{b}$, of the observed data, $\underline{b}$, is strictly in the direction of the largest eigenvectors of the matrix $\underline{M}$, the resulting solution vector $\underline{x} + \Delta\underline{x}$ will not change drastically as compared to the case if the same perturbation magnitude occurs in the components of $\underline{b}$ that are in the same direction as the smallest eigenvectors of $\underline{M}$. For the latter case, the resulting change of the solution vector, $\underline{x}$, would be drastically increased, with respect to the first case, by approximately the condition number of the $\underline{M}$ matrix times the perturbation of the data, $\Delta\underline{b}$.

The condition number, CN, and the stiffness factor, σ, are closely related. The context in which they are used is their only difference. In particular, the condition number of the $\underline{M}$ matrix, CN, reveals valuable information about expected round-off when taking the inverse of $\underline{M}$. Similarily the stiffness factor, σ, gives a measure of how an extreme spread in the component values affecting the eigenvalues of $\underline{A}$ can effect the numerical integration of the state equations (time constant problem).

.Thus, special attention must be given to the specific integration routine employed when the $\underline{A}$ matrix within the governing state equation becomes ill-conditioned (a large ratio of its largest to smallest eigenvalue magnitudes). The larger this ratio, the more ill-conditioned the $\underline{A}$ matrix, and consequently the stiffer the governing state equations which contain $\underline{A}$ become.

The degree of system stiffness has a great impact on the efficiency (computer costs per solution) and the accuracy of the numerical integration routines. This is because, in order to track the fastest time constant in a stable and/or accurate sense, small time steps are required throughout the entire simulation period. This is the case even though the fastest transient may have died out and consequently no longer contributes significantly to the system's long term response associated with the slower time constants. More

precisely, the maximum allowable integration step size is determined by the smallest time constant (or eigenvalue of $\underline{A}$), while the total number of integration steps required to reach steady state is strictly determined by the largest time constant (or eigenvalue of $\underline{A}$). Hence, whenever the time constants (eigenvalues of the $\underline{A}$ matrix) differ by many orders of magnitude, many integration routines (specifically explicit ones) suffer from the requirement of excess computer time in order to obtain a desired amount of simulation time.

In order to illustrate the effects of stiffness, two commercially available IMSL routines were used to obtain numerical solutions for the example network of Figure (2.6-1). The defining system of first order differential equations, for this network, can be set to any desired degree of stiffness by varying the value of σ. The two IMSL routines used in this example are DVERK and DGEAR. DVERK is an explicit initial-value differential equation solver which employs a 5th and 6th order Runge-Kutta variable step method. DGEAR, on the other hand, is an implicit initial value differential equation solver using a Predictor-Corrector method with variable step size capability. DGEAR's integration step size does not have to be limited to guarantee numerical stability. DVERK, on the other hand, is limited to a maximum step size in order to guarantee numerical stability. This restriction is inherent in all

explicit integration routines. Even though DVERK has the internal capability to automatically maximize its step size throughout a given simulation run, it will not exceed an internally generated upper limit in order to guarantee numerical stability and/or satisfy the programmer's specified maximum local error estimate, TOL. Hence, internal to DVERK is an error estimator which limits the maximum step size in order to satisfy a specified degree of accuracy. DGEAR, on the other hand, can exceed DVERK's maximum step size and still satisfy the same accuracy requirements. Details of the numerical analysis of both methods can be obtained in references [3, 5, 20].

The exact solution to the example network is given in equations (2.6-2) and (2.6-3). The corresponding numerical solutions from DVERK and DGEAR for $\sigma=10^6$, and TOL=10^{-7}, are presented in Figures (2.6-3) through (2.6-6). The exact solution, in each of these cases, is plotted with the corresponding numerical solution for comparison. The global relative error, which is defined as the accumulated local relative error, is presented within these figures as the smaller graph. The global relative error for each of the figures is defined as follows:

$$\text{Relative Error} = \frac{(\text{Exact } i_1(t) - \text{DGEAR's } i_1(t))}{\text{Exact } i_1(t)} \qquad (2.6\text{-}13)$$

$$\text{Relative Error} = \frac{(\text{Exact } i_2(t) - \text{DGEAR's } i_2(tT))}{\text{Exact } i_2(t)} \qquad (2.6\text{-}14)$$

$$\text{Relative Error} = \frac{(\text{Exact } i_1(t) - \text{DVERK's } i_1(T))}{\text{Exact } i_1(t)} \qquad (2.6\text{-}15)$$

$$\text{Relative Error} = \frac{(\text{Exact } i_2(t) - \text{DVERK's } i_2(T))}{\text{Exact } i_1(t)} \qquad (2.6\text{-}16)$$

A comparison of the computation times, memory requirements, and solution accuracies of the two IMSL routines is presented in Table (2.6-2) for three different degrees of stiffness. Based upon these results, it can be seen that DGEAR, which is designed specifically for stiff systems, out performed DVERK in all of the above catagories.

Specifically, for a stiffness, $\sigma=10^6$, and a specified local relative-error tolerance, TOL=10^{-7}, it can be seen from this table that DVERK could not keep its maximum global relative error (MGRE) within this specified tolerance. DGEAR, on the other hand, did a much better job of tracking the exact solution. In fact, with this value of stiffness, the MGRE of DVERK is nearly one thousand times that of DGEAR.
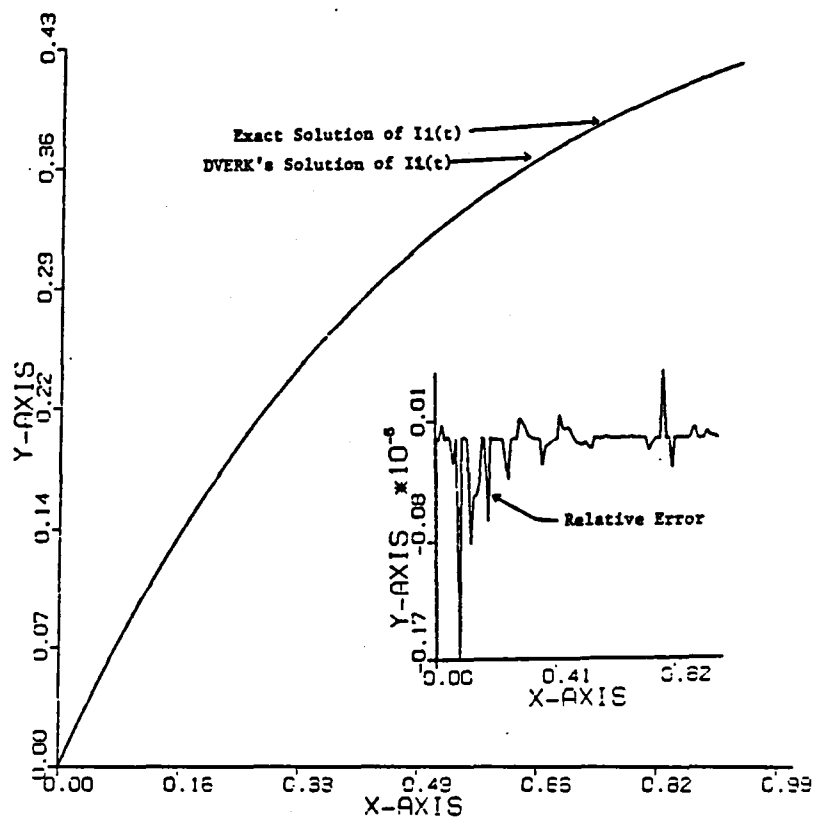
Figure (2.6-3)   DGEAR versus EXACT for $i_1(t)$ for $\sigma=10^6$
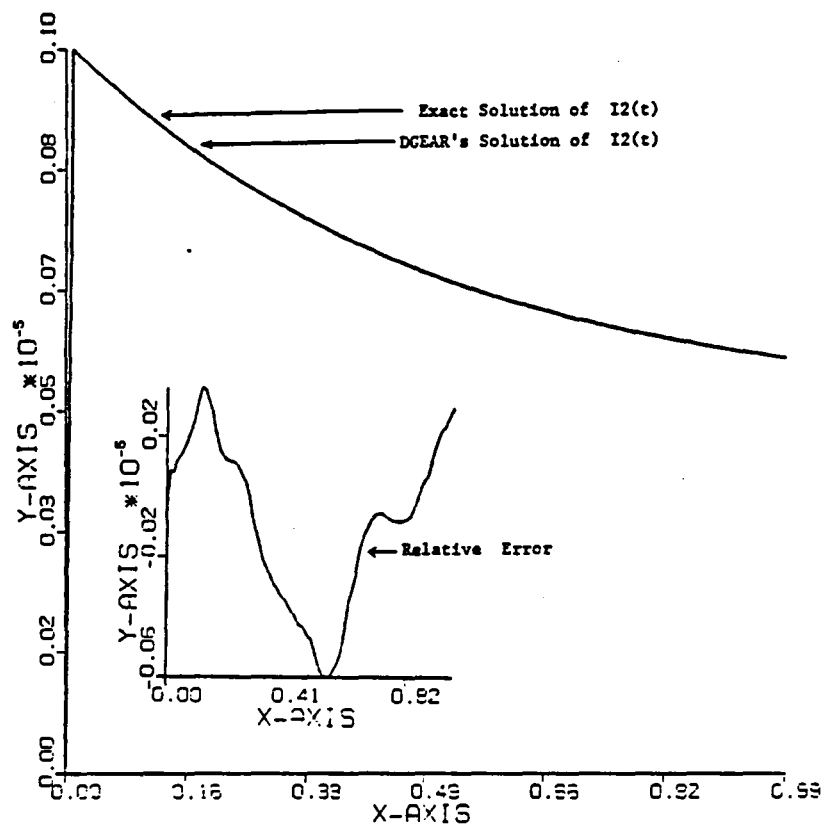
Figure (2.6-4) DGEAR versus EXACT for $i_2(t)$ for $\sigma=10^6$

Y-AXIS

0.43 0.36 0.29 0.14 0.07 0.00

Exact Solution of I1(t) ⟶

DGEAR's Solution of I1(t) ⟶

Y-AXIS *10⁻⁴

-0.01 -0.06 -0.11

⟵ Relative Error

0.00   0.4!   0.82
X-AXIS

0.00 0.16 0.33 0.49 0.66 0.82 0.99
X-AXIS
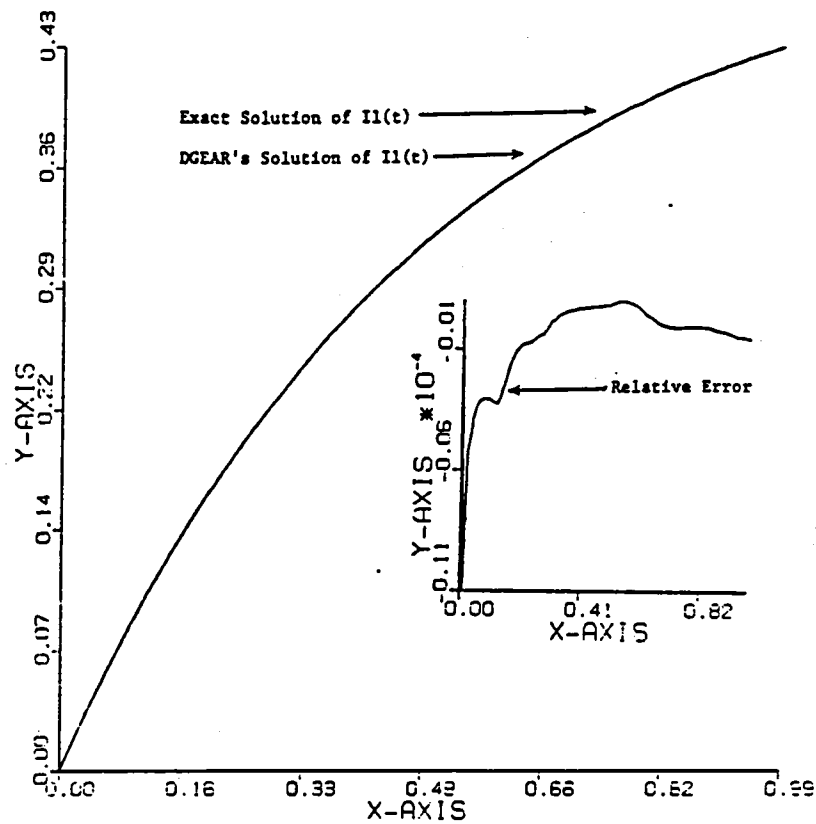
Figure (2.6-5)   DVERK versus EXACT for $i_1(t)$ for $\sigma=10^6$
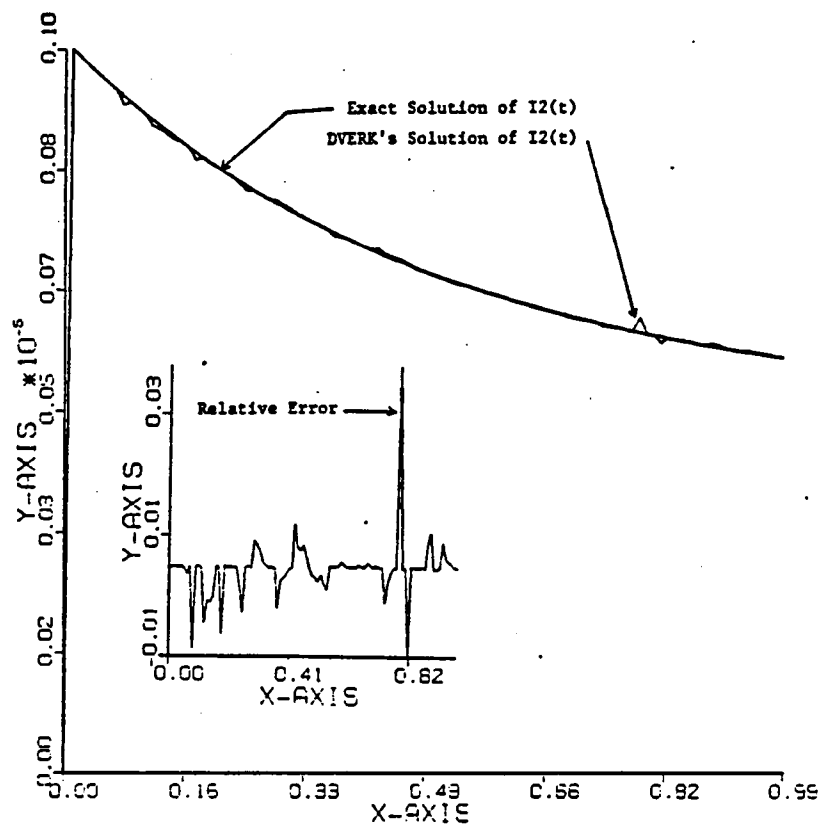
Figure (2.6-6)   DVERK versus EXACT for $i_2(t)$ for $\sigma=10^6$

Table (2.6-2)   Comparison Table for DVERK and DGEAR

DVERK Verner-Runge-Kutta 5th, 6th order Method	DGEAR Adam's Predictor-Corrector Variable order (GEAR's) Method

$$\sigma = 1.0 \; E + 4$$

00.00.30 seconds (CPU) 6.83 E - 6 MGRE * 449 KBS **	---------- ---------- ----------

$$\sigma = 1.0 \; E + 6$$

00.03.26 seconds (CPU) -1.0 E - 2 MGRE * 231468 KBS **	00.00.05 seconds (CPU) -1.1 E - 5 MGRE * 7492 KBS **

$$\sigma = 1.0 \; E + 14$$

---------- ---------- ----------	00.00.06 seconds (CPU) 2.0 E - 2 MGRE * 1346 KBS **

*   MGRE   is   defined,   using   equations   (2.6-3)   through (2.6-6), as the maximum relative error for either $i_1(t)$ or $i_2(t)$.

**KBS   is   defined   as   kilobyte-sec   which   is   equal   to storage (in kilobytes) times CPU time (in seconds).

The true cost of each routine is directly proportional to its use of both memory and execution time. The cost is a function of the product of storage used and CPU time. This cost can be expressed in terms of kilobyte-seconds (KBS) utilized by each routine to obtain its numerical approximation of the exact solution. For example, DVERK required approximately thirty times the KBS used by DGEAR to obtain the numerical solution for the case mentioned above. Even though DGEAR used about twice as much storage as DVERK, in this case, DVERK required about sixty-five times longer than DGEAR to execute because of its time step restriction mentioned earlier. Consequently, for this case, DGEAR was approximately thirty times less expensive and had a MGRE three orders of magnitude smaller than DVERK.

Finally, a case illustrating extreme stiffness, where $\sigma = 1.0 \text{ E}^{14}$ and TOL $= 1.0 \text{ E}^{-3}$, was examined. The results for this case are given in the last row of Table (2.6-1). Notice that DVERK was not able to track the exact solution for this large stiffness. This case illustrates that DGEAR can handle much stiffer systems that DVERK. Thus, even though the order of stiffness was increased by a factor of eight to $\sigma = 1.0 \text{ E}^{14}$, DGEAR still tracked the exact solution as well as DVERK did for the less stiff case when $\sigma = 1.0 \text{ E}^{6}$. Furthermore for this case, DGEAR also excelled in the other two categories (of CPU seconds of execution time and KBS) even when the stiffness was increased by eight

orders of magnitude, as shown in Table (2.6-2).

The comparison of the two IMSL routines, DVERK and DGEAR, yields the conclusion that DGEAR is far superior to DVERK when solving stiff systems of differential equations. Even though DGEAR uses more memory than DVERK, DVERK's excessive CPU time requirements far outweigh this memory advantage. Further, DVERK is not only more expensive but is less accurate (as summarized in Table (2.6-2)) to use than DGEAR, when integrating stiff systems of differential equations. Thus, DGEAR was chosen over DVERK as an appropriate integration routine for solving the differential equations associated with electromechanical systems employing solid state switching devices.

DGEAR was used for integrating the state equations for all the simulation runs presented later in this dissertation. These runs were made economically feasible because of the employment of DGEAR as well as the diode routine discussed previously within Section 2.1. Specifically, the diode algorithm does not interrupt DGEAR's control of the variable integration step size except for diode zero crossings. Hence, it allows DGEAR to integrate as economically as it can (maximizing its step size) for the majority of the simulation duration. This combination is most suitable for the types of machine systems considered in this report.

2.7 Verification of Modeling Approach

This section deals with the verification of the modeling approach presented in previous sections of this chapter. The system chosen for this purpose was an advanced electronically-commutated brushless dc motor designed for electric-vehicle propulsion, [20, 21, 22]. The performance and operating voltage and current waveforms of this system are well documented in these references. A block diagram of the propulsion system is presented in Figure (2.7-1).

The verification of the modeling approach presented in this section is based upon the favorable comparison of actual system measurements and simulated results. This section presents verification of the modeling approach's ability to simulate systems containing transistor and diode switching devices as well as mutual inductances.

A detailed schematic of the electric vehicle propulsion unit is given in Figure (2.7-2). The corresponding lumped parameter network model is given in Figure (2.7-3).
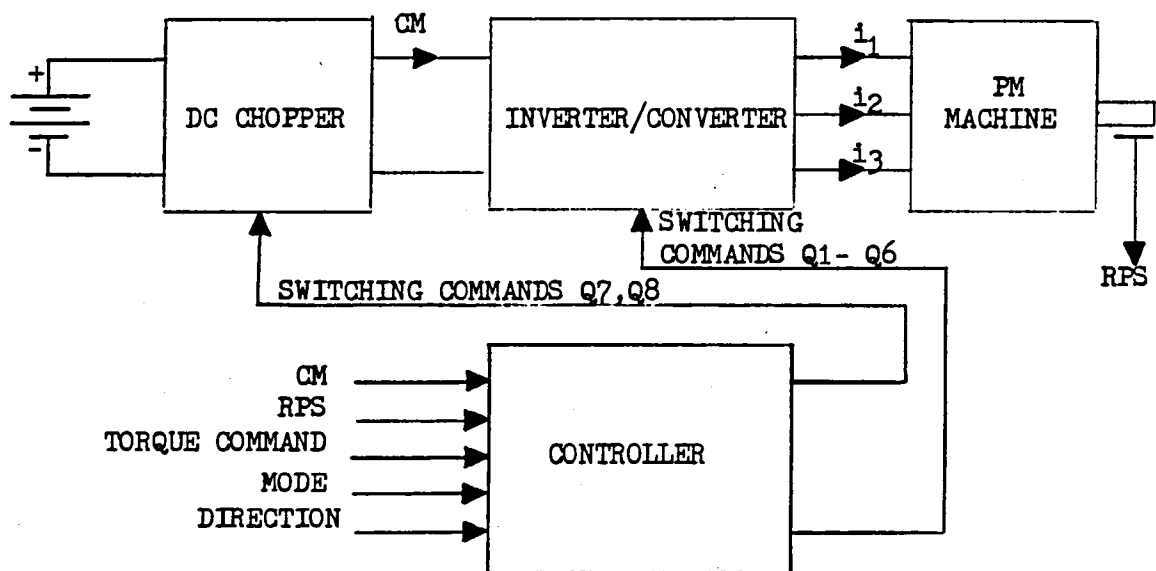
Figure (2.7-1) Block Diagram of the Electric Vehicle Propulsion Unit

The chosen test runs correspond to the rated 15 hp operation of this system and additional simulation data are presented in Table (2.7-1). The diodes and transistors of Figure (2.7-2) were all modeled as seperate (nonlinear) piece-wise linear resistors as shown in Figure (2.7-3). The oscillograms and other test data presented in this section were obtained with the brushless dc machine coupled to a dynamometer.

The parameters of the electric-vehicle propulsion unit as well as the control signals for all the transistors were obtained from reference [21]. The emf voltage waveforms were obtained from a field analysis [38] while the inductance values (self and mutuals) were obtained from the motor. The machine-inductance values (self and mutuals) were obtained from test measurements made on the actual machine modeled.

Two operating modes were simulated using the modeling approach presented in this report. The first mode simulated was motoring without chopping. The second mode was motoring with chopping. Details of these two motoring modes can be obtained in reference [21].
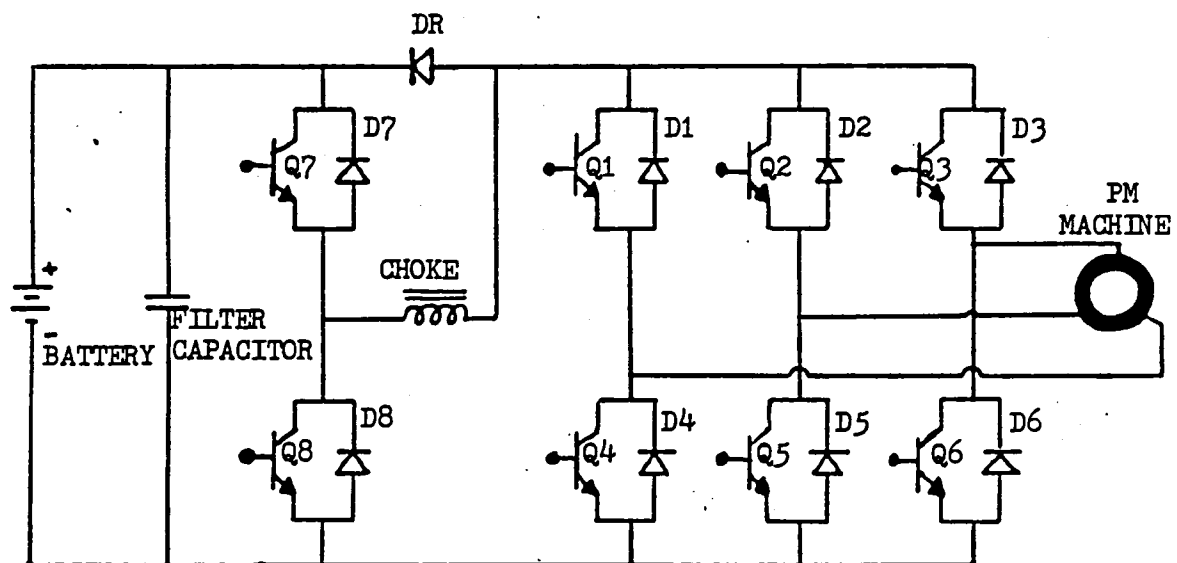
Figure (2.7-2)   Detailed Schematic and Corresponding Network
                  Model   of   the   Electric   Vehicle   Propulsion
                  Unit
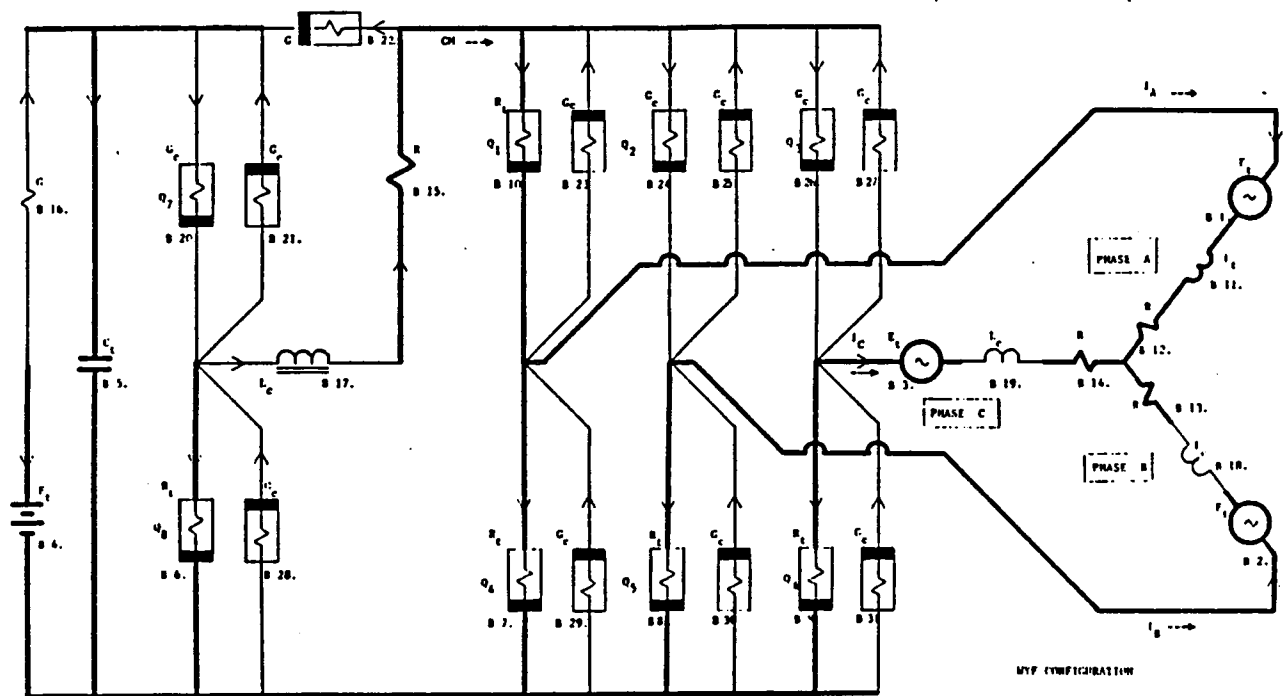
Figure (2.7-3) Lumped Parameter Network Model of the Electric Vehicle Propulsion Unit.

- 123 -

Table (2.7-1) Simulation Data for Electric Vehicle
Propulsion Unit (Verification Runs)

Brushless DC Motor Components:

field: Samarium Cobalt permanent magnet effects are
reflected as open circuit emf in armature.

armature: Three-phase wye-connected with floating neutral
- phase to neutral winding resistance = 6.8 milli-ohms
- phase to neutral winding inductance values:
    self = 47.82 micro-henries
    mutual =   4.18 micro-henries
- phase to neutral winding open circuit emf functional
representation is a truncated fourier series with
coefficients for the sine terms (a_n) and the
cosine terms (b_n), for the n-th harmonic, given
below:

n	a_n/RMVEL	b_n/RMVEL
1	74.400	3.550
3	-1.420	-0.221
5	0.000	0.000
7	0.553	-0.619
9	0.664	-0.278
11	0.373	-0.141
13	-0.037	-0.014

where:

$$\text{RMVEL} = (n_{RPM}/60.0) * 2 * pi * 10^{-3}$$

Power Conditioner Components:

diode: "on" resistance = 6.4 milli-ohms
"off" resistance = 20.0 kilo-ohms

transistor: "on" resistance = 6.4 milli-ohms
"off" resistance = 20.0 kilo-ohms

choke: winding resistance = 24.0 milli-ohms
self inductance   =   1.5 milli-henries

battery: thevenin equivalent resistance =   5.0 milli-ohms
thevenin equivalent voltage   = 120.0 volts

The first motoring mode was simulated at the rated 15 hp operating point. For this mode, the chopper transistor Q_7 is latched-on, in the saturation mode, and Q_8 is latched in its cutoff mode, Figure (2.7-2). This mode results in the full battery voltage being applied continuously across the inverter/converter bridge. The motoring results from periodic application of the battery voltage across the machine's terminals (line to line) in a specific sequence that is controlled by transistors Q_1 through Q_6. The oscillogram of the phase current of the electric-vehicle motor given in Figure (2.7-4) matches very closely the simulated waveform shown in Figure (2.7-5). The model was used also to predict the voltages across the transistor and diode switches. The oscillogram, Figure (2.7-6), and the predicted collector to emitter voltage waveform, Figure (2.7-7), of one of the inverter transistors are given for comparison. Inspection of these two waveforms reveals very close agreement between measured and simulated results for this first motoring mode of operation.

Another motoring mode was simulated and the results are compared with available oscillograms. This mode is called chopping. What is meant by chopping is that the conduction status of transistors Q_7 and Q_8 are controlled by logic base control signals which are determined by monitoring the magnitude of the current labeled CM, in Figure (2.7-3).
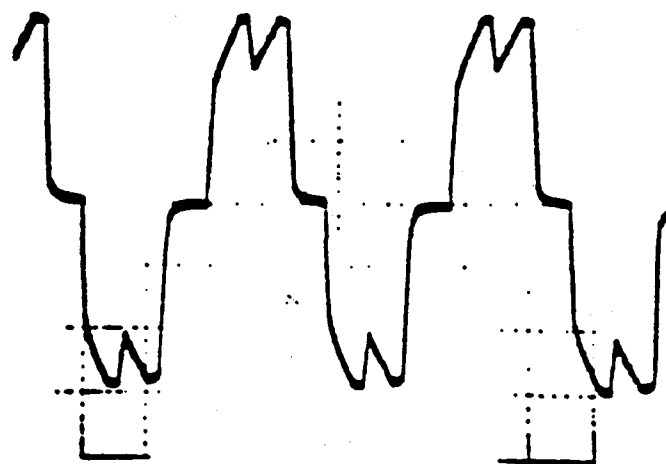
Figure (2.7-4) Oscillogram of the Phase Current

Y BASE IN VOLTS=62.2657
Y BASE IN AMPS.=146.1802

V
I E_T
E_T

+1.0

0.0

+1.0

-1.0

BRANCH 1.   X BASE IN SEC.=0.0100
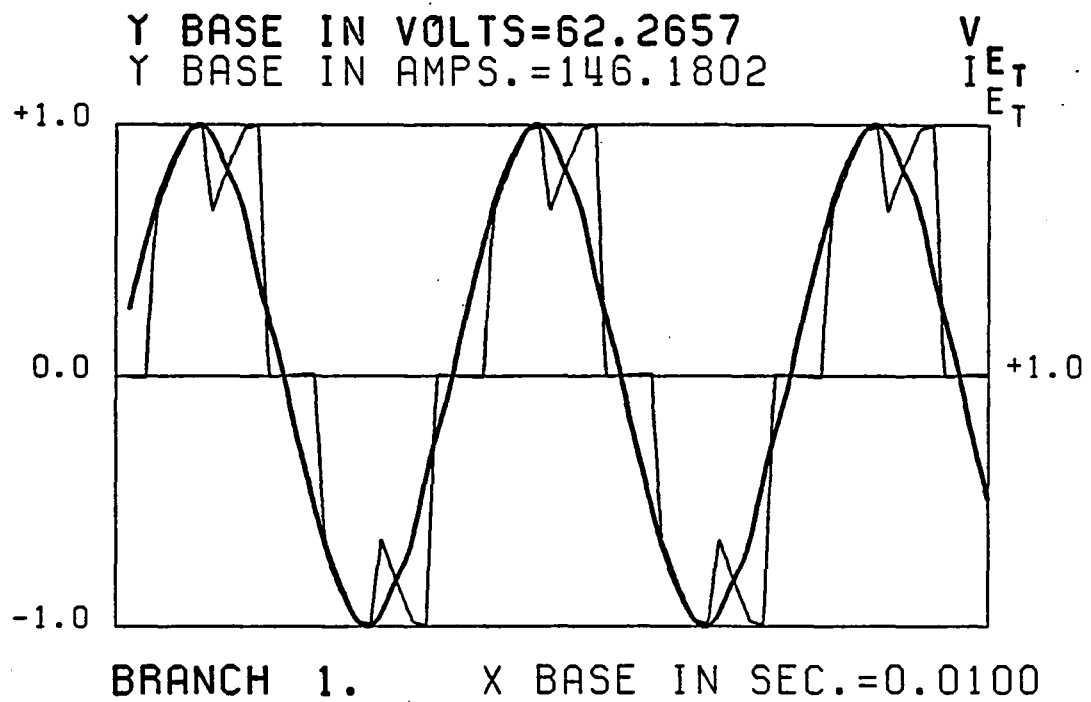
Figure (2.7-5) Predicted Waveform of the Phase Current

50.0 volts per division
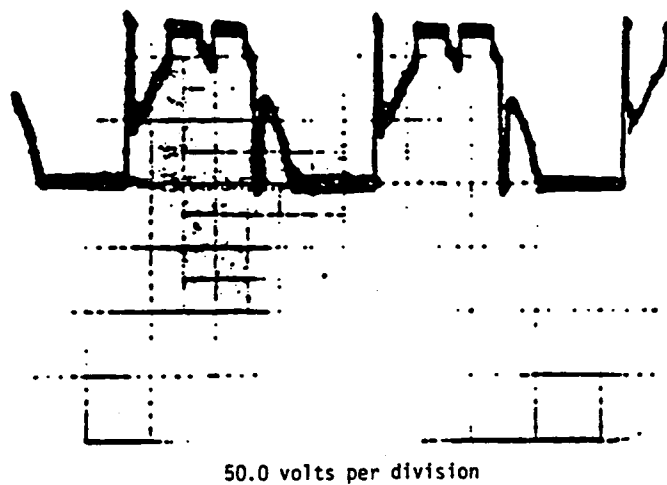
Figure (2.7-6) Oscillogram of the Inverter Switch Voltage
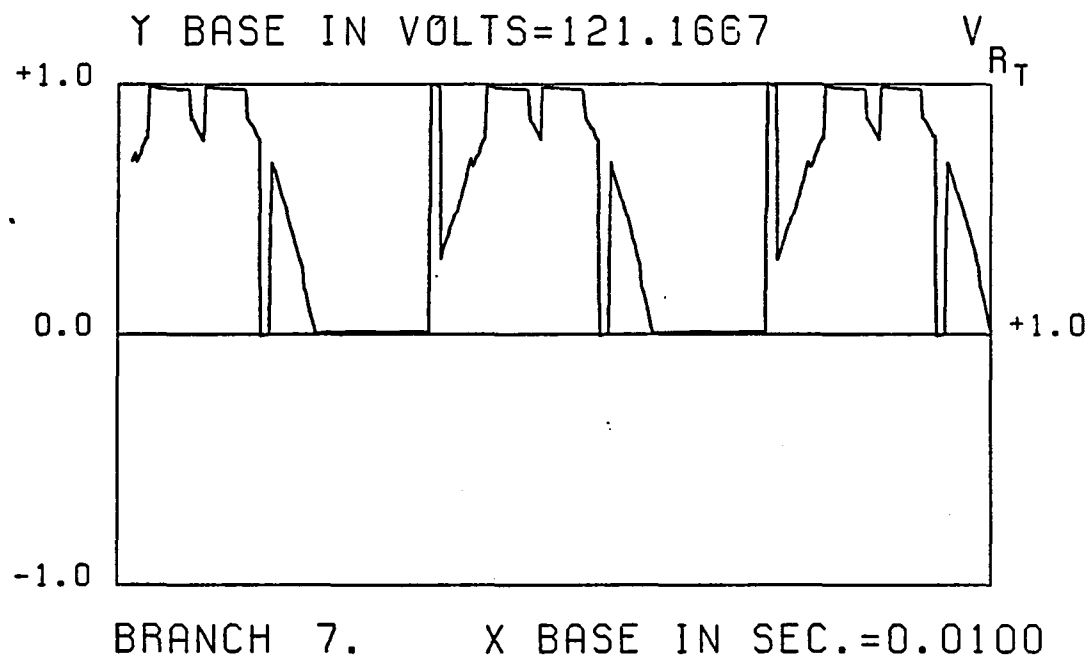
Figure (2.7-7) Predicted Waveform of the Inverter Switch Voltage

This feedback control is accomplished by external circuitry for the actual system and by a logical subroutine within the program. Both of the simulated waveforms and their corresponding oscillograms presented in Figure (2.7-8) through (2.7-11), reveal excellent correlation. Hence, both simulated motoring modes (with and without chopping) agree excellently with the actual system measurements.

Both of these motoring modes (with and without chopping) as well as additional verification of a portion of this modeling approach was presented earlier in reference [20] for the same system and will not be repeated here. In all cases, the agreement between measured and simulated results was excellent. What was not shown in reference [20] was the added feature to have a capability for handling mutual inductive coupling between the tree and cotree of a network. Also, the incorporation of an implicit versus an explicit integration routine , [19], reveals excellent correlation in every branch, with the improvement of less computation time. Also, the employment of the diode algorithm presented in Section 2.5 along with the implicit routine account for the improvement in computational efficiency and accuracy. The verification of the capability to handle mutual inductances between the tree and cotree of the overall system model will be discussed next.
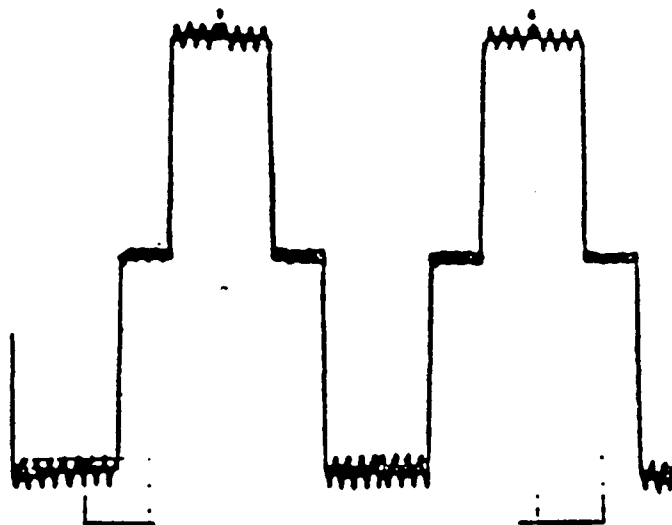
Figure (2.7-8) Oscillogram of the Phase Current
(Motoring with Chopping Control)

Y BASE IN VOLTS=24.8982
Y BASE IN AMPS.=85.0591
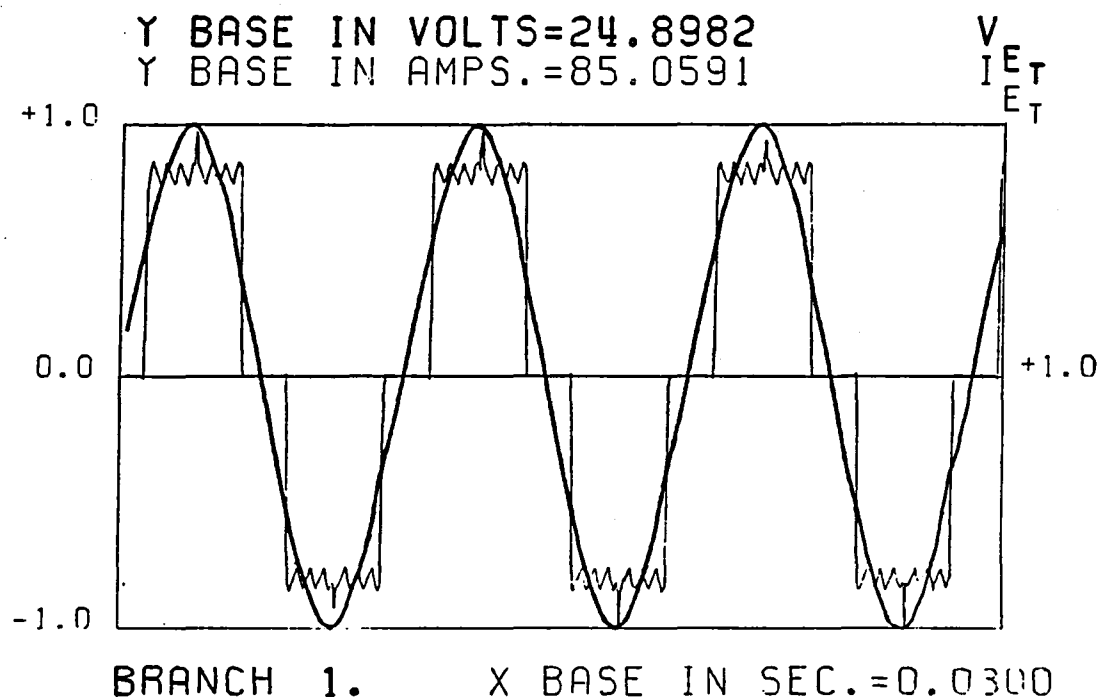
Figure (2.7-9) Predicted Waveform of the Phase Current
(Motoring with Chopping Control)
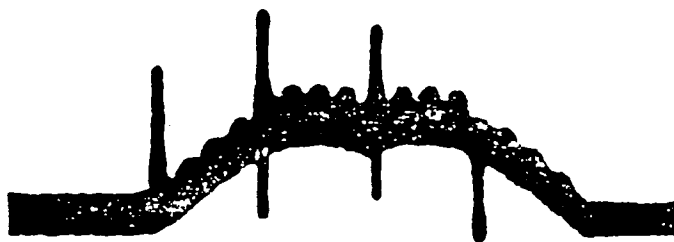
Figure (2.7-10)   Oscillogram of the Inverter Switch Voltage
(Motoring with Chopping Control)
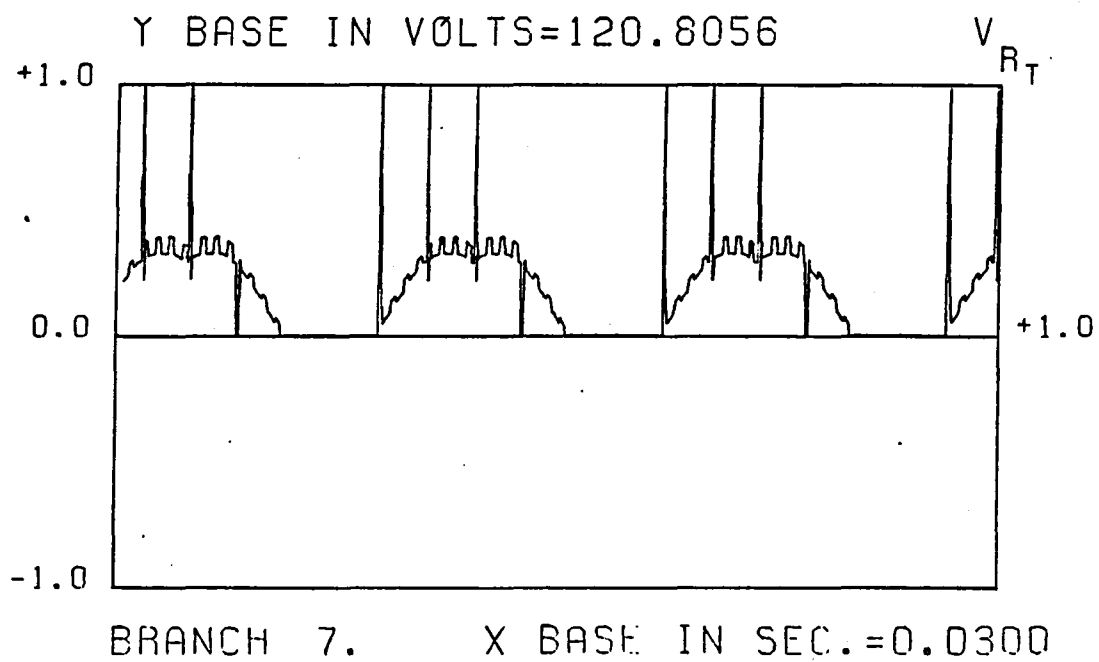
Figure (2.7-11) Predicted Waveform of the Inverter Switch
Voltage (Motoring with Chopping Control)

Further verification of the proposed modeling approach shall address the equality of representing the balanced machine's inductances as a lumped diagonal inductive matrix versus a full symmetric inductive matrix. Comparison of the simulated results obtained by both inductive matrices indicates the validity of the proposed matrix algebra. This novel approach includes the added feature which can automatically account for mutual coupling between the tree and cotree of the system network model, for any arbitrary windings. Further, the proposed matrix algebra is not restricted to balanced machine operation and is therefore directly amendable to fault analysis. Figures (2.7-5) and (2.7-7) represent the simulated phase current and inverter switch voltage, respectively, when the mutual terms are lumped with the self inductances.

Figures (2.7-12) and (2.7-13) represent the simulated phase current and inverter switch voltage, respectively, when the inductance matrix is full. A comparison of these waveforms reveals excellent correlation between these two sets of results. Details of the algebraic manipulations relating to this discussion can be seen in equations (2.3-62) and (2.3-64). The mutual inductance terms (those between the tree and cotree) are coupled via the hybrid matrix pre- and postmultiplications as shown in equation (2.3-62).

Y BASE IN VOLTS=62.2657
Y BASE IN AMPS.=147.5921

BRANCH 1.   X BASE IN SEC.=0.0100
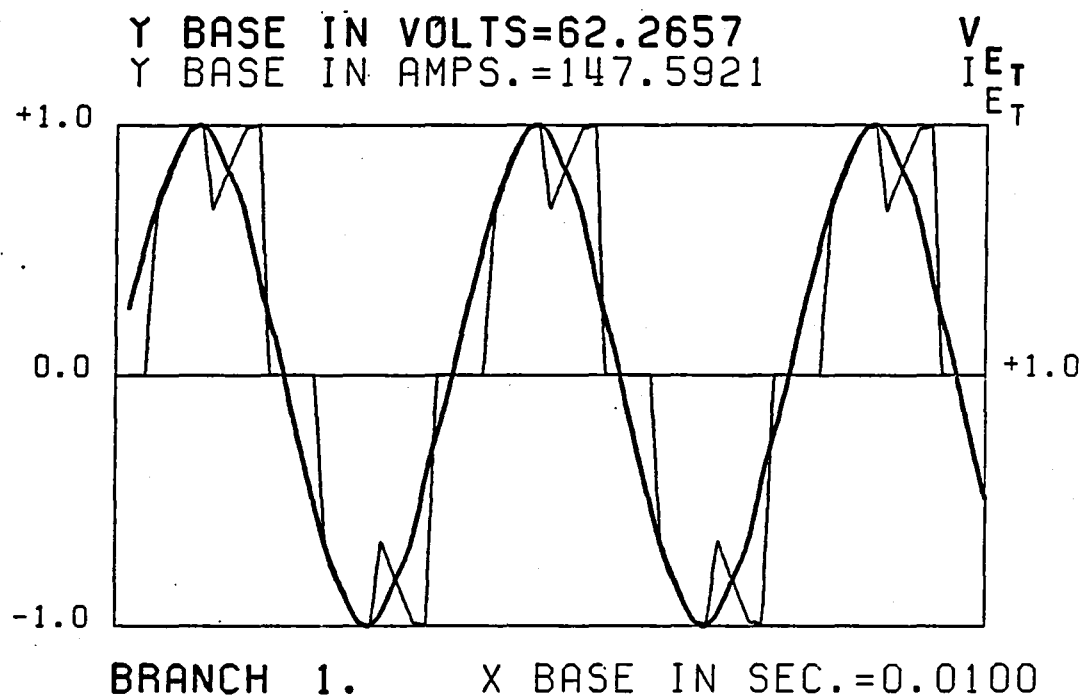
Figure (2.7-12) Predicted Waveforms of the Phase Current

Y BASE IN VOLTS=121.1273   V
Y BASE IN AMPS.=147.0264   I R_T
    R_T

BRANCH 7.   X BASE IN SEC.=0.0100
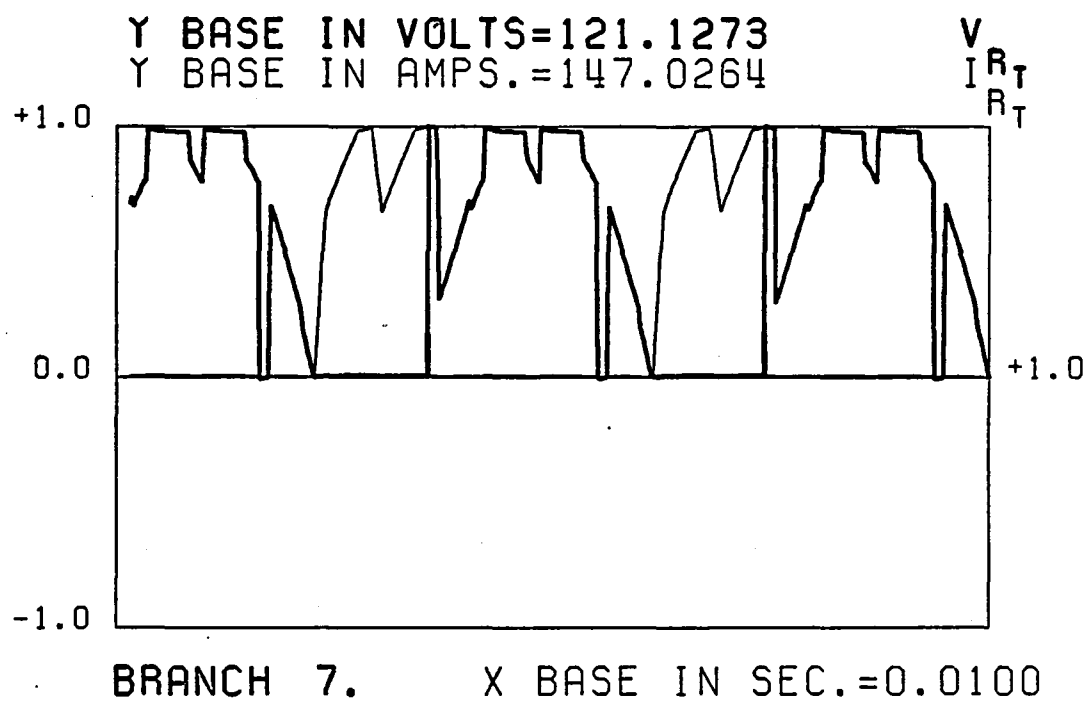
Figure (2.7-13) Predicted Waveforms of the Inverter Switch

To assess the validity of this verification, the influence of the mutuals upon the overall system performance was determined by simulating this same system while completely eliminating the mutuals from the full inductance matrix. The simulated waveforms, given in Figure (2.7-14), indicate an approximate 3 percent increase in the magnitude of the phase current for the case when the mutual terms were removed. The effects of the mutuals are mild, but noticeable, in this case and should not in general be ignored when simulating such systems considered in this report. The physical reason for the relatively weak (3 percent) effect of the mutuals is due to the relatively large effective air gap (which magnetically couples each of the stator windings). The effective air gap is larger because the permeability of the samarium-cobalt permanent magnets, located on the rotor, is very close to that of air. Hence, the mutual coupling between any of the armature windings is weak as indicated by these simulated results.

The next point of interest is how much influence the "off" resistance values of the diodes have upon the simulated waveshapes and magnitudes as well as the effect upon power delivered from the battery power source. Three

Y BASE IN VOLTS=62.2657   V
Y BASE IN AMPS.=150.0739   I E T
                                  E T

+1.0 ┤

0.0   +1.0

-1.0 ┤

BRANCH 1.   X BASE IN SEC.=0.0100
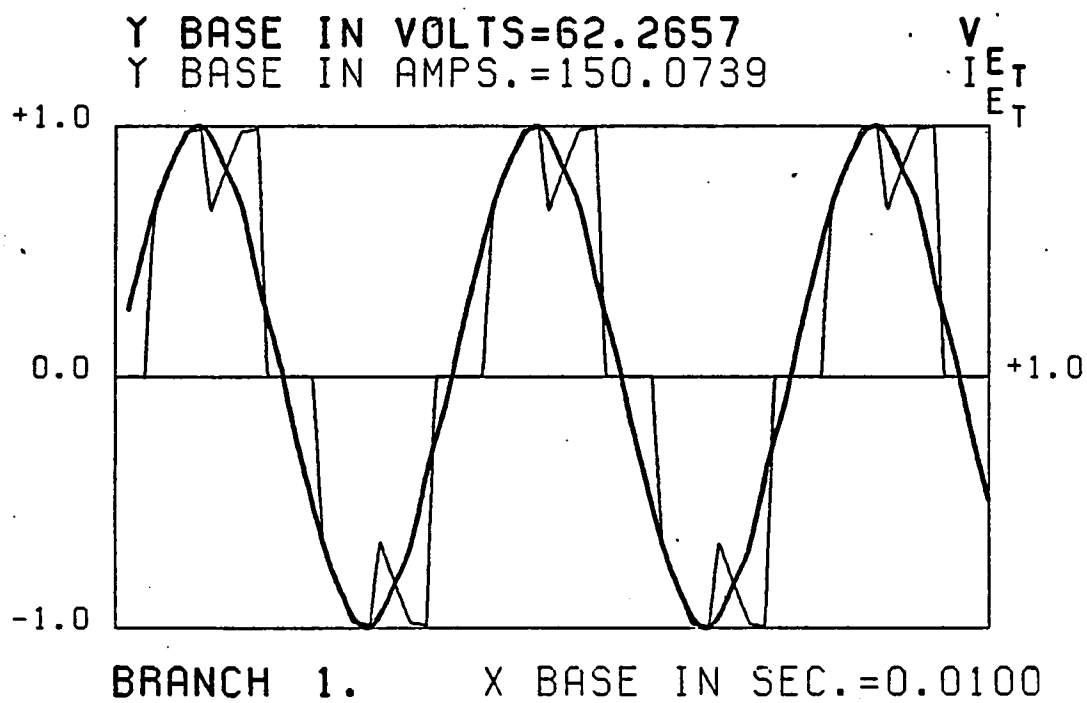
Figure (2.7-14) Predicted Waveforms of the Phase Current
(Mutuals Removed)

cases were run for different "off" resistance values but only the two extreme (minimum and maximum) cases are displayed. The low value of "off" resistance was set equal to 200 ohms and the maximum value was set at 20,000 ohms. This hundred fold difference in "off" resistance values resulted in less diode leakage current during the "off" state but the waveshapes were effectively unaltered. These runs were made by only varying the "off" resistance of the diodes not the transistors.

The two sets of diode waveforms agree closely for these two cases, as shown in Figures (2.7-15) through (2.7-18). The first set of diodes waveforms are for branch 23, the positive-Bus phase-A diode. The second set of voltage and current waveforms are for branch 22, the flyback diode. The actual location of these two branches in the overall network can be seen in Figures (2.7-2) and (2.7-3). Both sets of waveforms show little alteration in magnitude and waveshape as a result of the two values of R_{off}. This is also true for the next set of figures to be discussed. The average battery current can be obtained from Figures (2.7-19) and (2.7-20) for these two values of R_{off}. The ripple peak to peak is unaltered, hence the difference in the YBASE values of these Figures is equal to the difference in their average currents.
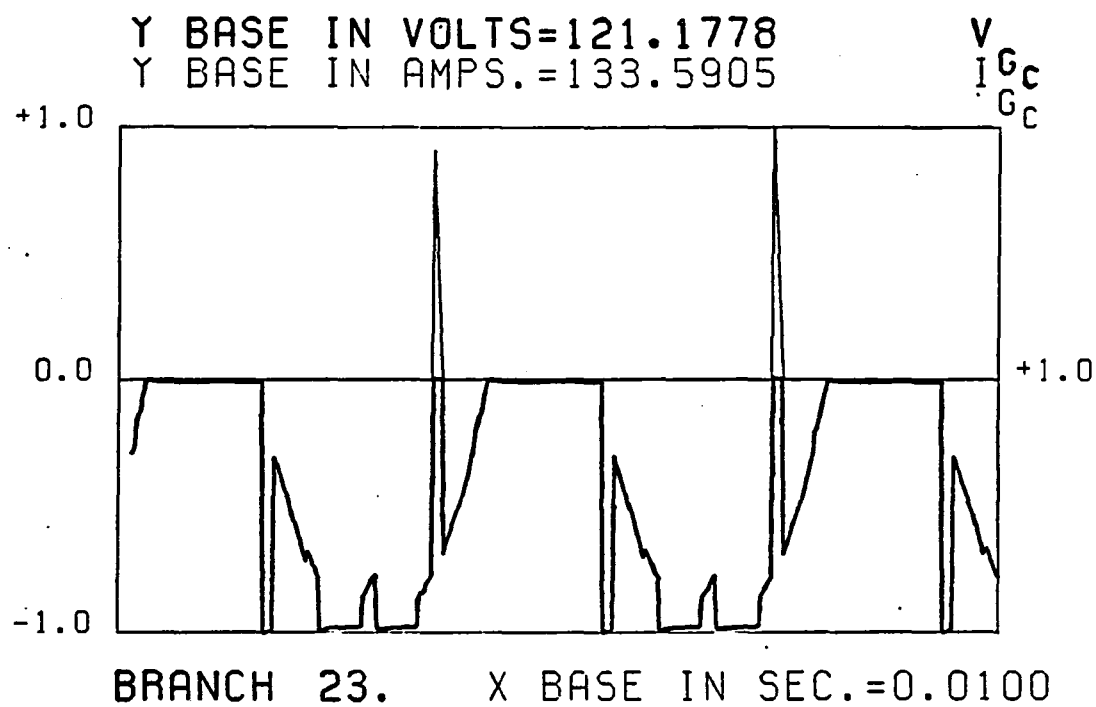
Figure (2.7-15)   Predicted phase A (+ bus) diode waveforms
for R_{off} = 20.0 kilo-ohms

Y BASE IN VOLTS=121.1359   V_{G_c}
Y BASE IN AMPS.=131.3243   I_{G_c}
                               G_c

BRANCH 23.   X BASE IN SEC.=0.0100
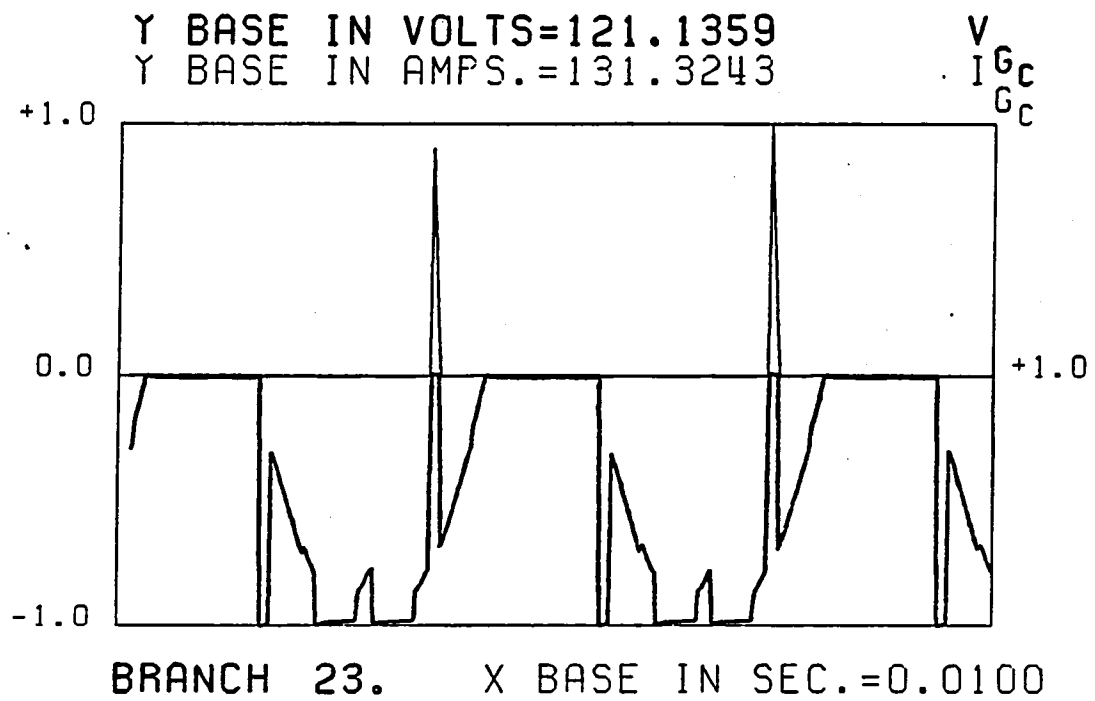
Figure (2.7-16)   Predicted phase A (+ bus) diode waveforms
                  for R_{off} = 0.2 kilo-ohms
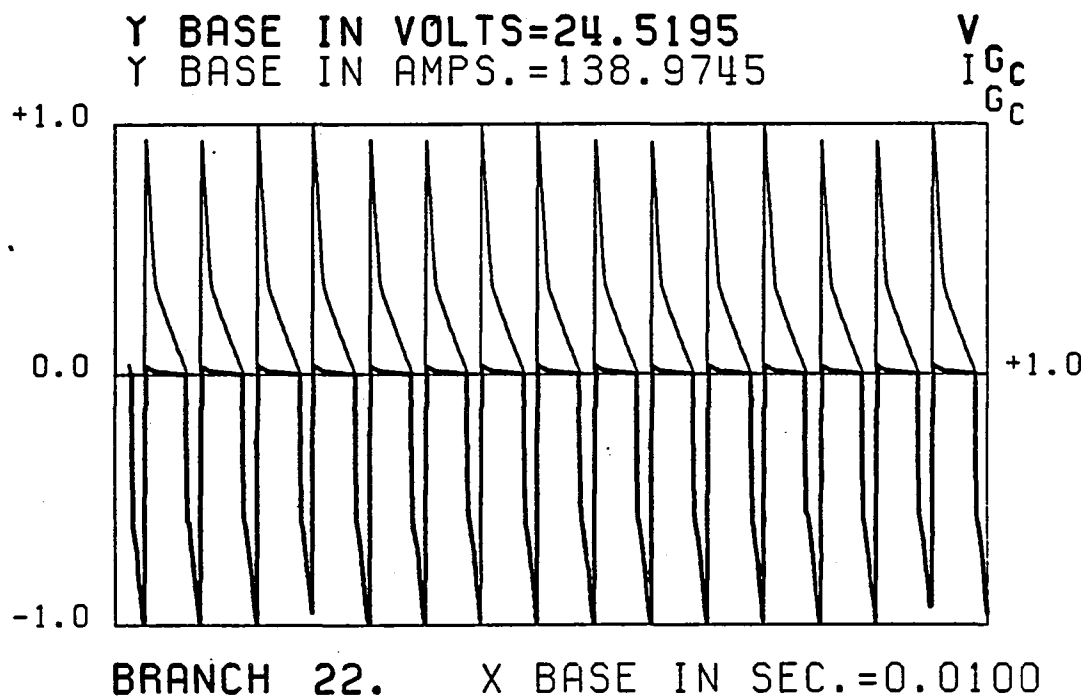
Figure (2.7-17)   Predicted (flyback) diode waveforms for
R_{off} = 20.0 kilo-ohms

- 143 -
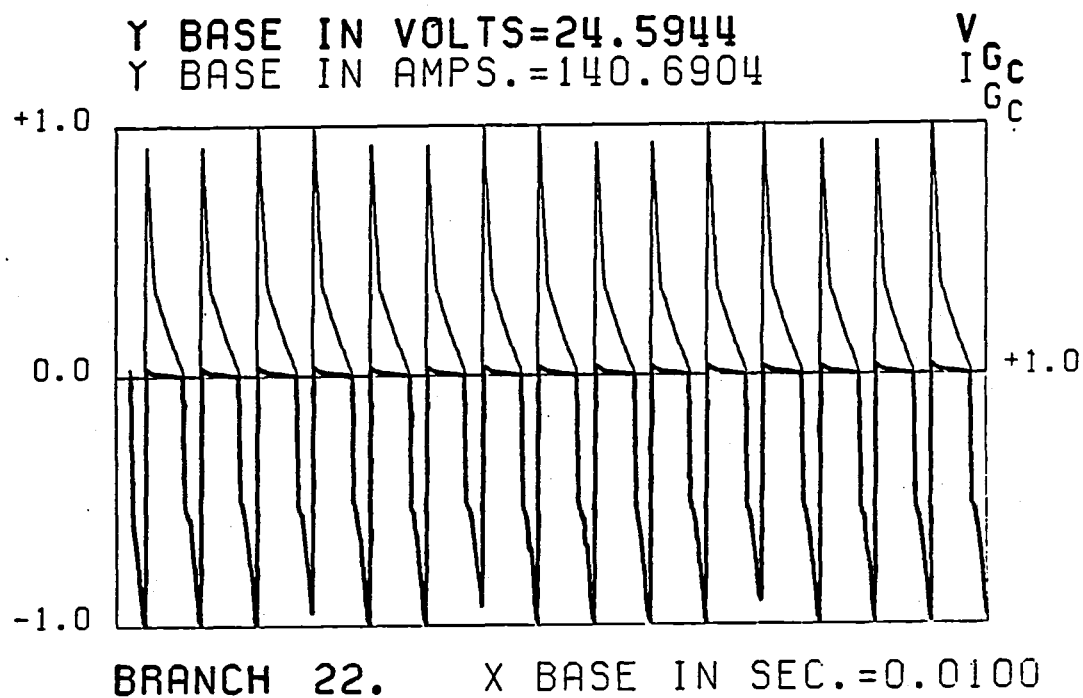
Figure (2.7-18)   Predicted (flyback) diode waveforms for
R_{off} = 0.20 kilo-ohms
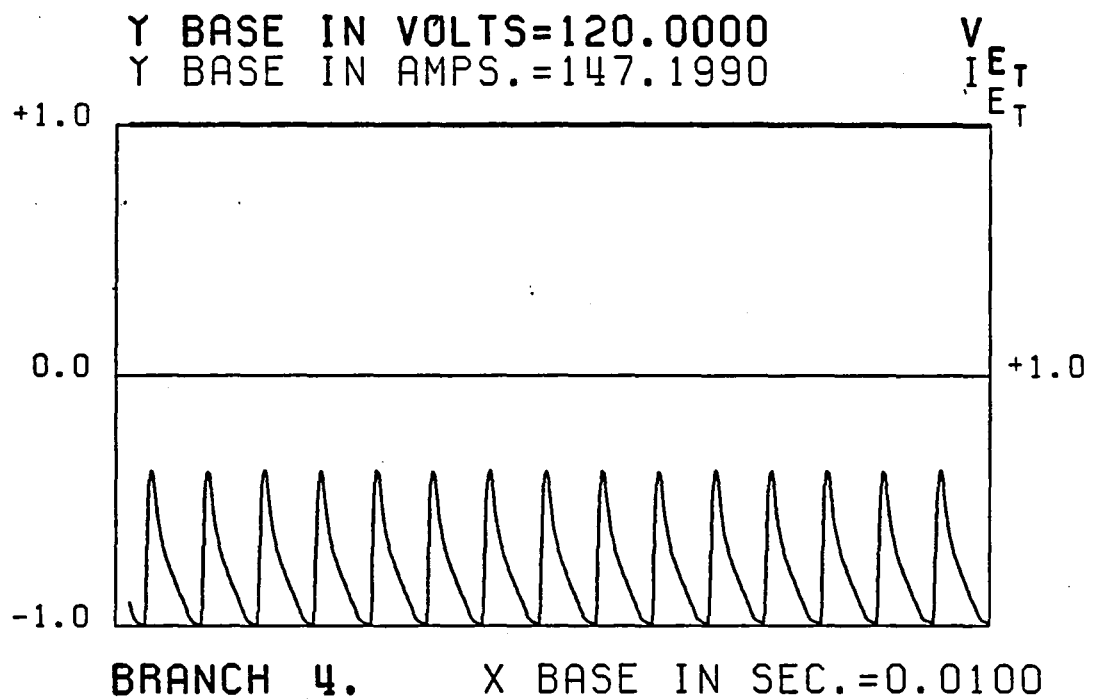
Figure (2.7-19) Predicted battery waveforms for R_{off} = 20.0 kilo-ohms

Y BASE IN VOLTS=120.0000   V E_T
Y BASE IN AMPS.=149.5750   I E_T

BRANCH 4.   X BASE IN SEC.=0.0100
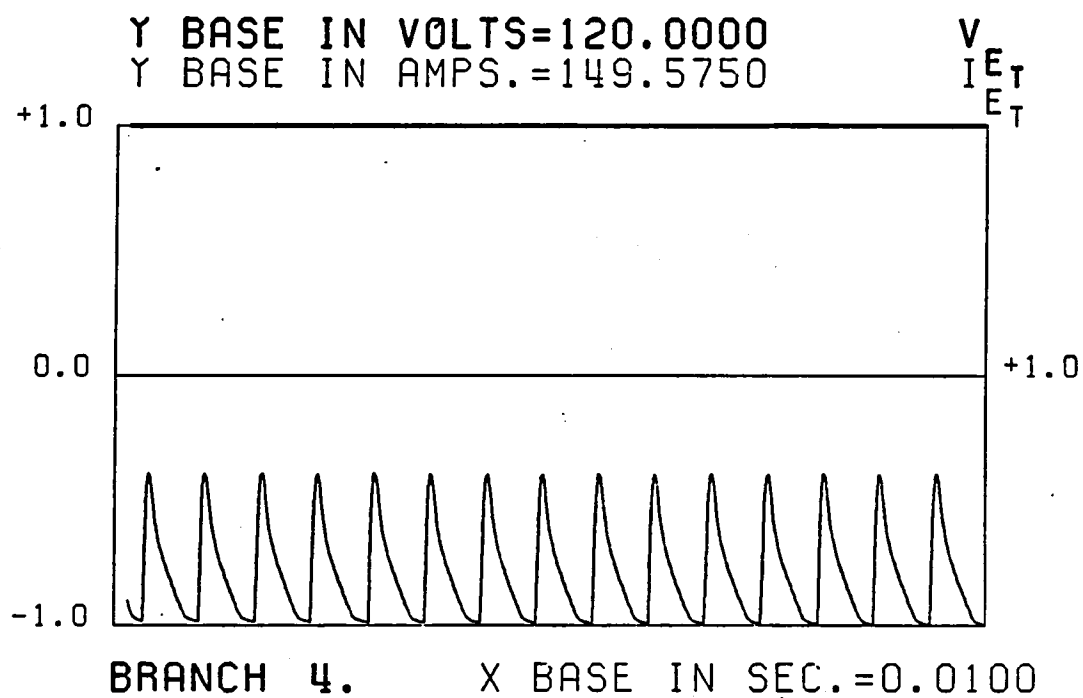
Figure (2.7-20)   Predicted battery waveforms for R_{off} = 200 kilo-ohms

In conclusion, the modeling approach presented here gives excellent results in comparison with test data for the types of systems considered in this report. It was shown that the voltage and current waveshapes are not affected noticeably by the choice of the "off" resistance, above 200 ohms in this case, for the solid state switches. However it was demonstrated that the "off" resistance is significant when calculating system efficiencies. Therefore, if efficiency calculations are not of interest when simulating such systems, the value of R_{off} can be relaxed. This relaxation is desirable since the computation cost increases with the increase of the value chosen for R_{off}. Furthermore, the ability to include mutual inductances in the machine model was demonstrated and verified against test data.

2.8 References Cited in Chapter (2.0)

1. Balabanian, N. and Bickert, T. A., _Electrical Network Theory_, New York: John Wiley and Sons, Inc., 1969.

2. Chua, L. O. and Lin, P., _Computer-Aided Analysis of Electronic Circuits: Algorithms and Computational Technique_. New Jersey: Prentice-Hall, Inc. 1975.

3. Arkadan, A. A. "Analysis of ac Brushless Exciters of Large Turbogenerators using Finite Elements", M. Sc. Thesis, _Virginia Polytechnic Institute and State University_, Aug. 1981.

4. F. A. Fouad, "Finite Element Analysis for Design of Classical and Electronically Operated Electric Machines," Ph.D. dissertation, Dept. Elec. Engr., Virginia Polytechnic Institute and State University, Blacksburg, VA, May, 1981.

5. Fouad, F. A., Nehl, T. W., and Demerdash, N. A., "Magnetic Field Modeling of Permanent Magnet Type Electronically Operated Synchronous Machines Using Finite Elements", _IEEE Transactions on Power Apparatus and Systems_, PAS-Vol. 100, 1981, pp. 4125-4135.

6. McMurray, W., "Hybrid Computer Simulation of a Controlled-Current Inverter Under Normal and Fault Conditions", _IEEE Transactions on Industry Applications Society_, No. 2, 1983, pp. 268.

7. Nehl, T. W., et. al., "Automatic Formulation of Models for Simulation of the Dynamic Performance of Electronically Commutated D. C. Machines", accepted by PES-IEEE for presentation at the PES 1985 Winter Meeting and for publication in the _IEEE Transactions on Power Apparatus and Systems_.

8. Edge, J. T., "An Electromechanical Actuator Technology Development Program", Paper No. 780581, _Society of Automotive Engineers_, Proceedings of the Aerospace _Fluid Power and Control Technologies Symposium_, 1978.

9. El-Sherbiny, M. K. and El-Serafi, A. M., "Analysis of Dynamic Performance of Saturated Machine and Analog Simulation", _IEEE Transactions on Power Apparatus and Systems_, July, 1982, pp. 1899.

10. Fink, D. G. and Carroll, J. M., _Standard Handbook for Electrical Engineers_, Tenth Edition, New York: McGraw-Hill Book Company, 1968.

11. Wu, F. F., "Existence of an Operating Point for a Nonlinear Circuit the Degree of Mapping", _IEEE Transactions on Circuits and Systems_, Vol. CAS-21, No. 5, 671-677, 1974.

12. Codrington, J. B., Pereira, L., and Falvey, H. T., "Computer Representation of Electrical System Interaction with a Hydraulic Turbine and Penstock", _IEEE Transactions on Power Apparatus and Systems_, No. 8, August, 1982, pp. 2611.

13. Cornell, E. P. and Lipo, T. A., "Modeling and Design of Controlled Current Induction Motor Drive Systems," _IEEE Transactions on Industry Applications_, Vol. IA-13, No. 4, 321-330, 1977.

14. Demerdash, N. A. and Nehl, T. W., "Dynamic Modeling of Brushless DC Motors -Power Conditioner Unit for Electromechanical Actuator Application", _IEEE Transactions on Aerospace and Electronis Systems_, 1979, pp. 333.

15. Demerdash, N. A. and Nehl, T. W., "Dynamic Modeling of Brushless DC Motors for Aerospace Actuation", _IEEE Transactions on Aerospace and Electronis Systems_, Vol., AES-16, No. 6, 1980, pp. 811-821.

16. Demerdash, N. A., Nehl, T. W., and Maslowski, E., "Dynamic Modeling of Brushless DC Motors in Electrical Propulsion and Electromechanical Actuation by Digital Techniques", _IEEE Transactions on Industry Applications Society_, 1980, pp. 570.

17. Carnahan, B., Luther, H. A. and Wilkes, J. O., _Applied Numerical Methods_. New York: John Wiley and Sons, Inc., 1969.

18. Gear, C. W., _Numerical Initial Value Problems in Ordinary Differential Equations_, Prentice-Hall, Englewood Cliffs, NY, 1971.

19. IMSL Library General Information Manual, Volume 1, International Mathematical and Statistical Libraries, Inc., Houston, TX.

20. Hijazi, M., "Automatic Formulation and Solution for the Nonlinear State Equations, for Electronically Operated Machines", M. S. Thesis, Virginia Polytechnic Institute and State University, August 1981.

21. Nehl, T. W., "A Discrete Time Model for a Power Conditioner Fed Permanent Magnet Brushless DC Motor

System for Aerospace and Electric Vehicle Applications for Design Purposes Using Finite Elements for Machine Parameter Determination", Ph.D. Dissertation, Dept. of Electrical Engineering, VPI&SU, Blacksburg, VA, May 1980.

22. Nehl, T. W., Fouad, F. A., Demerdash, N. A. and Maslowski, E., "Dynamic Simulation of Radially Oriented Permanent Magnet Type Electronically Operated Synchronous Machines with Parameters Obtained from Finite Element Field Solutions", IEEE Transactions on Industry Applications, Vol. IA-18, No. 2, 1982, pp. 172-182.

3.0 APPLICATION OF THE ACTUATOR MODEL TO VARIOUS MACHINE-POWER CONDITIONER CONFIGURATIONS

The actuator model developed in the previous chapter will now be applied to four additional PSA-machine configurations. These are a delta, open-delta, a wye and a wye with a shorted turn. It is assumed here that each of these systems has a separate chopper network. In general, however, the transistor switching logic routine can handle a number of different system configurations. The various options available are listed in Table (3.0-1). These options increase the flexibility of this model by allowing a large variety of possible configurations with a minimum amount of USER supplied input data.

In order to properly use this model, several conventions must be followed, see Figure (3.0-1). First the relationship between the phase and line currents for the delta type machines must satisfy the following relationship with respect to the line currents i_1, i_2, and i_3:

$$i_1 = i_a - i_c \tag{3.0-1}$$

$$i_2 = i_c - i_b \tag{3.0-2}$$

$$i_3 = i_b - i_a \tag{3.0-3}$$

these constraints result from KCL taken at the terminals of that machine.

Table (3.0-1) PSA Options

Variable Value / Variable Name		1	2	3
INVTP		Wye Connected Machine	Delta Connected Machine	Open-Delta Connected Machine
ICHOP .		Separate Chopper	Chopping Performed by Inverter	-
ICHOPT		Hysteresis	PWM	-
MODE		Motoring	Regen	Plugging
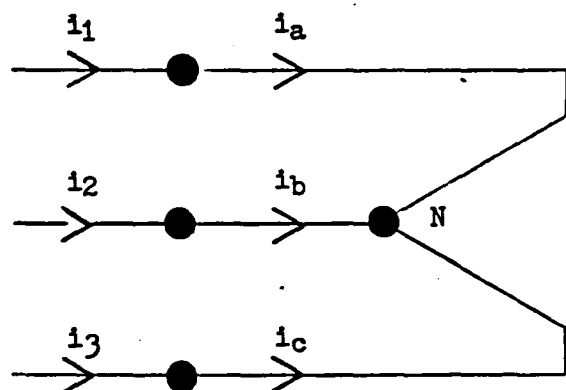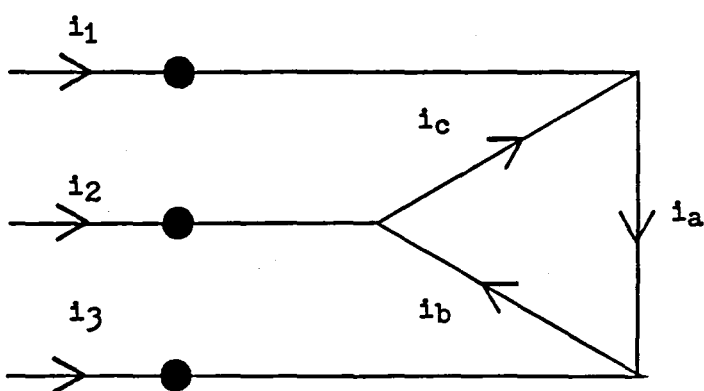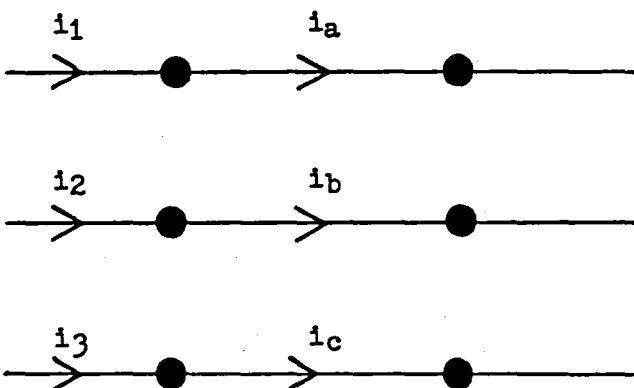
Figure (3.0-1)   Assumed Relationships Between Phase and Line
                 Currents

For the wye connected machine, the phase currents are equal to the line currents. This situation is shown in Figure (3.0-1). It is also assumed that the fundamental components of the forcing functions obey the following phase relationships:

$$e_a = E_m \sin(\delta t + \theta_x) \qquad (3.0-4)$$

$$e_b = E_m \sin(\delta t + \theta_x - 120) \qquad (3.0-5)$$

$$e_c = E_m \sin(\delta t + \theta_x - 240) \qquad (3.0-6)$$

The phase voltages must be of this form otherwise the transistor switching signals would be incorrect.

Another factor which must be taken into account when preparing a simulation run is the assignment of labels for the power transistors, Q_1, Q_2,...,Q_{12}. This information is given in Table (3.0-2). Notice that each of the inverter transistors is associated with one of the line currents i_1, i_2, or i_3. The sign of the line current into the machine, (+) or (-), is determined by which of the two transistors, attached at each machine terminal, is "on".

Similarily, the assumed numbering of the chopper transistors is given in Table (3.0-3). Transistors Q7 or Q13 are used for motoring while Q8 or Q14 are used for regeneration.

The line currents, in all cases, are assumed to be rectangular blocks of 120 electrical degrees duration. The line current i_1 is initiated 30 degrees after the emf of phase (A) passes through zero in the positive direction. The second and third line currents are initiated in a similar fashion 120 and 240 degrees later, respectively.

TABLE (3.0-2)   Inverter Transistor Numbering

MACHINE/ INVERTER TYPE	ACTIVE TRANSISTORS			SIGN OF INJECTED LINE CURRENT
	i_1	i_2	i_3	
WYE	Q1	Q2	Q3	(+)
	Q4	Q5	Q6	(−)
DELTA	Q1	Q2	Q3	(+)
	Q4	Q5	Q6	(−)
OPEN DELTA	Q1 Q2	Q3 Q4	Q5 Q6	(+) (−)
	Q7 Q8	Q9 Q10	Q11 Q12	(−) (+)

TABLE (3.0-3) Chopper Transistor Numbering

MACHINE/ INVERTER TYPE	CHOPPER TRANSISTORS	
	WITH SEPARATE CHOPPER	WITHOUT SEPARATE CHOPPER
WYE	Q7,Q8	Q1-Q6
DELTA	Q7,Q8	Q1-Q6
OPEN DELTA	Q13,Q14	Q1-Q12

The parameters used in the four simulations which are presented next are based upon the system analyzed in the previous chapter. In the case of the delta connected machine, the number of turns per phase is increased by a factor of $\sqrt{3}$. It was assumed that the copper volume remained constant, therefore one can write

$$Vol_{CU} = \ell_y A_y = \ell_\Delta A_\Delta \qquad (3.0-7)$$

$$\sqrt{3}\ell_y = \ell_\Delta \qquad (3.0-8)$$

where ℓ_y, A_y, ℓ_Δ, A_Δ are the lengths and crossectional areas of wye and delta machines, respectively. Using this information one can relate the winding resistances of the two cases as follows:

$$R_\Delta = 3R_y \qquad (3.0-9)$$

The inductances also increase by the square of the turns ratio, that is

$$L_\Delta = 3L_y \qquad (3.0-10)$$

Once all of the machine parameters were scaled properly, these parameters were then substituted into the model and the simulated waveforms were obtained. The network graphs corresponding to these three cases are given in Figures (3.0-2), (3.0-3) and (3.0-4). Representative samples of simulated branch voltage and current waveforms are given in Sections 3.1 through 3.3 for the network graphs (models) of Figures (3.0-2) through (3.0-4), respectively. Saturation effects in the machine were neglected in all three cases. It was also assumed that there were no faults . The machine speed in all three cases was 7750 rpm (4 poles).

The effects of a shorted turn in phase (A) of the wye connected machine are given in Section 3.4.
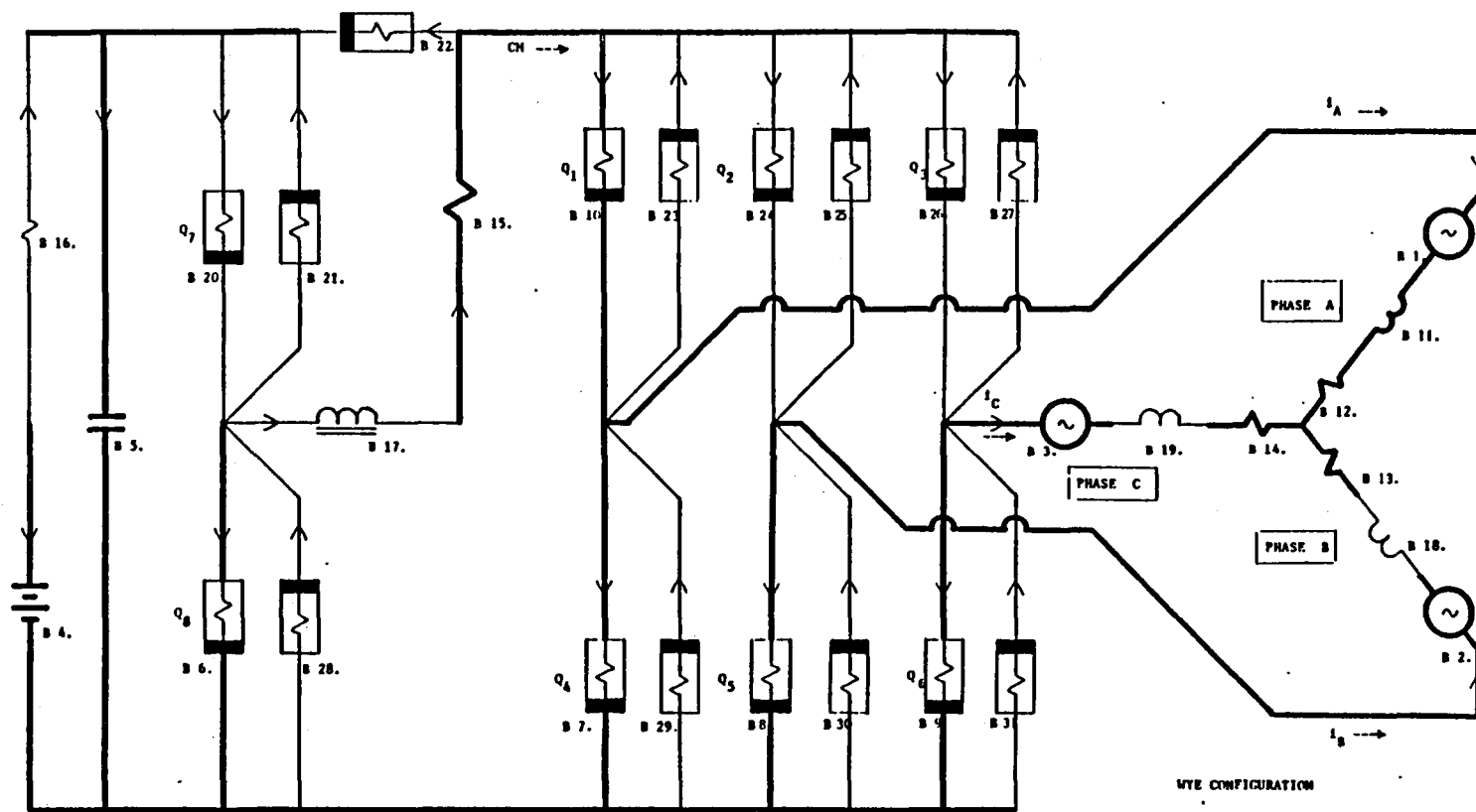
Figure (3.0-2) Network Graph of WYE Configuration
(Unfaulted)

Figure (3.0-3) Network Graph of DELTA Configuration
(Unfaulted)
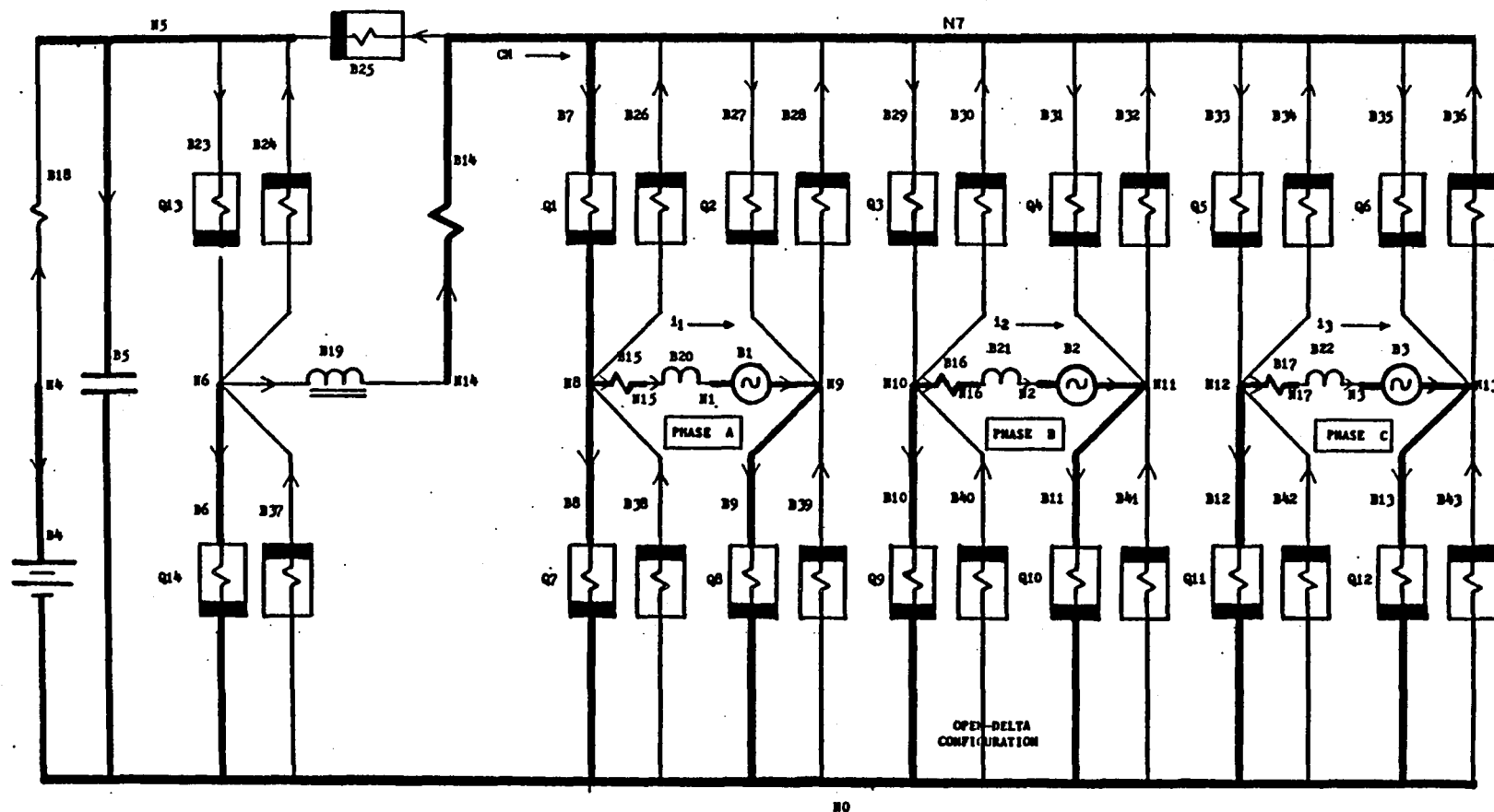
Figure (3.0-4) Network Graph of Open-DELTA Configuration
(Unfaulted)

3.1 Simulated Waveforms of the WYE Configuration

The simplified (with chopper) schematic diagram of Figure (1.0-1) for the WYE configuration, and its corresponding complete network graph (including chopper) of Figure (3.0-2) should be referred to in reviewing the results of simulations presented in this section. These simulations represent unfaulted normal motoring operation. The input data used in obtaining these results are given in Table (3.1-1). Identification of all the displayed voltage and current simulated waveforms is given in Table (3.1-2).

The calculated average electromagnetic machine power during the last cycle is 12,617 watts. The corresponding copper losses in the machine totaled 218.7 watts.

TABLE (3.1-1) Input Data for Network Model of the WYE

Configuration (Unfaulted)

```
 _____

    Three Phase Balanced Machine Model:


  Branch #12 Phase(A) Winding Resistance=6.8 milli-ohms
  Branch #11 Phase(A) Winding Inductance=52 micro-henries

 Inverter/Converter Bridge & Chopper Switching Components:

          Branch #10 (+Bus) Phase(A) Transistor
          Saturation Resistance "on" = 6.4 milli-ohms
          Cutoff Resistance     "off" = 2.0 killo-ohms

          Branch #23 (+Bus) Phase(A) Diode
          Forward-Biase Resistance "on" = 6.4 milli-ohms
          Reverse-Biase Resistance "off"= 2.0 killo-ohms

 Chopper Choke:

    Branch #15 Choke Resistance = 24 milli-ohms
    Branch #17 Choke Inductance = 1.5 milli-henries

 DC Power Source:

    Branch #5 Filter Capacitor = 7.8 milli-farrads
    Branch #4 Battery(Internal) Voltage = 120.0 Volts
    Branch #16 Battery(Internal) Resistance = 5 milli-ohms

 _____
```

Table (3.1-2) Branch Identification WYE Configuration
              (Unfaulted)

| Figure Number	Branch Number	Branch Identification
3.1-1	1	Phase (A) Back Emf
3.1-2	11	Phase (A) Winding Inductance
3.1-3	10	Phase (A) Transistor (+Bus)
3.1-4	23	Phase (A) Diode (+Bus)
3.1-5	7	Phase (A) Transistor (-Bus)
3.1-6	29	Phase (A) Diode (-Bus)
3.1-7	4	Battery Internal Voltage
3.1-8	17	Chopper Inductance
3.1-9	20	Chopper (+Bus) Transistor
3.1-10	21	Chopper (+Bus) Diode
3.1-11	6	Chopper (-Bus) Transistor
3.1-12	28	Chopper (-Bus) Diode
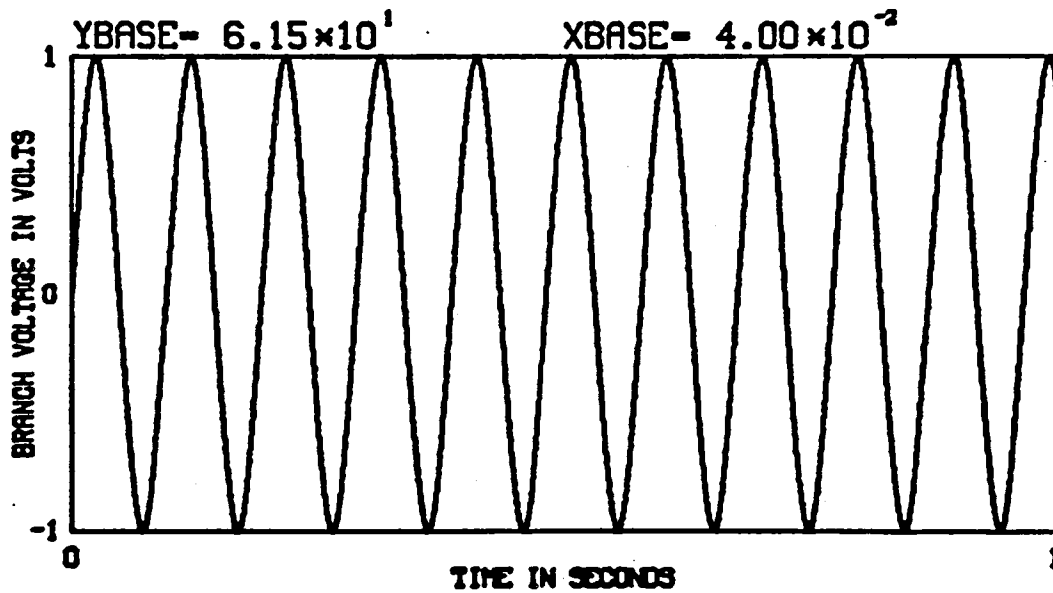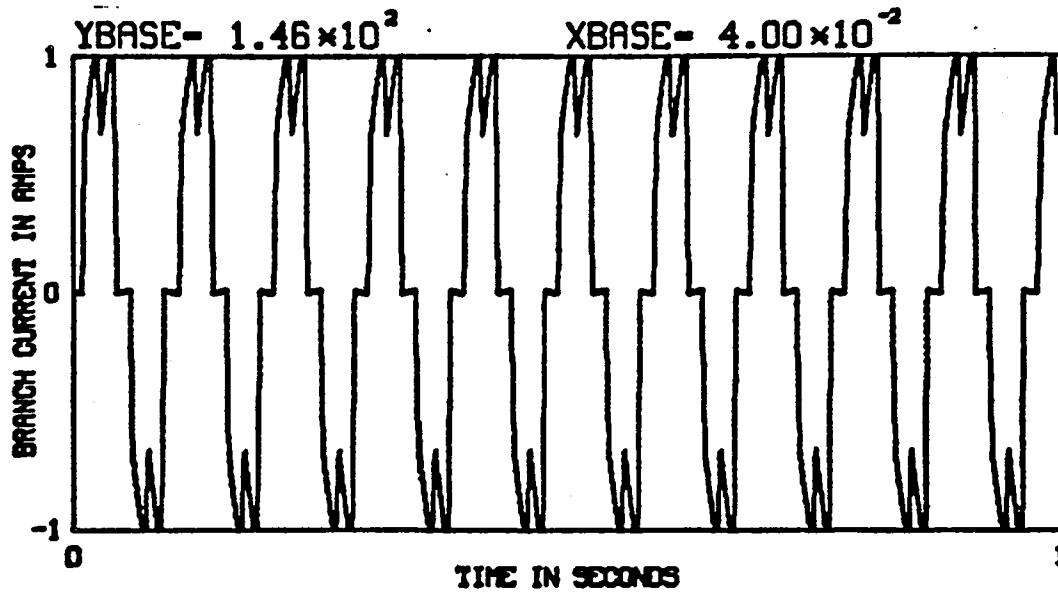
Figure (3.1-1)   Simulated Current and Voltage Waveforms for
Branch #1, WYE Configuration (Unfaulted)
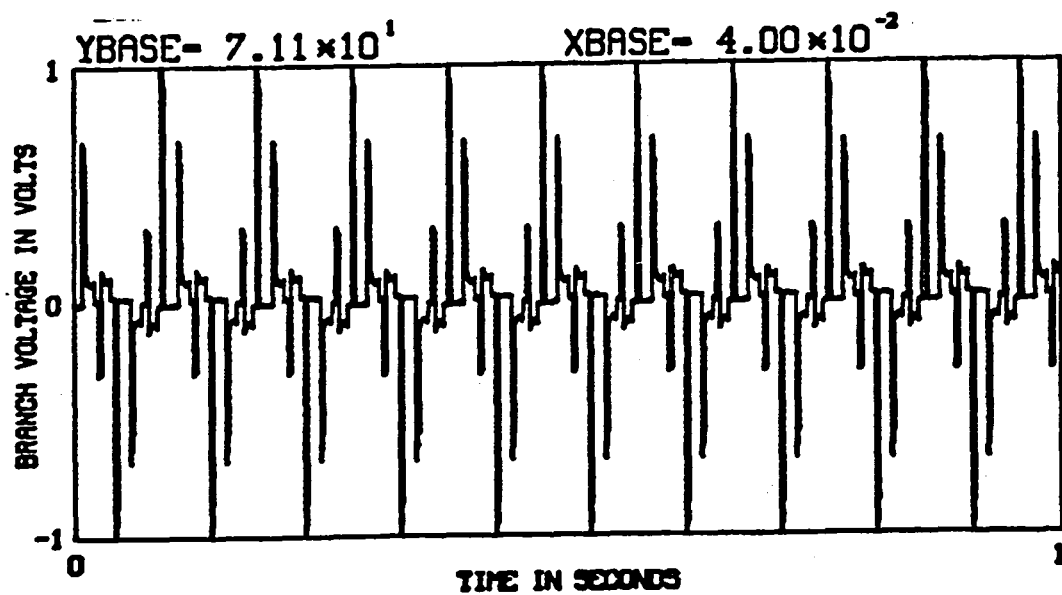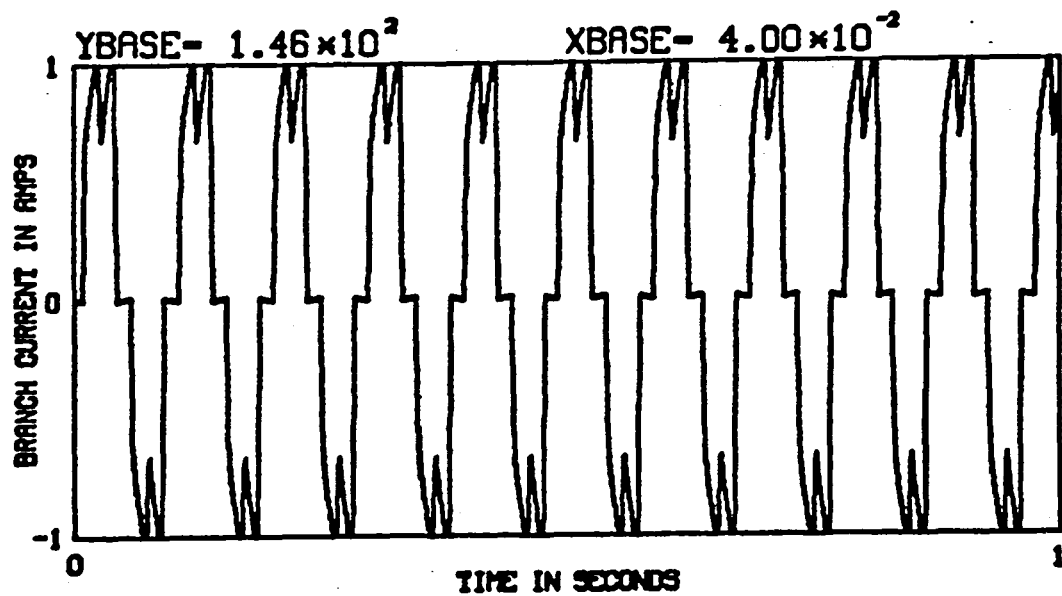
Figure (3.1-2)   Simulated Current and Voltage Wavefors for
                 Branch #11, WYE Configuration (Unfaulted)
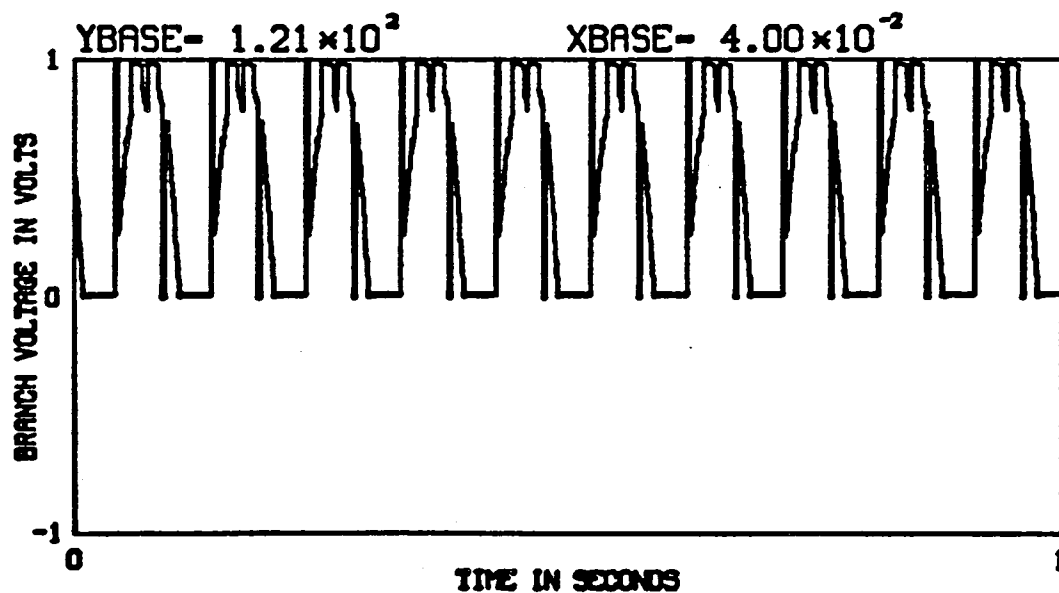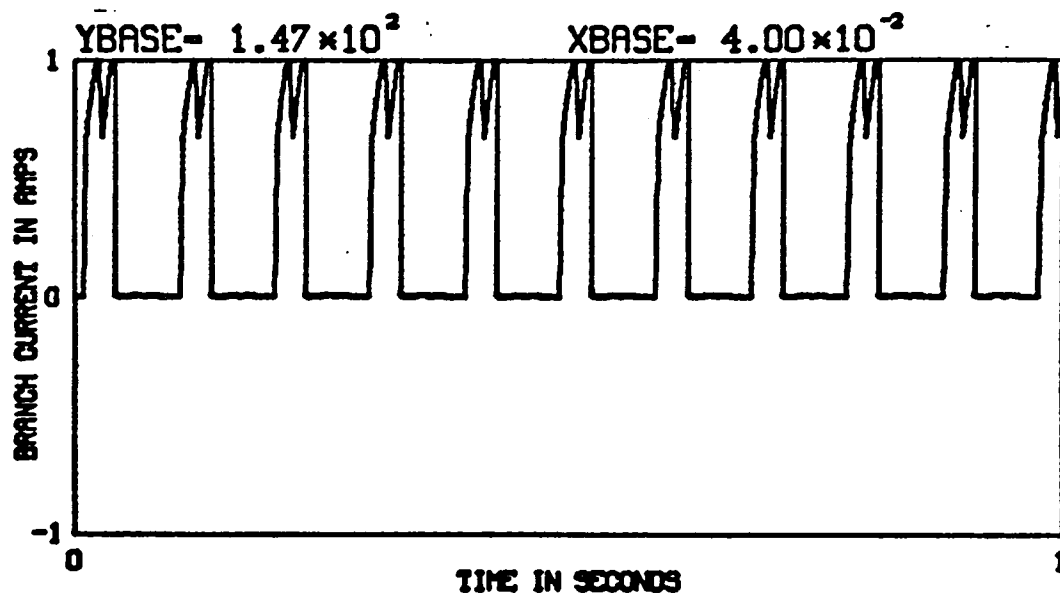
Figure (3.1-3)   Simulated Current and Voltage Waveforms for
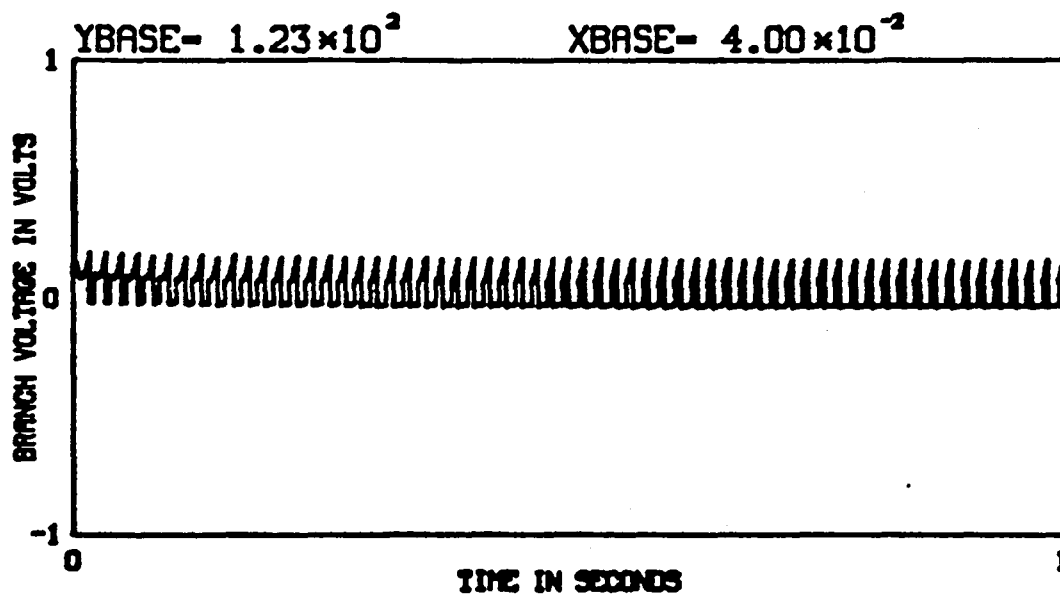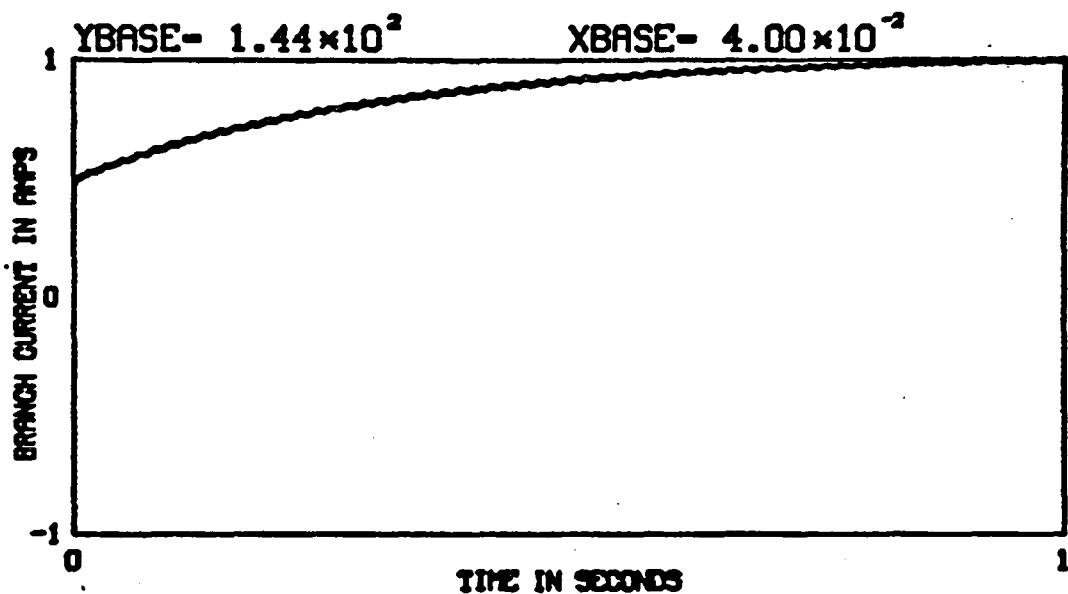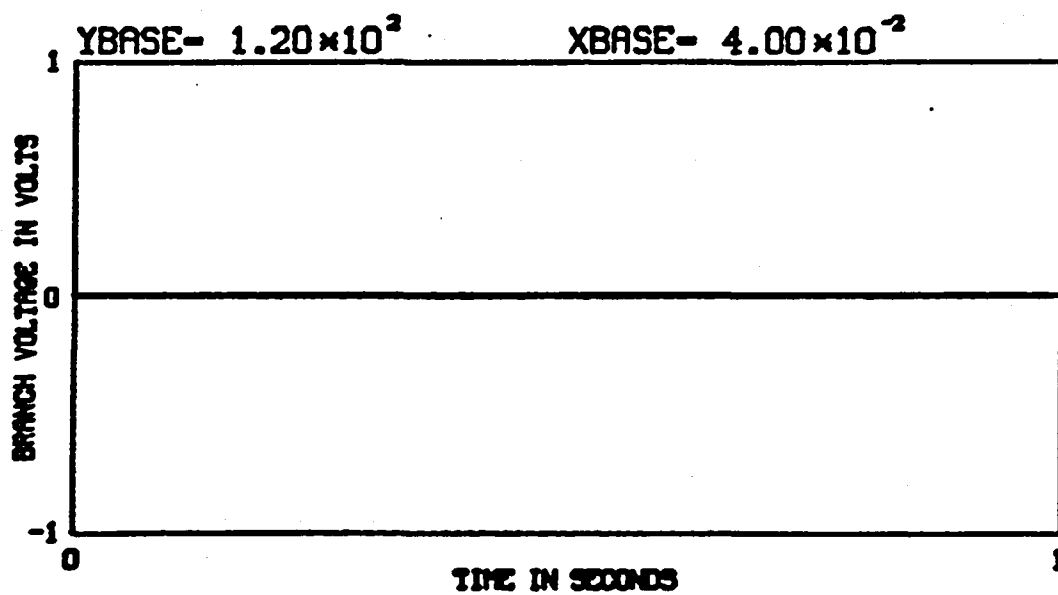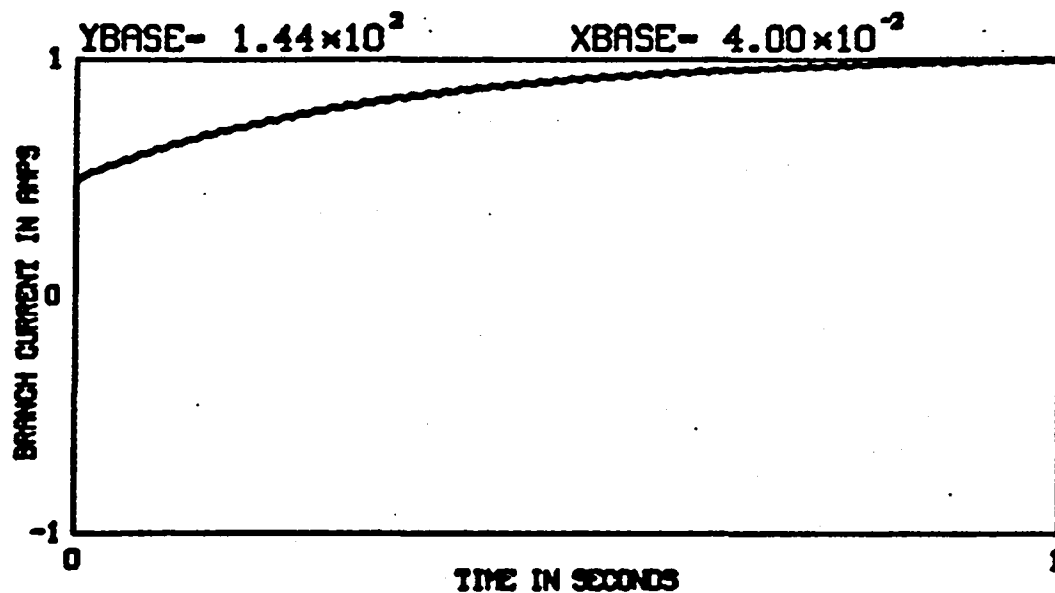   Branch #10, WYE Configuration (Unfaulted)
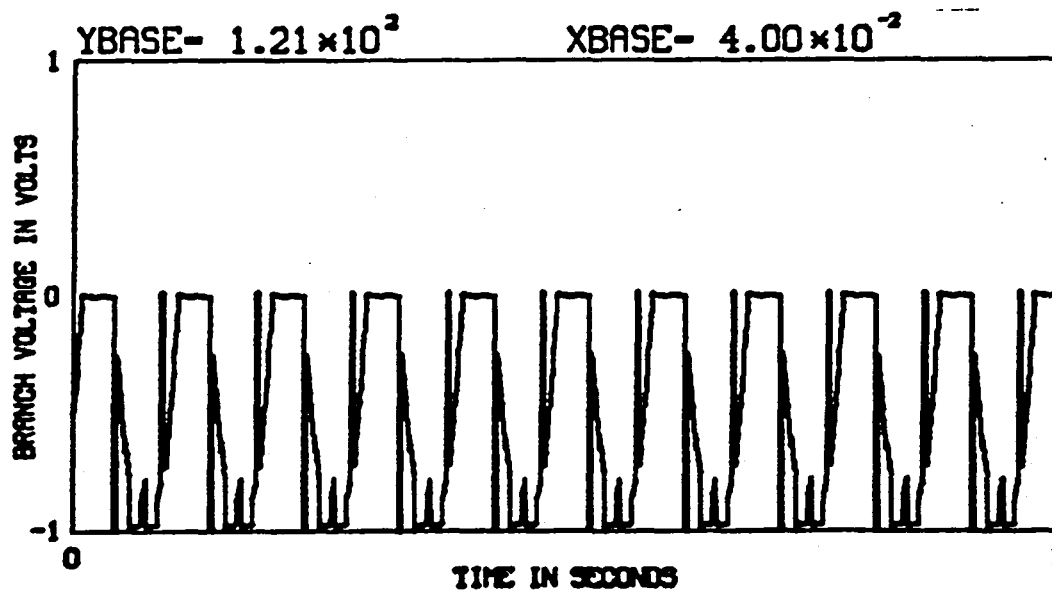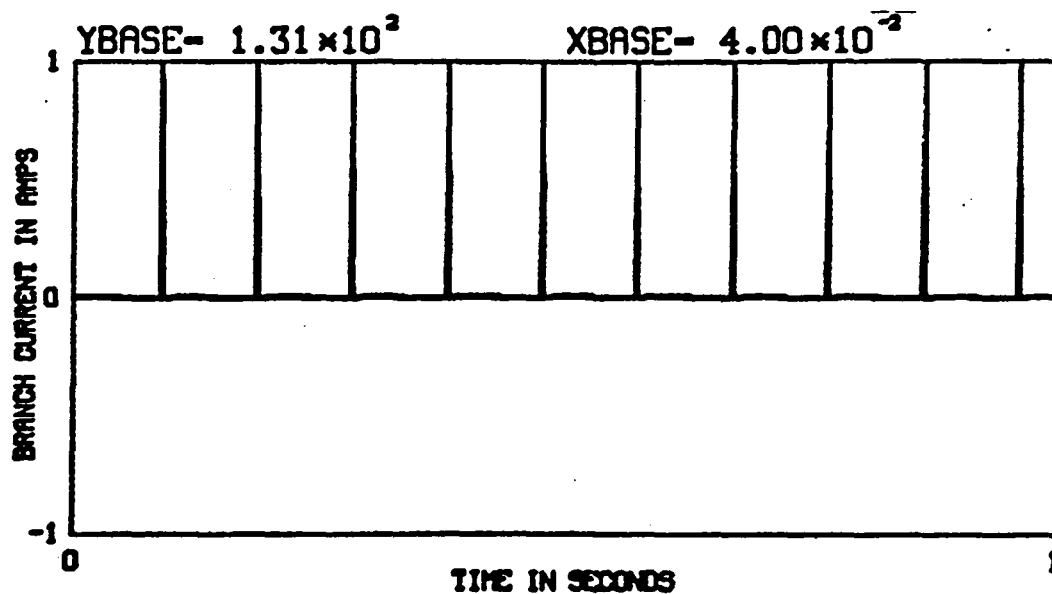
Figure (3.1-4)   Simulated Current and Voltage Waveforms for
                 Branch #23, WYE Configuration (Unfaulted)

- 166 -
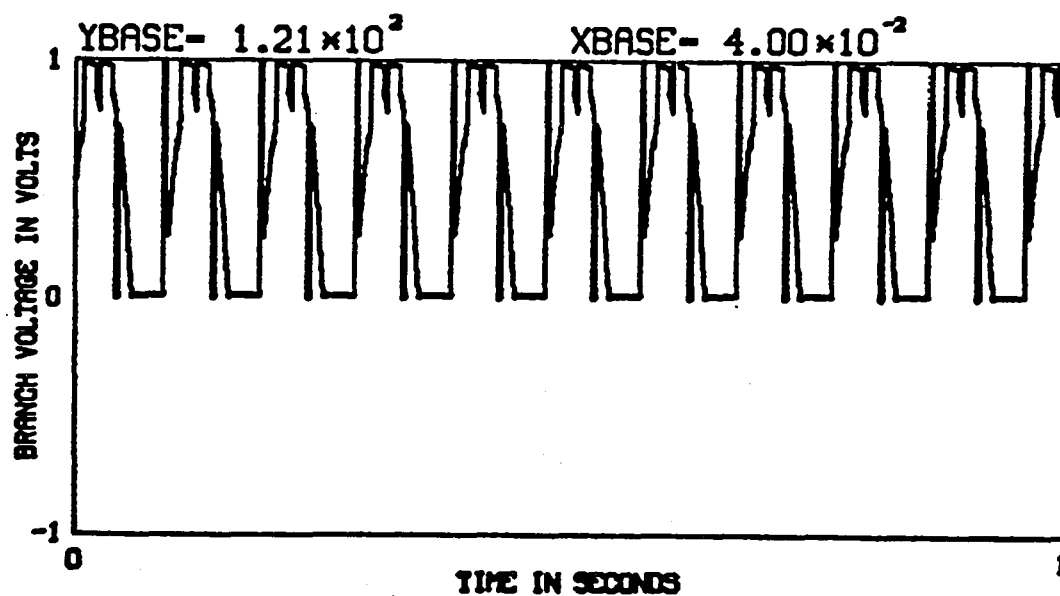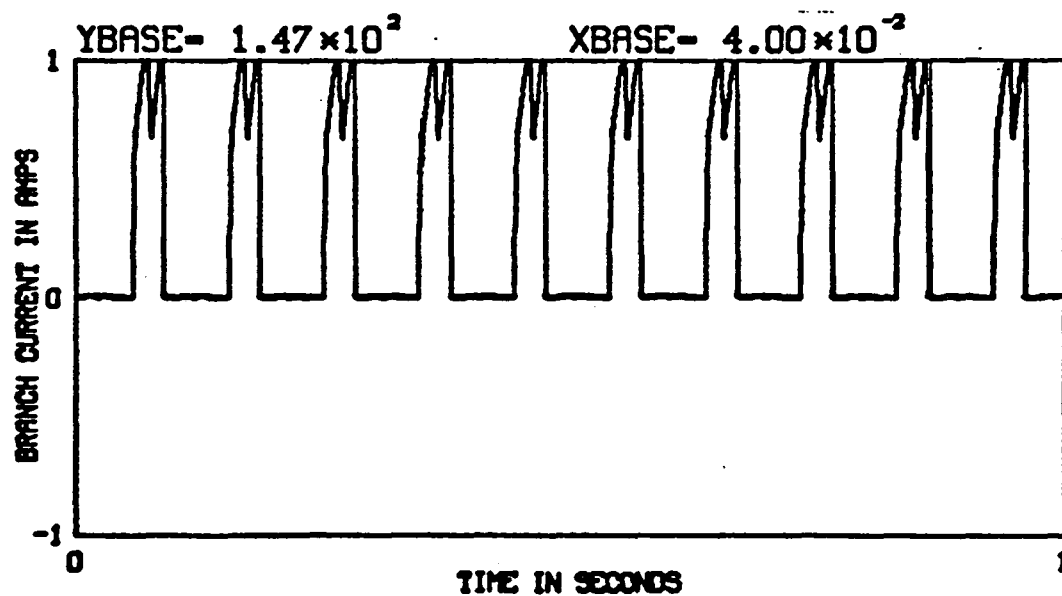
Figure (3.1-5)   Simulated Current and Voltage Waveforms for
Branch #7, WYE Configuration (Unfaulted)
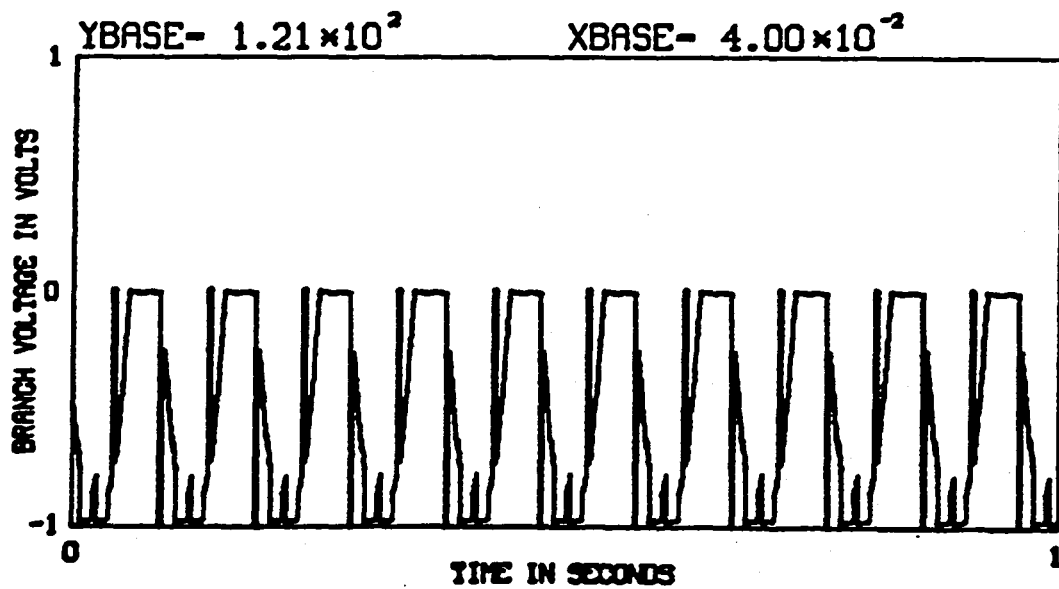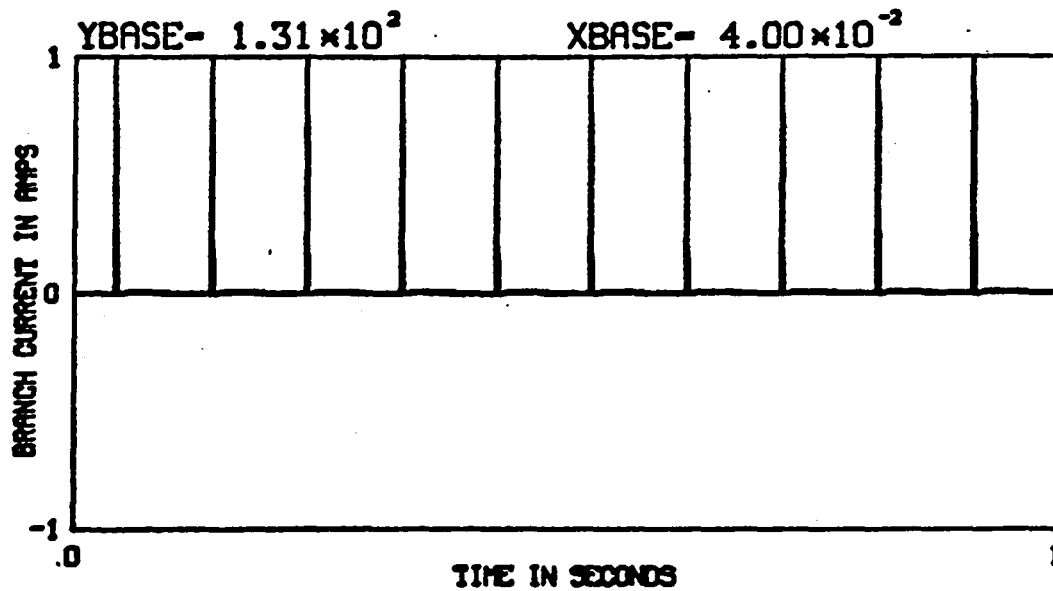
Figure (3.1-6)   Simulated Current and Voltage Waveforms for
                 Branch #29, WYE Configuration (Unfaulted)
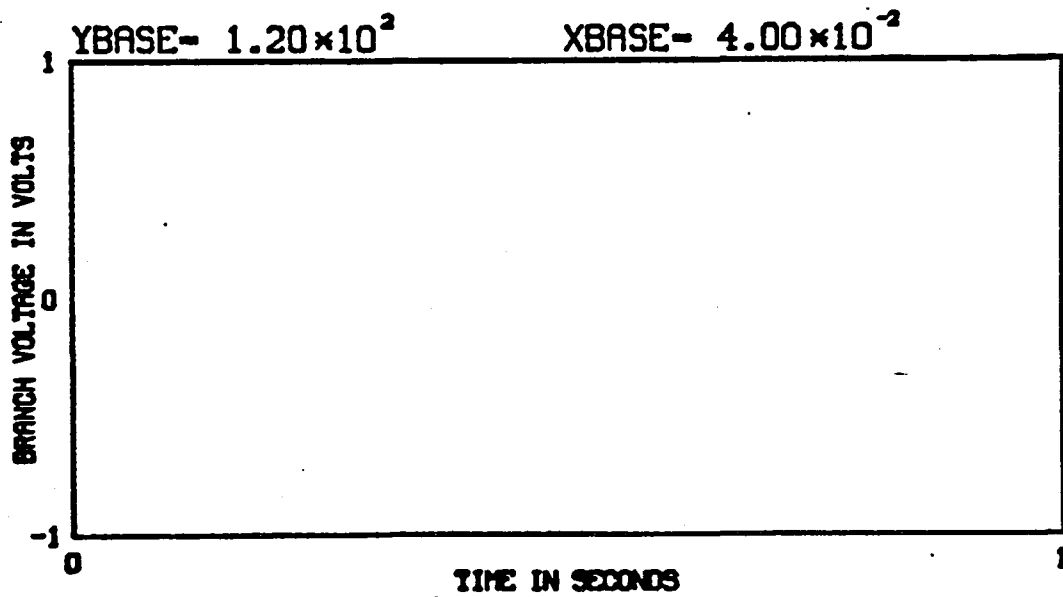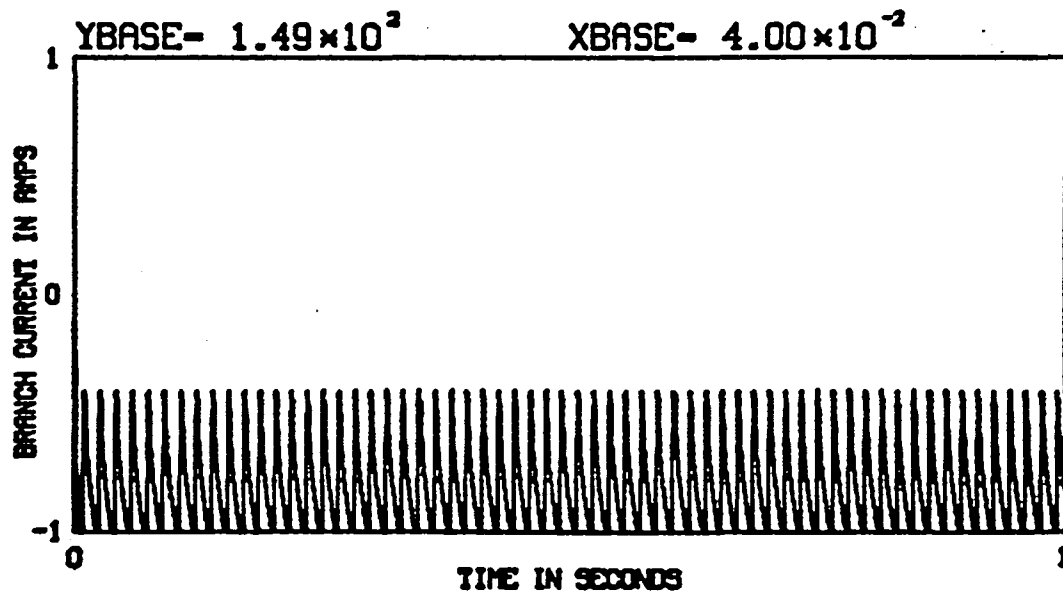
Figure (3.1-7)   Simulated Current and Voltage Waveforms for
Branch #4, WYE Configuration (Unfaulted)
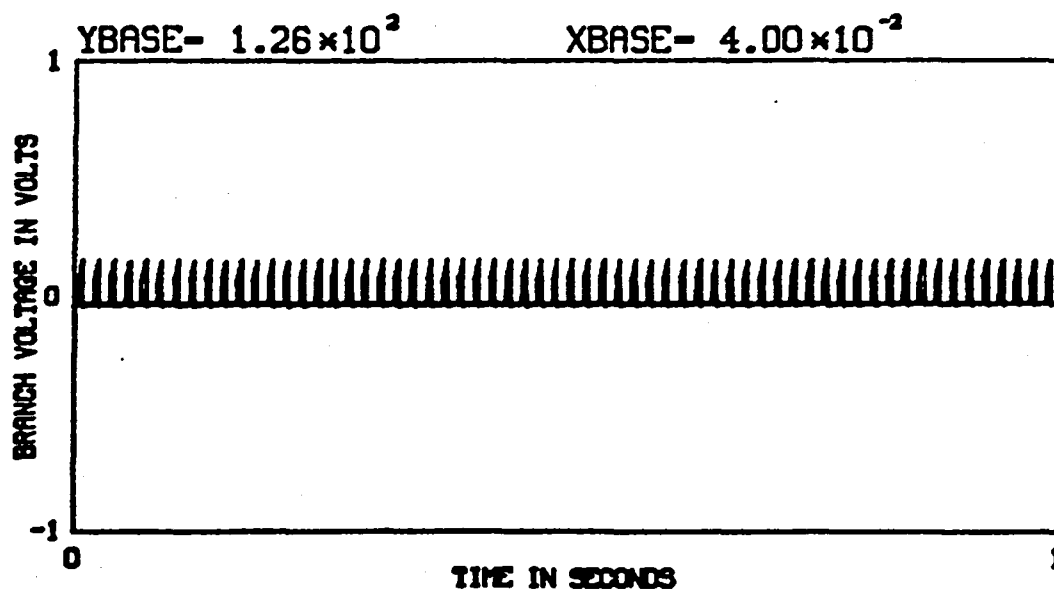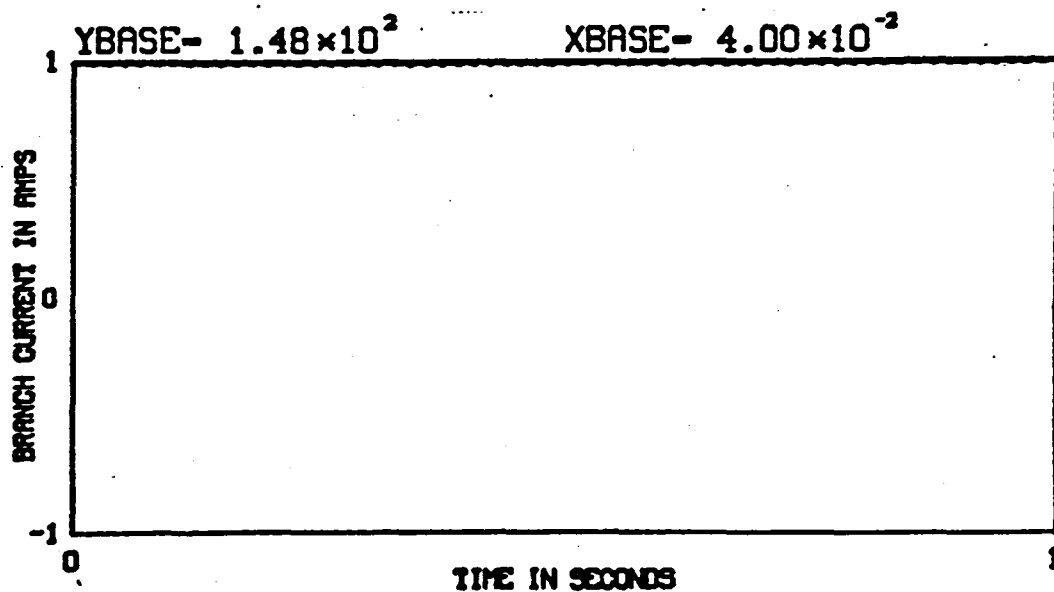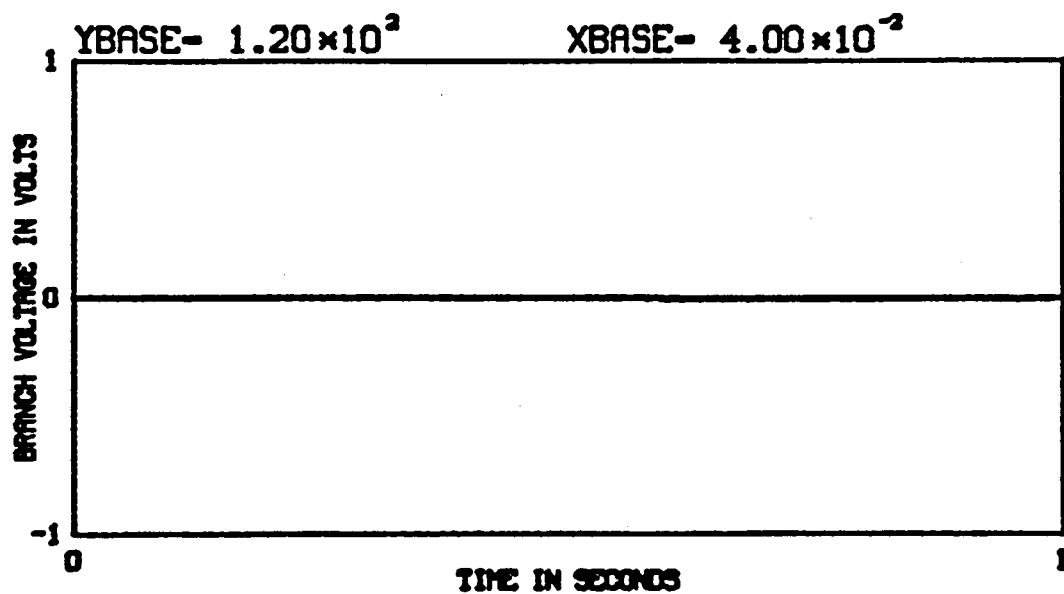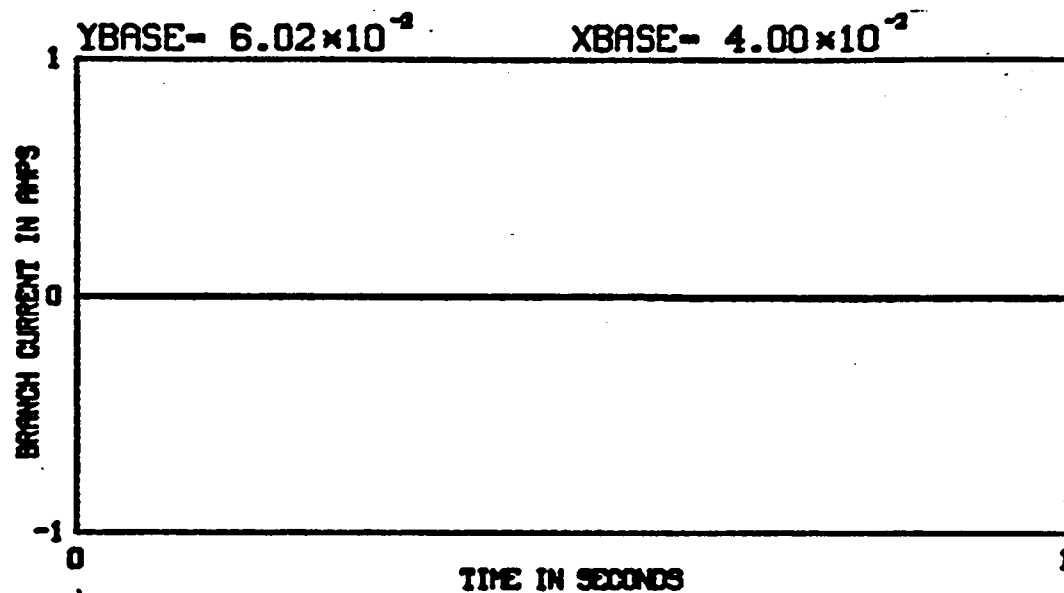
Figure (3.1-8)   Simulated Current and Voltage Waveforms for
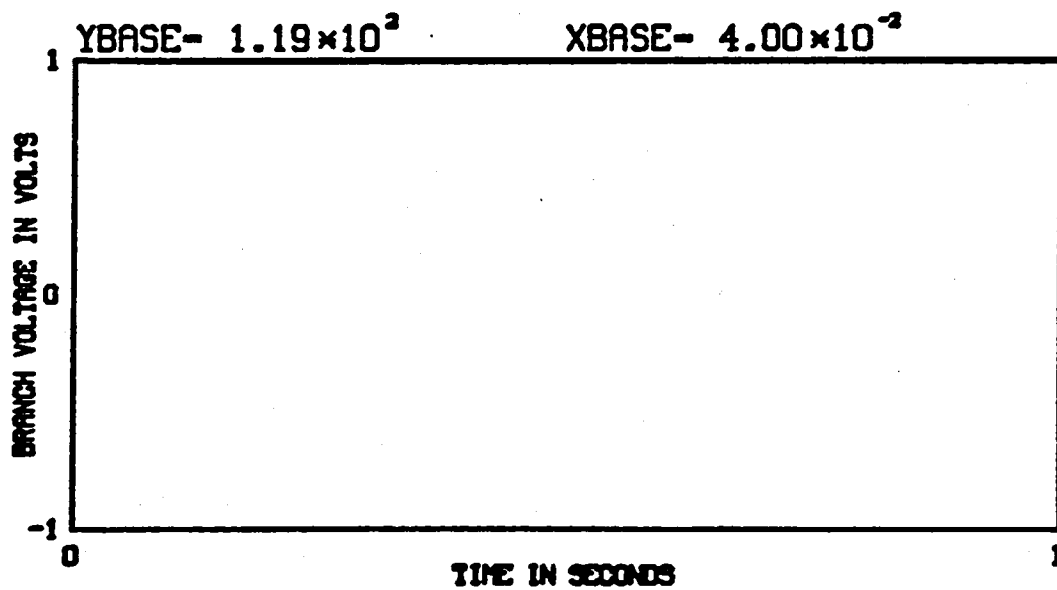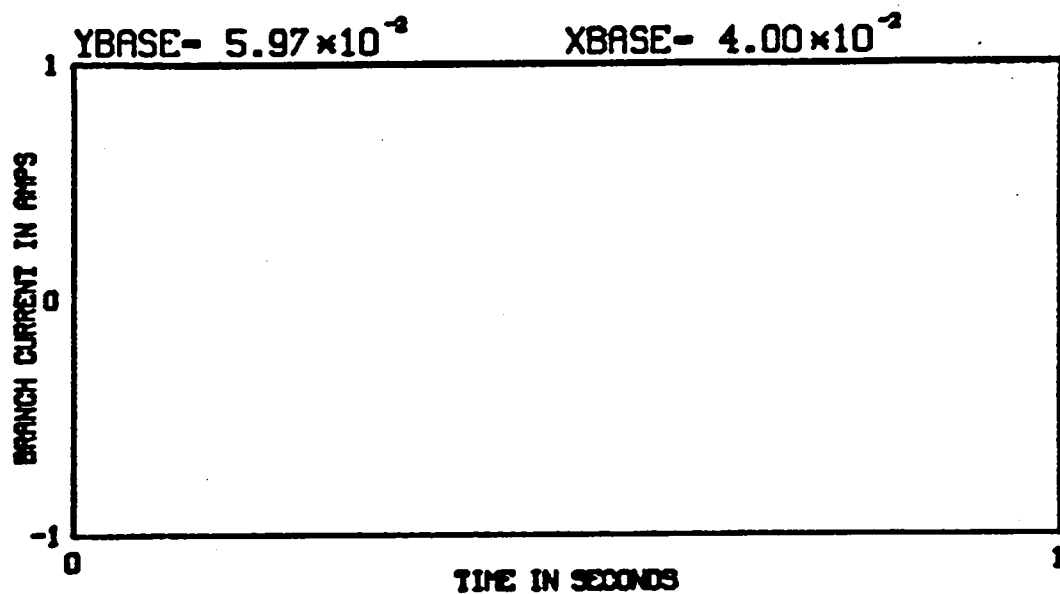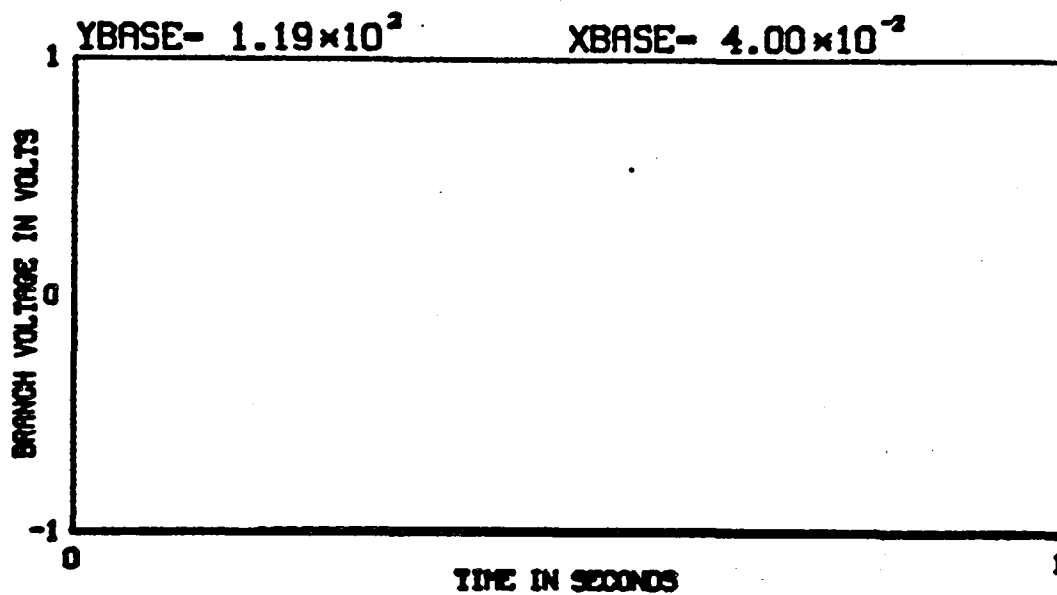   Branch #17, WYE Configuration (Unfaulted)

YBASE= 1.49×10^2 XBASE= 4.00×10^{-2}

BRANCH CURRENT IN AMPS

TIME IN SECONDS

YBASE= 1.21×10^2 XBASE= 4.00×10^{-2}

BRANCH VOLTAGE IN VOLTS

TIME IN SECONDS
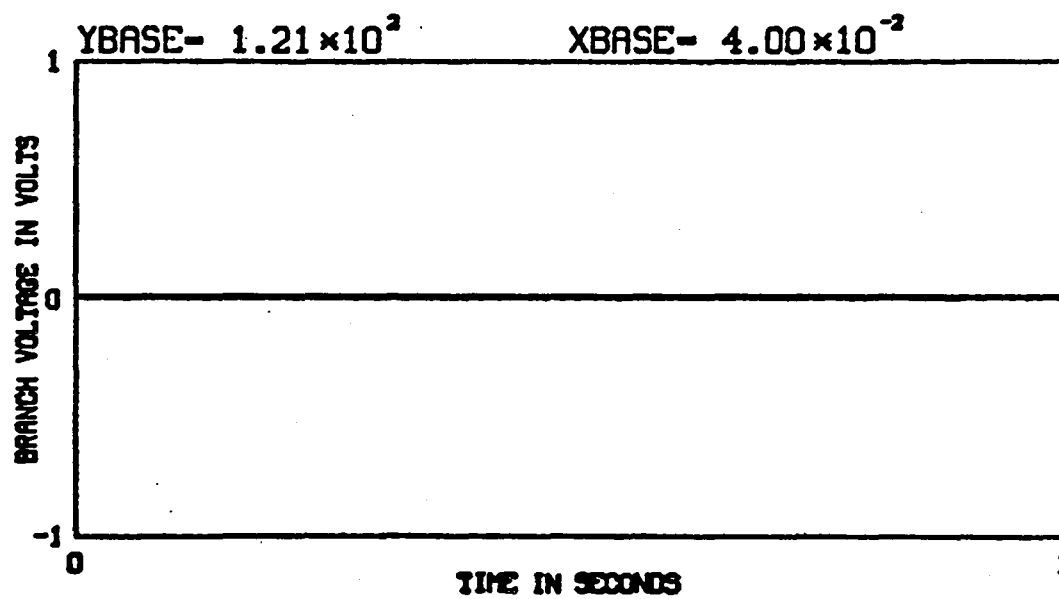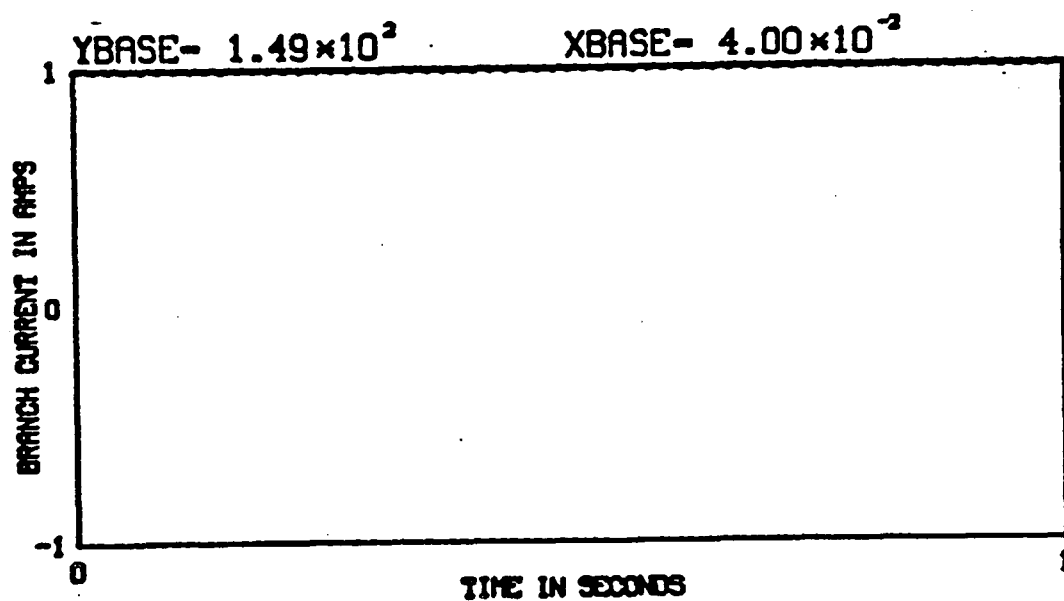
Figure (3.1-9)   Simulated Current and Voltage Waveforms for
                  Branch #20, WYE Configuration (Unfaulted)

YBASE= 6.05×10^{-1} XBASE= 4.00×10^{-2}

BRANCH CURRENT IN AMPS

TIME IN SECONDS

YBASE= 1.21×10^{2} XBASE= 4.00×10^{-2}

BRANCH VOLTAGE IN VOLTS

TIME IN SECONDS
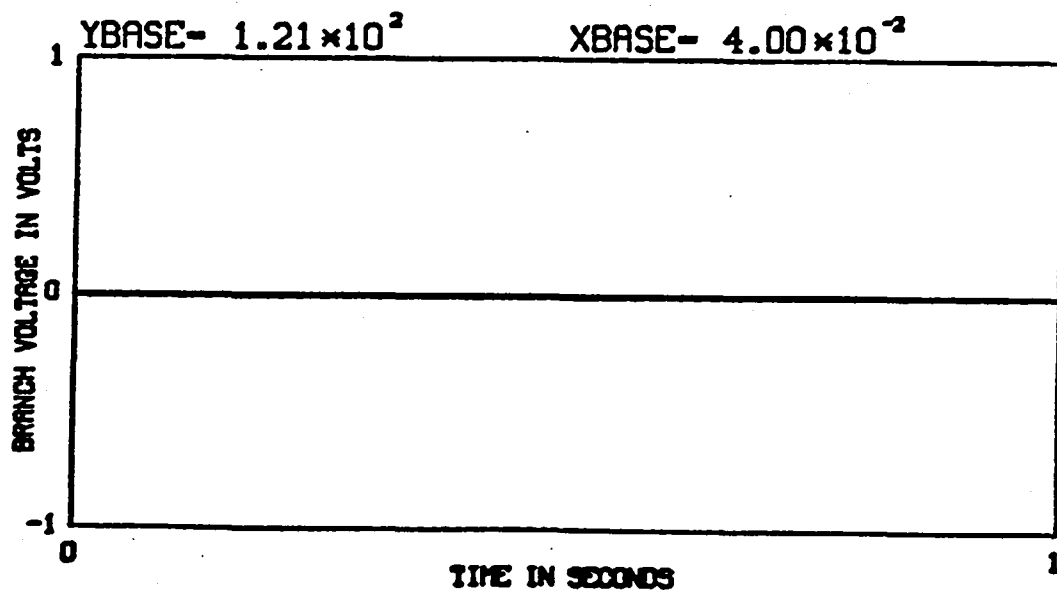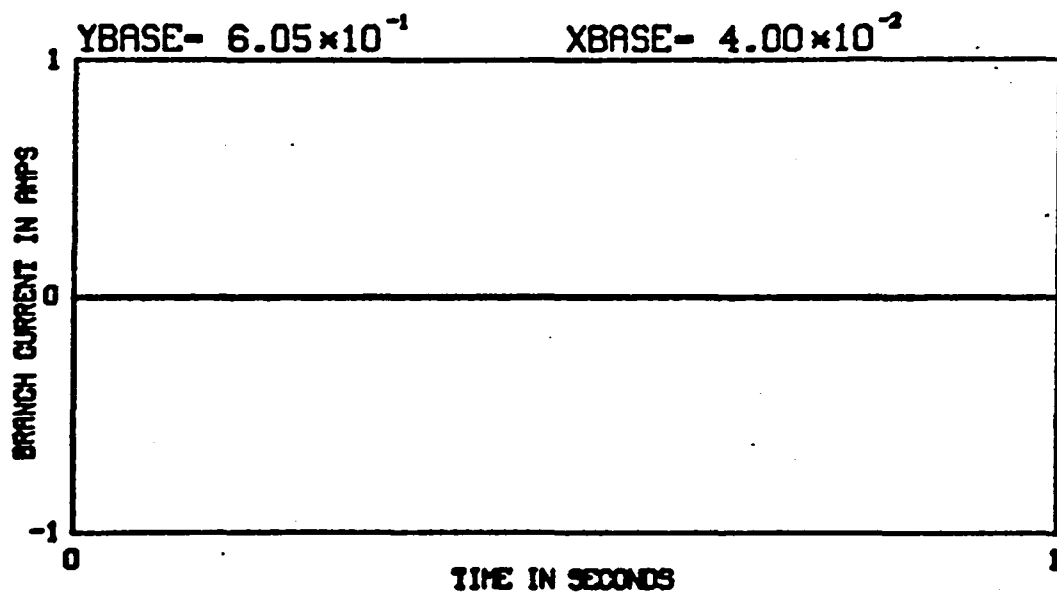
Figure (3.1-10)   Simulated Current and Voltage Waveforms for
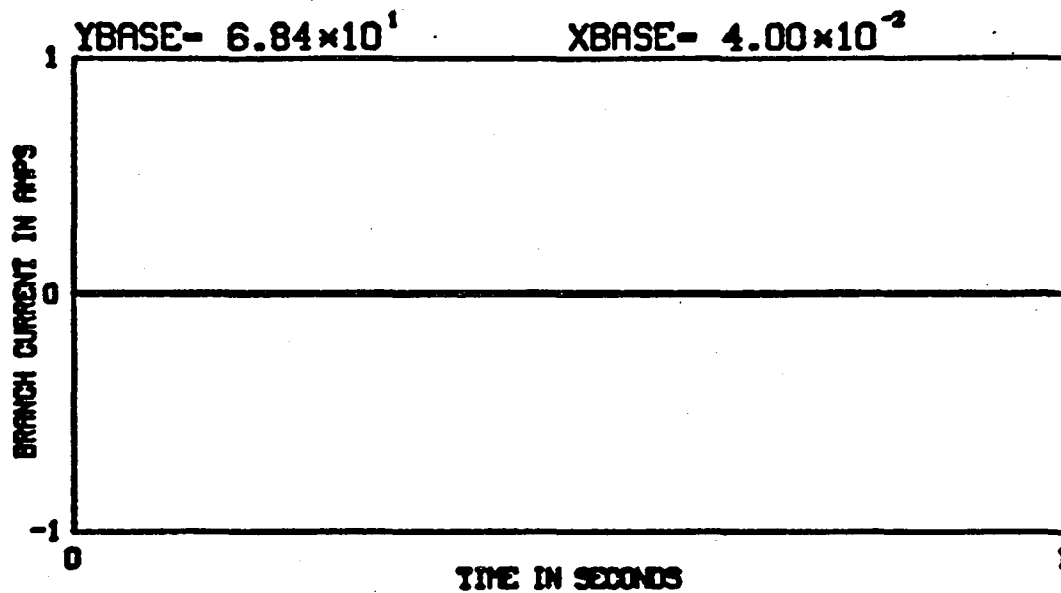   Branch #21, WYE Configuration (Unfaulted)

YBASE- 5.95×10^{-1} XBASE- 4.00×10^{-2}

BRANCH CURRENT IN AMPS

TIME IN SECONDS

YBASE- 1.19×10^{2} XBASE- 4.00×10^{-2}

BRANCH VOLTAGE IN VOLTS

TIME IN SECONDS
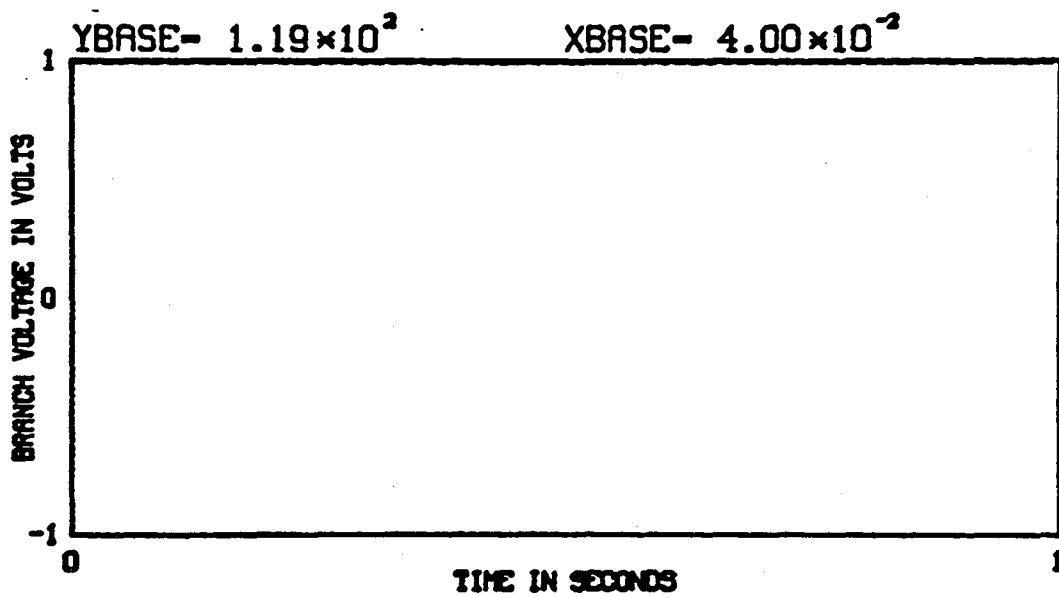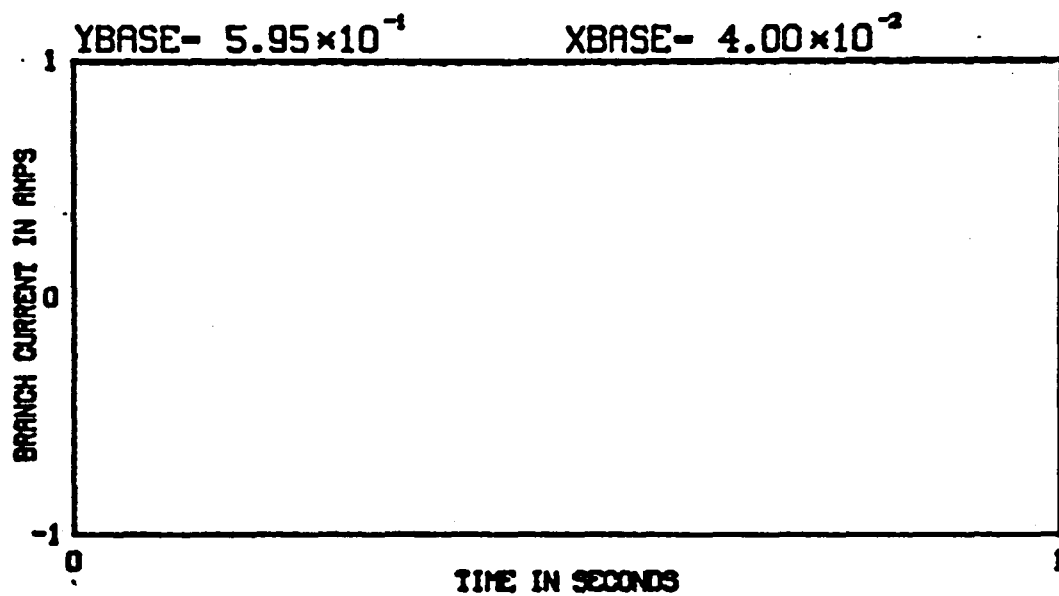
Figure (3.1-11)   Simulated Current and Voltage Waveforms for
                  Branch #6, WYE Configuration (Unfaulted)
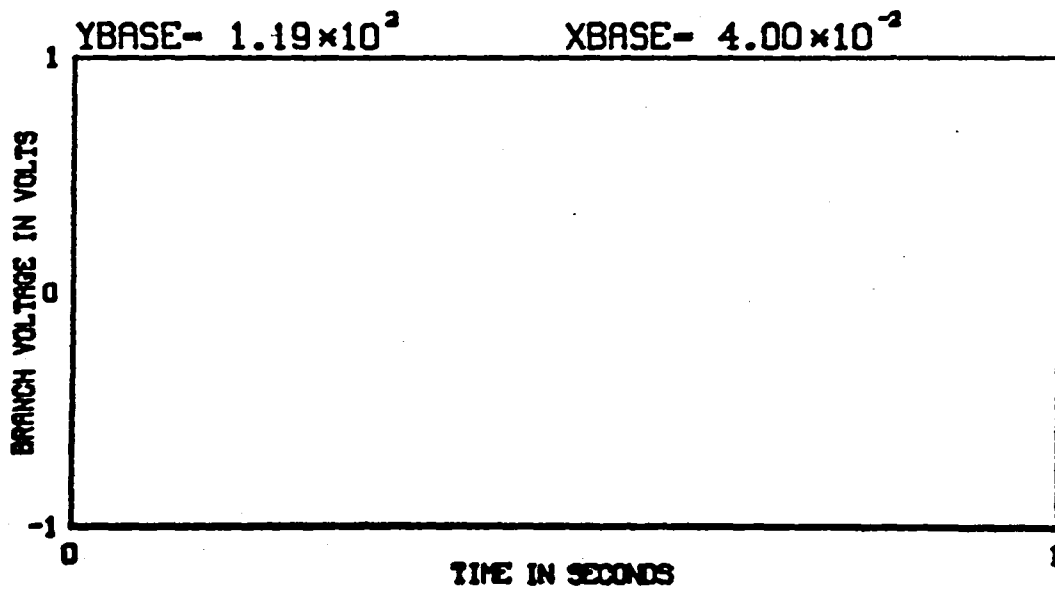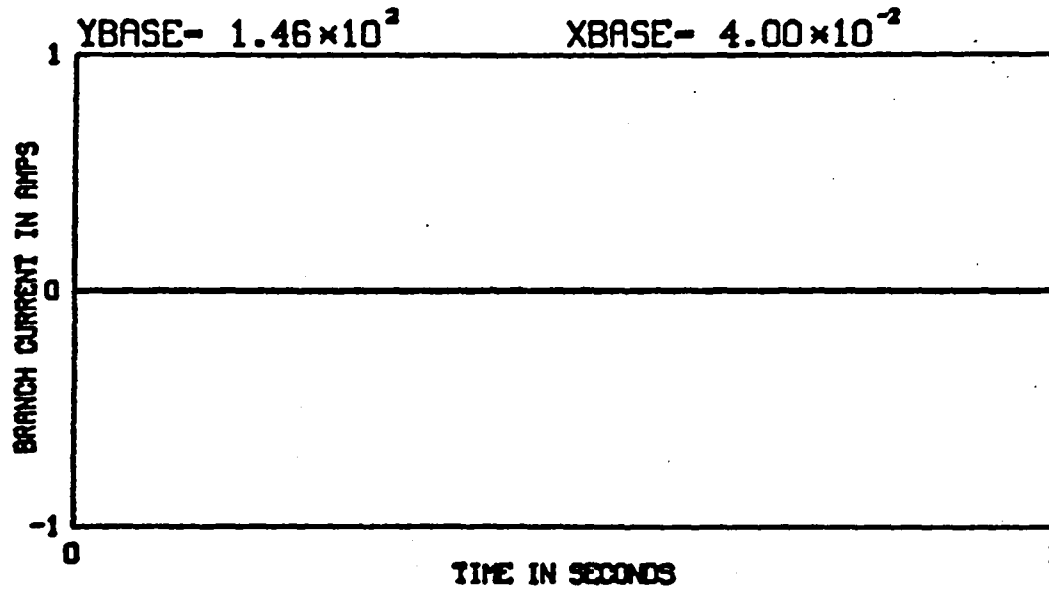
Figure (3.1-12)   Simulated Current and Voltage Waveforms for
                  Branch #28, WYE Configuration (Unfaulted)

3.2 Simulated Waveforms of the DELTA Configuration

The simplified (with chopper) schematic diagram of
Figure (1.0-2) for the DELTA configuration, and its
corresponding complete network graph (including chopper) of
Figure (3.0-3) should be referred to in reviewing the
results of simulations presented in this section. These
simulations represent unfaulted normal motoring operation.
The input data used in obtaining these results are given in
Table (3.2-1). Identification of all the displayed voltage
and current simulated waveforms is given in Table (3.1-2).

The calculated average electromagnetic machine power during the
last cycle is 12,594 watts. The corresponding copper losses in the
machine totaled 217.4 watts. These values are almost identical to the
ones obtained from the WYE connected machine. This is to be expected
since the machine parameters were chosen such that their terminal per-
formances are identical.

Table (3.2-1)   Input Data for Network Model of the DELTA

Configuration (Unfaulted)

```
 Three Phase Balanced Machine Model:


  Branch #11 Phase(A) Winding Resistance=20.4 milli-ohms
  Branch #17 Phase(A) Winding Inductance=156 micro-henries

Inverter/Converter Bridge & Chopper Switching Components:

        Branch #7 (+Bus) Phase(A) Transistor
        Saturation Resistance "on" = 6.4 milli-ohms
        Cutoff Resistance     "off" = 2.0 killo-ohms

        Branch #22 (+Bus) Phase(A) Diode
        Forward-Biase Resistance "on" = 6.4 milli-ohms
        Reverse-Biase Resistance "off"= 2.0 killo-ohms

Chopper Choke:

   Branch #14 Choke Resistance = 24 milli-ohms
   Branch #16 Choke Inductance = 1.5 milli-henries

DC Power Source:

   Branch #5 Filter Capacitor = 7.8 milli-farads
   Branch #4 Battery(Internal) Voltage = 120.0 Volts
   Branch #15 Battery(Internal) Resistance = 5 milli-ohms
```

Table (3.2-2) Branch Identification DELTA Configuration
(Unfaulted)

Figure Number	Branch Number	Branch Identification
3.2-1	1	Phase (A) Back Emf
3.2-2	17	Phase (A) Winding Inductance
3.2-3	7	Phase (A) Transistor (+Bus)
3.2-4	22	Phase (A) Diode (+Bus)
3.2-5	8	Phase (A) Transistor (-Bus)
3.2-6	28	Phase (A) Diode (-Bus)
3.2-7	4	Battery Internal Voltage
3.2-8	16	Chopper Inductance
3.2-9	31	Chopper (+Bus) Transistor
3.2-10	20	Chopper (+Bus) Diode
3.2-11	6	Chopper (-Bus) Transistor
3.2-12	27	Chopper (-Bus) Diode
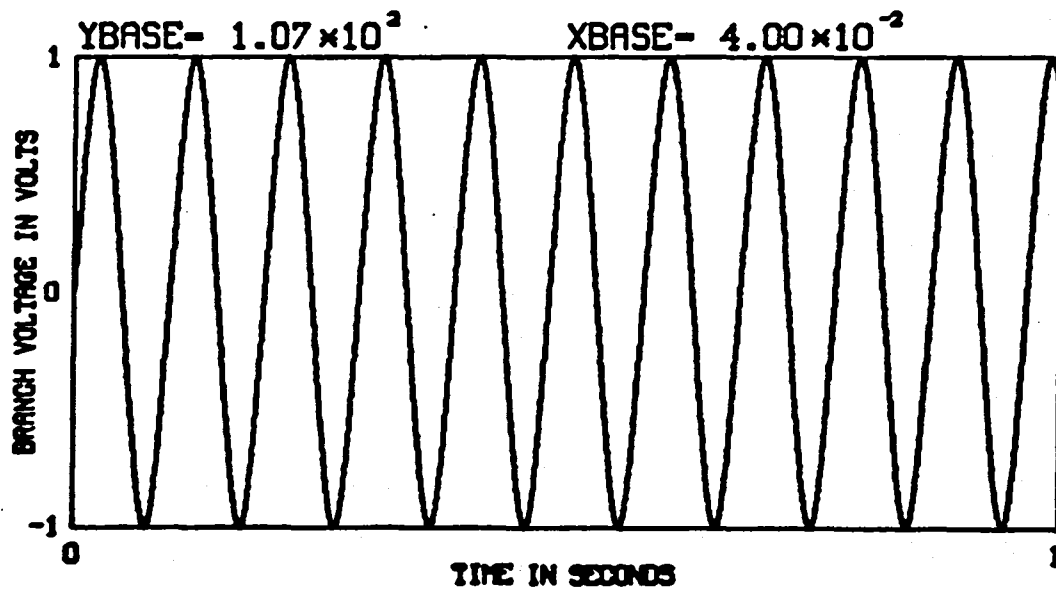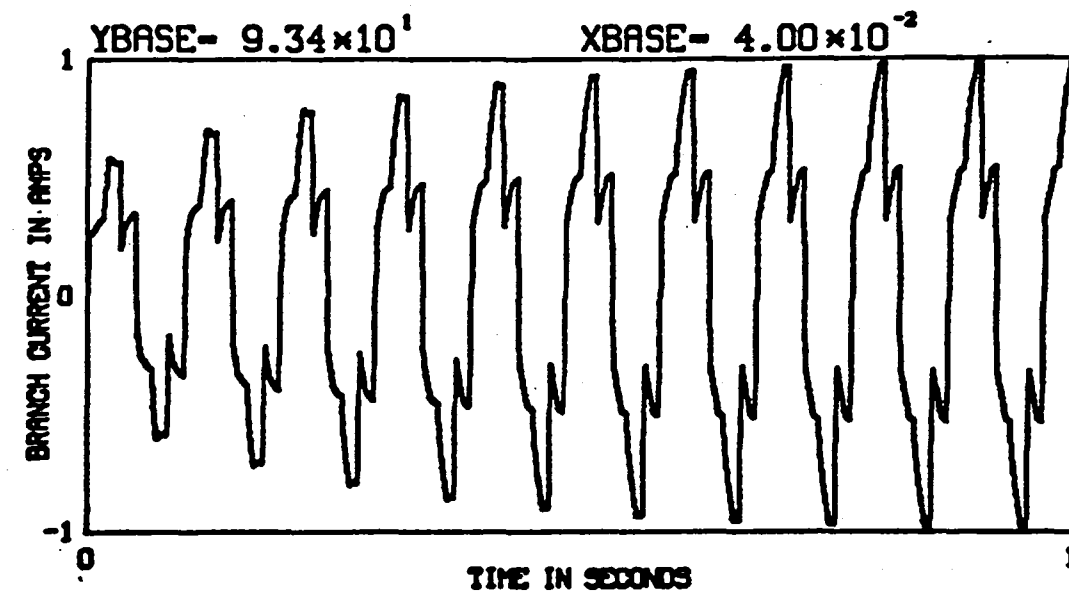
Figure (3.2-1)   Simulated Current and Voltage Waveforms for Branch #1, DELTA Configuration (Unfaulted)
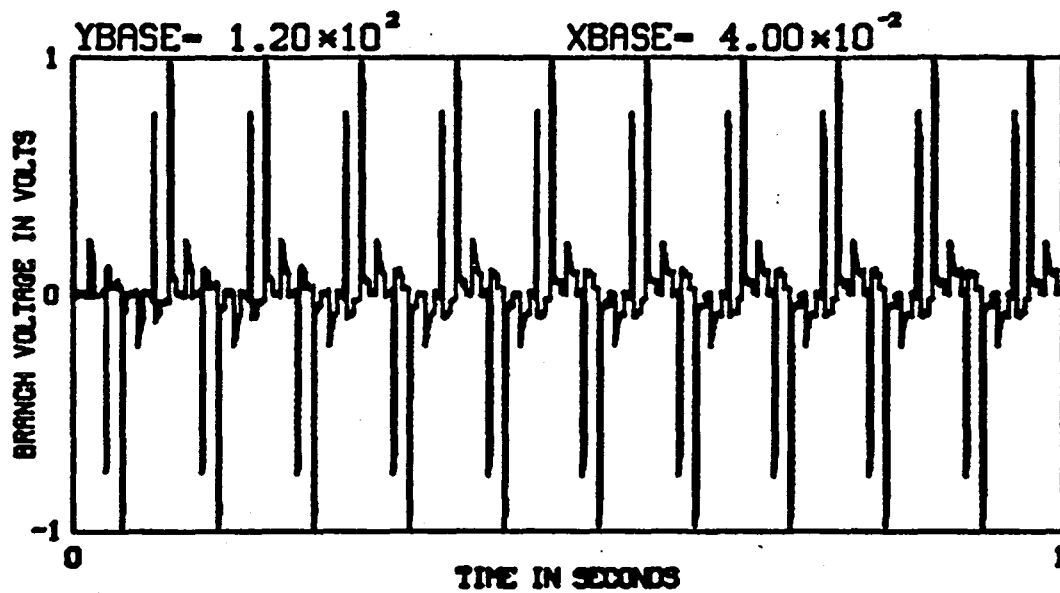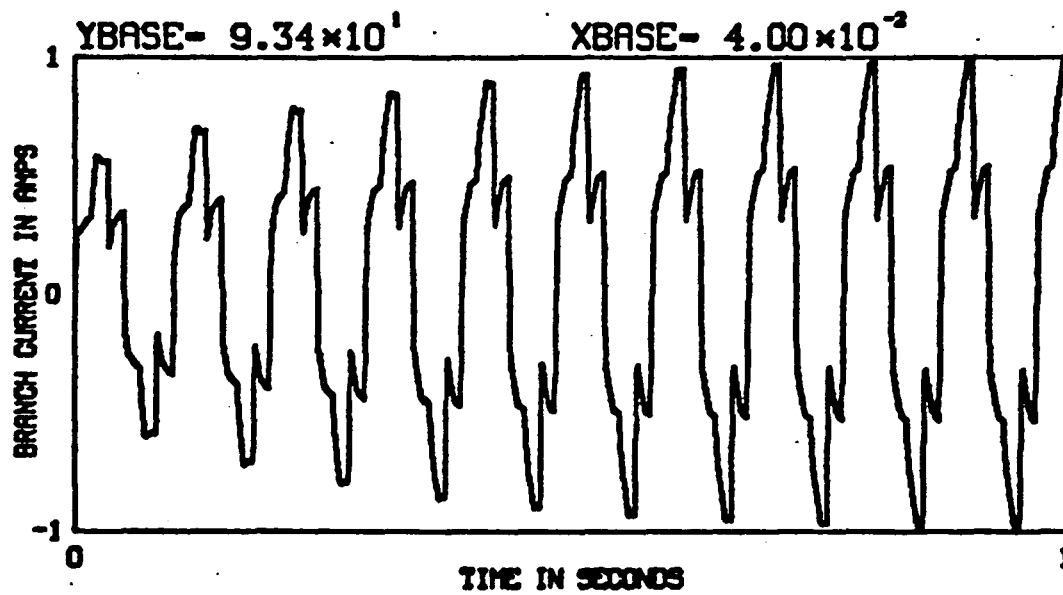
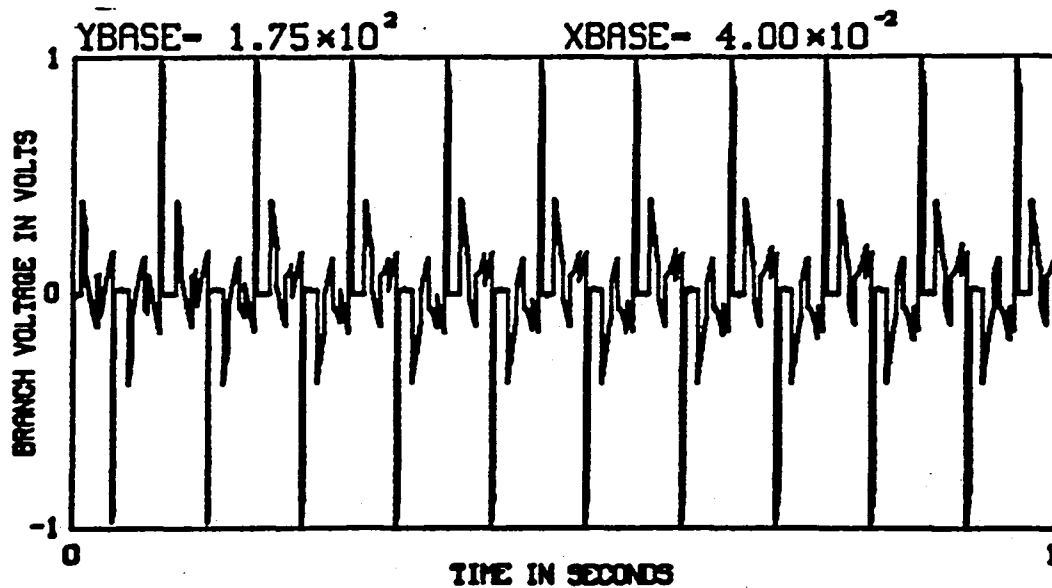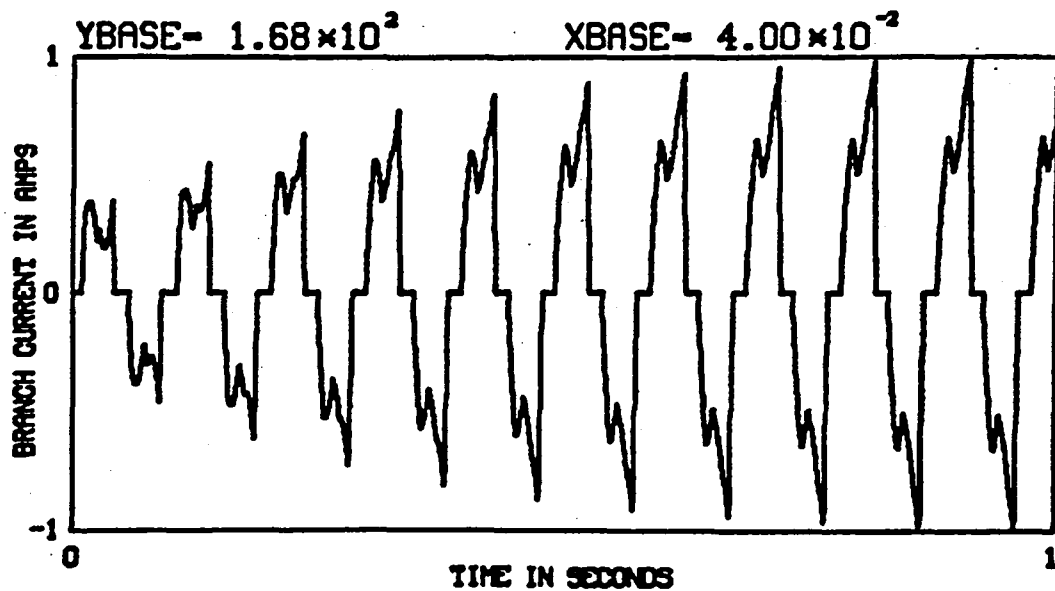Figure (3.2-2) Simulated Current and Voltage Waveforms for Branch #17, DELTA Configuration (Unfaulted)
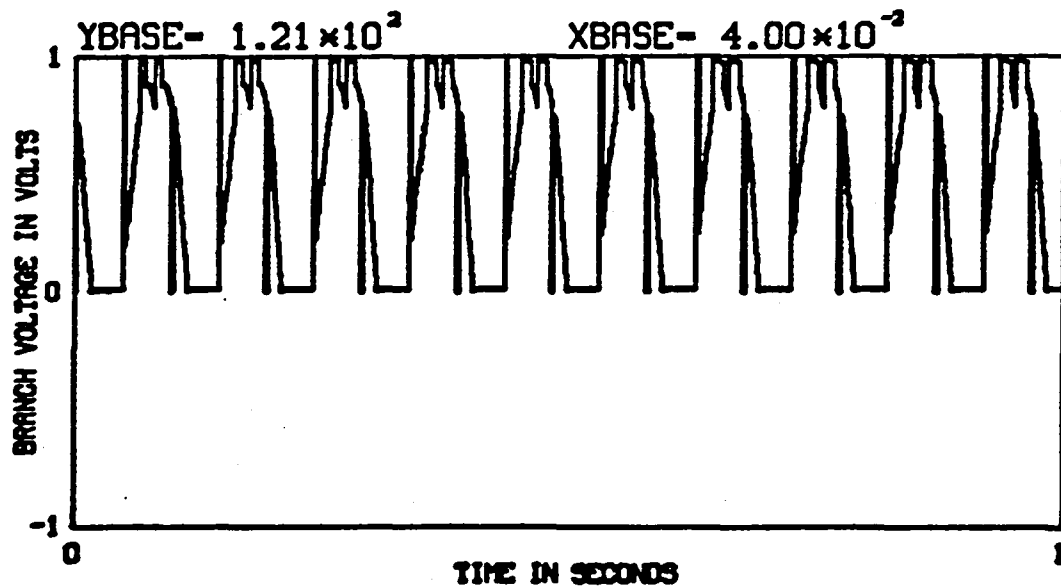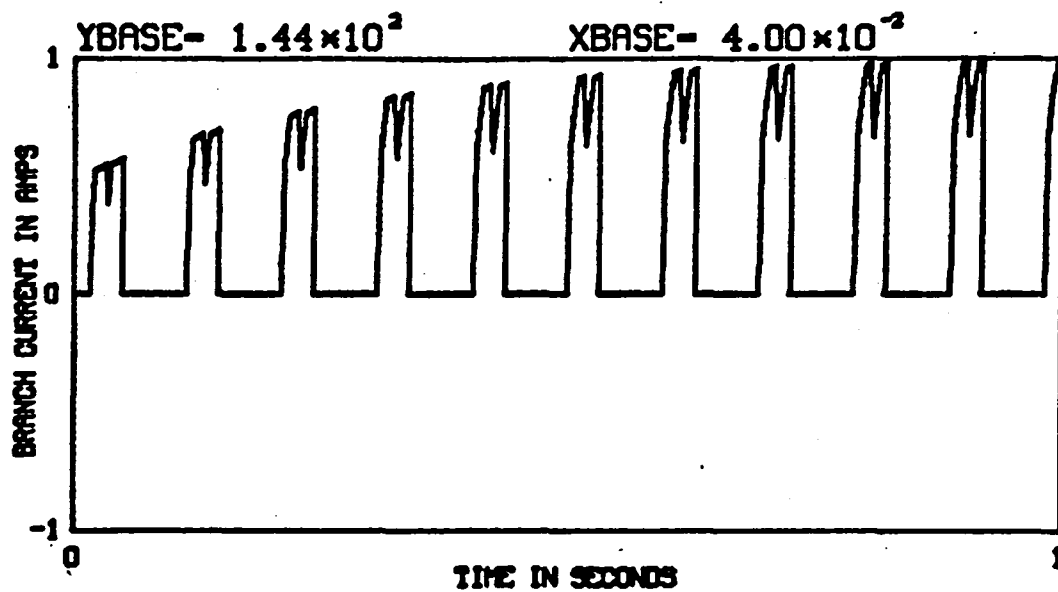
Figure (3.2-3)   Simulated Current and Voltage Waveforms for
                  Branch #7, DELTA Configuration (Unfaulted)
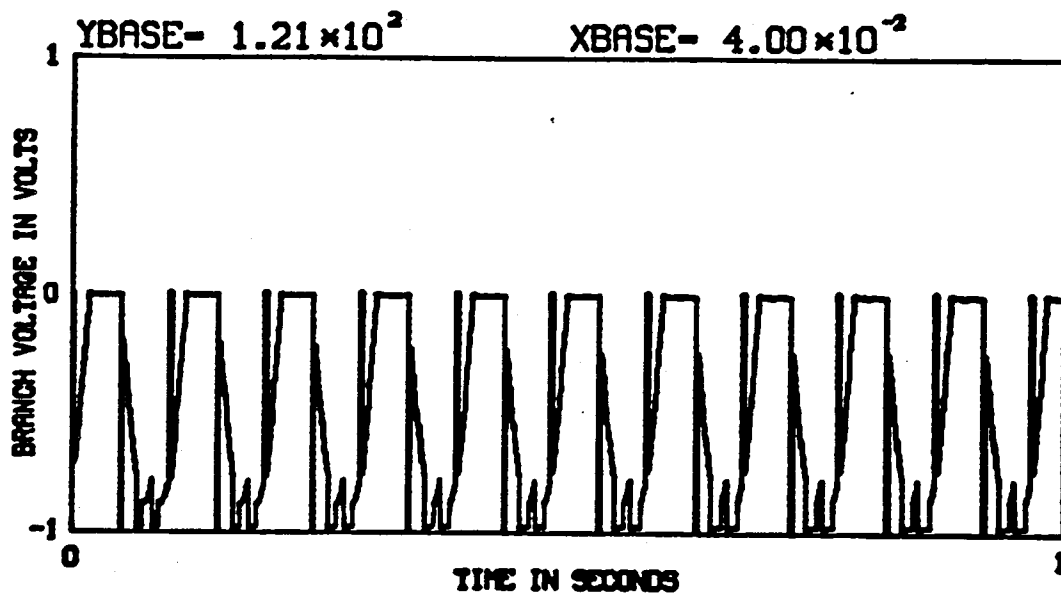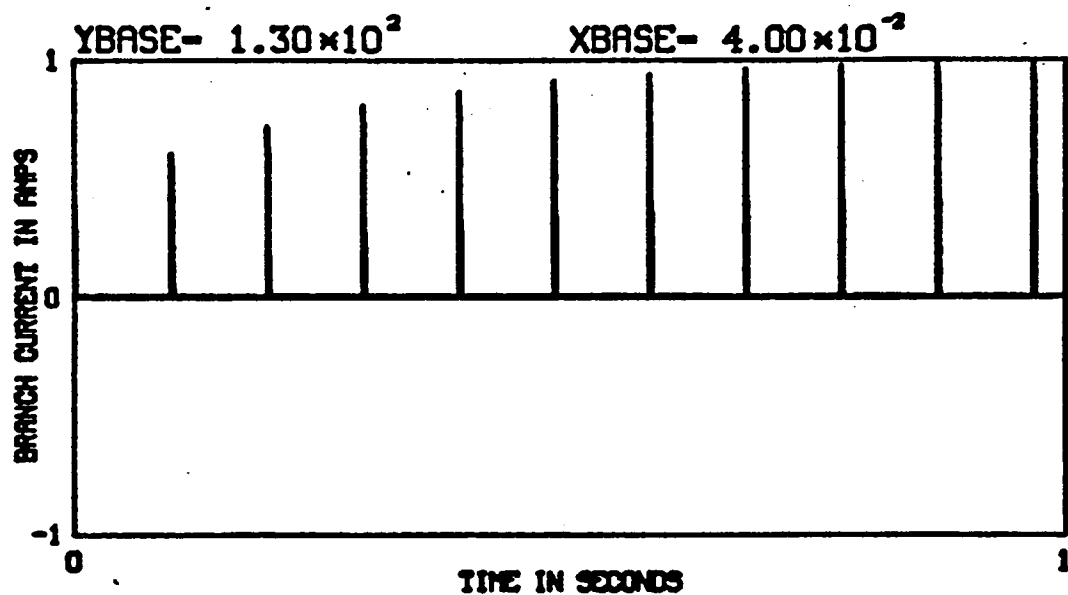
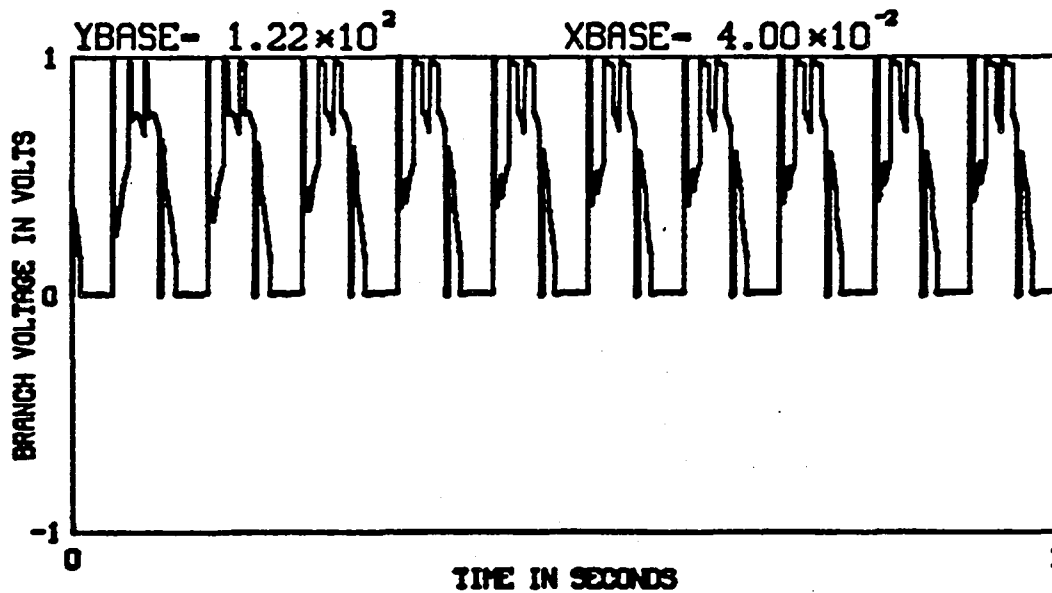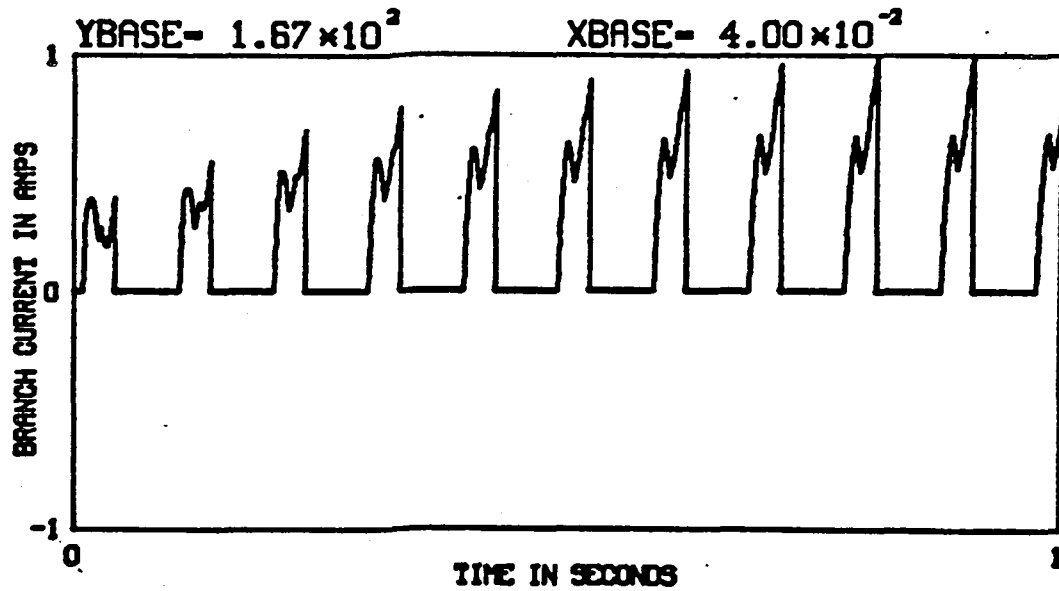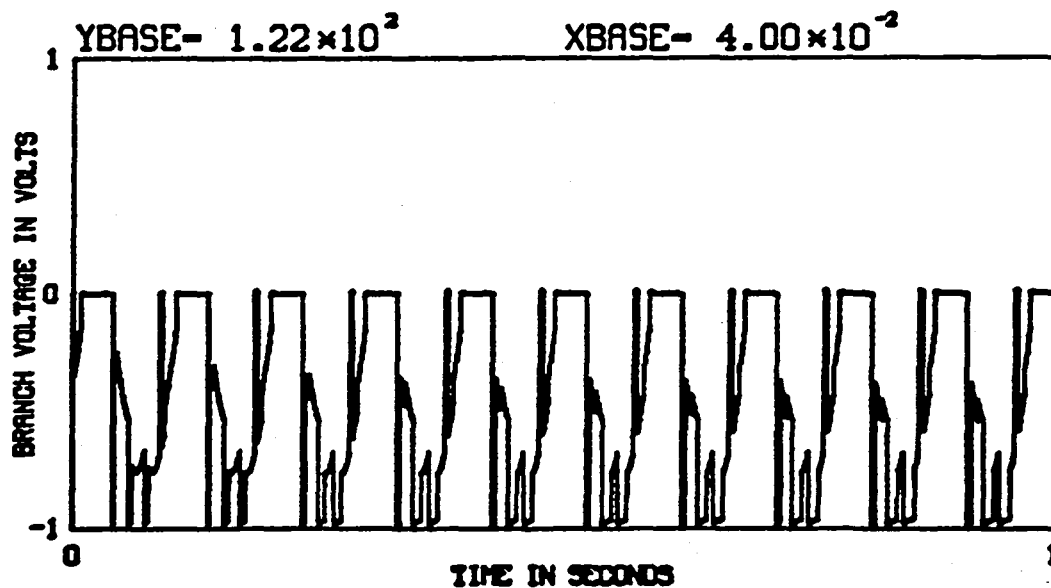Figure (3.2-4)   Simulated Current and Voltage Waveforms for Branch #22, DELTA Configuration (Unfaulted
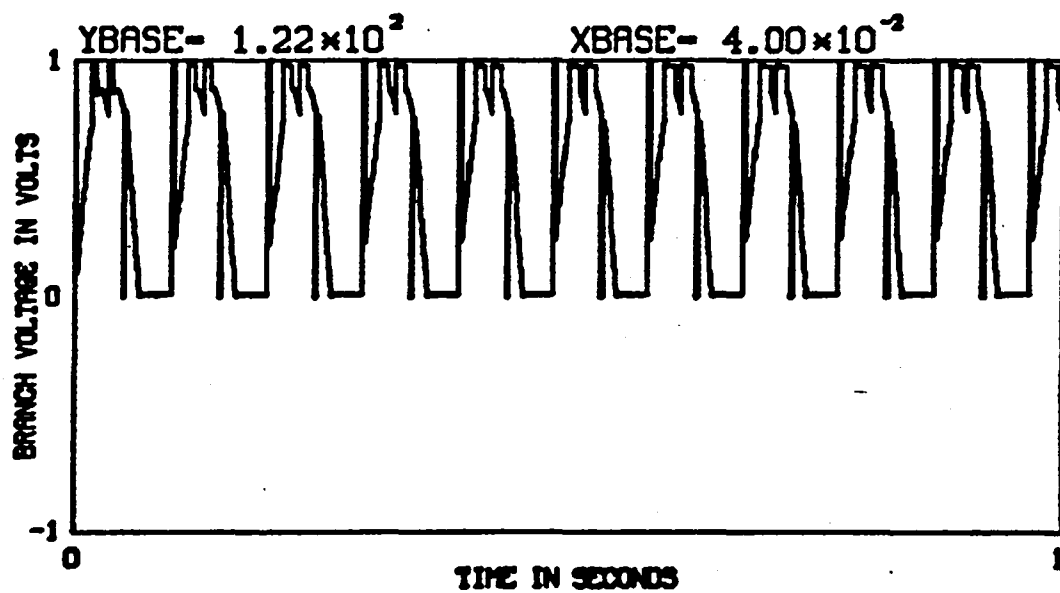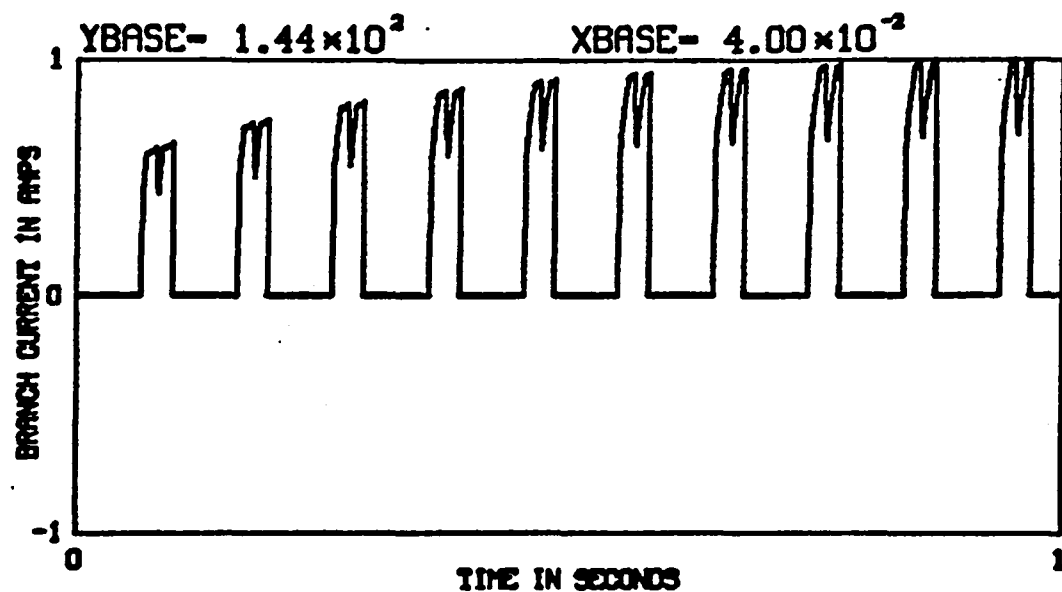
Figure (3.2-5)   Simulated Current and Voltage Waveforms for
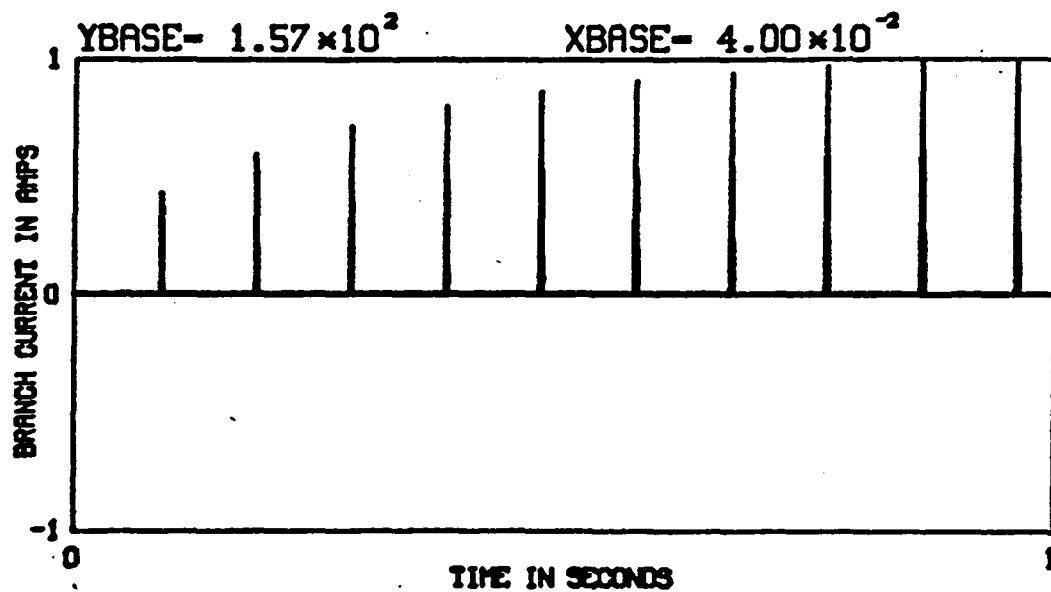   Branch #8, DELTA Configuration (Unfaulted)

- 182 -
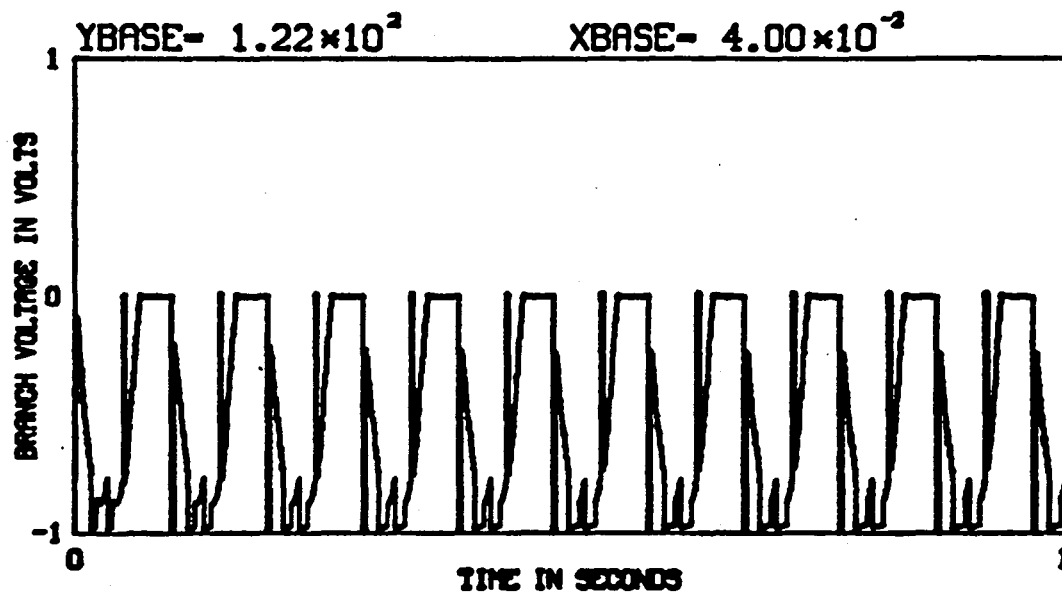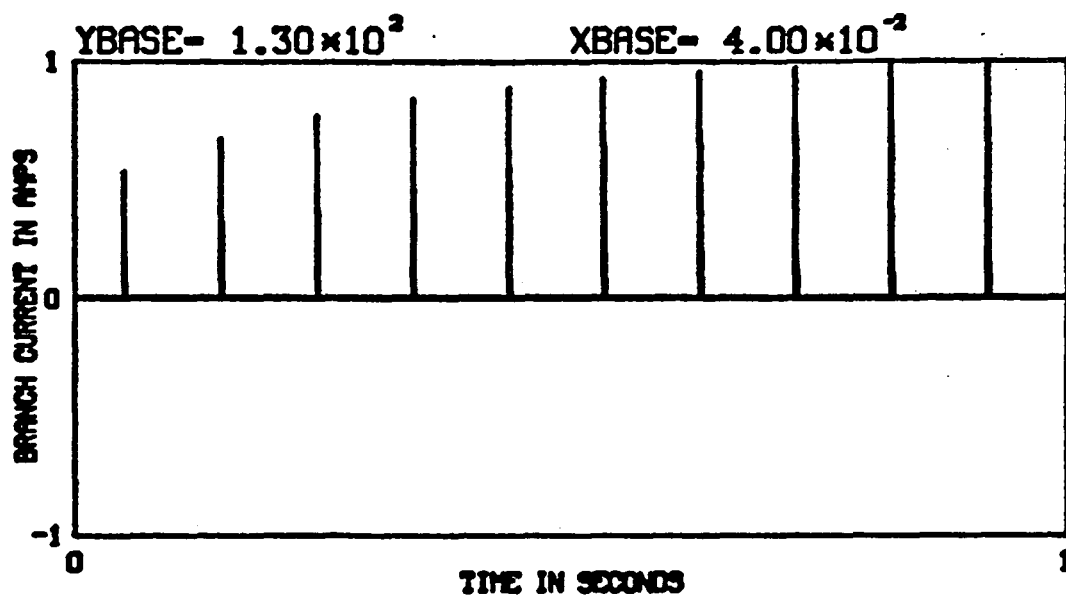
Figure (3.2-6)   Simulated Current and Voltage Waveforms for
                 Branch #28, DELTA Configuration (Unfaulted)
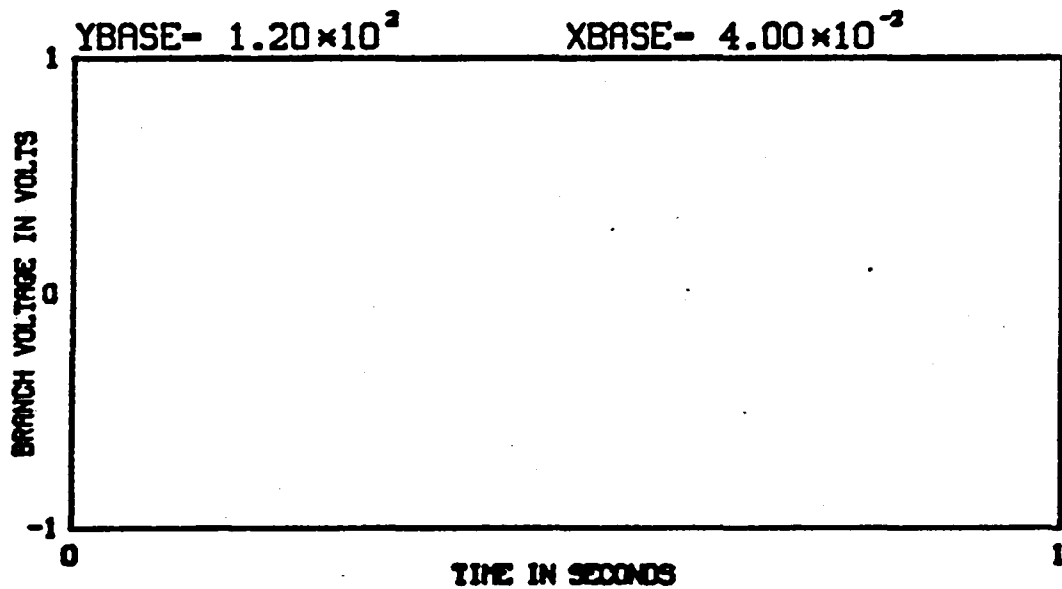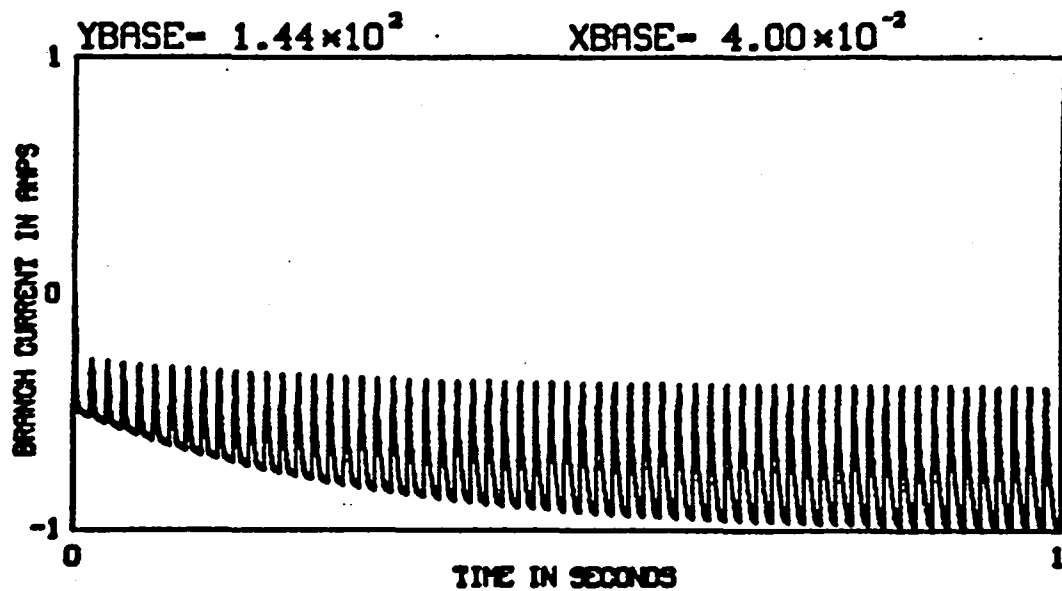
Figure (3.2-7) Simulated Current and Voltage Waveforms for
Branch #4, DELTA Configuration (Unfaulted)

- 184 -
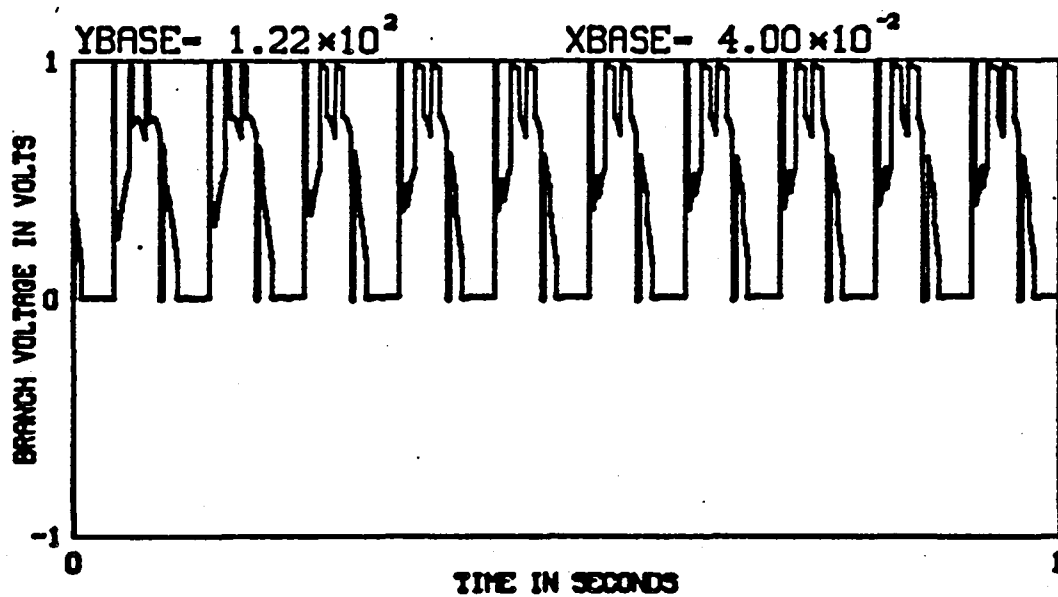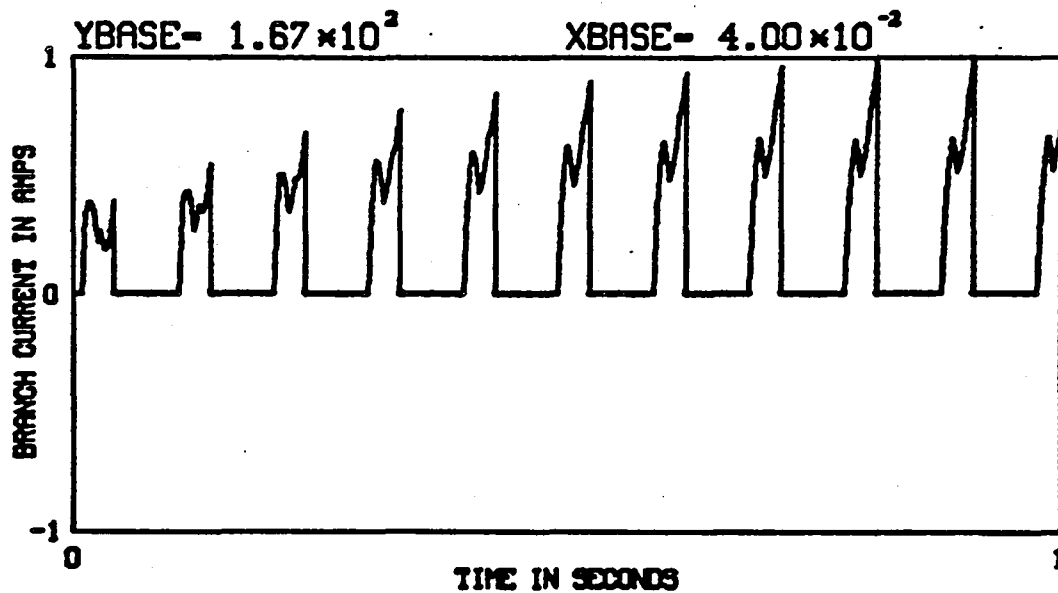
Figure (3.2-8)   Simulated Current and Voltage Waveforms for
                 Branch #16, DELTA Configuration (Unfaulted)

Figure (3.2-9) Simulated Current and Voltage Waveforms for Branch #31, DELTA Configuration (Unfaulted)

Figure (3.2-10)   Simulated Current and Voltage Waveforms for
Branch #20, DELTA Configuration (Unfaulted)

YBASE= 5.97×10^{-2} XBASE= 4.00×10^{-2}

BRANCH CURRENT IN AMPS

TIME IN SECONDS

YBASE= 1.19×10^{2} XBASE= 4.00×10^{-2}
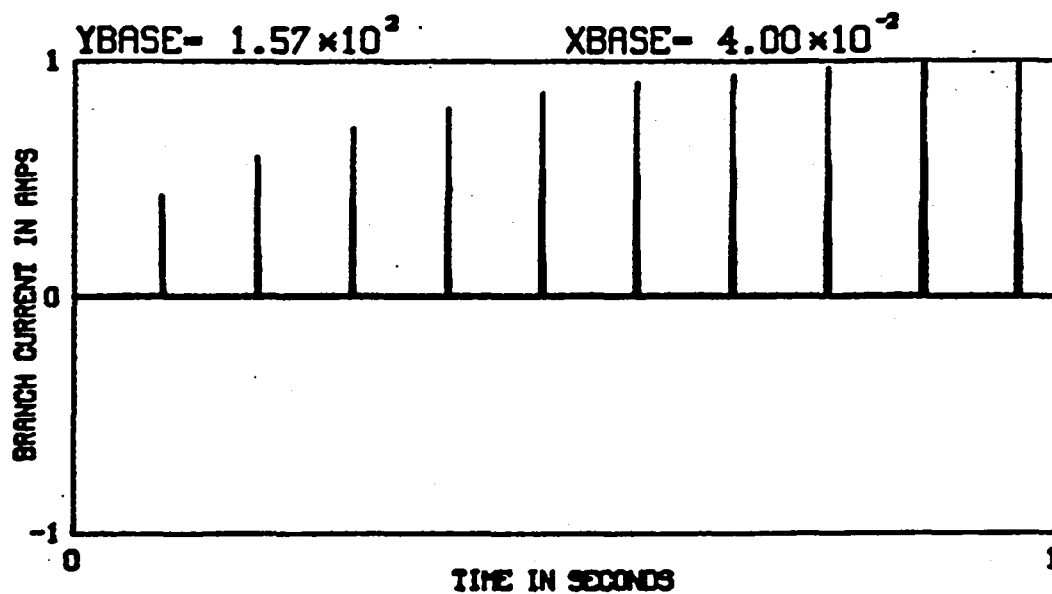
BRANCH VOLTAGE IN VOLTS

TIME IN SECONDS

Figure (3.2-11)   Simulated Current and Voltage Waveforms for Branch #6, DELTA Configuration (Unfaulted)

Figure (3.2-12)   Simulated Current and Voltage Waveforms for
                   Branch #27, DELTA Configuration (Unfaulted)
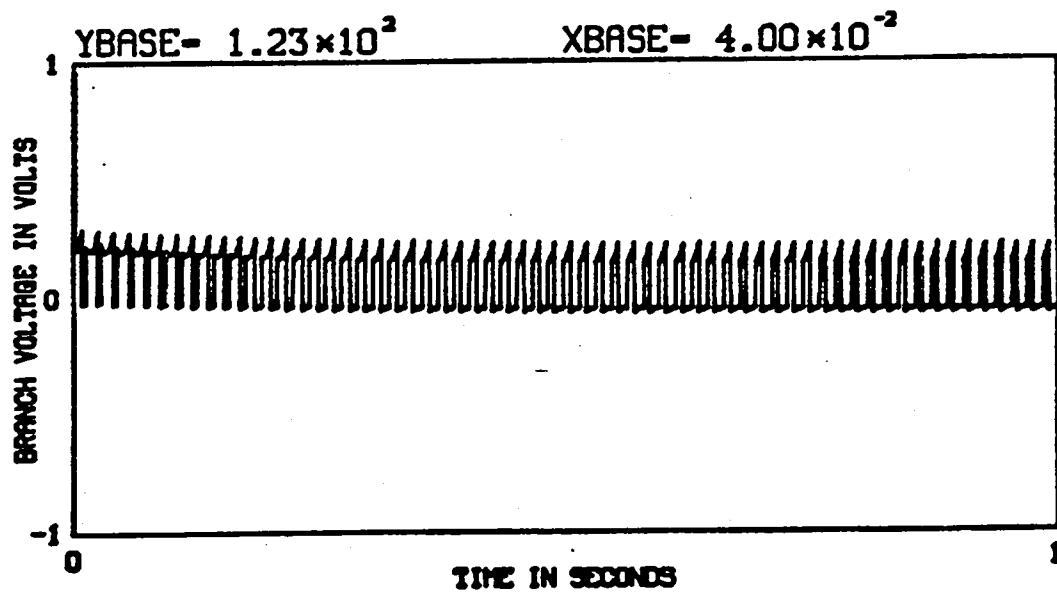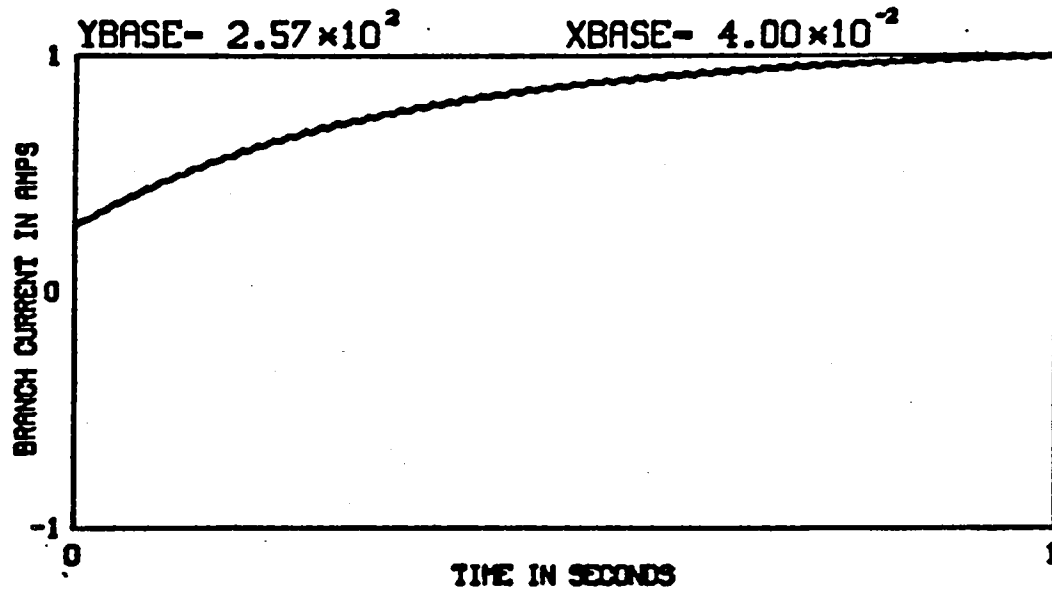
- 189 -

3.3 Simulated Waveforms of the OPEN-DELTA Configuration

The simplified (with chopper) schematic diagram of Figure (1.0-3) for the DELTA configuration, and its corresponding complete network graph (including chopper) of Figure (3.0-4) should be referred to in reviewing the results of simulations presented in this section. These simulations represent unfaulted normal motoring operation. The input data used in obtaining these results are given in Table (3.3-1). Identification of all the displayed voltage and current simulated waveforms is given in Table (3.3-2).

The calculated average electromagnetic machine power during the last cycle is 18,407 watts. The corresponding copper losses in the machine totaled 515 watts.

Table (3.3-1) Input Data for Network Model of the
OPEN-DELTA Configuration (Unfaulted)

Three Phase Balanced Machine Model:

Branch #15 Phase(A) Winding Resistance=20.4 milli-ohms
Branch #20 Phase(A) Winding Inductance=156 micro-henries

Inverter/Converter Bridge & Chopper Switching Components:

Forward Motoring Mode:

Branch #7 (+Bus) Phase(A) Transistor
Saturation Resistance "on" = 6.4 milli-ohms
Cutoff Resistance "off" = 2.0 killo-ohms

Branch #26 (+Bus) Phase(A) Diode
Forward-Biase Resistance "on" = 6.4 milli-ohms
Reverse-Biase Resistance "off"= 2.0 killo-ohms

Chopper Choke:

Branch #14 Choke Resistance = 24 milli-ohms
Branch #19 Choke Inductance = 1.5 milli-henries

DC Power Source:

Branch #5 Filter Capacitor = 7.8 milli-farads
Branch #4 Battery(Internal) Voltage = 120.0 Volts
Branch #18 Battery(Internal) Resistance = 5 milli-ohms

Table (3.3-2)   Branch Identification OPEN-DELTA Configuration
                (Unfaulted)

| Figure Number	Branch Number	Branch Identification
3.3-1	1	Phase (A) Armature EMF and Phase Current
3.3-2	20	Phase (A) Inductive Voltage and Phase Current
3.3-3	7	Phase (A) (+ Bus) Transistor
3.3-4	26	Phase (A) (+ Bus) Diode
3.3-5	9	Phase (A) (-Bus) Transistor
3.3-6	39	Phase (A) (-Bus) Diode
3.3-7	4	Battery Internal Voltage and Current
3.3-8	19	Chopper Inductive Voltage and Current
3.3-9	23	Chopper (+ Bus) Transistor
3.3-10	24	Chopper (+ Bus) Diode
3.3-11	6	Chopper (- Bus) Transistor
3.3-12	37	Chopper (- Bus) Diode
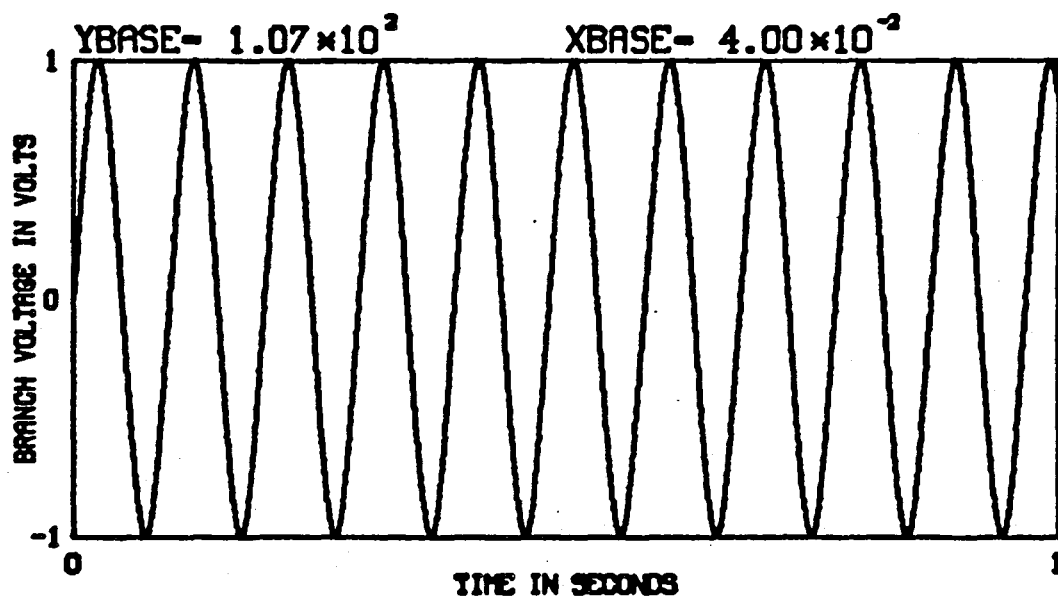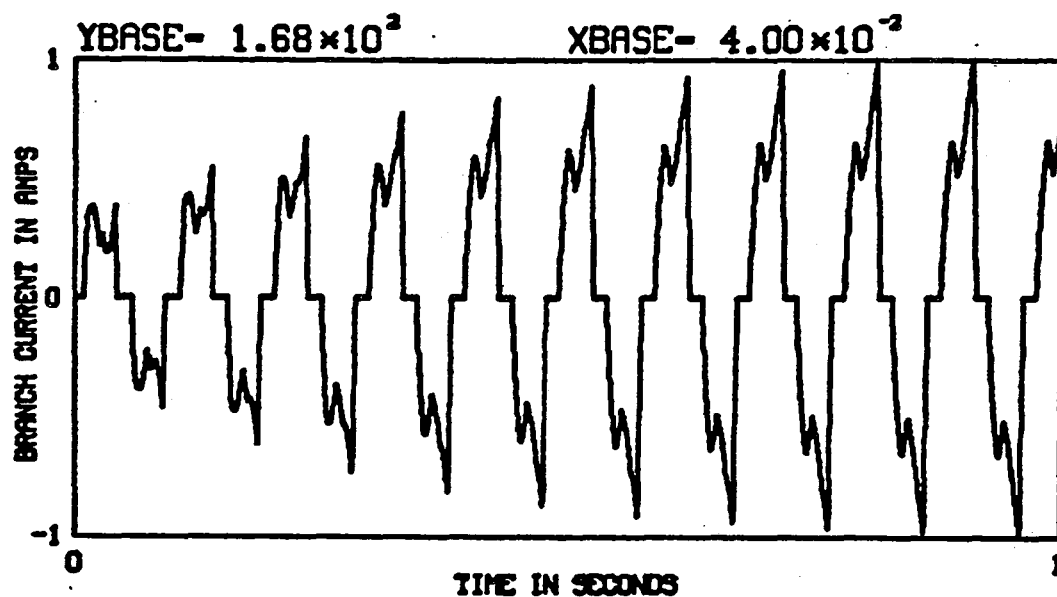
Figure (3.3-1)   Simulated Current and Voltage Waveforms for
                 Branch   #1,   OPEN-DELTA   Configuration
                 (Unfaulted)

Figure (3.3-2)   Simulated Current and Voltage Waveforms for
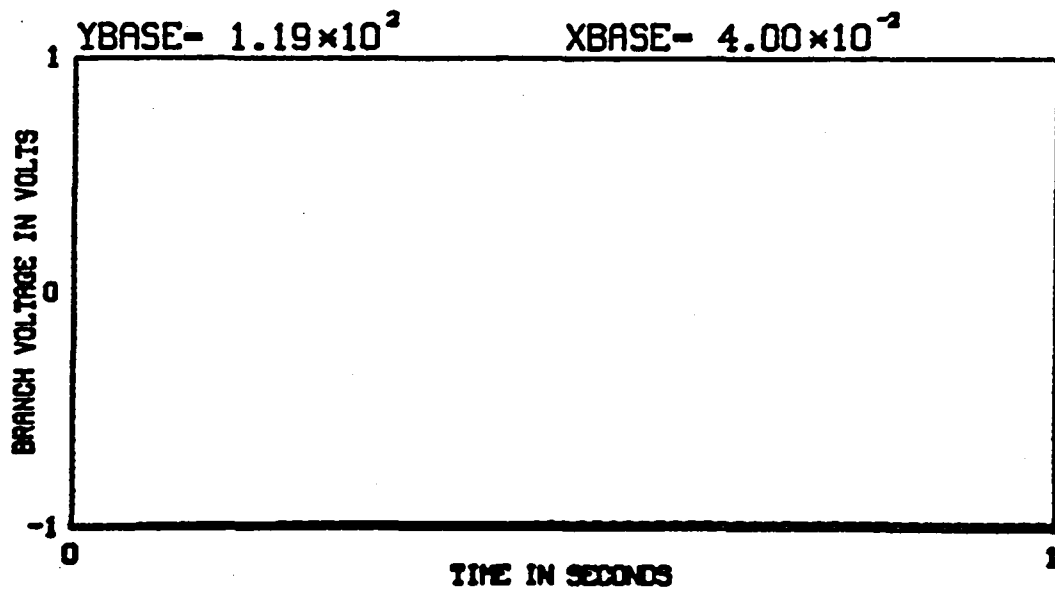   Branch   #20,   OPEN-DELTA   Configuration
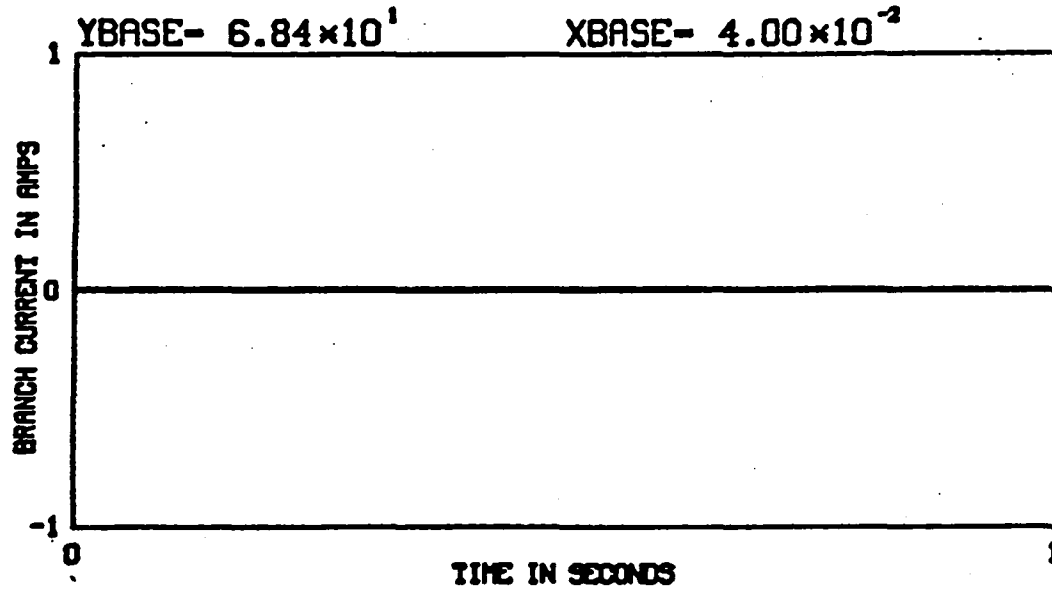   (Unfaulted)

YBASE- 1.67×10^{2} XBASE- 4.00×10^{-2}

BRANCH CURRENT IN AMPS

TIME IN SECONDS

YBASE- 1.22×10^{2} XBASE- 4.00×10^{-2}

BRANCH VOLTAGE IN VOLTS

TIME IN SECONDS

Figure (3.3-3)   Simulated Current and Voltage Waveforms for
                 Branch   #7 ,   OPEN-DELTA   Configuration
                 (Unfaulted)

Figure (3.3-4) Simulated Current and Voltage Waveforms for Branch #26, OPEN-DELTA Configuration (Unfaulted)

Figure (3.3-5)   Simulated Current and Voltage Waveforms for
                 Branch   #9,   OPEN-DELTA   Configuration
                 (Unfaulted)
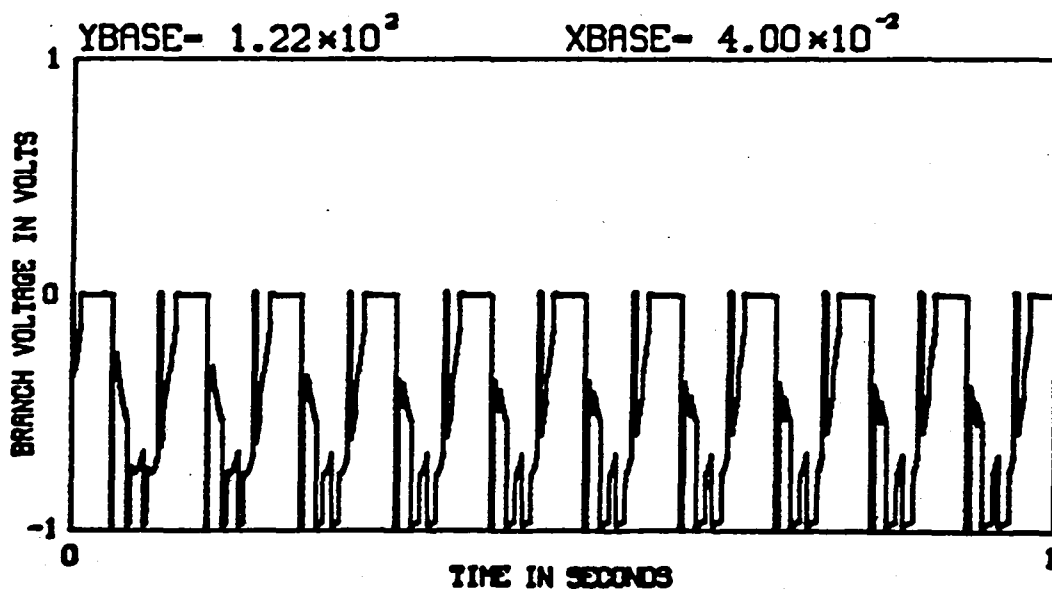
Figure (3.3-6)   Simulated Current and Voltage Waveforms for Branch #39, OPEN-DELTA Configuration (Unfaulted)
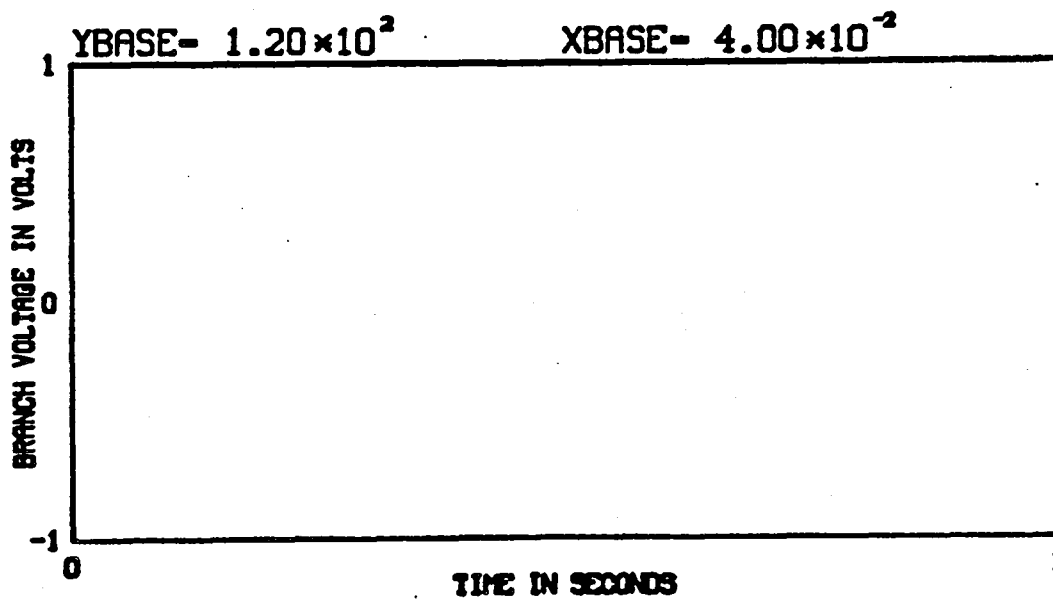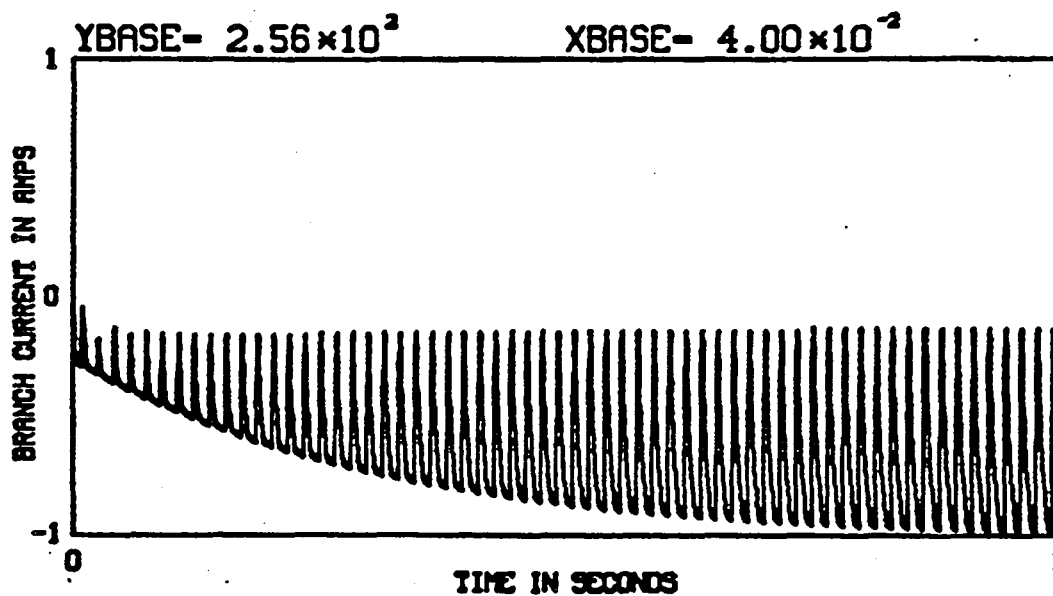
Figure (3.3-7) Simulated Current and Voltage Waveforms for Branch #4, OPEN-DELTA Configuration (Unfaulted)

YBASE- 2.57×10^{2} XBASE- 4.00×10^{-2}

BRANCH CURRENT IN AMPS

TIME IN SECONDS

YBASE- 1.23×10^{2} XBASE- 4.00×10^{-2}

BRANCH VOLTAGE IN VOLTS

TIME IN SECONDS

Figure (3.3-8)   Simulated Current and Voltage Waveforms for Branch #19, OPEN-DELTA Configuration (Unfaulted)
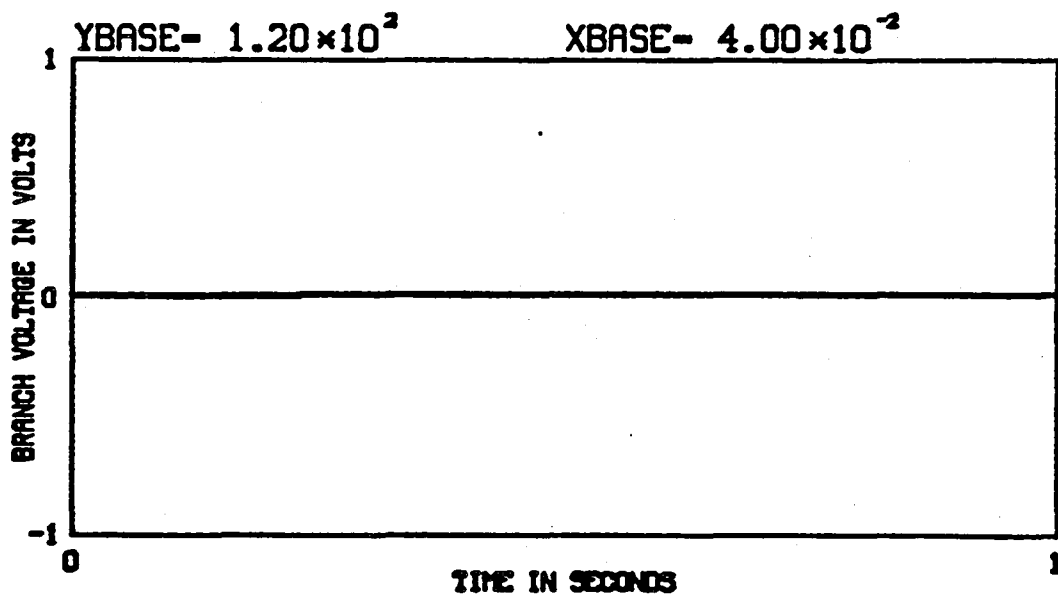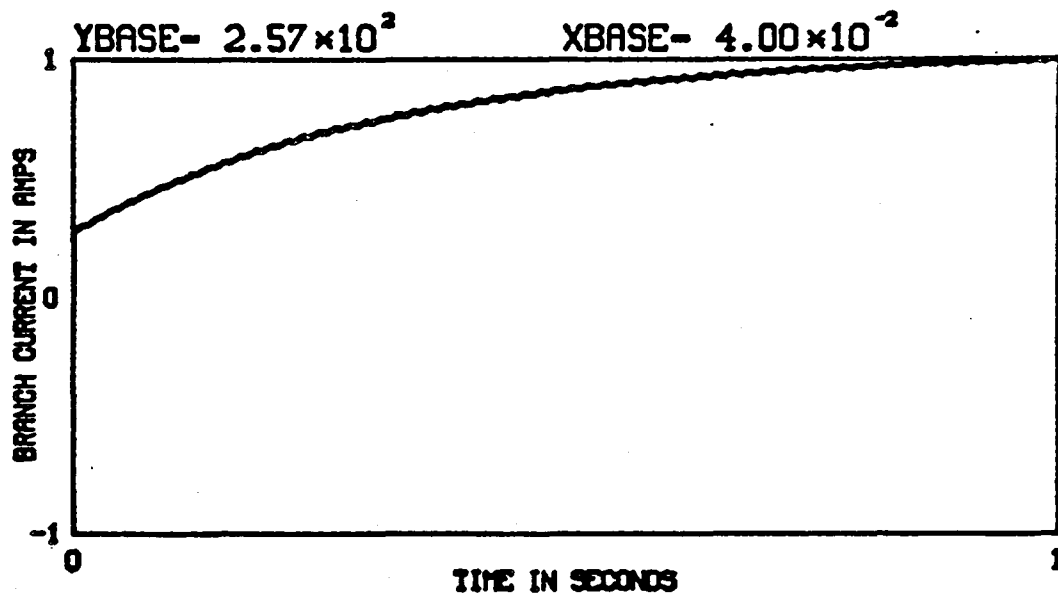
Figure (3.3-9)   Simulated Current and Voltage Waveforms for Branch #23, OPEN-DELTA Configuration (Unfaulted)
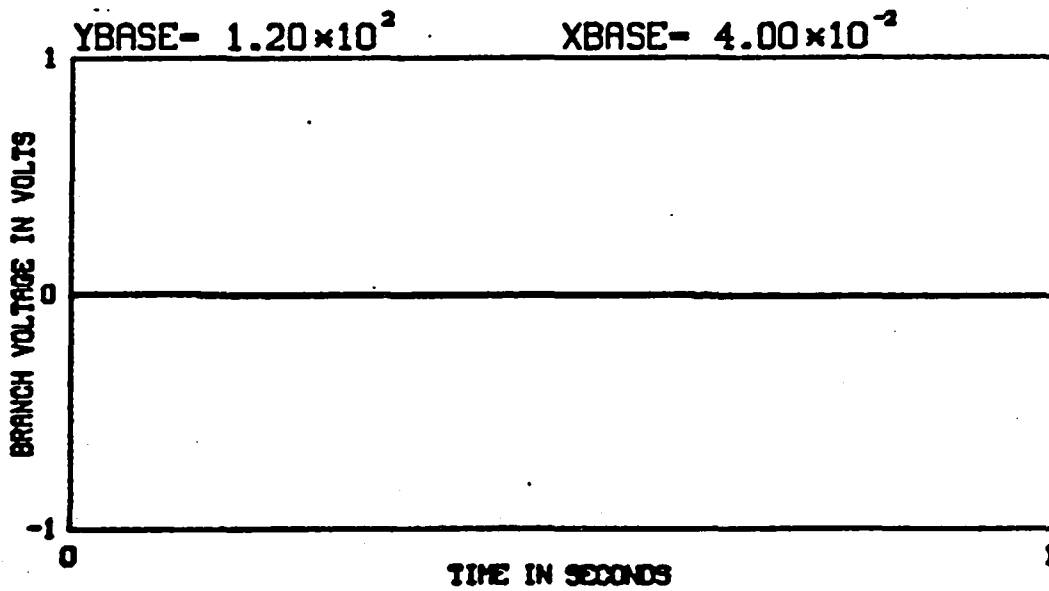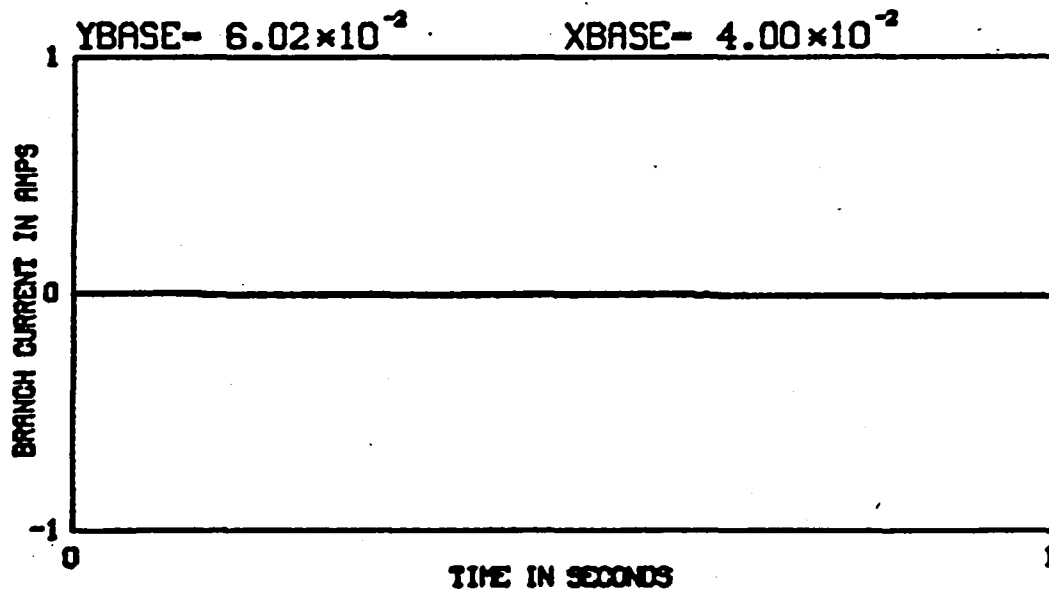
Figure (3.3-10)   Simulated Current and Voltage Waveforms for
                  Branch   #24,   OPEN-DELTA   Configuration
                  (Unfaulted)

YBASE= 5.97 × 10^{-2} XBASE= 4.00 × 10^{-2}

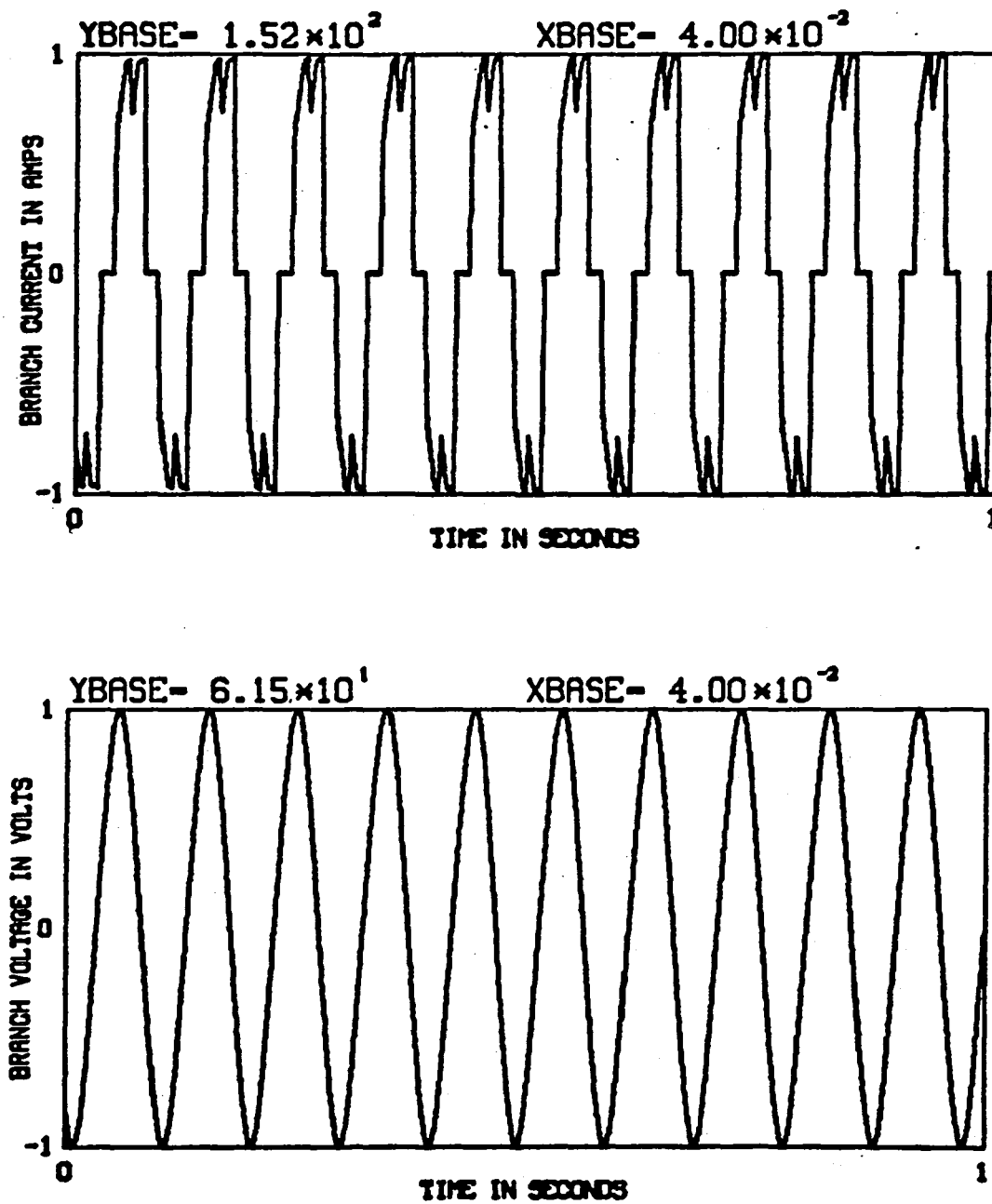YBASE= 1.19 × 10^{2} XBASE= 4.00 × 10^{-2}
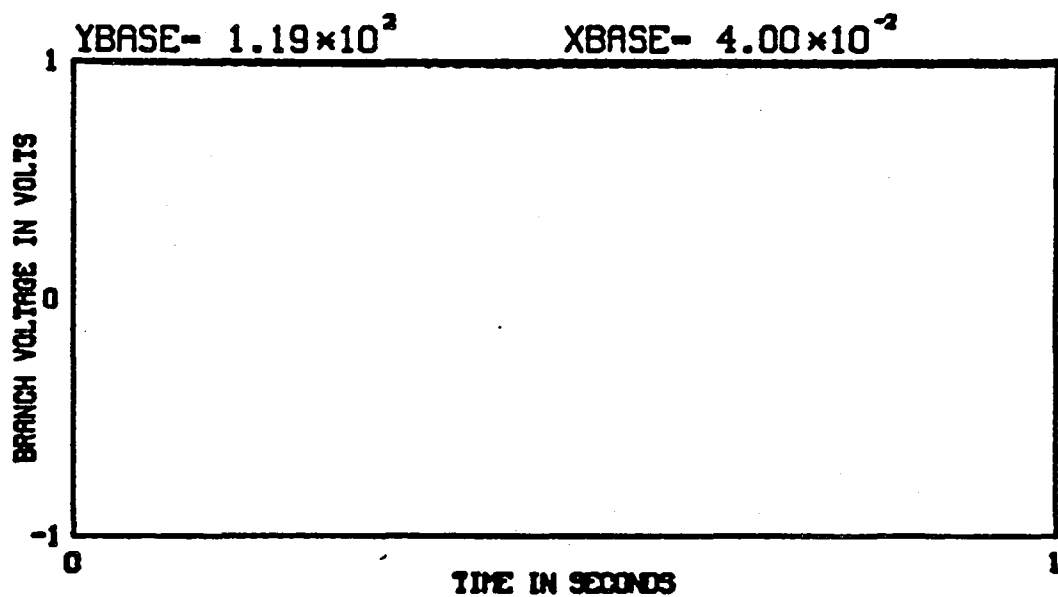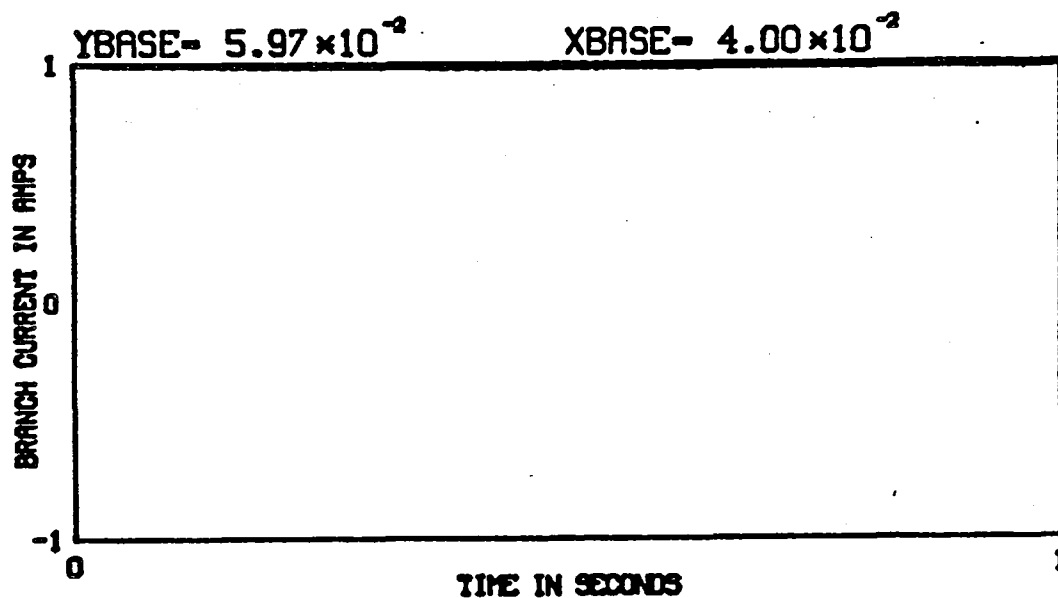
Figure (3.3-11)   Simulated Current and Voltage Waveforms for Branch #6, OPEN-DELTA Configuration (Unfaulted)

Figure (3.3-12)   Simulated Current and Voltage Waveforms for
                  Branch   #37,   OPEN-DELTA   Configuration
                  (Unfaulted)

3.4 Simulated Waveforms of the WYE Configuration (Containing Shorted Turn)

A simulation of the effects of a shorted turn in a WYE connected machine is presented in this section. This simulation is otherwise identical to the case presented in Section (3.3-1). The corresponding network graph is given in Figure (3.4-1) and should be referred to in reviewing the results of simulations presented in this section. The inductances used to simulate the effects of the shorted turn are given in Table (3.4-3).

The input data used in obtaining these results are given in Table (3.4-1). Identification of all the displayed voltage and current simulated waveforms is given in Table (3.4-2).

The calculated average electromagnetic machine power during the last cycle is 12,520 watts. This is only slightly less than that for the unfaulted case. The corresponding copper losses, however, are much greater (597.15 watts). The losses in the shorted turn are 40 times higher (366 watts) than the unfaulted losses (9.1 watts). It must be emphasized that saturation effects and changes in winding resistance due to increased temperatures were neglected in this analysis. These factors should be included in any future efforts in this area.
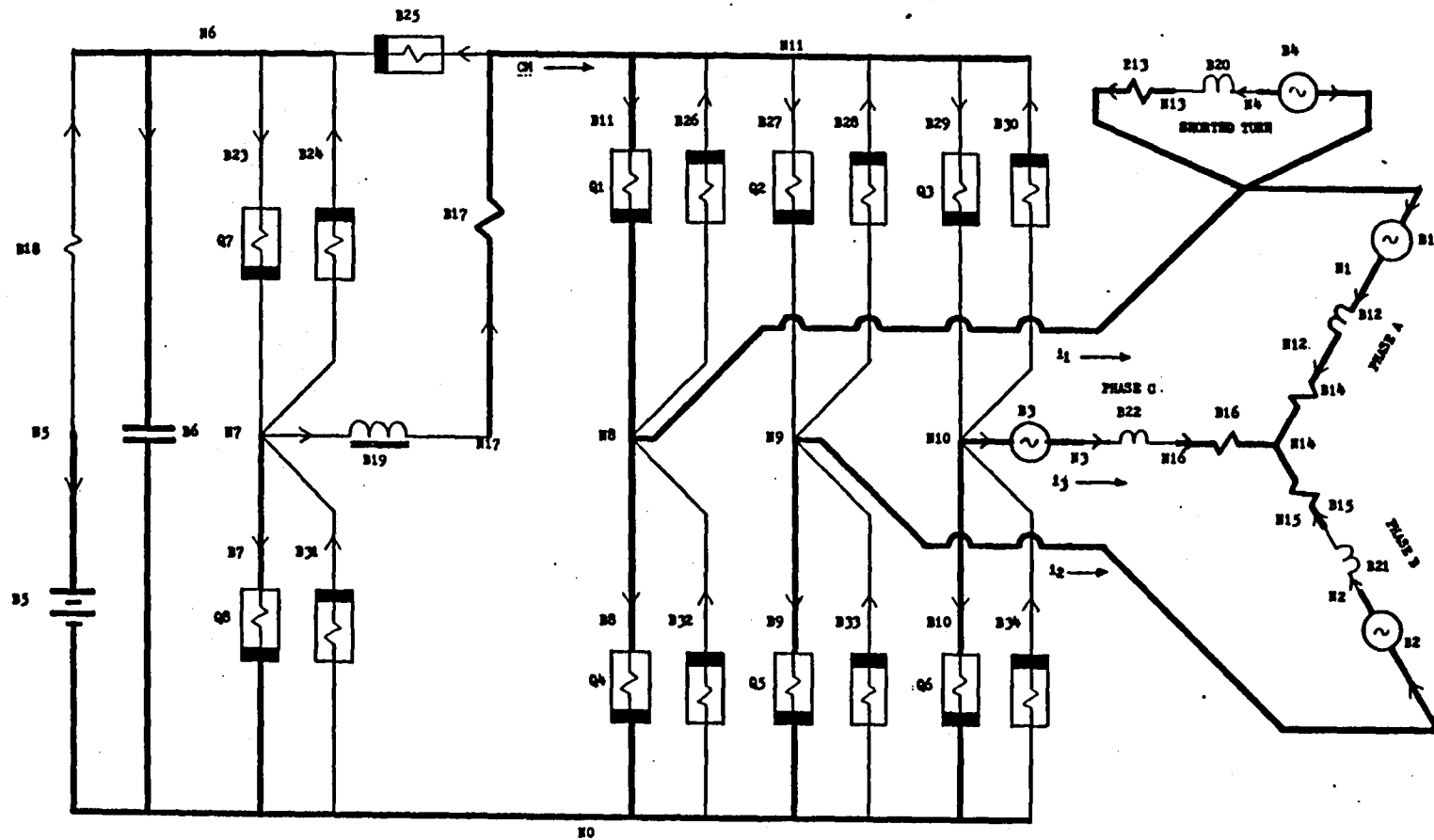
Figure (3.4-1) Network Model of the WYE Configuration
(Containing Shorted Turn)

Three Phase UnBalanced Machine Model:

Branch #14 Healthy Portion Phase(A) 7 TURNS
            Winding Resistance= 5.95 milli-ohms
Branch #13 Shorted Portion of Phase(A) 1 TURN
            Winding Resistance= 0.85 milli-ohms

Branch #15 Phase(B) Winding Resistance= 6.8 milli-ohms
Branch #16 Phase(C) Winding Resistance= 6.8 milli-ohms

See Inductance Matrix (Unbalanced Case) Attached in
Figure (3.4-2)

Inverter/Converter Bridge & Chopper Switching Components:

    Branch #11 (+Bus) Phase(A) Transistor
    Saturation Resistance "on" = 6.4 milli-ohms
    Cutoff Resistance   "off" = 2.0 killo-ohms

    Branch #26 (+Bus) Phase(A) Diode
    Forward-Bias Resistance "on" = 6.4 milli-ohms
    Reverse-Bias Resistance "off"= 2.0 killo-ohms

Chopper Choke:

    Branch #17 Choke Resistance = 24 milli-ohms
    Branch #19 Choke Inductance = 1.5 milli-henries

DC Power Source:

    Branch #6 Filter Capacitor = 7.8 milli-farads
    Branch #5 Battery(Internal) Voltage = 120.0 Volts
    Branch #18 Battery(Internal) Resistance = 5 milli-ohms

Table (3.4-2) Branch Identification WYE Configuration
(Containing Short Circuit)

Figure Number	Branch Number	Branch Identification
3.4-2	2	Phase (B) Armature EMF and Phase Current
3.4-3	21	Phase (B) Inductive Voltage and Phase Current
3.4-4	27	Phase (B) (+ Bus) Transistor
3.4-5	28	Phase (B) (+ Bus) Diode
3.4-6	9	Phase (B) (- Bus) Transistor
3.4-7	33	Phase (B) (- Bus) Diode
3.4-8	5	Battery Internal Voltage and Current
3.4-9	19	Chopper Inductive Voltage and Current
3.4-10	23	Chopper (+ Bus) Transistor
3.4-11	24	Chopper (+ Bus) Diode
3.4-12	7	Chopper (- Bus) Transistor
3.4-13	31	Chopper (- Bus) Transistor
3.4-14	1	(H) Phase (A) Armature EMF and Phase Current
3.4-15	12	(H) Phase (A) Inductive Voltage and Phase Current
3.4-16	4	(S) Phase (A) Armature EMF and Phase Current
3.4-17	20	(S) Phase (A) Inductive Voltage and Phase Current

	A(H)	CHOKE	A(S)	B(H)	C(H)
A(H)	36.6	0.	4.97	-3.66	-3.66
CHOKE	0.	1500.	0.	0.	0.
A(S)	0.747	0.	4.97	-0.523	-0.523
B(H)	-3.66	0.	-0.523	47.8	-4.18
C(H)	-3.66	0.	-0.523	-4.18	47.8

ALL INDUCTANCES IN MICROHENRIES

Table (3.4-3) Inductance Matrix of Unbalanced (Faulted) Case

Figure (3.4-2)   Simulated Current and Voltage Waveforms for
                  Banch #2, WYE Configuration (faulted)
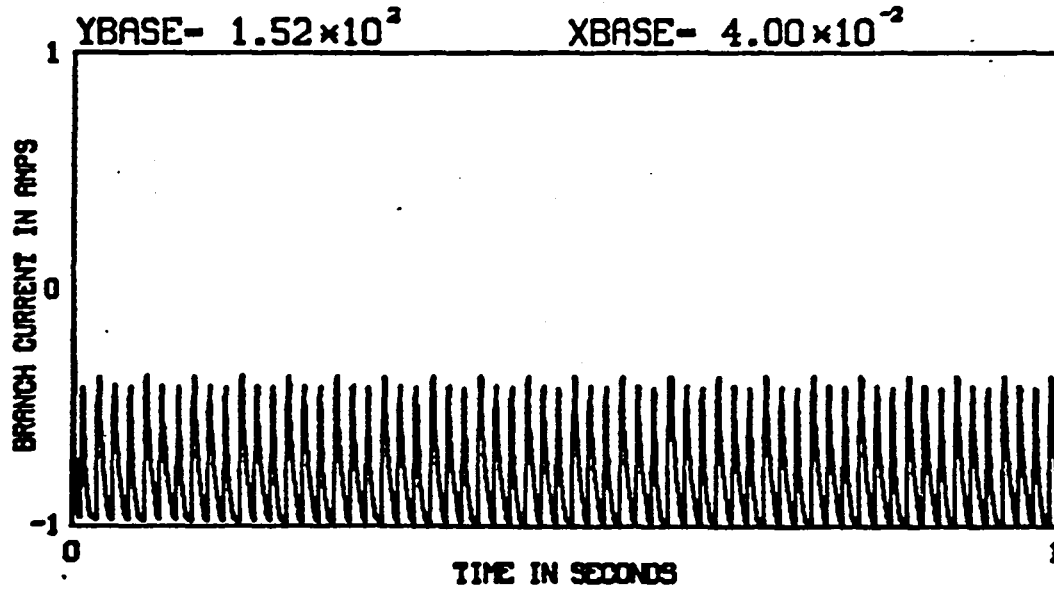
- 210 -
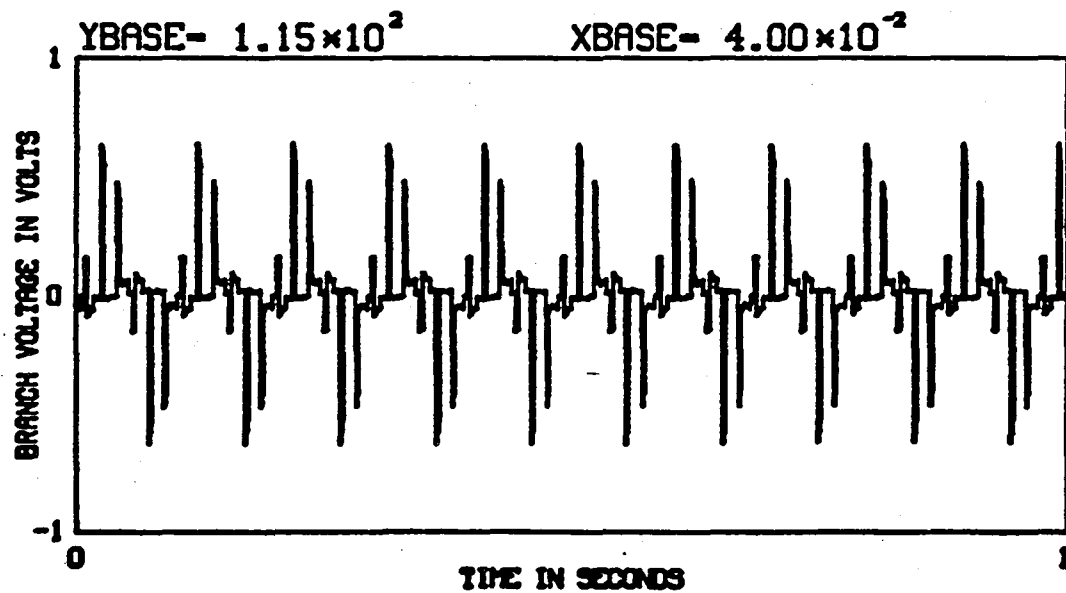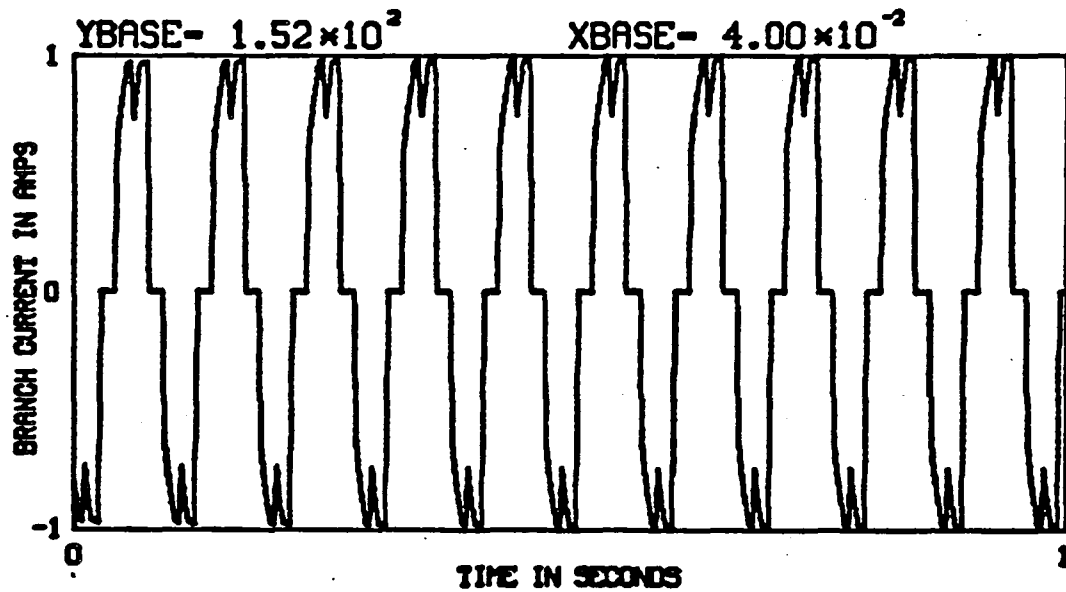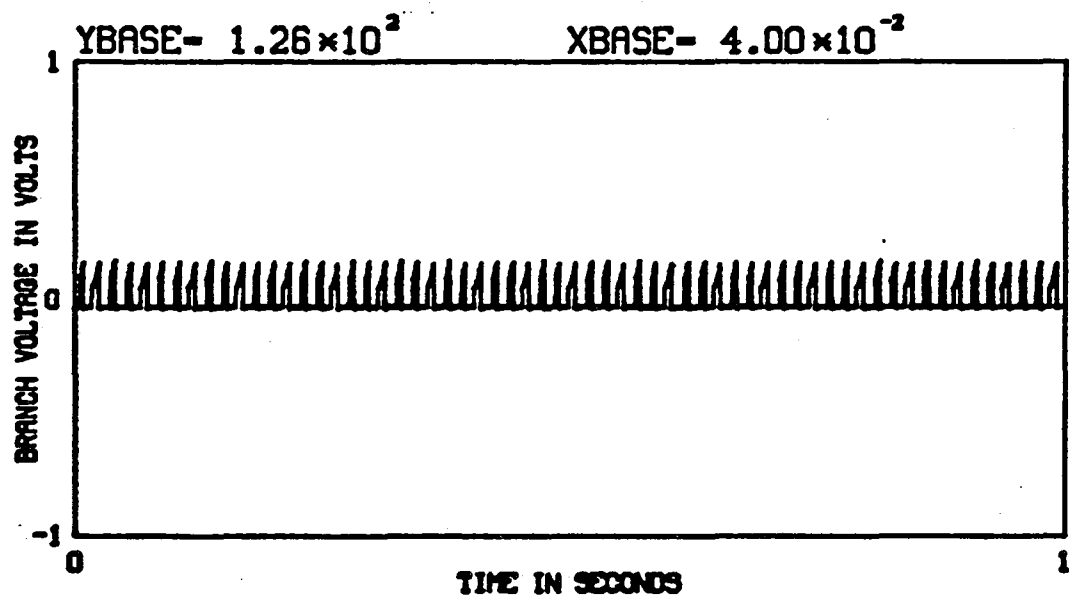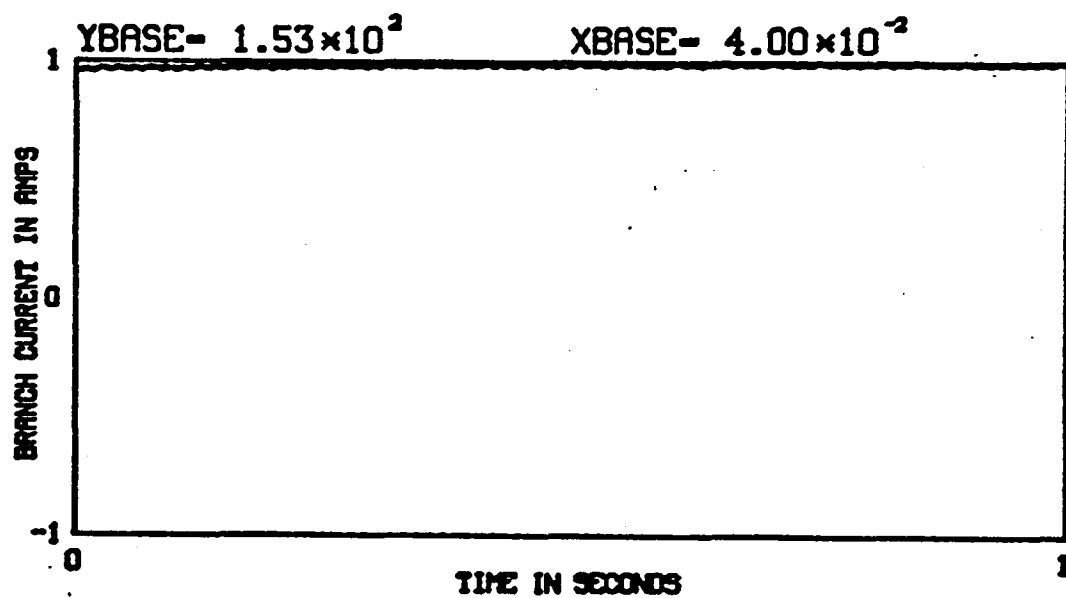
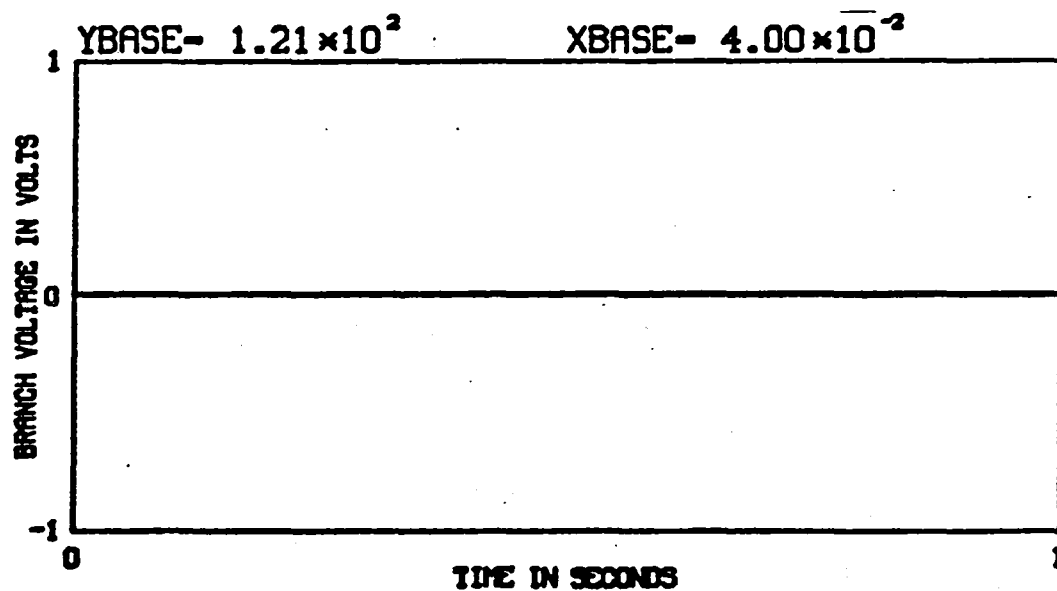Figure (3.4-3)   Simulated Current and Voltage Waveforms for Banch #21, WYE Configuration (faulted)
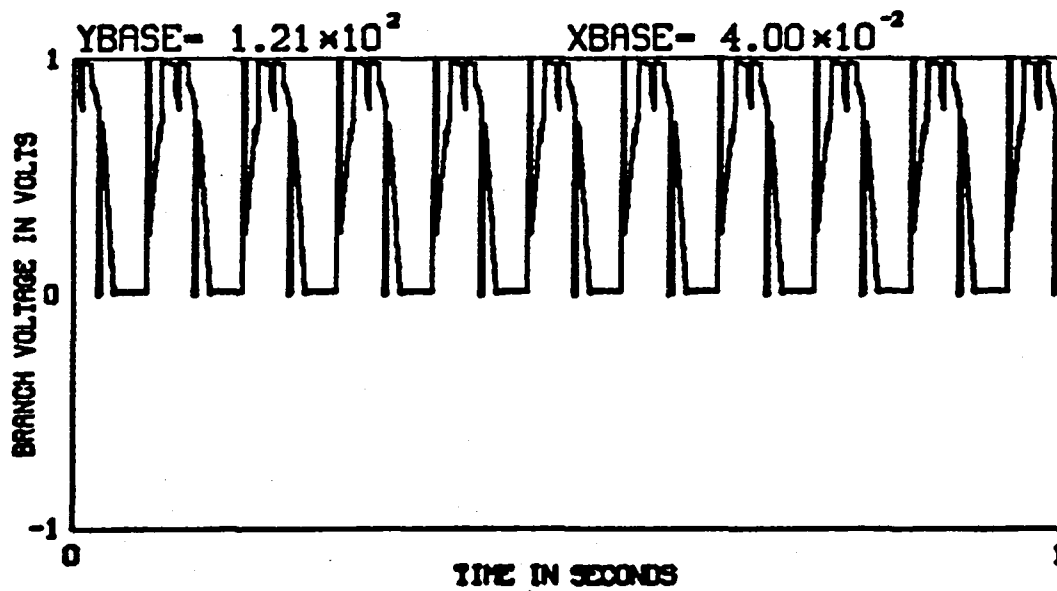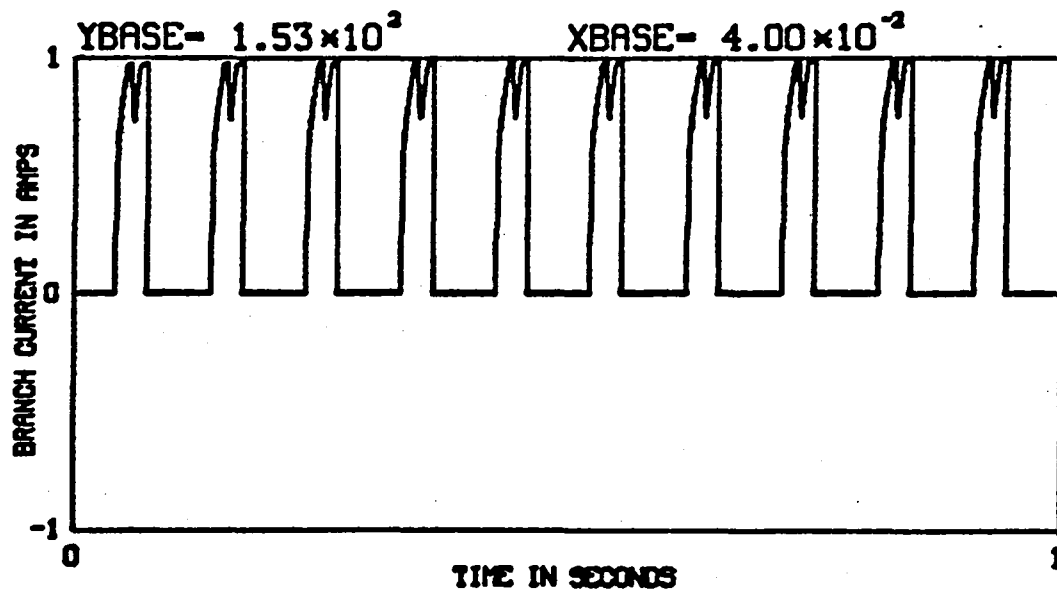
Figure (3.4-4)   Simulated Current and Voltage Waveforms for
Branch #27, WYE Configuration (faulted)
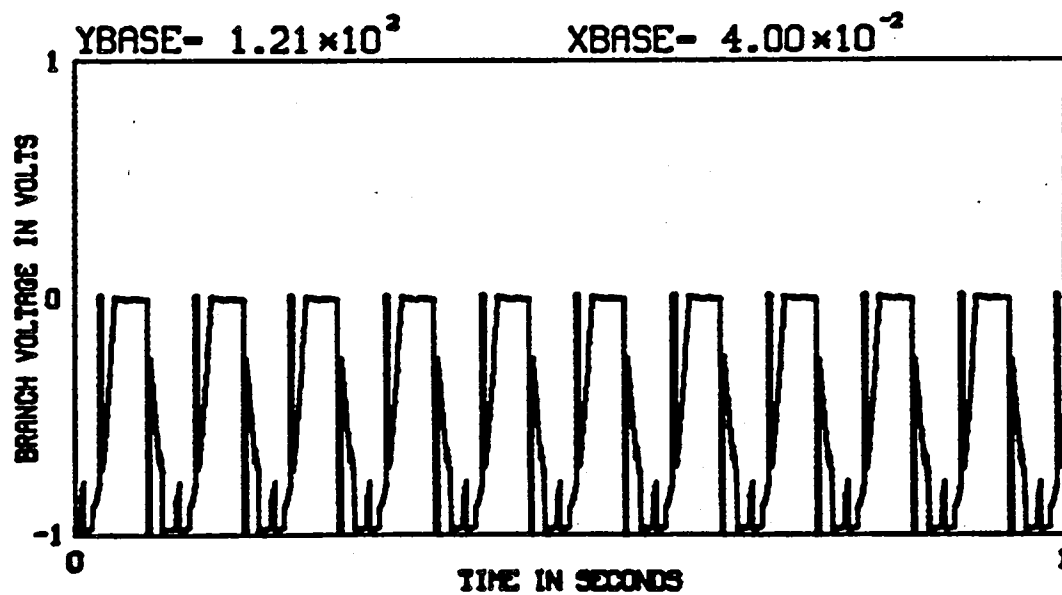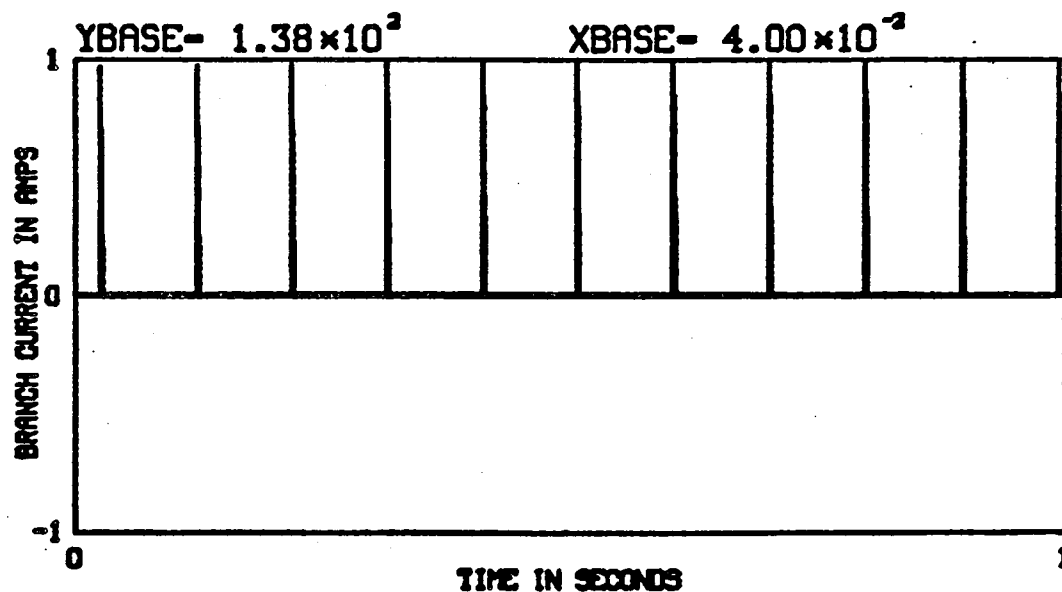
Figure (3.4-5)   Simulated Current and Voltage Waveforms for
                  Branch #28, WYE Configuration (faulted)
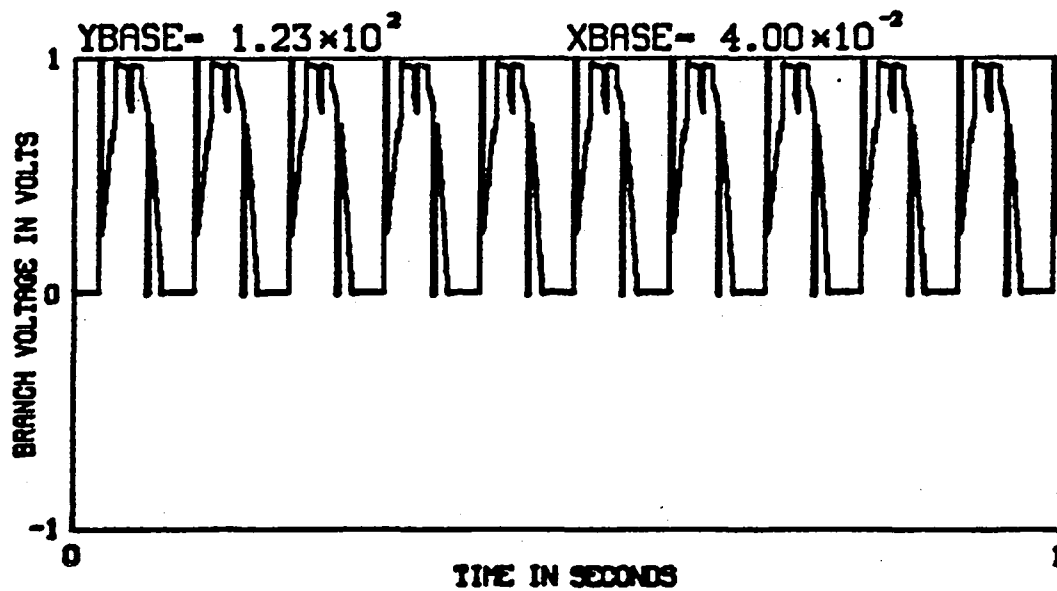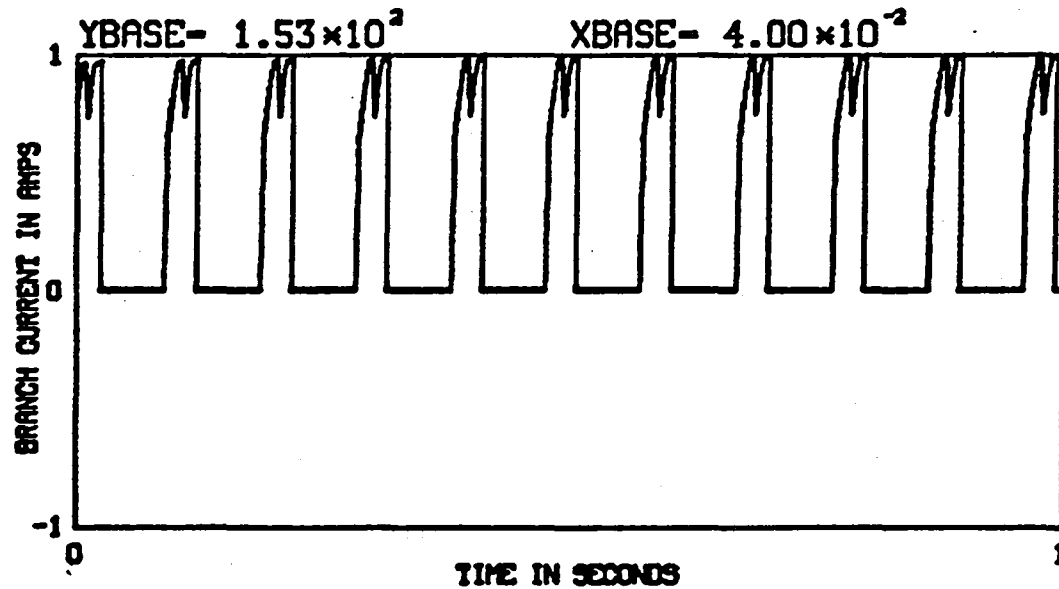
Figure (3.4-6)   Simulated Current and Voltage Waveforms for
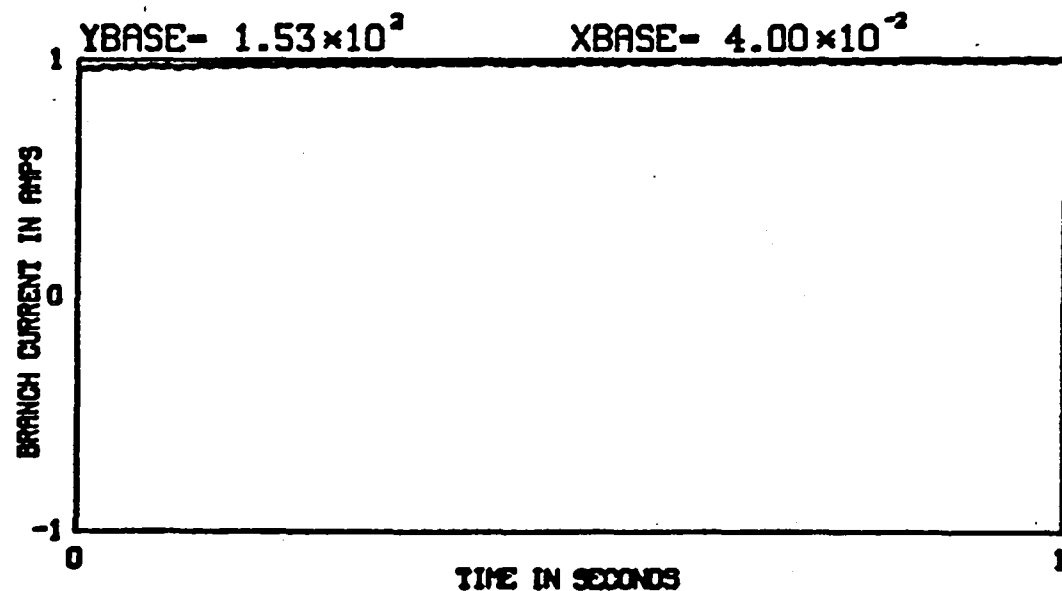   Branch #9, WYE Configuration (faulted)

YBASE- 1.38×10^{2} XBASE- 4.00×10^{-2}

YBASE- 1.23×10^{2} XBASE- 4.00×10^{-2}
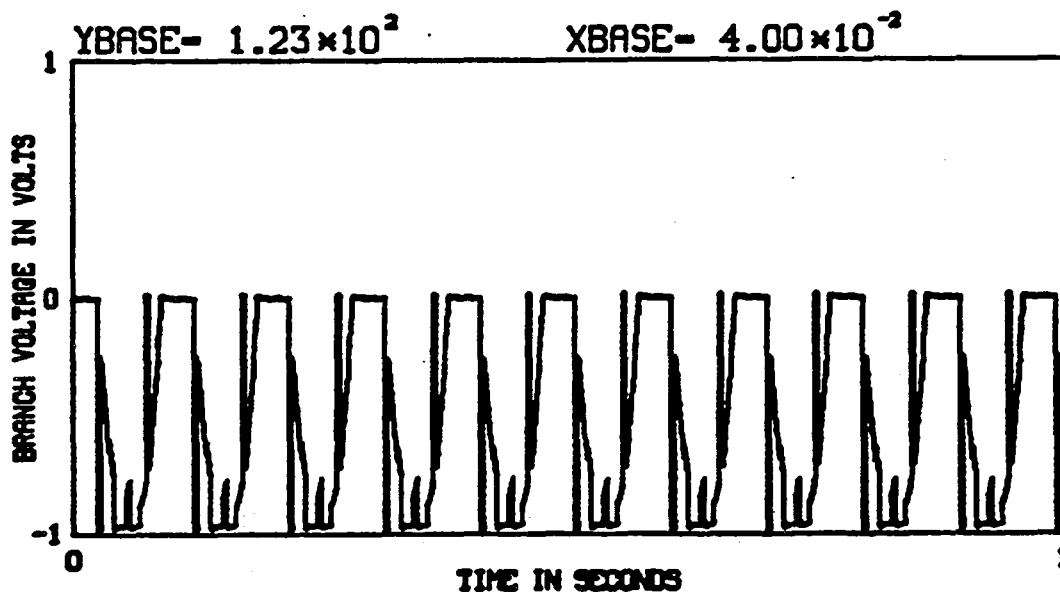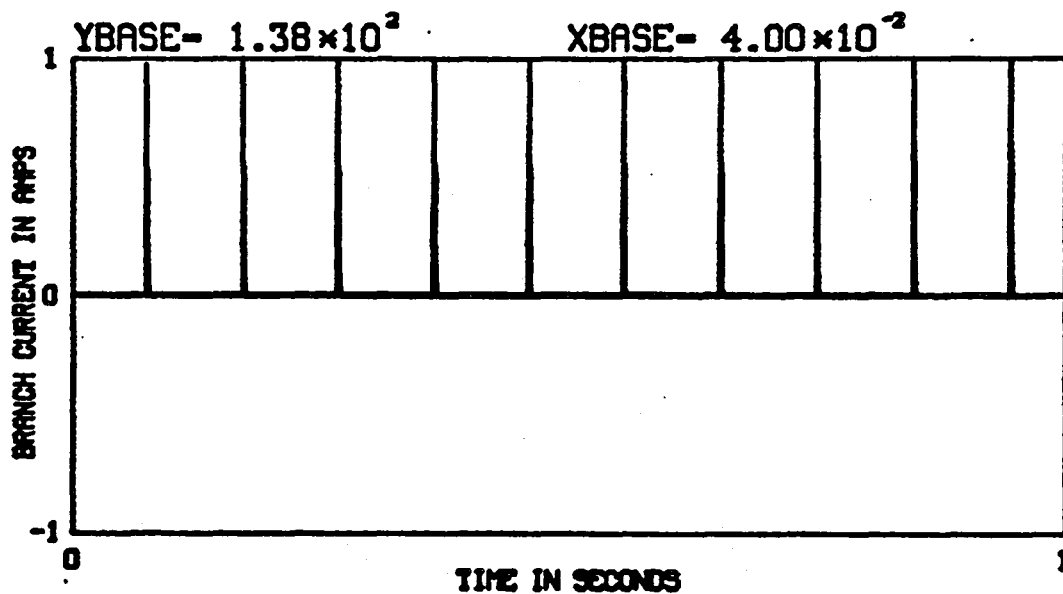
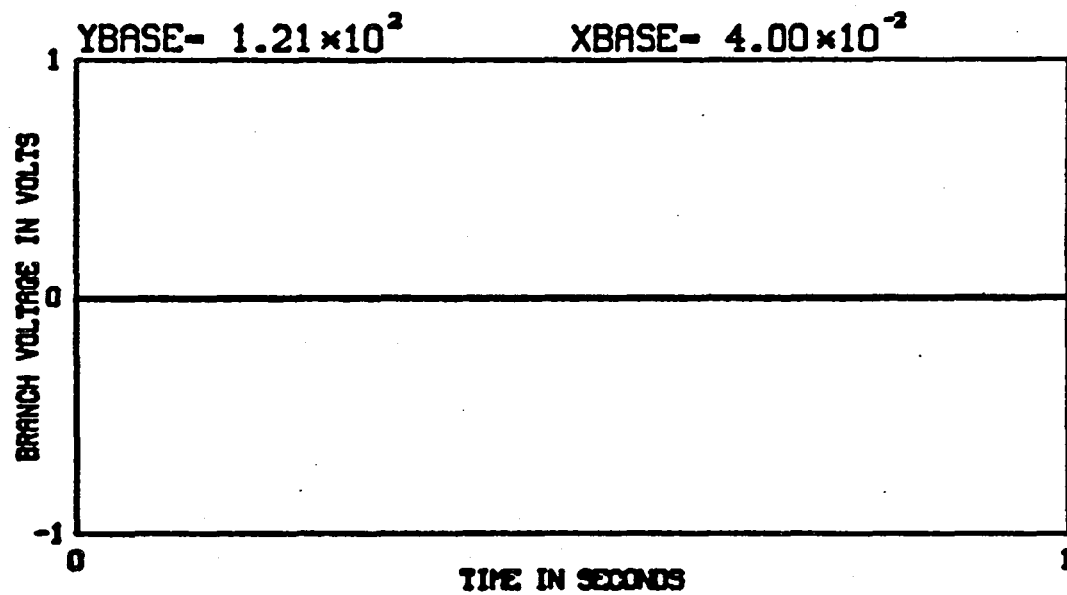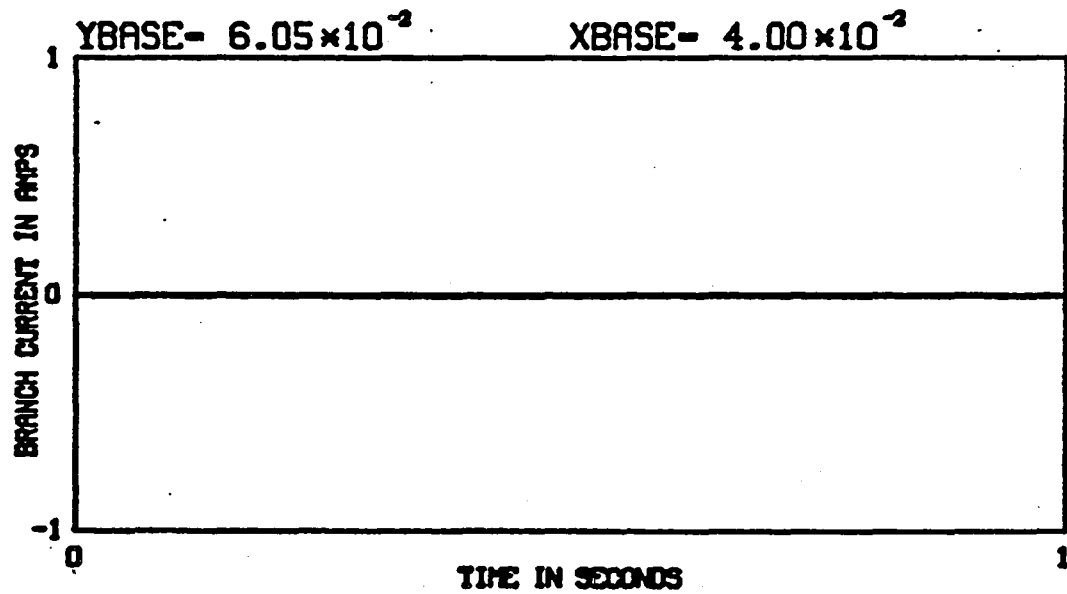Figure (3.4-7)   Simulated Current and Voltage Waveforms for Branch #33, WYE Configuration (faulted)
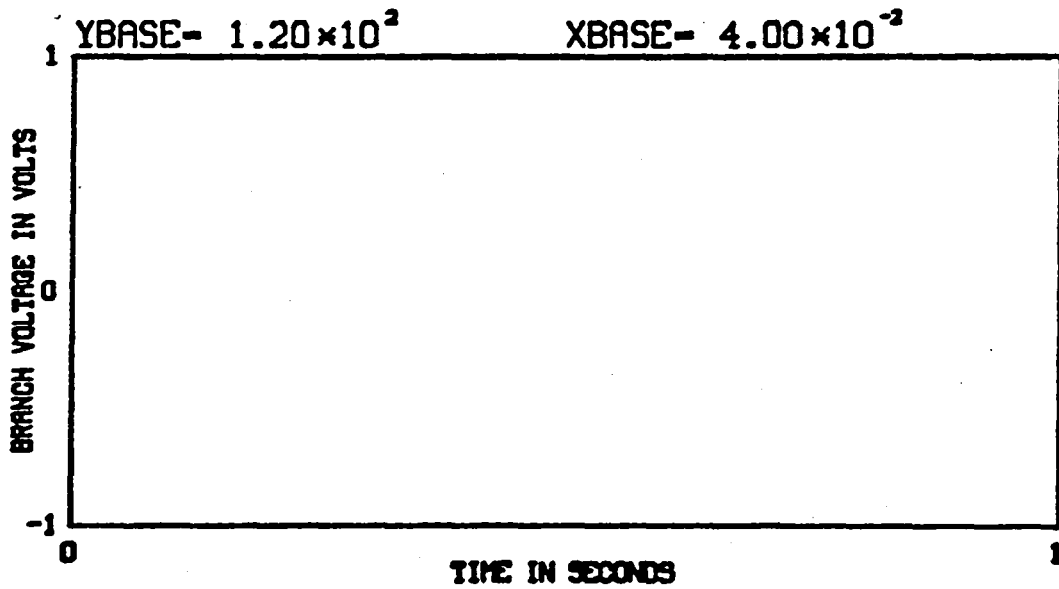
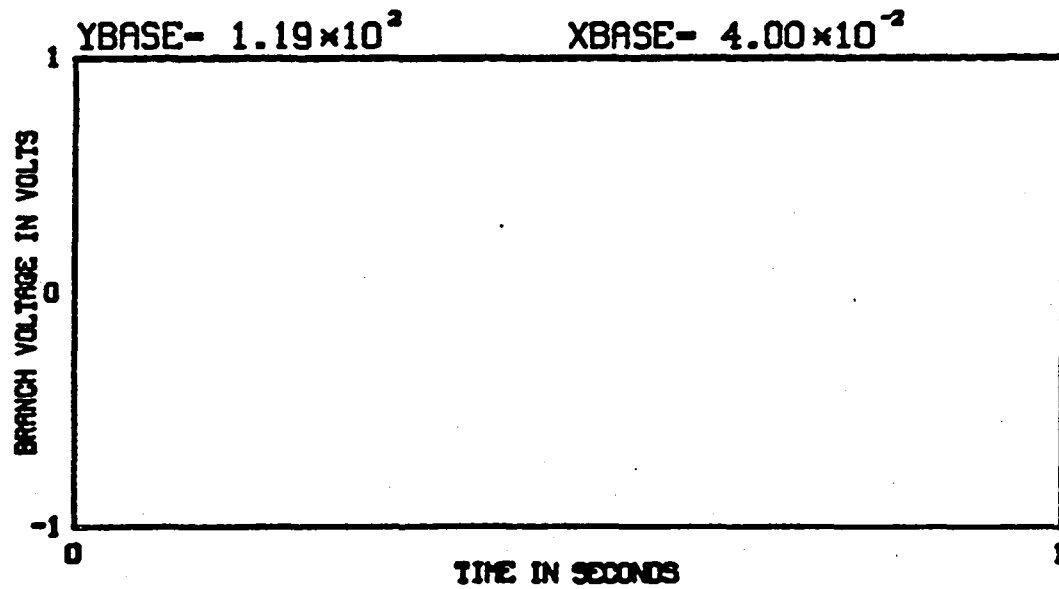Figure (3.4-8)   Simulated Current and Voltage Waveforms for Branch #5, WYE Configuration (faulted)

Figure (3.4-9) Simulated Current and Voltage Waveforms for Branch #19, WYE Configuration (faulted)

YBASE- 1.53 ×10²   XBASE- 4.00 ×10⁻²

BRANCH CURRENT IN AMPS

TIME IN SECONDS

YBASE- 1.21 ×10²   XBASE- 4.00 ×10⁻²

BRANCH VOLTAGE IN VOLTS

TIME IN SECONDS

Figure (3.4-10)   Simulated Current and Voltage Waveforms for
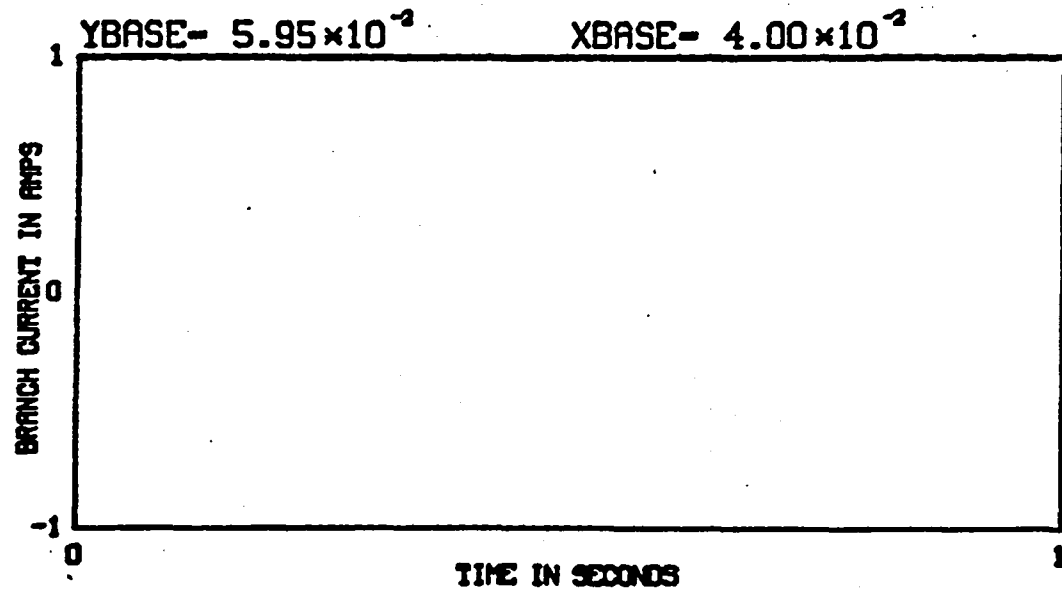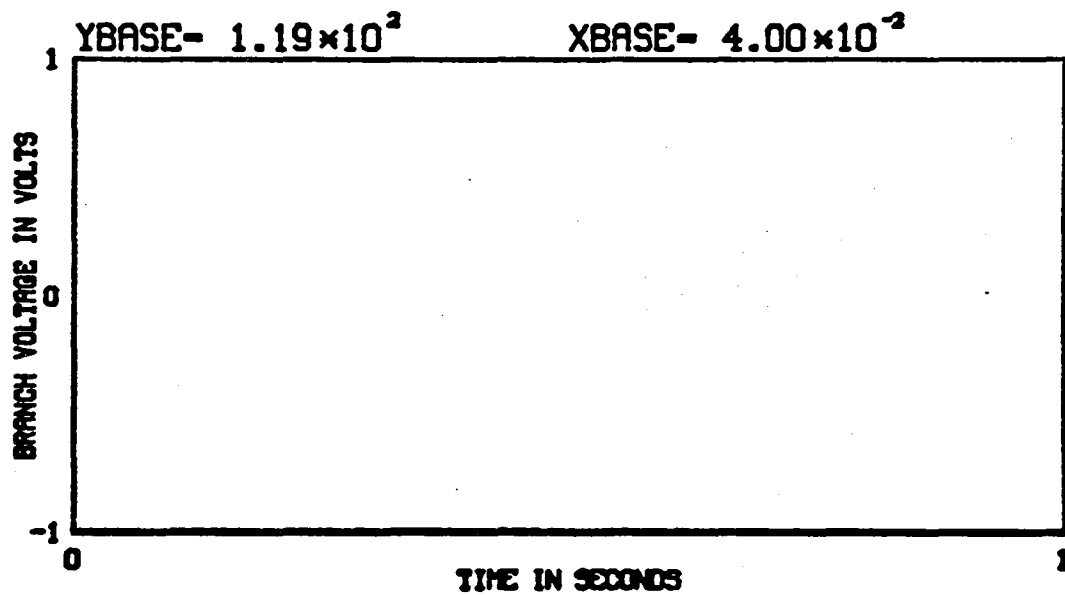Branch #23, WYE Configuration (faulted)

YBASE= 6.05×10^{-2} XBASE= 4.00×10^{-2}

BRANCH CURRENT IN AMPS

TIME IN SECONDS

YBASE= 1.21×10^{2} XBASE= 4.00×10^{-2}

BRANCH VOLTAGE IN VOLTS

TIME IN SECONDS

Figure (3.4-11)   Simulated Current and Voltage Waveforms for
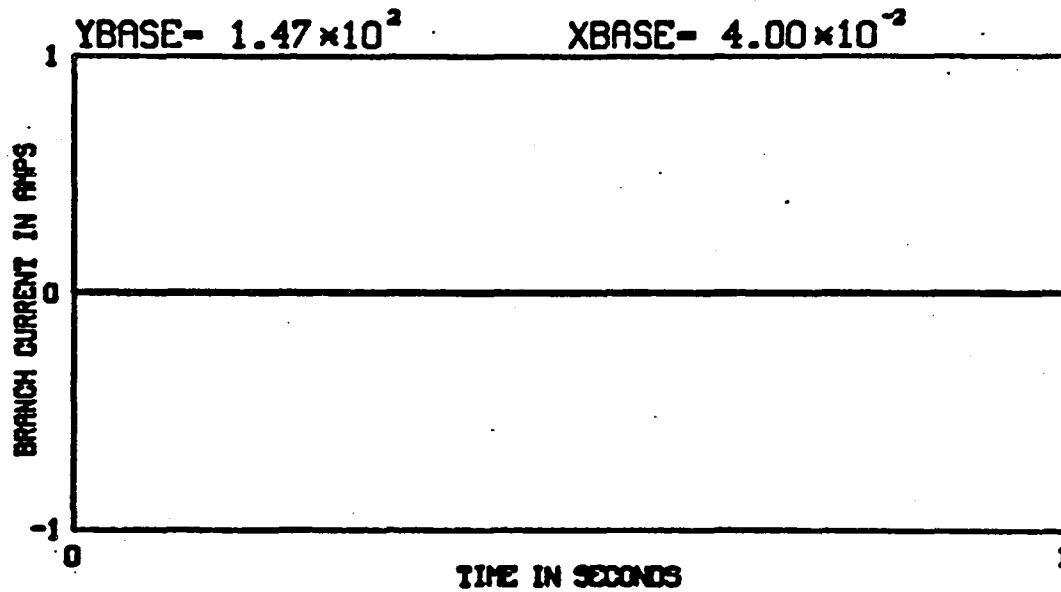   Branch #24, WYE Configuration (faulted)

YBASE- 5.95×10^{-2} XBASE- 4.00×10^{-2}

BRANCH CURRENT IN AMPS

1

0

-1

0   TIME IN SECONDS   1

YBASE- 1.19×10^{2} XBASE- 4.00×10^{-2}

BRANCH VOLTAGE IN VOLTS

1

0

-1

0   TIME IN SECONDS   1

Figure (3.4-12)   Simulated Current and Voltage Waveforms for
                  Branch #7, WYE Configuration (faulted)

YBASE- 1.47×10^{2} XBASE- 4.00×10^{-2}

BRANCH CURRENT IN AMPS

1

0

-1

0   TIME IN SECONDS   1

YBASE- 1.19×10^{2} XBASE- 4.00×10^{-2}

BRANCH VOLTAGE IN VOLTS

1

0

-1
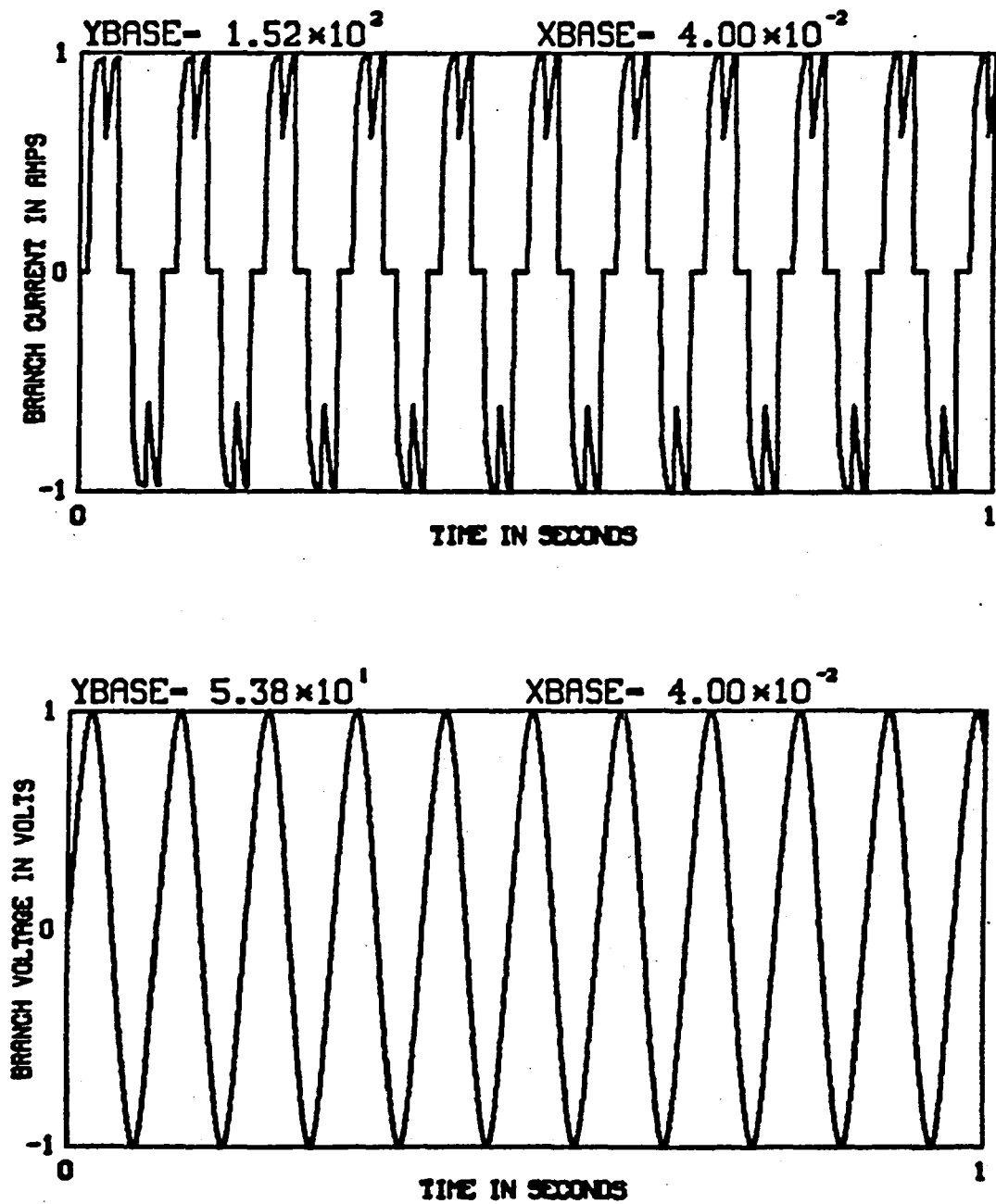
0   TIME IN SECONDS   1

Figure (3.4-13)   Simulated Current and Voltage Waveforms for
Branch #31, WYE Configuration (faulted)

Figure (3.4-14)   Simulated Current and Voltage Waveforms for
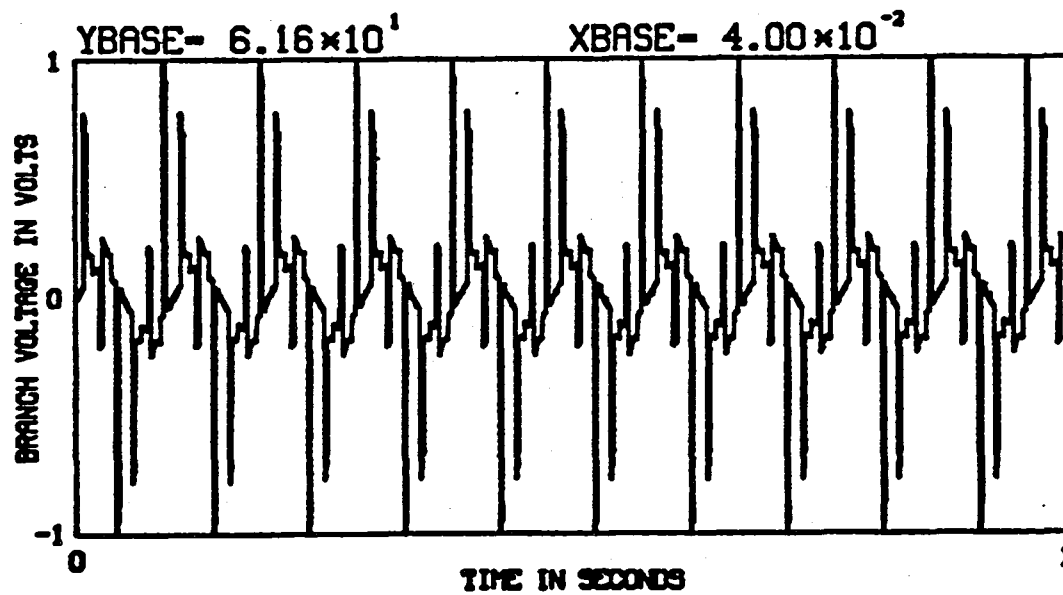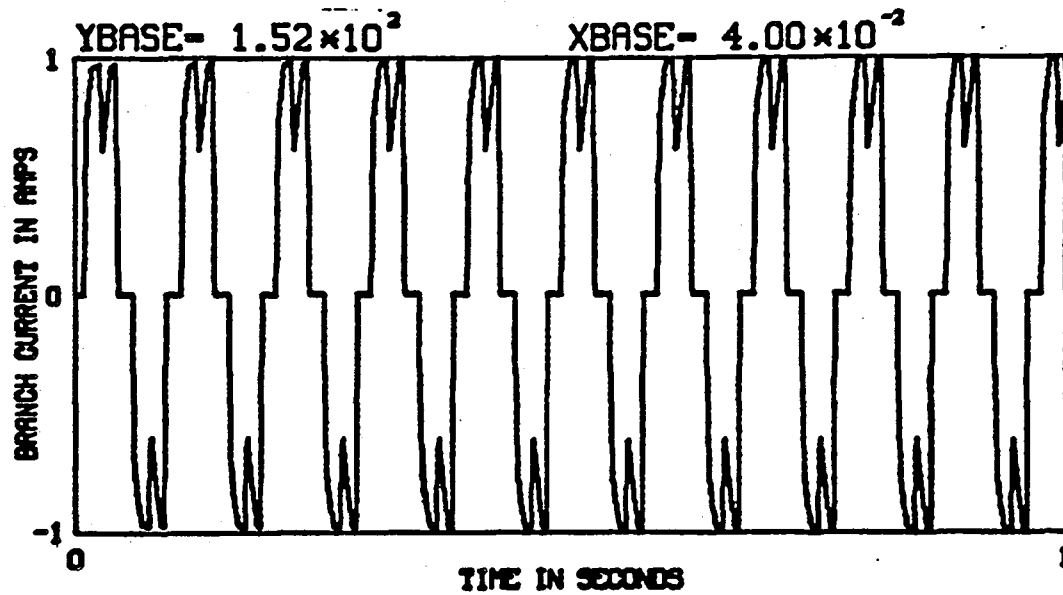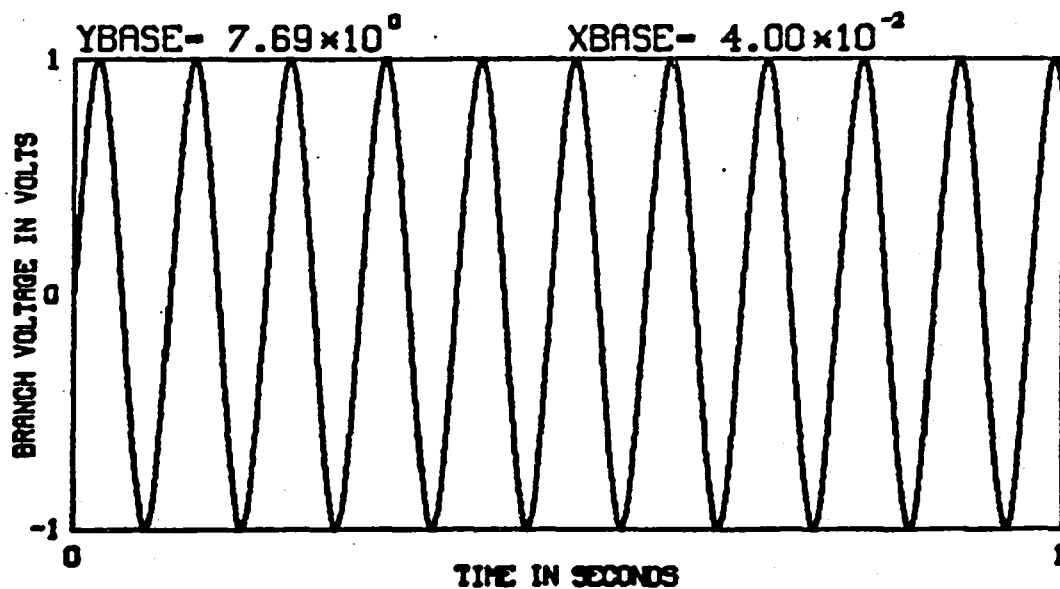   Branch #1, WYE Configuration (faulted)

- 222 -

Figure (3.4-15)   Simulated Current and Voltage Waveforms for
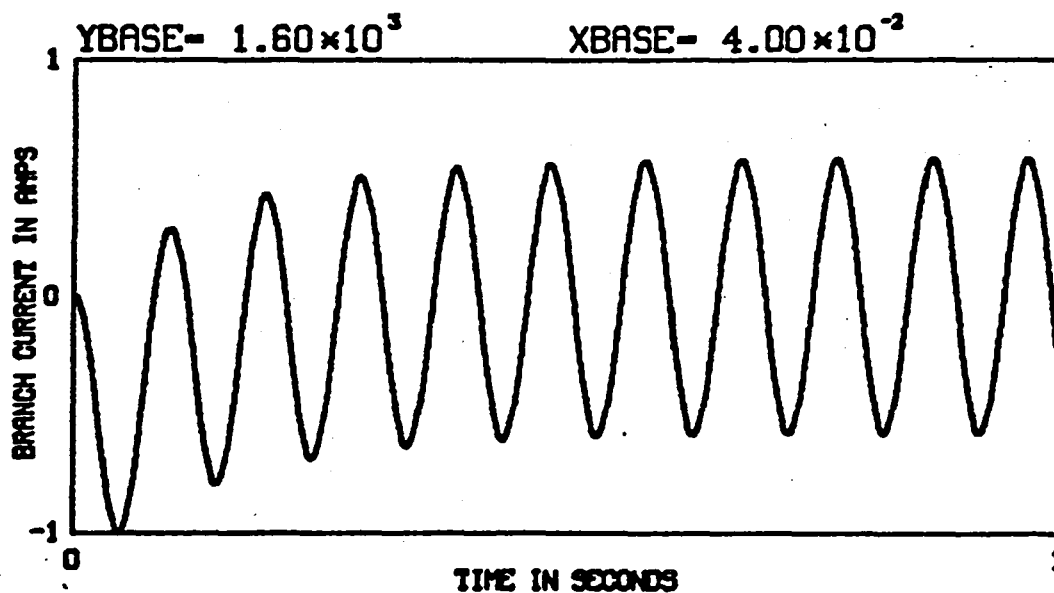   Branch #12, WYE Configuration (faulted)

Figure (3.4-16)   Simulated Current and Voltage Waveforms for
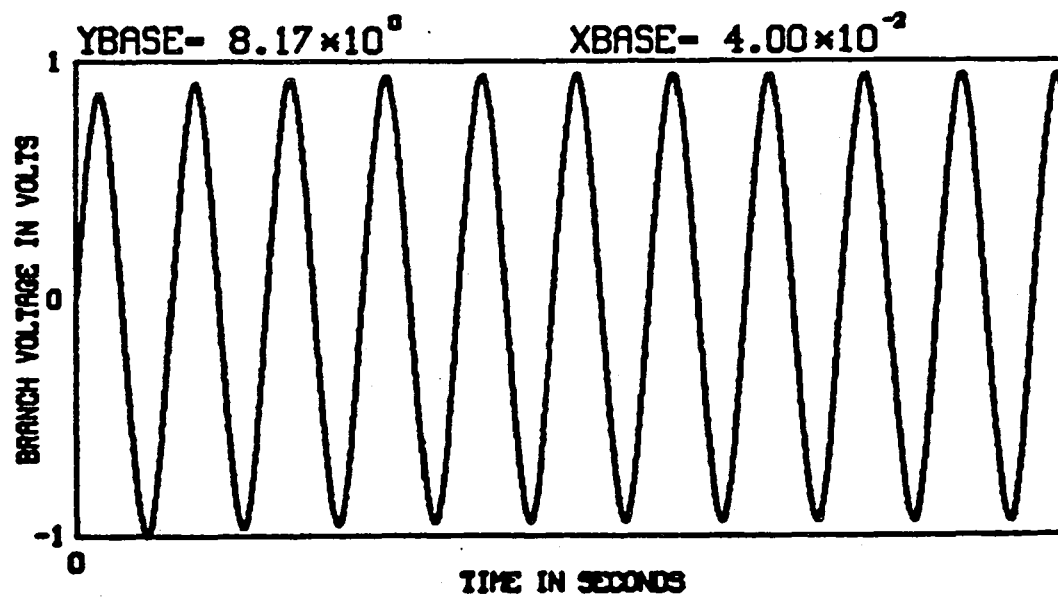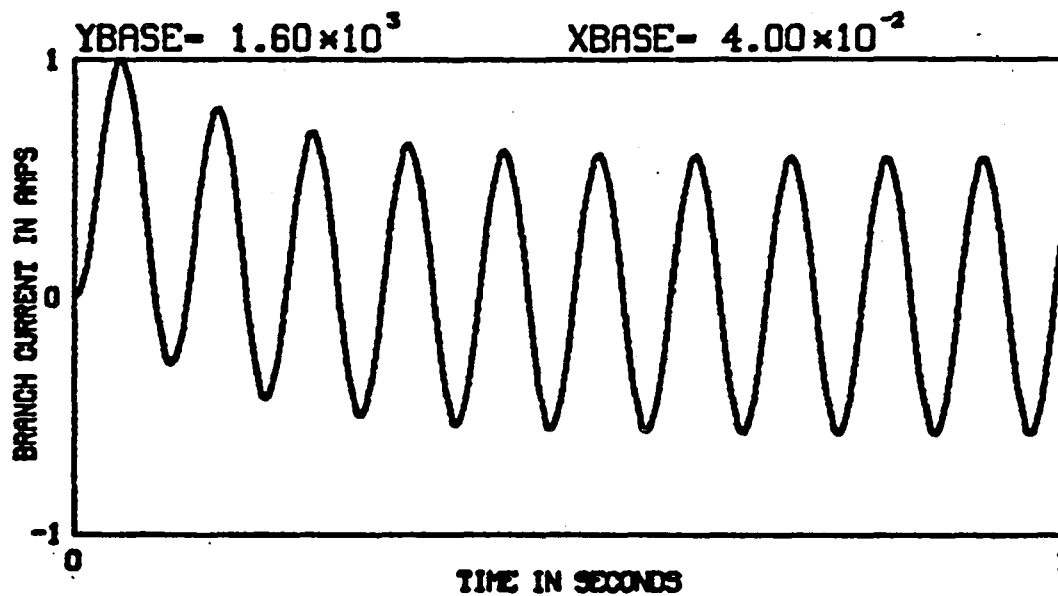Branch #4, WYE Configuration (faulted)

Figure (3.4-17) Simulated Current and Voltage Waveforms for
Branch #20, WYE Configuration (faulted)

4.0 CONCLUSIONS AND RECOMMENDATIONS

A network topology based modeling approach designed for the simulation of electromechanical drive and actuator systems has been presented and verified against actual test measurements. The salient features of this model are:

1. The state equations are automatically generated from the USER specified network topology using standard network graph theory concepts.

2. The type of control unit used to operate the power conditioner can be USER specified from a number of preprogrammed controllers. Additional control schemes can be implemented, if required, by modifying SUBROUTINE QLOGIC.

3. The program can handle a number fault scenarios including shorted turns and failures in the power electronics.

4. The program can handle mutual inductances and can be adopted to include nonlinearities in the machine parameters.

5. The integration routine employed by this program is the IMSL SUBROUTINE DGEAR which is widely available and well suited to solving the ill conditioned systems of differential equations resulting from these types of machine systems.

The model was shown to be successful in simulating the machines with connections such as WYE, DELTA, OPEN-DELTA, and WYE with SHORTED TURN IN ARMATURE WINDING. The model was used successfully in determining currents and voltages in and across the various branches, respectively. The present computer algorithm can be easily supplied with a post processor (external subroutines) which would calculate input power, output power, and losses in the systems studied here. However, the present resources did not permit the development of this post processor, which must be added in future research efforts on such machine system simulation models.

There are a number of improvements which would greatly expand the capabilities of this model. These include:

1. A more detailed switch model may be necessary in future investigations especially if power conditioner efficiencies are of great importance. Such improvements may include a more accurate representation of the static I-V characteristics as well as accounting for switching and base drive losses.

2. A model of SCR switches should also be implemented to increase the versatility of the model.

3. The program should be modified to accept dependent sources.

4. This model should be linked to a finite element machine model when studying the effects of shorted turns. This is necessary due to the heavy saturation produced by the fault currents.

5. The program should be streamlined and upgraded to enable the USER to perform simulations with a minimum amount of input data. This should include a preprocessor to automatically generate a proper network graph for the system under study. Postprocessors to calculate losses, efficiencies, etc. and well as plotting routines to display the results would also be useful.

The results and experimental verification presented in this report demonstrate the usefulness and accuracy of this model in predicting both the faulted and unfaulted performance of electromechanical actuators. Much work remains to be done to link this network model with the finite element based machine parameter estimation model required for accurate simulation of the shorted turn behavior of such systems.

End of Document